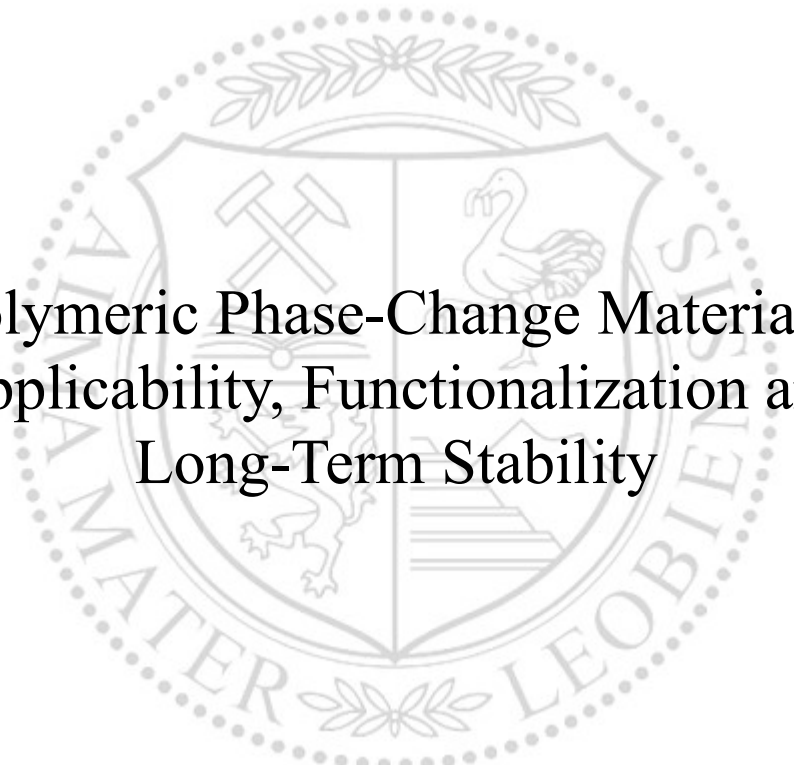Chair of Materials Science and Testing of Polymers

Doctoral Thesis

Polymeric Phase-Change Materials: Applicability, Functionalization and Long-Term Stability

Dipl.-Ing. Helena Marion Weingrill, BSc

April 2019

Helena Marion WEINGRILL

Dissertation

Helena Marion WEINGRILL

Dissertation

Polymeric Phase-Change Materials: Applicability, Functionalization and Long-Term Stability

April 2019

Chair of Materials Science and Testing of Polymers
Department Polymer Engineering and Science, Montanuniversitaet Leoben

Part I.

Preamble

AFFIDAVIT

I declare on oath that I wrote this thesis independently, did not use other than the specified sources and aids, and did not otherwise use any unauthorized aids.

I declare that I have read, understood, and complied with the guidelines of the senate of the Montanuniversität Leoben for "Good Scientific Practice".

Furthermore, I declare that the electronic and printed version of the submitted thesis are identical, both, formally and with regard to content.

Date 18.04.2019

Signature Author
Helena Marion, Weingrill
Matriculation Number: 00935143

Acknowledgement

I would like to express my sincere gratitude to all persons who supported and inspired me during my thesis.

First and foremost, I would like to thank Assoc.-Prof. Dr. Katharina RESCH-FAUSTER (Materials Science and Testing of Polymers, Montanuniversitaet Leoben) for guiding me through my PhD and my personal development as a PhD student. During our scientific discussions, she taught me how to combine my knowledge on polymers with my creativity to explain the results of my research. She always promoted my independent work with sufficient guidance to guarantee a successful completion of my PhD. I am also very thankful that Katharina gave me the opportunity to spend time abroad to fulfill my craving for learning about different cultures and speaking foreign languages despite the rigors of my time as a PhD student.

Second, I would like to express my appreciation to my reviewer Univ.-Prof. Dr. Gerald PINTER (Materials Science and Testing of Polymers, Montanuniversitaet Leoben) for offering me the possibility to perform this thesis and for establishing such a warm and welcoming working atmosphere at our institute. He thereby contributed significantly to the outcome of my research.

Next, I must voice my gratitude to my mentor Assoc.-Prof. Dr. Thomas LUCYSHYN (Polymer Processing, Montanuniversitaet Leoben) and to Univ.-Prof. Dr. Clemens HOLZER (Polymer Processing, Montanuniversitaet Leoben) for their guidance concerning the processing aspects of my research and the valuable input for my project-related work and publications.

Furthermore, I could not have completed my PhD without Dr. Susanne KAHLEN's (Borealis GmbH, Linz) technical support and helpful input about polyolefins.

Abstract

This dissertation deals with the development of polymeric phase-change materials (PCM) for thermal energy storages. PCM are applied in latent heat storages (LHS) as storage media as they can store and release large amounts of thermal energy in the form of latent heat when they undergo a phase transition (melting and crystallization is used most commonly). They are preferable over sensible heat storage media as they possess higher energy density. PCM for different application temperature ranges already exist but all still face several challenges during their application including incongruent melting, subcooling instead of crystallizing (which is necessary for the energy release), corrosion issues with the construction materials and low thermal conductivity (TC) leading to slow heat transfer rates. In spite of their broad variety of melting temperatures, polymers have been almost completely neglected for the application as PCM up to now. However, they exhibit many of preferable properties of PCM such as cost efficiency, commercial availability and the possibility to easily tailor their properties via compounding with various fillers and additives. Therefore, the first part of the dissertation presents the results of an extensive material screening process of suitable semi-crystalline polymers. Focus was put on commodity and engineering plastics. Their application-relevant thermo-physical properties such as their heat of fusion which equals the storage capacity of the PCM and their melting and crystallization behavior which reflects the charging and discharging mechanism, were investigated in detail. The following groups of semi-crystalline polymers were thereby identified as potential PCM: polyethylene (PE), polypropylene (PP), polyoxymethylene (POM), polyamides (PA) and their recyclates. As polymers have not been considered as PCM yet, no data about their long-term stability (ability to maintain their preferable thermo-physical properties during the application as PCM) were available in the scientific literature. They encounter severe conditions when applied as PCM as they lose their crystalline structure in the melt state which typically shields the atmospheric oxygen from diffusing into the material and

initiating thermo-oxidative degradation. As degradation alters the morphologic structure of the polymer, also its thermo-physical properties are typically affected. Therefore, a high-density polyethylene (HDPE) grade, a copolymer of POM (POM-C) and a PA 6 grade were exposed to static thermal load in air in the melt state for up to 15 days as application-oriented stability investigations. The exposed specimens of both, the HDPE and PA 6 grade showed superficial degradation only (which was attributed to diffusion-limited oxidation) but maintained the majority of their storage capacity after the applied thermal loads. The POM-C, however, proved not to be stable and degraded to low-molecular organic substances which was ascribed to multiple chain cleavage. Nonetheless, by the use of HDPE and PA 6 as PCM an application temperature range from approximately 100 °C to 250 °C can be covered. The exposure parameters were then further refined (higher exposure temperature and bulkier specimen dimensions) to better imitate the thermal loads during the application for long-term stability testing. For this purpose, a selected HDPE grade (as the most promising polymeric PCM) was exposed in air in the melt state for up to 10 months along with several additionally stabilized variations of this polymer (hindered amine stabilizers were applied). During the exposure, different aging phenomena occurred which pointed out the challenges that come along with the application of polymers in the melt state. A constant melt movement coming from natural convection within the specimens was detected due to the combination of the melt movability and minor temperature gradients in the ovens. The degradation eventually caused an immobilization of the specimen surface. The immobilized surface acted as oxygen scavenger (atmospheric oxygen only diffused through the specimen surface into the specimen) and impeded oxygen diffusion into the rest of the specimen as soon as thermo-oxidation sealed the surface. Oxidation penetration depth (OPD) measurements revealed that an additional stabilization which delayed the immobilization of the specimen surface as compared to the non-additionally stabilized HDPE, increased the amount of superficial degradation of the specimen. Thus, the additional stabilization was found to be obsolete which is beneficial for the material price. Nevertheless, merely minor losses in the storage capacity of all exposed specimens had occurred as no thermo-oxidative degradation was detected in those specimen parts which were out of the reach of oxygen diffusion. After proving the applicability of semi-crystalline polymers as PCM, the second part of the dissertation deals with the functionalization of the polymeric PCM to enhance their TC via the incorporation of highly conductive particles. Incorporated filler particles typically lower the storage capacity of polymeric PCM compounds (compared to the neat polymers) as they do not

undergo a phase transition during the PCM's application temperature range. Therefore, the most efficient fillers for the enhancement of TC needed to be found via a sound filler screening. Nine filler types with varying shapes and sizes were incorporated into an HDPE matrix at different filler loadings and the compounds' TC was determined. As measuring the TC of polymeric materials is still a highly complex field of testing, parts of the investigations focused on the exact determination of this material property. For this purpose, a sound analysis of technology- and material-induced impacts on the TC of polymeric compounds was elaborated. The thereby gained knowledge was applied for the filler screening and aluminum, copper and expanded graphite particles were selected due to their ability to increase the TC of HDPE efficiently even at low filler loadings. However, the TC of the compounds containing expanded graphite exceeded by far the TC of the compounds containing aluminum and copper. Furthermore, the expanded graphite did not reduce the short-term thermo-oxidative stability of the HDPE as opposed to the other filler types. Therefore, these compounds were optimized for the application as PCM in terms of expanded graphite type, filler loading and processing conditions. Varying the filler loading pointed out the filler's impact on the compounds' properties as its flowability was steadily reduced up to reaching dimensional stability in the melt state at a certain filler loading. Thus, further possible impacts on application-relevant properties needed to be examined via an additional characterization. For this purpose, compounds containing expanded graphite and aluminum were exposed under identical conditions as it was done for the long-term stability investigations of the neat HDPE. The filler particles affected the melting and crystallization behavior only little whereas the viscosity of the compounds was increased over the neat HDPE. However, this contributed to maintain a sufficiently homogeneous filler distribution in the melt state during the applied thermal loads. Moreover, the incorporated particles increased the thermo-oxidative stability of the compounds over the neat HDPE (comparably smaller OPD). The hereby conducted investigations therefore demonstrate the applicability of neat and functionalized polymers as novel, cost-efficient PCM. Their outstanding stability upon high thermal loads in air in the melted state is revealed for the first time. The neat polymeric PCM can be successfully functionalized to achieve an improved applicability as PCM and a better well-functioning of the LHS. Furthermore, the comprehension of measuring the TC of polymeric materials is significantly expanded.

Kurzfassung

Die vorliegende Dissertation befasst sich mit der Entwicklung von polymeren Phasenwechselmaterialen (PCM für „phase-change materials") für Wärmespeicher. Diese werden als Speichermaterial in Latentwärmespeichern (LHS für „latent heat storage") eingesetzt da sie während ihres Phasenübergangs große Mengen an thermischer Energie zusätzlich zur sensiblen Wärme speichern und wieder freigeben können wofür großteils der Schmelz- und Kristallisationsvorgang genutzt wird. PCM werden gegenüber sensiblen Speichermedien bevorzugt, da sie höhere Speicherdichten aufweisen. Es existiert bereits eine Vielzahl an PCM für unterschiedliche Temperaturbereiche. Derzeit üblicherweise eingesetzte PCM weisen vereinzelt Komplikationen in der Anwendung auf wie z.B. inkongruentes Schmelzen, Unterkühlen statt Kristallisieren (was notwendig ist um die gespeicherte Wärme wieder abzugeben), Korrosion der Konstruktionsmaterialen und niedrige Wärmeleitfähigkeiten die langsame Lade- und Entladevorgänge zur Folge haben. Obwohl Kunststoffe eine große Bandbreite an Schmelzpunkten aufweisen, wurden sie bis dato nur vereinzelt als PCM erprobt und eingesetzt. Sie besitzen jedoch viele der gewünschten Eigenschaften von PCM wie Kosteneffizienz, Handelsverfügbarkeit und die Möglichkeit der Eigenschaftsanpassung durch Compoundierung mit diversen Füllstoffen und Additiven. Die erste Hälfte der Dissertation befasst sich deshalb mit einem umfangreichen Screening von teilkristallinen Kunststoffen hinsichtlich ihrer Eignung als PCM, wobei der Fokus dabei auf Standardkunststoffe und technische Kunststoffe gelegt wurde. Deren anwendungsrelevante thermophysikalische Eigenschaften wie die Schmelzenthalpie (entspricht der Speicherkapazität) und das Schmelz- und Kristallisationsverhalten (spiegelt den Lade- und Entlademechanismus wider) wurden für diesen Zweck detailliert untersucht. Die folgenden Polymergruppen wurden dabei als potentielle PCM identifiziert: Polyethylen (PE), Polypropylen (PP), Polyoxymethylen (POM), Polyamide (PA) sowie deren Rezyklate. Da Kunststoffe bis jetzt jedoch noch nicht großflächig als

PCM untersucht wurden, sind keine Daten über deren Langzeitverhalten als PCM vorhanden. Teilkristalline Kunststoffe in der Verwendung als PCM werden hoher thermischer Belastung ausgesetzt, da sie in ihrem geschmolzenen Zustand ihre kristalline Struktur verlieren, welche die Luftsauerstoffdiffusion in das Material und somit die Initiierung eines thermo-oxidativen Abbau hemmt. Der thermo-oxidative Abbau verändert die Morphologie des Kunststoffs, was sich wiederum auf die thermophysikalischen Eigenschaften des Materials auswirken kann. Um die anwendungsrelevante Langzeitstabilität von Kunststoffen als PCM zu untersuchen, wurde eine High-Density Polyethylen (HDPE)-Type, ein POM-Copolymer (POM-C) und eine PA 6-Type im geschmolzenem Zustand in Luft für 15 Tage in anwendungsnahen Bedingungen ausgelagert. Dabei wurde nur ein oberflächlicher thermo-oxidativer Abbau der ausgelagerten HDPE- und PA 6-Prüfkörper festgestellt, was auf diffusionslimitierte Oxidation zurückgeführt wurde. Somit wurde der Großteil der Speicherkapazität der ausgelagerten Prüfkörper erhalten. Das ausgelagerte POM-C hielt den Auslagerungsbedingungen jedoch nicht Stand und wurde durch mehrfache Kettenspaltung zu niedermolekularen Substanzen abgebaut. Nichtsdestotrotz wird mit den durch die Selektion ausgewählten polymeren PCM (HDPE und PA 6) ein Speichertemperaturbereich von ca. 100 °C bis 250 °C abgedeckt. Die Auslagerungsparameter wurden im Anschluss für Langzeituntersuchungen weiter an die tatsächliche Anwendung in einem Wärmespeicher angepasst (erhöhte Auslagerungstemperatur und größere Prüfkörperdimensionen). Dafür wurde eine ausgewählte HDPE-Type und mehrere zusätzlich gegen thermo-oxidativen Abbau stabilisierte (mittels „hindered amine stabilizer") HDPE-Typen in Luft für 10 Monate im geschmolzenen Zustand ausgelagert. Während der Auslagerung traten unterschiedliche Alterungserscheinungen auf, welche die Herausforderungen bei der Verwendung von Kunststoffen im geschmolzenen Zustand veranschaulichten. Die Kombination aus Schmelzbeweglichkeit und geringer Temperaturgradienten während der Auslagerung führten zu kontinuierlichen Umwälzungen der Schmelze. Mit fortgeschrittener Alterung verlor die Oberfläche der Prüfkörper jedoch ihre Beweglichkeit. Diese versiegelte Prüfkörperoberfläche diente als Fänger des Luftsauerstoffs und verhinderte eine weitere Sauerstoffdiffusion in das Prüfkörperinnere. Messungen zur Bestimmung der Oxidationseindringtiefe (OPD für „oxidation penetration depth") zeigten einen größeren Anteil an oberflächlich abgebauten Material der zusätzlich stabilisierten HDPE-Typen aufgrund einer verzögerten Versiegelung der Prüfkörperoberfläche gegenüber der nicht zusätzlich stabilisierten Type. Eine zusätzliche Stabilisierung gegen thermo-oxidativen

Abbau wirkte sich somit kontraproduktiv auf den Erhalt der Speicherkapazität aus und wurde als obsolet für die Anwendung als PCM eingestuft. Dies wirkt sich auch vorteilhaft auf den Materialpreis aus. Nichtsdestotrotz wurde die Speicherkapazität aller ausgelagerten Prüfkörper der unterschiedlich stabilisierten HDPE-Typen nur minimal reduziert, da außerhalb des Prüfkörperbereichs, in den der Luftsauerstoff diffundieren konnte, kein thermo-oxidativer Abbau festgestellt wurde. Nach dem Nachweis der prinzipiellen Eignung von teilkristallinen Kunststoffen als PCM, befasst sich der zweite Teil der Dissertation mit der Funktionalisierung der Werkstoffe zur Verbesserung der Wärmeleitfähigkeit durch die Beimengung von hochleitfähigen Partikeln. Da diese Partikel im Anwendungsbereich von polymeren PCM jedoch keinen Phasenübergang aufweisen, reduzieren sie die Speicherdichte des polymeren Materials im Allgemeinen. Deshalb wurden zunächst jene Füllstofftypen eruiert, welche die Wärmeleitfähigkeit des polymeren PCM möglichst effizient steigern. Neun Füllstofftypen mit unterschiedlichen Partikelgrößen und -formen wurden zu verschiedenen Füllgraden in HDPE eingearbeitet und die Wärmeleitfähigkeit dieser Compounds ermittelt. Da die exakte Messung der Wärmeleitfähigkeit von Kunststoffen nach wie vor ein sehr komplexes Thema ist, widmete sich ein Teil der Arbeit der akkuraten Messung eben dieser Materialeigenschaft. Dabei wurde eine umfangreiche Darstellung werkstofflicher und messtechnischer Einflussfaktoren auf die Wärmeleitfähigkeit erarbeitet. Durch die dabei gewonnenen Erkenntnisse wurden Aluminium-, Kupfer- und expandierte Graphitpartikel aufgrund ihres Vermögens die Wärmeleitfähigkeit von HDPE bereits bei niedrigem Füllstoffgehalt effizient zu steigern, ausgewählt. Aus diesen drei Füllstofftypen, erhöhte der expandierte Graphit die Wärmeleitfähigkeit des HDPE jedoch am effizientesten und zeigte den geringsten Einfluss auf die Kurzzeitbeständigkeit des Compounds, weswegen diese Compounds in weiterer Folge in puncto Type, Partikelgröße und Herstellungsparameter für die Anwendung als PCM optimiert wurden. Während der Optimierung kam der Einfluss der Füllstoffe auf die Fließfähigkeit des HDPE zum Vorschein, welche mit steigendem Füllgrad signifikant bis hin zur Formstabilität im geschmolzenen Zustand abnahm. Um nun weitere Einflüsse auf anwendungsrelevante Eigenschaften zu untersuchen, wurde die Langzeitstabilität von HDPE-Compounds gefüllt mit expandiertem Graphit und Aluminium geprüft (parallel zu den Untersuchungen des reinen HDPEs). Während die Füllstoffpartikel das Schmelz- und Kristallisationsverhalten nur minimal beeinflussten, erhöhte ihre Beimengung die Viskosität des Materials wesentlich. Dies trug schlussendlich aber auch dazu bei, dass eine homogene Füllstoffverteilung

während der Auslagerung im geschmolzenen Zustand großteils erhalten blieb, da sich durch die erhöhte innere Reibung zwischen den Partikel und den Partikeln und der Polymerketten eine Form der Fixierung ergeben hatte. Zusätzlich erhöhten die Partikel die thermo-oxidative Stabilität des Materials (geringere OPD im Vergleich zum ungefüllten HDPE). Dies wurde auf die Barrierewirkung der beigemengten Partikel gegenüber der Sauerstoffdiffusion in das Prüfkörperinnere zurückgeführt. Die für diese Dissertation durchgeführten Untersuchungen demonstrieren somit die Eignung von Kunststoffen sowohl in der Form von Reinpolymeren als auch als Compounds mit erhöhter Wärmeleitfähigkeit als neuartige, kosteneffiziente PCM. Es wird ihre herausragende Stabilität unter der hohen thermischen Belastung in Luft im geschmolzenen Zustand erstmalig enthüllt. Die Reinpolymere können hingehend ihrer Anwendbarkeit effizient funktionalisiert werden um ihre Einsatzfähigkeit in Wärmespeichern weiter zu erhöhen. Darüber hinaus leistet die Arbeit durch umfassende morphologische Analysen einen signifikanten Beitrag zum vertieften Verständnis der Wärmeleitfähigkeitsermittlung für Kunststoffe.

Contents

Part II.

Introduction and motivation of the thesis

1.   Motivation and theoretical background

"Energy will do anything that can be done in the world." – Johann Wolfgang von Goethe

1.1.   Fossil-fueled civilization and its environmental impact

Our civilization is depleting finite fossil fuel deposits that cannot be restocked in a time span longer than the existence of humans [1]. In 2015, fossil fuels accounted for 86 % of the world's primary energy. This is only 4 % less than in 1990 even though alternatives for energy generation such as nuclear fission, wind- and photovoltaic systems for the generation of electricity, geothermal power plants, hydropower plants and new ways of converting phytomass to fuels exist [1]. Part of the reason for fossil fuel's dominance in the world wide energy share is its facile transportation of stored energy in the form of coal, crude oil or natural gas. Its ubiquitous availability as energy resource resulted in major advances in agricultural productivity, rapid industrialization and urbanization, in the expansion and acceleration of transportation and worldwide effortless accessibility of information [1]. This revolutionized the structure of modern societies as it increased the average food availability far above subsistence needs and assured the provision of health care which are both regarded as the key factors behind the steady increase in average life expectancy [2]. Furthermore, it provided occupational and intellectual opportunities and turned international trade into a mass-scale global affair [2]. This is further demonstrated by the relationship between the Human Development Index (HDI) which takes into account life expectancy, education and per capita income and the energy use per capita in Figure 1.1. A higher HDI indicates a higher human development.

Thus, it is clear that energy supply contributes to a country's wealth as it is a key factor for economic prosperity and technological competitiveness [5]. Nevertheless, the fossil fuel's extensive use has also been a key factor behind income inequality, it enabled the construction of modern high-energy weapons which created the possibility of destroying an entire civilization and contributed to severe environmental degradation [1].
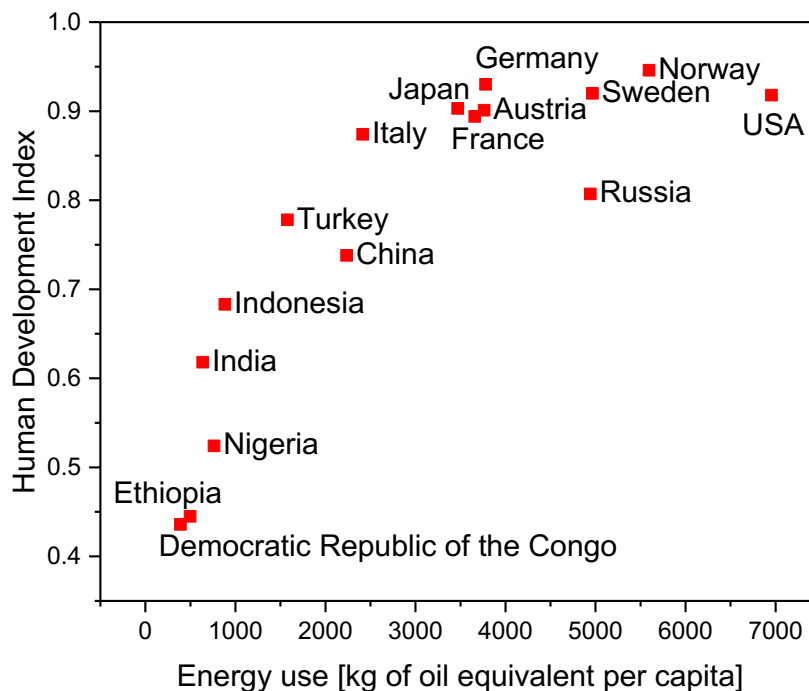
Figure 1.1: Relationship between the human development index of 2014 [3] and the energy use per capita 2014 for selected countries [4]. The higher the energy use per capita, the higher the Human Development Index.

The environmental degradation associated with energy is taking place at a global level and the most striking changes comprise [1,2]:

- increasing water pollution caused by accidental oil spills and acid mine drainage
- partial destruction of the ozone layer by the release of chlorofluorocarbons
- loss of global bio diversity
- pollution of the atmosphere by greenhouse gas emissions

The main greenhouse gas is CO_2 and it is the end-product of the combustion of fossil and biomass fuels. Fossil fuels account for 60 % of the increasing anthropogenic generation of CO_2 whereas land use changes account for 10 % and methane emissions mainly from livestock for approximately 20 % [1]. The increasing generation of greenhouse gases has resulted in the increasing concentration of greenhouse gases in the atmosphere. The greenhouse effect per se is natural and necessary for the philanthropic average global temperature of approximately +15 °C. Without the greenhouse effect, the global average temperature would be -18 °C [6].

4

However, the increased greenhouse effect caused by humans is affecting our climate. It has raised the average global temperature by 0.65 °C to 1.06 °C between 1880 and 2012 and another rise between 1.8 - 4°C is expected by 2100 [2]. The climate of our world has been changing for millions of years as there have been several ice ages and interglacial periods before. A simple energy balance determines the world's climate: the thermal energy which is emitted from the world into space needs to equalize the absorbed solar radiation [6]. Climate changes are the result of a disequilibrium of the world's energy balance which can be caused by three possibilities: the solar radiation varies due to changes of the world's orbit around the sun or changes of the sun, the reflected part of solar radiation changes due to changes in the world's surface (e.g. moving of continents, ice surface coverage) or the outgoing thermal radiation changes due to absorbing gases and aerosols in the atmosphere (i.e. a change in the greenhouse effect) [6]. Our current geological epoch the Holocene is an interglacial period that started about 10000 years. Without small exceptions, the Holocene has shown a rather stable average global temperature. However, during the last century the average global temperature has risen to a high which the world has only seen in the interglacial period Eem before the last ice age about 120000 years ago [6]. Indicators of the ongoing climate change include inter alia the shrinkage of glaciers, the melting of the icecap and permafrost, change in the marine currents, rise of the sea level, weather extremes such as tropic thunderstorms and impacts on the ecosystems [6]. The latter implies changes in the agriculture as temperature and precipitation change. Whereas in rather cold regions which are mainly in industrialized countries such as Canada, the agricultural conditions will be improved and agriculture can be adjusted by the choice of crops [6]. However, the agricultural condition of subtropical regions where mostly poor countries are present will be most likely deteriorated due to excessive heat and water scarcity [6]. Thus, the fight against the ongoing climate change represents an ethical issue in the end.

1.2.   Europe 2020 and thermal energy storages

"Over 70% of global energy investments will be government-driven and as such the message is clear – the world's energy destiny lies with decisions and policies made by governments." – Dr. Fatih Birol, Executive Director of the International Energy Agency

In 2010 the European Commission defined the Europe 2020 strategy for "smart, sustainable and inclusive growth" for the upcoming decade as a reaction to the economic crisis in 2009 [7]. The strategy was divided into five

target areas: employment, research and development, climate change and energy, education and poverty and social exclusion. The climate change and energy includes the following goals [7]:

- reducing greenhouse gas emissions by at least 20 % compared with 1990 levels
- increasing the share of renewable energy in final energy consumption to 20 %
- moving towards a 20 % increase in energy efficiency

The strategy strives to turn the EU into a low-carbon economy (refers to the main greenhouse gas CO_2 which accounts for 81 % of the EU's total greenhouse gas emissions in 2016 [8]). A low-carbon economy is based on renewable energy sources and energy efficiency and should not only mitigate climate change, climate and energy policies but should also help to reduce health risks by lowering air pollution and reduce energy dependence [9].

According to the latest edition of Eurostat's "Smarter, greener, more inclusive?" which monitors the progress of the Europe 2020 strategy by different indicators, the countries of the European Union are on track to achieving the goal for greenhouse gas emissions. They were already lowered by 22.4 % in 2016 compared with 1990 levels [9]. The reduction in greenhouse gas emissions is partly due to the increased share of renewable energy which made up 17.0 % of the gross final energy consumption in 2016. For improving energy efficiency further to the targeted increase of 20 %, however, the EU needs to reduce its primary energy consumption by 3.9% down to 1483 Mtoe (million tonnes of oil equivalent) [9]. For this purpose, energy storage systems can be applied as they contribute not only to reduced energy costs but also to a reduced energy consumption by closing the gap between energy demand and supply [5]. The energy storage systems which are available nowadays can be divided into the following categories (reproduced from [5]):

- mechanical energy storages
- chemical energy storages
- biological storages
- magnetic storages
- thermal energy storages

Out of these energy storage methods, only mechanical, chemical and thermal energy storages have emerged and will be discussed in further detail. A widely applied type of mechanical energy storages are

6

hydrostorages, where water is pumped upward from a river to a reservoir when energy demand is low. When energy demand increases, the filled reservoir releases water which turns a turbine to generate electricity. A pumped water plant only takes 30 s to reach its maximum power [5]. A hydrostorage's applicability, however, is geographically limited. Reservoirs are also used for compressed-air storages (mechanical energy storage), where compressed air is stored underground in natural caverns, old oil or gas wells or porous rock formations during off-peak hours [5]. When energy is required, the air is released and drives a gas turbine generator. Furthermore, the heat generated during air compression can be stored and used to preheat the expanding air in the turbine. The most-known chemical energy storage is the electrochemical battery where energy is stored chemically and released as electric energy on demand. Examples are the lead-acid, nickel-zinc or lithium-iron sulfide batteries. They can be used for electric utility load management, electric vehicles and storage for renewable energy systems such as wind or photovoltaic systems [5].

The last category of the emerged energy storage systems are thermal energy storages. Thermal energy is crucial for many aspects in our daily routine such as cooking food or even to survive as the human body requires a minimum ambient temperature. Thus, there is and will always be strong demand for thermal energy. It comes from different sources such as the sun via solar radiation due to nuclear fission at the sun's core, the planet's core in the form of geothermal energy, fossil-fuel power plants, nuclear power plants, excess heat generated by manufacturing plants often referred to as industrial waste heat and by burning phytomass [10]. However, a gap between the demand and supply is due to the time difference between generation and consumption, the difference in the cost between peak and off-peak hours of the day and the distance between the thermal energy source and place of consumption [10]. In spite of that, heating and cooling in buildings and industry causes half of the energy consumption in the European Union [11,12]. In households, roughly 80 % of the energy is used for heating or hot water which equals 192.5 Mtoe. In industry, about 71 % of the energy (193.6 Mtoe) is consumed due to space and industrial process heating. This indicates a large potential for increasing energy efficiency via increasing thermal energy efficiency as thermal energy storages can be integrated into energy systems of both, renewable energy sources such as solar, wind, geothermal and non-renewable resources such as industrial waste heat recovery [13]. Thermal energy storages typically store high- or low-temperature thermal energy for later use and can be seen as a link and a buffer between heat source and heat user [5]. Summer heat can be used for

winter heating, winter ice for cooling in the summer or solar energy is used for overnight heating [5]. They are designed to operate on a cyclical basis (diurnally, occasionally or seasonally) [5]. The scheme of the basic principle of thermal energy storages is given in Figure 1.2. It comprises three processes being charging, storing and discharging which may occur simultaneously. The thermal energy is stored within the storage media.
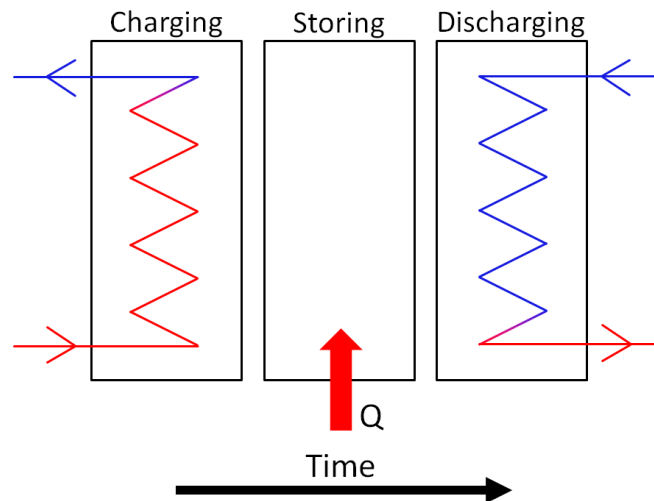
Figure 1.2: Basic principle of a thermal energy storage. It comprises three steps: charging, storing and discharging which may occur simultaneously. Adapted from [5].

Thermal energy storages are mainly associated with heating and cooling. For buildings, thermal energy storage systems can be categorized into active and passive systems [14,15]. Active thermal energy storages are usually applied for off-peak storage (the off-peak times refer to the time during each day where less energy is consumed which is mainly during the night hours) [15]. The off-peak rates for electricity are typically 33-75 % lower than peak rates [5]. An example is the storage of heat produced by off-peak electricity which helps to reduce the heating costs. Electrical resistance heaters with an efficiency of nearly 100 % produce heat. For this purpose, electric heat grids need to be placed 0.5 m to 2 m in the ground beneath the relevant construction (e.g. house, building) [5]. Either earth materials or ceramic bricks in insulated containers are typically used as storage media. When thermal energy is needed for room heating, the stored energy is transferred via a heat transfer fluid to the rooms to be heated. Besides that, thermal energy storages are also often combined with solar energy as heat coming from solar radiation is only available during the day. An example for such an active thermal energy storage for buildings is a so-called rock-bed (Figure 1.3). To store the heat from during the day, the heat is collected in air which

is moved by a blower towards a rock-bed. This is the actual storage and the rock functions as the storage material. In the rock-bed, the air is cooled as it transfers its contained heat to the storage media and the cooled air is transported to the solar collector again. The scheme of the complete cycle is given in Figure 1.3. The stored energy in the rock-bed can then be transferred to houses for heating following the same principle as the storage of heat from off-peak electricity.
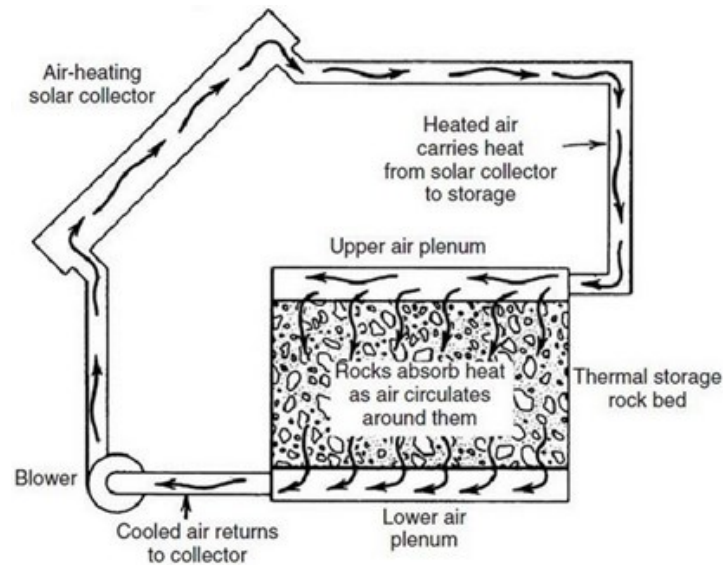
Figure 1.3: Principle of a solar rock-bed [16].

Passive thermal energy storages for buildings comprise technologies or design features for heating and cooling where mechanical devices are not necessary [18]. For this purpose, panels or walls with different storage media are integrated into the interior. Above a temperature threshold, the storage media absorbs the excessive heat and releases it when a lower threshold is reached. It thereby helps to keep the room temperature at the comfort level with less energy consumption [14].

Apart from buildings, thermal energy storages can also be integrated into power plants such as concentrated solar power plants or nuclear power plants. For both plants, heat is generated to heat up water for running a turbine to generate electricity. However, not all of the generated heat is necessary to boil the water and the excess heat can be withdrawn and stored in e.g. concrete as storage media as seen in Figure 1.4. From the thermal energy storage, the heat can then be transferred and used for the preheating of different devices.
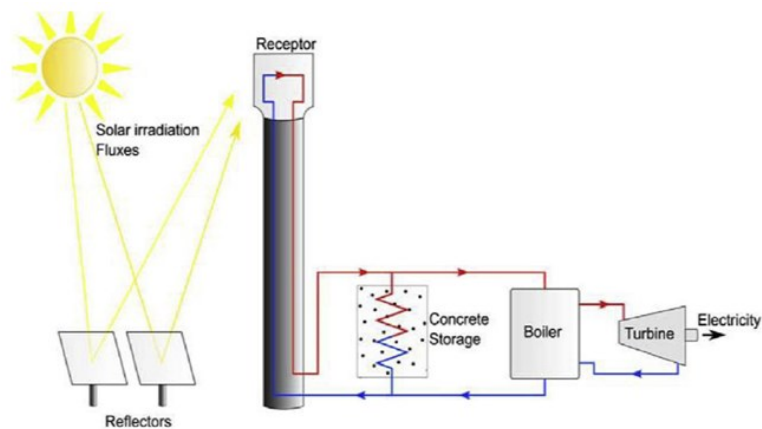
Figure 1.4: Thermal energy system integrated in a concentrated solar power plant [17].

Thermal energy storages can also be used at a much smaller scale in thermal comfort textiles also known as "smart textiles" [15]. For that purpose, the storage media is incorporated into the textile either directly into the fiber of the textile, via coating or via lamination [10,15]. The heat is absorbed by the textile if the body temperature reaches a threshold and releases it when it gets to cold similar to the principle of passive thermal energy storages for buildings as described above. Smart textiles are therefore considered as thermoregulating [19]. They were first developed by the NASA for astronauts to reduce the impact of extreme temperature variations during space missions [20]. Nowadays, they are used for blankets, outdoor clothing, mattresses, pillow wear and duvets [19].

Manifold other fields of application for thermal energy story systems can be found in the automotive industry, in space applications, in biomedical applications, in electronics and in the food industry [15].

Depending on the charging and discharging mechanism of the storage material, thermal energy storages are classified as either chemical or physical thermal energy storages. Chemical thermal energy storages can be further categorized as sorption storage and thermochemical energy storage [21,22]. For both, thermal energy is stored and released via the breaking and forming of chemical bonds. However, chemical thermal energy storages are still in the research phase [23] and will not be discussed here in further detail. In physical thermal energy storages, the storage mechanism depends upon the thermo-physical properties of the utilized storage media. This helps to divide physical thermal energy storages into sensible heat storages and latent heat storages [5,10,23]. For sensible heat storages, the stored energy increases steadily with increasing temperature and depends upon the mass,

specific heat capacity of the storage media and the temperature difference between the initial and final state. Typically applied solid storage media are either earth materials (concrete, rock, gravel, brick, marble, granite, sandstone, graphite etc.) or metals (copper, aluminum, cast iron, pure iron and different alloys) [10,24,25]. Materials with high thermal conductivity such as metal or graphite are applied for applications where fast charging and discharging is required whereas stone, rock and gravel exhibit low thermal diffusivity and result in slow charging and discharging [23]. Molten salts, water and thermal oils are applied as liquid storage media. Out of these materials, water with an outstandingly high specific heat capacity of approximately 4 J/(gK), low cost and non-toxicity is the most promising one for temperatures below 100 °C [5,26]. Molten salts are implemented for high-temperature applications. However, their tendency for corrosion requires specific construction of the energy storage [27]. Via liquid storage media thermal energy can more easily be transported than via solid storage media and they exhibit good-heat transfer rates [5]. Solid storage media, however, exhibit higher specific heat capacities than solid storage media [5].

For latent heat storages, the stored energy increases also steadily with increasing temperature until the storage media undergoes a phase transition (e.g. melting) and stores additionally the latent heat required for the phase transition. Storage media used for latent heat storages are therefore called phase-change materials (PCM). During their phase-transition, the temperature of the PCM stays constant and only increases further after the phase change of the storage medium is completed. Hence, the storage capacity of latent heat storages depends upon the mass, the specific heat capacity of the PCM and upon the latent heat which is necessary to undergo the phase transition. High latent heat and high specific heat capacity therefore result in high storage capacities. PCM and their applications will be discussed in more detail in 1.3.

The major advantage of sensible heat storages over latent heat storages is their market maturity as they are commercially available and show service life of up to 20 years [23]. They cover a temperature range from approximately 50 °C to 450 °C. However, latent heat storages cover a broader temperature range from several degrees above 0 °C up to 1000 °C [23] and offer an up to 10 times higher energy density. This results in a reduction of the storage dimensions and further in the costs of the storage. The choice between a sensible and a latent heat storage depends upon economic viability, on the storage period required (diurnal or seasonal) and most important on the temperature at which the thermal energy should be stored [5].

1.3. Phase-change materials

PCM must possess several properties to be suitable for the application in latent heat storages. They are illustrated in Figure 1.5 and ranked according to their priority (categorization starts with "show stoppers" (most fundamental requirements), continues with "game changers", "enablers" and ends with "differentiators" as the high level selection criteria).
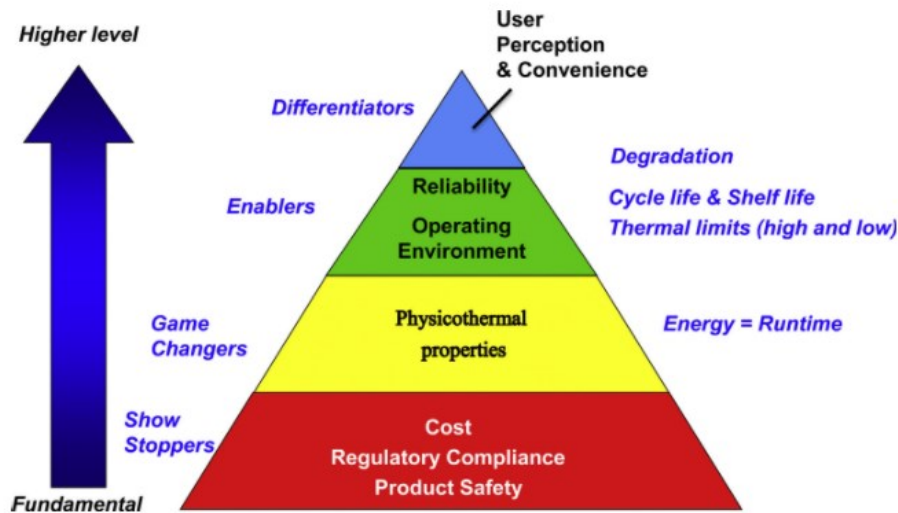
Figure 1.5: Selection criteria for phase-change materials. Taken from [23].

As mentioned in the preceding section, PCM undergo a phase-transition during their energy storing and releasing process. The solid-liquid phase transition is mainly used as it shows the smallest change in volume of up to ~10 % [15]. PCM of which the liquid-gas or solid-gas phase transition is used are not practical because of large volumetric changes and an increase in pressure that both occur during the phase transition [23]. For solid-solid PCM the heat required from changing from one crystalline form into another is taken advantage of. Their crosslinked material character helps them to remain solid even after undergoing the phase transition and leakage cannot occur in the charged state. However, their heat required to undergo the phase transition is relatively small compared to the heat of fusion of solid-liquid PCM [23].

The simplest way to use solid-liquid PCM as storage media is illustrated in Figure 1.5. The PCM is contained in a tank to prevent leakage and thermal losses in the charged state. A heat transfer fluid transfers the excess thermal energy to the PCM. The pipes through which the heat transfer fluid runs are surrounded by the PCM (right part of Figure 1.6). As the heat is transferred, the PCM around the pipes starts to melt and thereby stores the thermal

energy. To release the stored energy, a comparably cooler heat transfer fluid is run through the tank and the PCM solidifies again. The tank therefore works as heat exchanger.
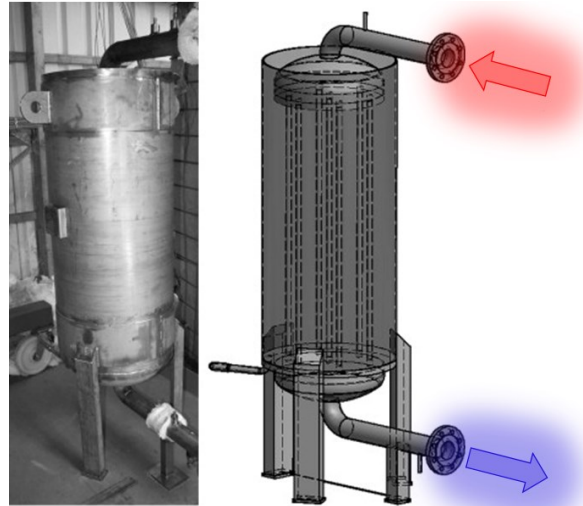
Figure 1.6: Tank for storing the PCM. A heat transfer fluid transports the heat to be stored to the PCM during charging and forcing it to melt. During the melting process, the PCM stores the energy to undergo the phase transition. Taken and partially adapted from [28].

Solid-liquid PCM can be classified according to their material class into organic, inorganic and eutectic phase-change materials. Each PCM class can then further be categorized according to its application temperature for low-temperature (phase transition occurs until 220 °C), intermediate-temperature (phase transition occurs between 220 °C to 420 °C) and high-temperature applications (phase transition occurs above 420 °C) [23,29,30]. Organic PCM (paraffins, fatty acids, esters, alcohols, glycols) show adequate phase transitions from approximately -5 °C to 160 °C. Thus, they are only available for low-temperature applications. Most organic PCM show heat of fusions between 100 kJ/kg and 340 kJ/kg and their energy densities range from approximately 150 MJ/m³ up to 500 MJ/m³ [30]. Their main advantages comprise compatibility with conventional construction materials, no segregation, high heat of fusion and recyclability. However, low thermal conductivity, low heat capacity and flammability account for their major drawbacks. Inorganic PCM (salt hydrates, salts, hydroxides, metals, metal alloys) exhibit phase transitions from approximately 30 °C to 1400 °C and can therefore cover all three types of application temperature ranges [23,29,30]. They exhibit higher heats of fusion from 70 – 1040 kJ/kg and higher energy densities from 220 MJ/m³ up to 2700 MJ/m³ [30]. In general,

they also exhibit higher thermal conductivities than organic PCM. However, compatibility issues with construction materials arise because they are highly corrosive. Furthermore, phase segregation of the salt hydrates might occur after several consecutive charging and discharging cycles due to incongruent melting. Eutectic PCM (organic, inorganic) represent the third group with melting points from approximately 10 °C to 770 °C [23,29,30]. They show heats of fusions from 70 – 790 kJ/kg and their energy densities range from 150 MJ/m³ to 960 MJ/m³ [30]. However, not sufficient data of their thermo-physical properties is available yet, they are expensive and highly corrosive and show also low thermal conductivity. An overview of each phase-change including their most relevant properties material class is presented in Table 1.1.

Table 1.1: Overview of different PCM classes including their application-relevant properties (partially taken and adapted from [23] and [30]).

Type	Class	Phase-change temperature range [°C]	Latent heat [kJ/kg]	Energy density [MJ/m³]	Cost estimation [$/kg]
Organic	Paraffins	-5 - 82	148 - 255	158 - 204	2 - 1150
	Fatty acids	16 - 69	149 - 209	146 - 197	28 - 41
	Esters	11 - 63	100 - 216	~ 250	16 - 453
	Alcohols	93 - 165	110 - 344	164 - 499	90 - 430
	Glycols	4 - 70	118 - 176	120-200	12 - 20
In-organic	Salt hydrates	30 - 117	116 - 280	226 - 550	5 - 21
	Nitrate salts	306 - 426	145 - 266	306 - 389	6 - 226
	Carbonate salts	732 - 1330	142 - 509	416 - 1074	3 - 111
	Chloride salts	192 - 802	75 - 452	218 - 1049	3 - 55
	Sulfate salts	858 - 1460	84 - 212	187 - 564	3 - 180
	Fluoride salts	850 - 1418	391 - 1044	1109 - 2756	8 - 220
	Hydroxides	318 - 462	165 - 873	306 - 1275	8 - 220
	Metals	419 - 1084	113 - 397	807 - 1864	10 - 84
	Metal alloys	340 - 946	92 - 757	375 - 2257	not commer-cially available
Eu-tectics	Organic eutectics	21 - 52	143 - 183	n. a.	
	Inorganic eutectics	13 - 767	74 - 790	155 - 959	

As stated above, the use of solid-liquid PCM as storage media in thermal energy storages faces several challenges which include inter alia issues with leakage in the charged state, interaction with the surroundings (e.g. corrosion of the container) and the low thermal conductivity which results in slow heat transfer rates [31,32]. To overcome the low thermal conductivity, several approaches have been made including the use of metallic inserts such as fins that reach into the storage media, the incorporation of highly thermally conductive particles and encapsulation (via an increased interface between PCM and heat transfer fluid) [32]. However, only encapsulation also prevents leakage and possible interaction with the surrounding. Encapsulation can be

done on either a macroscopic, microscopic or nanoscopic scale. For macroscopic encapsulation, the required volume of the PCM is contained in tubes or spheres with dimensions of several centimeters instead of one single bulky piece or blended with a non-melting supporting material to achieve dimensional stability [33]. Microencapsulation is defined as the procedure of coating individual droplets or particles with a continuous coating to fabricate capsules on a micrometer to millimeter scale [34]. Microcapsules typically possess a PCM as core and a polymer or inorganic material shell as container [31]. They appear in different shapes (e.g. oval, spherical, tubular or irregular) which mainly depend on the core material and the fabrication of the shell [31,35]. Microencapsulation can be categorized into physical (pan coating, air-suspension coating, centrifugal extrusion, vibrational nozzle, spray drying and solvent evaporation), physical-chemical (ionic gelation, coacervation and sol-gel methods) and chemical methods (interfacial polymerization, suspension polymerization and emulsion polymerization) [31]. Nanoencapsulated PCM provide higher stability than microencapsulated ones [36] and increase the heat transfer fluid's viscosity [37]. They are typically fabricated via interfacial polymerization or sol-gel methods and prove to be the most promising solution to overcome the effect of subcooling of certain phase-change materials [31].

1.4. Polymers as phase-change materials

As pointed out above, all existing PCM possess major drawbacks and the perfect PCM has not been found yet. Therefore, many PCM are still emerging and the development of new PCM is still taking place. Interestingly, polymers have been mainly neglected for the application as PCM which might be due to their susceptibility towards thermal and thermo-oxidative degradation. However, this material class offers many of the fundamental properties for PCM (Figure 1.5) such as low cost due to their commercial availability and product safety. Additionally, properties such as their thermal conductivity or thermal/thermo-oxidative stability can easily be adapted via the incorporation of additives (highly conductive particles or stabilizers, respectively) into the polymer. Furthermore, the different polymer classes cover a broad application temperature range with melting peaks from approximately 60 °C up to 330 °C [38].

Several polymeric materials such as polyalcohols [39], crosslinked polyethylene [40-43] and shape-stabilized polyethylene glycol [44-49] have been tested as polymeric solid-solid PCM to overcome the issue of leakage in the charged state. Polyalcohols show solid-state transformations in the form of changes in their crystalline morphology which are used as phase-

transition [15]. For the shape-stabilized polyethylene glycol, the polyethylene glycol was either blended with form stable polymers or chemically inserted into a polyurethane or polyhydroxybutyrate-co-hydroxyvalerate network in the form of segments [15]. Nonetheless, only the polyethylene glycol part was responsible for the heat required for the phase-change within the blends and the networks. Neat polyethylene glycol, however, has also been extensively studied as solid-liquid polymeric PCM without an additional material for structural support [50-52]. Depending on the molecular weight of the polyethylene glycol, its heat of fusion and melting point varies. It was observed that with increasing molecular weight of up to 35000, its heat of fusion and thus its storage capacity was increased which was attributed to more convenient geometrical alignment during crystallization [50]. Its melting temperature is equally strongly dependent on its molecular weight. It can therefore cover a broad application temperature range with melting peaks between 4 °C and 70 °C (Table 1.1). However, polyethylene glycol's major drawback as a polymeric PCM is its comparably higher price over other polymers. It has been applied inter alia in smart textiles [20].

Furthermore, polyethylene has been tested as solid-liquid PCM by several authors [53-57]. Its chemical structure is very similar to the widely applied organic low-temperature PCM paraffin as both consist mostly of a repeating methylene unit $-CH_2-$ in their carbon backbone. However, due to morphological differences that imply different types of branching and differences in the chain lengths, their thermo-physical properties do not coincide. Whereas paraffins exhibit melting temperatures between -5 °C and 82 °C and heats of fusion between approximately 150 kJ/kg and 250 kJ/kg (Table 1.1), the different types of polyethylene (low-density, linear low-density, high-density and ultra-high molecular weight polyethylene) show melting peaks between 100 °C and 135 °C and heats of fusion between approximately 120 kJ/kg and 240 kJ/kg [38,58]. Out of the different types of polyethylene, high-density polyethylene (HDPE) exhibits the highest heat of fusion due to its small amount of branching resulting in a higher degree of crystallinity. HDPE's typical melting temperatures and heats of fusion lay within 131 °C and 135 °C and 205 kJ/kg and 239 kJ/kg, respectively [58]. Zauner et al. [53,57] built a fin-tube latent heat storage with 170 kg of HDPE as storage media as displayed in Figure 1.7a. The fins were added to accelerate the heat transfer rate and to compensate the low thermal conductivity of the HDPE. The granule was poured on top of the fin-tubes and flowed in between them during the first charging cycles of the storage. The same authors also used HDPE in a commercial shell-and-tube heat exchanger (Figure 1.7b) and investigated its thermo-physical characteristics

via experiments and simulations [55]. The tubes were filled with the HDPE. The heat transfer fluid flowed around the tubes acted as sensible heat storage material turning the storage into a hybrid sensible-latent heat storage. Both storage types proved to be viable for different applications.
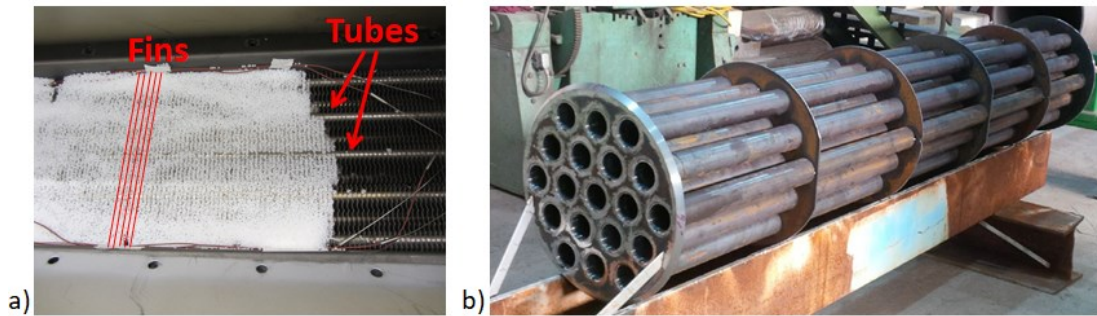
Figure 1.7: a) A fin-tube latent heat storage with 170 kg of HDPE as storage media: a) the granule is poured on top of the fines and the tubes and flows in between them during the first charging of the storage (slightly adapted from [53]); b) A shell-and-tube heat exchanger [55]. The tubes were filled with high-density polyethylene and the heat transfer fluid ran around them. Both acted as storages media turning it into a hybrid sensible-latent heat storage.

To address the HDPE's thermal stability as storage media in latent heat storages, cyclic testing up to 1000 heating and cooling cycles as imitation for the consecutive charging and discharging cycles during application was executed [57]. Only small changes in its heat of fusion were detected. This indicated its large potential as polymeric PCM. However, HDPE has not been applied in industry as its long-term cycle stability (more than 1000 cycles) and especially its thermo-oxidative stability have not been investigated in detail yet. Additionally, HDPE's inherent low thermal conductivity when applied as PCM has only been addressed via the insertion of metal fins [53] but it has not been examined profoundly yet via the incorporation of highly conductive particles into the polymeric PCM.

1.5.   Thermal conductivity enhancement of polymers

In general, a material's thermal conductivity is defined as the heat quantity in J that is conducted through a stationary body during a defined time with a temperature gradient of 1 K [59]. Just like other low-temperature PCM, polymers exhibit inherent low thermal conductivities. They are therefore categorized as insulators with thermal conductivities in the approximate range of 0.1 - 0.6 W/(mK) [60,61]. Their low thermal conductivity is due to the transport mechanism of heat which is governed by phonons since no freely moving electrons like in metals are available. Phonons can be seen as the

heat packets responsible for the heat transport and are the quantized form of thermal energy [61]. Any material can be envisioned as a set of mass and springs and each atom vibrates when subjected to heat as given in Figure 1.8a and b. This vibration generates phonons i.e. elastic waves which transfer heat from one atom to another.
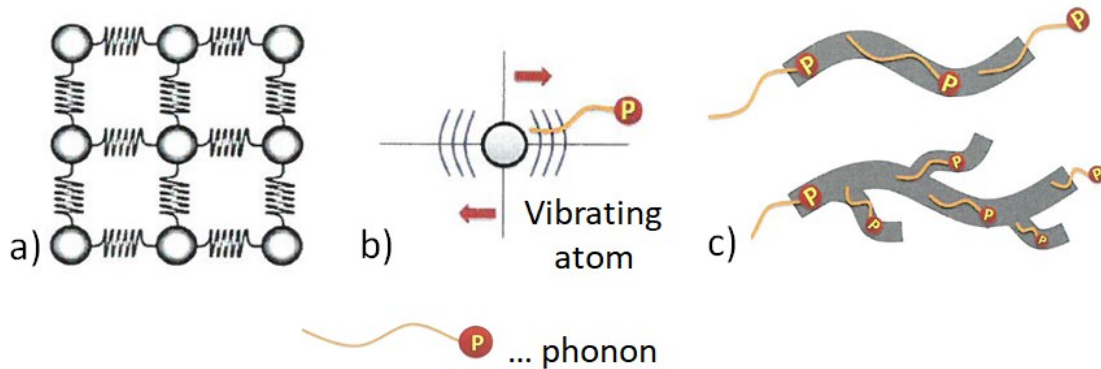
Figure 1.8:   a) Lattice of a material though as a set of mass points and springs; b) every atom which is subjected to heat vibrates and therefore phonons (elastic waves) are produced; c) phonon propagation in a linear and in a branched polymer chain. The branches results in phonon scattering and thus smaller thermal conductivity (all figures taken and/or partially adapted from [61])

However, phonons can be scattered within the material which is the main reason for the low heat conduction in non-metal materials [61]. The thermal transport by phonons is mainly controlled by the specific heat capacity, the phonon group velocity and the mean free path length [61]. The thermal conductivity λ is therefore given by the Debye theory according to equation [61] (1),

$$\lambda = \frac{1}{3} \int C_v(\omega) * v(\omega) * L(\omega) d\omega \tag{1}$$

with ω as the vibration frequency of the phonon, C_V as the heat capacity at constant volume, v as the phonon group velocity and L as the phonon mean free path length which is the characteristic length before a phonon is scattered. The heat capacity is the ability of a material to absorb heat. It is seen as the sum of kinetic energy of atomic motions and potential energy of distortion of interatomic bonds [61]. The phonon group velocity reflects the propagation velocity of a wave packet. It is large for long wavelengths and almost negligible for short wavelengths [61]. It equals the speed of sound in a crystal [62]. The mean free path length of a phonon is mainly determined by phonon scattering [63]. There are three types of phonon scattering that occur: phonon-phonon scattering, phonon-impurity scattering and phonon-

boundary scattering [64]. For phonon-phonon scattering the energy is conserved and phonons are scattered in different directions. When a phonon collides with an impurity such as point defects, dislocations, vacancy defects etc. [65], the frequency of the phonon does not change. Nonetheless, even small amounts of impurity show great impact on the material's thermal conductivity [61]. The third type of phonon scattering i.e. phonon-boundary scattering occurs when a phonon travels across boundaries of the lattice e.g. in composite materials. All these types of phonon scattering ad up to the effective mean path length of a phonon in a material which greatly affects the polymer's thermal conductivity [61].

Interestingly, ultradrawn polyethylene nanofibers with diameters from 50 nm to 500 nm can exhibit a thermal conductivity of approximately up to 104 W/(mK) [66], whereas the author discovered polyethylene's thermal conductivity to be in the range of 0.4 – 0.6 W/(mK) determined on specimens with a thickness of 4 mm [67]. The phenomenon of the large discrepancy in the thermal conductivity caused by differently sized measurement specimens is due to increased phonon scattering caused by the disordered structure and entanglements in the bulk polymer [68]. Intra-chain molecular interaction along the carbon backbone (strong covalent bonding) and inter-chain molecular interaction (weak van der Waals forces and strong hydrogen bonding) strongly affect the thermal conductivity of polymers [69]. The covalent bonds offer an efficient path for phonons, whereas the weak van der Waals bonds offer a 10 times higher thermal resistance due to increased phonon scattering [70]. Hydrogen bonding, however, helps to develop paths for phonon transport and rather increases thermal conductivity [61]. In general, a better order of the structure contributes to a higher thermal conductivity. This phenomenon is reflected by the 1D propagation of phonons in a single polymer chain compared to the 2D propagation of a phonon in a branched polymer chain as depicted in Figure 1.8c. The phonon can travel along the single polymer chain without being scattered as presented by its constant size (head and tail of the phonon). As opposed to that, the phonons are strongly scattered within the branched polymer chain which leads to a decrease in thermal conductivity as more open paths for phonon transport are available [71]. The higher morphological order of semi-crystalline polymers also results in higher thermal conductivities compared to amorphous polymers.

The inherent low thermal conductivity of polymers results in a slow heat transfer rate when applied as PCM which may further inhibit a complete melting of the PCM if the little time for charging is available. To prevent an

underuse of the thermal energy storage, a higher thermal conductivity can be achieved via encapsulation of the PCM as discussed above, via constructive ways by implementing metallic inserts into the storage media (e.g. fins in Figure 1.6a) or via the incorporation of highly conductive particles into the phase-change material [72,73]. The latter is typically done on a compounder where the filler is incorporated into the melted matrix polymer. Typically four filler types are applied for increasing the thermal conductivity of polymers: metallic fillers, carbon-based fillers, ceramic fillers and hybrid systems of the preceding three types [61,74].

Metallic fillers comprise inter alia aluminum, brass, copper, nickel, steel and zinc [61,74]. In metals, electrons are the main contributor for thermal transport leading to intrinsic thermal conductivities from 158 W/(mK) for nickel to 483 W/(mK) for copper [75]. Once metallic filler particles show efficient connection with neighboring particles, high thermal conductivities can be reached [61]. For example, the thermal conductivity of polypropylene could be enhanced from 0.5 W/(mK) to 3.6 W/(mK) by the incorporation of approximately 35 vol% of aluminum particles [76]. Additionally, the metals' ductile material character makes them available in different shapes (spheres, platelets, rods and irregular shapes). However, their high densities result in a large increase in the compound's weight over the neat polymer's when incorporated.

Ceramic fillers such as aluminum nitride, alumina, boron nitride, wollastonite, silicon carbide etc. are typically applied if electrical insulation is demanded like in electronic applications [61]. Similar to polymers, thermal energy is transported via phonons in ceramic fillers, but due to their higher crystallinity, less phonon scattering occurs. Therefore, their thermal conductivities range from 20-29 W/(mK) for alumina up to approximately 300 W/(mK) for boron nitride [75]. Certain ceramic fillers such as silicon carbide, however, exhibit very high hardness making them difficult to process due to their abrasiveness towards the compounding equipment. As opposed to that, the hexagonal form of boron nitride is a comparably soft ceramic filler and is therefore widely applied. The thermal conductivity of polyethylene can be increased from 0.26 W/(mK) to approximately 1.02 W/(mK) by the incorporation of 35 vol% of boron nitride [77].

Carbon fillers include inter alia natural and expanded graphite, graphene, carbon fibers, carbon nanotubes, diamond and carbon black [61]. Even though all carbon fillers mainly comprise only carbon, they greatly differ in their morphology and hence in their intrinsic thermal conductivities. Natural graphite is built of multiple hexagonal carbon sheets. Expanded graphite is

produced from natural graphite by intercalating these individual carbon sheets and fanning them out via an exothermic shock of the intercalating substances [78]. Graphene refers to the individual sheets of graphite and can be produced from expanded graphite by an additional intercalation step [78]. By the separation of the individual graphite sheets, the thermal conductivity of graphite can be enhanced from approximately 100-140 W/(mK) to a thermal conductivity for graphene of 800 W/(mK) or higher [75]. Similar to polymers, strong covalent bonds between the carbon atoms and weak van der Waals bonds holding the individual sheets together are present in the material. By reducing the van der Waals bonds also the thermal resistance in the material is reduced leading to a higher intrinsic thermal conductivity of graphene over graphite [79]. Nonetheless, the fabrication of graphene is still very expensive and not economically viable yet. Yang et al. [54] increased the thermal conductivity of recycled polyethylene from 0.51 W/(mK) to 1.31 W/(mK) by incorporating 20 wt% of graphite.

Synergistic effects can be achieved by combining the three filler types. For that purpose, the packing fraction is maximized by combining differently shaped fillers and producing conductive pathways thereby [77,80]. However, the fillers do not only come in varying shapes, but also sizes and size distributions and different surface treatments which all affect the final thermal conductivity of the compound [81-83]. Also the processing type and specimen preparation may affect the thermal conductivity of the final compound [84,85]. For comparison reasons, Zhao and co-workers [86] accumulated results of the thermal conductivity enhancement of polymers via the incorporation of carbon fillers. Interestingly, the authors indicated not only the materials (polymeric matrix and carbon filler type) but also the applied measurement method which raised awareness to a possible impact of the testing procedure. This issue was addressed in more detail in publication 3 in Part 5 of the thesis.

1.6. References

[1]   V. Smil, Energy and Civilization: A History, MIT Press, Cumberland, 2017.

[2]   V. Smil, Energy: A beginner's guide, 2nd ed., Oneworld, London, 2017.

[3]   United Nations Development Programme, Human Development Reports. http://hdr.undp.org/en/indicators/137506 (accessed 30 January 2019).

[4]   The World Bank Group, Energy use (kg of oil equivalent per capita). https://data.worldbank.org/indicator/EG.USE.PCAP.KG.OE (accessed 30 January 2019).

[5]   İ. Dinçer, M.A. Rosen, Thermal energy storage: Systems and applications, 2nd ed., Wiley, Hoboken, N.J, 2011.

[6]   S. Rahmstorf, H.-J. Schellnhuber, Der Klimawandel: Diagnose, Prognose, Therapie, 8th ed., C.H.Beck, München, 2018.

[7]   European Commision, Europe 2020 strategy. https://ec.europa.eu/info/business-economy-euro/economic-and-fiscal-policy-coordination/eu-economic-governance-monitoring-prevention-correction/european-semester/framework/europe-2020-strategy_en (accessed 17 January 2019).

[8]   European Environment Agency, Annual European Union greenhouse gas inventory 1990–2016 and inventory report 2018. https://www.eea.europa.eu/publications/european-union-greenhouse-gas-inventory-2018 (accessed 17 January 2019).

[9]   Smarter, greener, more inclusive?: Indicators to support the Europe 2020 strategy 2018 edition, 2018th ed., Publications Office of the European Union, Luxembourg, 2018.

[10]   G. Alva, Y. Lin, G. Fang, An overview of thermal energy storage systems, Energy 144 (2018) 341–378.

[11]   European Commision, Heating & Cooling. https://ec.europa.eu/energy/en/topics/energy-efficiency/heating-and-cooling (accessed 17 January 2019).

[12]   European Commision, Commision launches plans to curb energy use in heating and cooling.

https://ec.europa.eu/energy/en/news/commission-launches-plans-curb-energy-use-heating-and-cooling (accessed 17 January 2019).

[13] A. Gil, M. Medrano, I. Martorell, A. Lázaro, P. Dolado, B. Zalba, L.F. Cabeza, State of the art on high temperature thermal energy storage for power generation. Part 1—Concepts, materials and modellization, Renewable and Sustainable Energy Reviews 14 (1) (2010) 31–55.

[14] J. Heier, C. Bales, V. Martin, Combining thermal energy storage with buildings – a review, Renewable and Sustainable Energy Reviews 42 (2015) 1305–1325.

[15] K. Pielichowska, K. Pielichowski, Phase change materials for thermal energy storage, Progress in Materials Science 65 (2014) 67–123.

[16] Norman C. Harris, Irving E. Thomas, Cydney E. Miller, Solar energy systems design, New York, 1985.

[17] U. Pelay, L. Luo, Y. Fan, D. Stitou, M. Rood, Thermal energy storage systems for concentrated solar power plants, Renewable and Sustainable Energy Reviews 79 (2017) 82–100.

[18] H.-Y. Chan, S.B. Riffat, J. Zhu, Review of passive solar heating and cooling technologies, Renewable and Sustainable Energy Reviews 14 (2) (2010) 781–789.

[19] G. Nelson, Application of microencapsulation in textiles, International Journal of Pharmaceutics 242 (1-2) (2002) 55–62.

[20] S. Mondal, Phase change materials for smart textiles – An overview, Applied Thermal Engineering 28 (11-12) (2008) 1536–1550.

[21] K. Lim, J. Che, J. Lee, Experimental study on adsorption characteristics of a water and silica-gel based thermal energy storage (TES) system, Applied Thermal Engineering 110 (2017) 80–88.

[22] P. Pardo, A. Deydier, Z. Anxionnaz-Minvielle, S. Rougé, M. Cabassud, P. Cognet, A review on high temperature thermochemical heat energy

storage, Renewable and Sustainable Energy Reviews 32 (2014) 591–610.

[23] H. Nazir, M. Batool, F.J. Bolivar Osorio, M. Isaza-Ruiz, X. Xu, K. Vignarooban, P. Phelan, Inamuddin, A.M. Kannan, Recent developments in phase change materials for energy storage applications: A review, International Journal of Heat and Mass Transfer 129 (2019) 491–523.

[24] R. Tiskatine, A. Aharoune, L. Bouirden, A. Ihlal, Identification of suitable storage materials for solar thermal power plant using selection methodology, Applied Thermal Engineering 117 (2017) 591–608.

[25] P. Tatsidjodoung, N. Le Pierrès, L. Luo, A review of potential materials for thermal energy storage in building applications, Renewable and Sustainable Energy Reviews 18 (2013) 327–349.

[26] A. Simons, S.K. Firth, Life-cycle assessment of a 100% solar fraction thermal supply to a European apartment building using water-based sensible heat storage, Energy and Buildings 43 (6) (2011) 1231–1240.

[27] S. Guillot, A. Faik, A. Rakhmatullin, J. Lambert, E. Veron, P. Echegut, C. Bessada, N. Calvet, X. Py, Corrosion effects between molten salts and thermal storage material for concentrated solar power plants, Applied Energy 94 (2012) 174–181.

[28] D. Laing, T. Bauer, N. Breidenbach, B. Hachmann, M. Johnson, Development of high temperature phase-change-material storages, Applied Energy 109 (2013) 497–504.

[29] J. Pereira da Cunha, P. Eames, Thermal energy storage for low and medium temperature applications using phase change materials – A review, Applied Energy 177 (2016) 227–238.

[30] G. Alva, L. Liu, X. Huang, G. Fang, Thermal energy storage materials and systems for solar energy applications, Renewable and Sustainable Energy Reviews 68 (2017) 693–706.

[31]   A. Jamekhorshid, S.M. Sadrameli, M. Farid, A review of microencapsulation methods of phase change materials (PCMs) as a thermal energy storage (TES) medium, Renewable and Sustainable Energy Reviews 31 (2014) 531–542.

[32]   Z. Ge, Y. Li, D. Li, Z. Sun, Y. Jin, C. Liu, C. Li, G. Leng, Y. Ding, Thermal energy storage: Challenges and the role of particle technology, Particuology 15 (2014) 2–8.

[33]   K. Resch-Fauster, M. Feuchter, Thermo-physical characteristics, mechanical performance and long-term stability of high temperature latent heat storages based on paraffin-polymer compounds, Thermochim Acta 663 (2018) 34–45.

[34]   V.V. Tyagi, S.C. Kaushik, S.K. Tyagi, T. Akiyama, Development of phase change materials based microencapsulated technology for buildings: A review, Renewable and Sustainable Energy Reviews 15 (2) (2011) 1373–1391.

[35]   S.K. Ghosh, Functional Coatings, Wiley-VCH Verlag GmbH & Co. KGaA, Weinheim, FRG, 2006.

[36]   G. Sukhorukov, A. Fery, H. Möhwald, Intelligent micro- and nanocapsules, Progress in Polymer Science 30 (8-9) (2005) 885–897.

[37]   Y. Fang, H. Yu, W. Wan, X. Gao, Z. Zhang, Preparation and thermal performance of polystyrene/n-tetradecane composite nanoencapsulated cold energy storage phase change materials, Energy Conversion and Management 76 (2013) 430–436.

[38]   G.W. Ehrenstein, G. Riedel, P. Trawiel, Thermal analysis of plastics: Theory and practice, Hanser, Munich, 2004.

[39]   Q. Yan, C. Liang, The thermal storage performance of monobasic, binary and triatomic polyalcohols systems, Solar Energy 82 (7) (2008) 656–662.

[40]   I.O. Salyer, J.E. Davison, Thermal-energy storage in crosslinked pellets of high-density polythylene for home heating and cooling via

off-peak electric power utilization, J. Appl. Polym. Sci. 28 (9) (1983) 2903–2924.

[41]   Kamimoto, M., Abe, Y., Sawata, S., Tani, T., & Ozawa, T., Latent thermal storage unit using form-stable high density polyethylene: Part I: performance of the storage unit, Journal of solar energy engineering 108 (4) (1986) 282–289.

[42]   H. Inaba, Z. Li, Thermal energy storage characteristics of a latent heat storage vessel packed with surface cross-linked, form-stabilized, high-density polyethylene pellets by boiling phenomenon, Heat Trans. Asian Res. 28 (8) (1999) 649–663.

[43]   S.O. Han, D.W. Lee, O.H. Han, Thermal degradation of crosslinked high density polyethylene, Polymer Degradation and Stability 63 (2) (1999) 237–243.

[44]   X. Du, H. Wang, Y. Wu, Z. Du, X. Cheng, Solid-solid phase-change materials based on hyperbranched polyurethane for thermal energy storage, J. Appl. Polym. Sci. 134 (26) (2017) 456.

[45]   Q. Cao, P. Liu, Hyperbranched polyurethane as novel solid–solid phase change material for thermal energy storage, European Polymer Journal 42 (11) (2006) 2931–2939.

[46]   W. Kong, X. Fu, Z. Liu, C. Zhou, J. Lei, A facile synthesis of solid-solid phase change material for thermal energy storage, Applied Thermal Engineering 117 (2017) 622–628.

[47]   S. Sundararajan, A.B. Samui, P.S. Kulkarni, Shape-stabilized poly(ethylene glycol) (PEG)-cellulose acetate blend preparation with superior PEG loading via microwave-assisted blending, Solar Energy 144 (2017) 32–39.

[48]   C. Alkan, A. Sari, O. Uzun, Poly(ethylene glycol)/acrylic polymer blends for latent heat thermal energy storage, AIChE J. 52 (9) (2006) 3310–3314.

[49] H. Xiang, S. Wang, R. Wang, Z. Zhou, C. Peng, M. Zhu, Synthesis and characterization of an environmentally friendly PHBV/PEG copolymer network as a phase change material, Sci. China Chem. 56 (6) (2013) 716–723.

[50] K. Pielichowski, K. Flejtuch, Differential scanning calorimetry studies on poly(ethylene glycol) with different molecular weights for thermal energy storage materials, Polym. Adv. Technol. 13 (10-12) (2002) 690–696.

[51] K. Pielichowski, K. Flejtuch, Recent developments in polymeric phase change materials for energy storage: Poly(ethylene oxide)/stearic acid blends, Polym. Adv. Technol. 16 (2-3) (2005) 127–132.

[52] S. Han, C. Kim, D. Kwon, Thermal degradation of poly(ethyleneglycol), Polymer Degradation and Stability 47 (2) (1995) 203–208.

[53] C. Zauner, F. Hengstberger, M. Etzel, D. Lager, R. Hofmann, H. Walter, Durability of a fin-tube latent heat storage using high density polyethylene as PCM, IOP Conf. Ser.: Mater. Sci. Eng. 251 (2017) 12123.

[54] C. Yang, M.E. Navarro, B. Zhao, G. Leng, G. Xu, L. Wang, Y. Jin, Y. Ding, Thermal conductivity enhancement of recycled high density polyethylene as a storage media for latent heat thermal energy storage, Sol Energ Mat Sol C 152 (2016) 103–110.

[55] C. Zauner, F. Hengstberger, B. Mörzinger, R. Hofmann, H. Walter, Experimental characterization and simulation of a hybrid sensible-latent heat storage, Applied Energy 189 (2017) 506–519.

[56] A. Sciacovelli, M.E. Navarro, Y. Jin, G. Qiao, L. Zheng, G. Leng, L. Wang, Y. Ding, High density polyethylene (HDPE) — Graphite composite manufactured by extrusion: A novel way to fabricate phase change materials for thermal energy storage, Particuology (2018).

[57] C. Zauner, F. Hengstberger, M. Etzel, D. Lager, R. Hofmann, H. Walter, Experimental characterization and simulation of a fin-tube

latent heat storage using high density polyethylene as PCM, Applied Energy 179 (2016) 237–246.

[58]   H.M. Weingrill, K. Resch-Fauster, C. Zauner, Applicability of Polymeric Materials as Phase Change Materials, Macromol. Mater. Eng. 31 (2018) 1800355.

[59]   W. Grellmann, S. Seidler, V. Altstädt (Eds.), Polymer testing, 2nd ed., Hanser, Munich, 2013.

[60]   T.A. Osswald, E. Baur, S. Brinkmann, K. Oberbach, E. Schmachtenberg, International Plastics Handbook, Carl Hanser Verlag GmbH & Co. KG, München, 2006.

[61]   N. Mehra, L. Mu, T. Ji, X. Yang, J. Kong, J. Gu, J. Zhu, Thermal transport in polymeric materials and across composite interfaces, Applied Materials Today 12 (2018) 92–130.

[62]   W. Kim, Strategies for engineering phonon transport in thermoelectrics, J. Mater. Chem. C 3 (40) (2015) 10336–10348.

[63]   G.P. Srivastava, The physics of phonons, Hilger, Bristol, 1990.

[64]   R. Berman, Heat conductivity of non-metallic crystals, Contemporary Physics 14 (2) (1973) 101–117.

[65]   Aleksandr Chernatynskiy, David R. Clarke, Simon R. Phillpot, Thermal transport in nanostructured material, in: W.A. Goddard (Ed.), Handbook of nanoscience, engineering, and technology, 3rd ed., CRC Press, Boca Raton, Fla., 2012, pp. 568–595.

[66]   S. Shen, A. Henry, J. Tong, R. Zheng, G. Chen, Polyethylene nanofibres with very high thermal conductivities, Nat. Nanotechnol. 5 (4) (2010) 251–255.

[67]   H. Weingrill, W. Hohenauer, K. Resch-Fauster, C. Zauner, Analyzing Thermal Conductivity of Polyethylene-Based Compounds Filled with Copper, Macromol. Mater. Eng. 59 (2019) 1800644.

[68] A. Henry, THERMAL TRANSPORT IN POLYMERS, Annual Rev Heat Transfer 17 (N/A) (2014) 485–520.

[69] B. Nysten, P. Gonry, J.-P. Issi, Intra-and interchain thermal conduction in polymers, Synthetic Metals 69 (1-3) (1995) 67–68.

[70] K. Eiermann, Modellmäßige Deutung der Wärmeleitfähigkeit von Hochpolymeren, Kolloid-Z.u.Z.Polymere 198 (1-2) (1964) 5–16.

[71] A. Henry, G. Chen, S.J. Plimpton, A. Thompson, 1D-to-3D transition of phonon heat conduction in polyethylene using molecular dynamics simulations, Phys. Rev. B 82 (14) (2010) 141.

[72] Y. Lin, Y. Jia, G. Alva, G. Fang, Review on thermal conductivity enhancement, thermal properties and applications of phase change materials in thermal energy storage, Renewable and Sustainable Energy Reviews 82 (2018) 2730–2742.

[73] L. Fan, J.M. Khodadadi, Thermal conductivity enhancement of phase change materials for thermal energy storage: A review, Renewable and Sustainable Energy Reviews 15 (1) (2011) 24–46.

[74] H. Chen, V.V. Ginzburg, J. Yang, Y. Yang, W. Liu, Y. Huang, L. Du, B. Chen, Thermal conductivity of polymer-based composites: Fundamentals and applications, Prog Polym Sci 59 (2016) 41–85.

[75] Z. Han, A. Fina, Thermal conductivity of carbon nanotubes and their polymer nanocomposites: A review, Progress in Polymer Science 36 (7) (2011) 914–944.

[76] D. Kumlutas, Thermal conductivity of particle filled polyethylene composite materials, Compos Sci Technol 63 (1) (2003) 113–117.

[77] W. Zhou, S. Qi, Q. An, H. Zhao, N. Liu, Thermal conductivity of boron nitride reinforced polyethylene composites, Mater Res Bull 42 (10) (2007) 1863–1873.

[78] S.R. Dhakate, N. Chauhan, S. Sharma, J. Tawale, S. Singh, P.D. Sahare, R.B. Mathur, An approach to produce single and double layer

graphene from re-exfoliation of expanded graphite, Carbon 49 (6) (2011) 1946–1954.

[79]   S.H. Song, K.H. Park, B.H. Kim, Y.W. Choi, G.H. Jun, D.J. Lee, B.-S. Kong, K.-W. Paik, S. Jeon, Enhanced thermal conductivity of epoxy-graphene composites by using non-oxidized graphene flakes with non-covalent functionalization, Adv Mater 25 (5) (2013) 732–737.

[80]   G.-W. Lee, M. Park, J. Kim, J.I. Lee, H.G. Yoon, Enhanced thermal conductivity of polymer composites filled with hybrid filler, Compos Part A-Appl S 37 (5) (2006) 727–734.

[81]   H.S. Tekce, D. Kumlutas, I.H. Tavman, Effect of Particle Shape on Thermal Conductivity of Copper Reinforced Polymer Composites, J Reinf Plast Comp 26 (1) (2007) 113–121.

[82]   B. Debelak, K. Lafdi, Use of exfoliated graphite filler to enhance polymer physical properties, Carbon 45 (9) (2007) 1727–1734.

[83]   S. Ganguli, A.K. Roy, D.P. Anderson, Improved thermal conductivity for chemically functionalized exfoliated graphite/epoxy composites, Carbon 46 (5) (2008) 806–817.

[84]   H.J. Ahn, Y.J. Eoh, S.D. Park, E.S. Kim, Thermal conductivity of polymer composites with oriented boron nitride, Thermochim Acta 590 (2014) 138–144.

[85]   K. Wattanakul, H. Manuspiya, N. Yanumet, Thermal conductivity and mechanical properties of BN-filled epoxy composite: Effects of filler content, mixing conditions, and BN agglomerate size, J Compos Mater 45 (19) (2011) 1967–1980.

[86]   Y.-H. Zhao, Z.-K. Wu, S.-L. Bai, Study on thermal properties of graphene foam/graphene sheets filled polymer composites, Compos Part A-Appl S 72 (2015) 200–206.

2.   Objectives of the thesis

As mentioned in the introduction above, the exploitation of novel phase-change materials (PCM) is necessary to further increase energy efficiency. Up to now, the potential of the polymeric material class as PCM has been mainly neglected even though polymers exhibit many of their preferable properties. This may be due to the fact that all polymers exhibit susceptibility towards thermo-oxidative degradation. Material degradation can result in the deterioration of the preferable materials' characteristics and hence the loss of their applicability as PCM. It is therefore important to not only find candidate polymeric materials by characterizing their relevant thermo-physical properties but to equally investigate their ability to maintain those material characteristics during the application as PCM. An appropriate imitation of the severe conditions polymers face during the application as PCM needs to be found. The thereby developed exposure parameters can then be applied on selected polymers only to make detailed scientific research possible. Thereafter, the low thermal conductivity of polymers needs to be addressed to further increase their well-functioning as PCM in latent heat storages. However, typically applied fillers for enhancing thermal conductivity do not undergo a phase-transition during the phase-transition of polymers and thereby reduce the storage capacity of the polymer. Thus, the most efficient way for increasing the thermal conductivity of polymers by means of optimizing filler geometries and processing is demanded.

To sufficiently address the aspects described above, the following objectives were set for this thesis:

1. Screening of commercially available semi-crystalline polymer grades which are applicable as PCM

   - Finding of semi-crystalline polymer classes with high potential as PCM in terms of low-cost, high heat of fusion and different application temperature ranges

- Determining the heat of fusion and the application temperature range of individual polymer grades within different polymer classes
- Evaluation of recyclates for the use as PCM as economically and ecologically attractive alternatives to neat polymers

2. Investigation of long-term stability of candidate polymers applied as PCM
   - Evaluation of different types of accelerated testing in application-relevant conditions by identifying appropriate specimen dimensions, temperatures and other exposure parameters
   - Short-term stability testing as preliminary material selection for long-term stability testing
   - Long-term stability testing in application-oriented conditions with monitoring application-relevant material characteristics such as the heat of fusion and the application temperature range
   - Evaluation of necessity for additional stabilization against thermo-oxidative degradation

3. Enhancement of thermal conductivity of candidate polymeric PCM
   - Understanding the physics and impacts on thermal conductivity of polymeric materials
   - Finding of commercially available, economical and efficient fillers to increase the thermal conductivity of polymers
   - Fabrication of compounds containing different fillers types at different filler loadings and shapes
   - Determining the thermal conductivity of fabricated compounds and evaluating the most efficient filler types
   - Optimizing the processing and filler geometry (shape, mean particles size, size distribution) within the most efficient filler

types according to the requirements of an improved well-functioning of the latent heat storage

4. Investigation of long-term stability of polymers with enhanced thermal conductivity applied as PCM

- Characterization of application-relevant properties and the impact of incorporated fillers on the material's long-term stability of the incorporated fillers

3.   Structure of the thesis

According to the objectives, the thesis comprises a series of publications dealing with the development of novel polymeric phase change materials (PCM). It is divided into six parts which are:

I.   Preamble

II.   Introduction and motivation of the thesis

III.   Semi-crystalline polymers for latent heat storages

IV.   Long-term stability of polymeric phase-change materials

V.   Functionalized polymeric phase-change materials

VI.   Summary, conclusion and outlook

Part I consists of all mandatory sections and contents such as the affidavit, acknowledgment, the abstract and its German version and the table of content.

Part II gives an introduction to the thesis. It outlines the motivation behind the thesis and it offers the theoretical background for thermal energy storages and the applied storage media with focus on PCM. It further presents the state of the art of polymers applied in latent heat storages. The last section focuses on the thermal conductivity of polymers and its enhancement.

Part III deals with the feasibility of polymers as PCM and contains the publication 1. The screening of different semi-crystalline polymer classes as potential polymeric PCM according to application-relevant thermo-physical properties determined via Differential Scanning Calorimetry (DSC) is presented. The most appropriate polymers types are then selected out of several polymeric classes to cover a broad application temperature range. Two types of short-term stability testing (i.e. cyclic testing in a DSC in inert atmosphere and the exposure to thermal static loads in air) for the imitation of the thermal loads during the PCM's application are evaluated and are

further executed on candidate polymeric materials. Additionally, the economic benefits of recyclates instead of neat polymers as PCM are estimated and discussed based on the generated results and the latest material prices.

Part IV looks into the long-term stability of promising polymers as determined from the preliminary short-term testing in Part III. During their application as PCM, polymers encounter severe conditions due the combination of elevated temperatures and the presence of atmospheric oxygen. Therefore, bulky specimens of neat and additionally stabilized polymers are exposed in air to imitate application-related conditions up to 7200 h. Infrared spectroscopy, DSC and Polarized Light Microscopy are applied to investigate, monitor and explain the occurring aging phenomena. Relationships between the morphology and application-relevant properties are revealed. Furthermore, the need for an additional stabilization is evaluated. The outcome is presented in publication 2.

Part V focuses on polymeric PCM of which the thermal conductivity is enhanced to achieve faster heat transfer rates. For this purpose, the thermal conductivity of promising polymeric PCM is enhanced via the incorporation of highly thermally conductive particles. First, a comparative study of different commercially available measurement devices for determining thermal conductivity is presented in publication 3. The detected differences in the thermal conductivity of differently functionalized polymeric PCM are analyzed and ascribed to material-induced and technology-induced impacts. A consecutive filler screening is executed to determine the most efficient fillers for enhancing the thermal conductivity of polymers. As incorporated particles tend to interact with the surrounding polymeric matrix [1-5], publication 4 then focuses on the long-term stability of functionalized PCM and compares their long-term stability to the one of the neat polymers.

Prior to publications 1, 2 and 3 a brief introduction focuses on specific information about each publication. Afterwards, the concept of each publication is outlined. Prior to publication 4, the introduction additionally contains unpublished data on the screening procedure of different filler types in order to find the most efficient filler for enhancing the thermal conductivity of candidate polymeric materials. Filler loadings and processing parameters are optimized via combined thermal conductivity measurements and morphological considerations.

Part VI consists of a short summary and the conclusions of the thesis which come along with an outlook of future investigations.

3.1. References

[1]   L.M. Gorghiu, S. Jipa, T. Zaharescu, R. Setnescu, I. Mihalcea, The effect of metals on thermal degradation of polyethylenes, Polym Degrad Stabil 84 (1) (2004) 7–11.

[2]   E. Tarani, Z. Terzopoulou, D.N. Bikiaris, T. Kyratsi, K. Chrissafis, G. Vourlias, Thermal conductivity and degradation behavior of HDPE/graphene nanocomposites, J Therm Anal Calorim 129 (3) (2017) 1715–1726.

[3]   A.K. Pandey, K. Singh, K.K. Kar, Thermo-mechanical properties of graphite-reinforced high-density polyethylene composites and its structure–property corelationship, J Compos Mater 51 (12) (2016) 1769–1782.

[4]   Rusu, M., Sofian, N., & Rusu, D, Mechanical and thermal properties of zinc powder filled high density polyethylene composites., Polym Test 20 (4) (2001) 409–417.

[5]   A.S. Luyt, J.A. Molefi, H. Krump, Thermal, mechanical and electrical properties of copper powder filled low-density and linear low-density polyethylene composites, Polym Degrad Stabil 91 (7) (2006) 1629–1636.

Part III.

Semi-crystalline polymers for latent heat storages

4.   Introduction to publication 1

Out of the polymeric material class, only polyethylene glycol with melting peak temperatures between 40 °C and 70 °C (reflects the phase-change material's (PCM) application temperature) and heats of fusion up to 190 J/g (which is mainly responsible for the material's storage capacity) [1] has been extensively studied as solid-liquid PCM [2]. Several authors have equally considered high-density polyethylene (HDPE) with a melting temperature of approximately 135 °C due to its outstanding high heat of fusion of up to 240 J/g [3-7]. However, manifold other semi-crystalline polymers with melting peaks ranging from approximately 100 °C to 290 °C [3], are available, but have not been considered as PCM yet. Within each polymer class several polymer types (e.g. polyethylene comes in the form of low-density polyethylene, linear low-density polyethylene, HDPE and ultra-high molecular weight polyethylene) [3] may be available. Furthermore, varying synthesis parameters result in morphological differences (amount of branching, chain length, molecular weight, etc.) and thus numerous different polymer grades within one polymer class or type. This further affects the crystalline structure and thereby the heat of fusion and the melting and crystallization behavior of the polymer. Data about their thermo-physical properties is partially available but it mainly includes the polymer's melting and crystallization peak temperatures only. As opposed to metals, polymers do not exhibit well-defined melting and crystallization peaks but rather broad melting and crystallization regions which are caused by heterogeneous crystallite sizes [3]. Thus, to truly characterize a polymer's melting and crystallization behavior, also the on- and endset temperatures of the melting and crystallization transitions are significant for the application of polymers as PCM. Furthermore, the thermo-physical properties are strongly dependent on the preceding thermal treatment of a polymer and can only be compared if identical conditions i.e. identical testing parameters in terms of same specimen preparation, measurement method and evaluation are given.

Additionally to the above mentioned thermo-physical properties that determine the applicability of polymers as PCM (melting temperature range and heat of fusion), also the polymer's ability to maintain these properties

during the application as PCM is crucial as it undergoes several thousand charging and discharging cycles. Polymers are applied in a variance of application fields such as packaging, building and construction, electrical equipment etc. [8]. In many of them, they are constantly exposed to elevated temperatures and a broad range of scientific literature about their thermal and thermo-oxidative long-term stability is therefore available for semi-crystalline polymers in the solid state [9-11]. However, for the long-term stability of semi-crystalline polymers in the melt state sufficient data is not available.

Therefore, a systematic screening through semi-crystalline polymer classes is first necessary to select promising polymer grades and determine their application temperature range and storage capacity. For this purpose, the melting and crystallization behavior and heat of fusion are investigated in detail by Differential Scanning Calorimetry. Moreover, short-term stability investigations as further selection step are applied on polymers selected from the screening. Publication 1 presents the detailed outcome of this systematic screening of semi-crystalline polymers and of the preliminary short-term stability investigations to evaluate the applicability of promising polymer grades as PCM. Furthermore, benefits for the use of recyclates instead of the virgin polymer are estimated.

Besides the publication shown in the following, contributions in terms of oral presentations have been made by the author in this field and are given in the following:

Conference contribution: H. Weingrill, K. Resch-Fauster, T. Lucyshyn, C. Zauner.; "Applicability of polymeric materials for heat storages", The III Energy & Materials Research Conference, Lisbon, PT, 2017

Conference contribution: H. Weingrill, K. Resch-Fauster, T. Lucyshyn, C. Zauner.; "Selection and stability of polymeric phase change materials", 2nd International Conference on Renewable Energy and Resources, Boston, US, 2018

4.1. References

[1]   K. Pielichowski, K. Flejtuch, Differential scanning calorimetry studies on poly(ethylene glycol) with different molecular weights for

thermal energy storage materials, Polym. Adv. Technol. 13 (10-12) (2002) 690–696.

[2]   K. Pielichowska, K. Pielichowski, Phase change materials for thermal energy storage, Progress in Materials Science 65 (2014) 67–123.

[3]   G.W. Ehrenstein, G. Riedel, P. Trawiel, Thermal analysis of plastics: Theory and practice, Hanser, Munich, 2004.

[4]   C. Zauner, F. Hengstberger, B. Mörzinger, R. Hofmann, H. Walter, Experimental characterization and simulation of a hybrid sensible-latent heat storage, Applied Energy 189 (2017) 506–519.

[5]   C. Zauner, F. Hengstberger, M. Etzel, D. Lager, R. Hofmann, H. Walter, Experimental characterization and simulation of a fin-tube latent heat storage using high density polyethylene as PCM, Applied Energy 179 (2016) 237–246.

[6]   A. Sciacovelli, M.E. Navarro, Y. Jin, G. Qiao, L. Zheng, G. Leng, L. Wang, Y. Ding, High density polyethylene (HDPE) — Graphite composite manufactured by extrusion: A novel way to fabricate phase change materials for thermal energy storage, Particuology (2018).

[7]   C. Yang, M.E. Navarro, B. Zhao, G. Leng, G. Xu, L. Wang, Y. Jin, Y. Ding, Thermal conductivity enhancement of recycled high density polyethylene as a storage media for latent heat thermal energy storage, Sol Energ Mat Sol C 152 (2016) 103–110.

[8]   T.A. Osswald, E. Baur, S. Brinkmann, K. Oberbach, E. Schmachtenberg, International Plastics Handbook, Carl Hanser Verlag GmbH & Co. KG, München, 2006.

[9]   N. Billingham, Handbook of Polymer Degradation, Polymer Degradation and Stability 74 (3) (2001) 585.

[10]   K. Pielichowski, J. Njuguna, Thermal degradation of polymeric materials, Rapra Technology, Shawbury, 2005.

[11]   C. Krebs, K.W. Leu (Eds.), Langzeitverhalten von Thermoplasten: Alterungsverhalten und Chemikalienbeständigkeit, Hanser, München, 1999.

5.   Publication 1

5.1.   Bibliographic information

- Title: Applicability of polymeric materials as phase-change materials

- Authors:

    - Helena Weingrill[1]

    - Katharina Resch-Fauster[1]

    - Christoph Zauner[2]

- Affilitation:

    1. Materials Science and Testing of Polymers, Montanuniversitaet Leoben, Otto-Gloeckel-Strasse 2, 8700 Leoben, Austria

    2. Austrian Institute of Technology, Giefinggasse 2, 1020 Vienna, Austria

- Periodical: Macromolecular Materials and Engineering

- DOI: 10.1002/mame.201800355

Statement with regard to this publication: The manuscript presented here is an adapted accepted manuscript in order to fit the formatting of the thesis and does not necessarily reflect exactly the actually published version.

5.2.   Abstract

The applicability of more than 70 semi-crystalline polymer grades with different melting temperatures as phase change materials (PCM) is investigated. Their storage capacity (heat of fusion) and their application temperature range (defined by the melting temperature range and the degradation behavior) are analyzed via Differential Scanning Calorimetry (DSC). Application-oriented stability investigations (thermal cycling and exposure to static thermal load above the polymer's melting temperature) are applied on the most promising polymer types. The thermal and thermo-oxidative degradation behavior is monitored via DSC and Fourier-transform infrared spectroscopy (FTIR). Different aging phenomena are identified. However, these   have only little impact on the polymer's storage capacity. Therefore, a great potential of polymers as PCM is revealed. Additionally, the economic efficiency of polymers as PCM is estimated and discussed.

5.3.   Introduction and scope

Phase change materials (PCM) store and release large amounts of thermal energy when they undergo a phase change [1]. In contrast to conventional, sensible heat storage, PCM store between 5 to 14 times more thermal energy per unit volume due to an exceptional energy density [2]. The phase change (e.g. solid-liquid, liquid-gaseous) and therefore the storing and releasing process almost take place isothermally (latent heat storage). Preferably, the melting process is used as storing process because only a low volume change of 10 % or less occurs [3]. In this case the amount of thermal energy that can be stored and released depends on the PCM's heat of fusion. Depending on the field of application, the PCM should fulfill thermal (suitable phase-change temperature, high heat of phase change, high thermal conductivity), physical (high density, small volume change), kinetic (no subcooling, sufficient crystallization rate), chemical (long-term stability, no phase segregation, compatibility with materials of construction, no toxicity, no fire hazard) and/or economical (abundant, available, cost effective) requirements. With regard to their melting temperature range, PCM can be divided into low- and high-temperature PCM. Suitable low-temperature PCM (up to 200°C) are paraffins, polyalcohols, low-melting metallics, nonparaffin organics (e.g. fatty acids) and salt hydrates [2,4,5]. Suitable high-temperature PCM (up to 1000°C) are fluoride salts, chloride eutectic compositions, hydroxide compositions, nitrate compositions, carbonate salts and high-melting metallics and their eutectic compositions [6,7]. Semi-crystalline polymers exhibit a broad variety of melting temperatures ranges from ~50 °C

to ~340 °C and show therefore potential as low-temperature and high-temperature PCM. Nevertheless, concerning latent heat storages up to now polymeric materials have mostly been applied as form-stabilizer, e.g. [8-22]. Only a few polymers have been used as PCM per se: polyethylene glycol has been tested as PCM profoundly [11,13,14,17,20,22-28], whereas polyethylene has been considered by a few authors [29-34]. Also various other semi-crystalline polymers show great potential in terms of many of the above mentioned requirements (high heat of fusion, different suitable melting temperature ranges, cost effectiveness etc.). However, they have not been investigated yet as possible PCM. Thus, the overall objective of the present study is to evaluate the suitability and potential of different polymeric materials as PCM. Firstly, a sound scientific screening of a wide variety of polymer types and grades is done regarding their thermo-physical characteristics. Afterwards promising candidate materials are tested regarding the application-relevant thermal and thermo-oxidative stability. Finally, specific focus is on assessing the economic efficiency of polymeric PCM.

5.4.   Material selection

In the present study, the phase change from the solid-crystalline state to the liquid-amorphous state (i.e. melting) was used to store thermal energy. The application-relevant thermo-physical characteristics, i.e. heat of fusion and melting temperature range, were determined by means of Differential Scanning Calorimetry (DSC). For the material screening a wide variety of commercially available polymer types and grades from numerous manufacturers were analyzed. Primary selection criteria were a high degree of crystallinity and an outstanding crystallization capability of the particular polymer type. The relationship between the heat of fusion ΔH_M and the degree of crystallinity k of a polymer is outlined in equation (1)

$$k = \frac{\Delta H_M}{\Delta H_M^0} * 100\% \qquad (1)$$

with ΔH_M as the polymer's heat of fusion in J/g and ΔH_M^0 as the theoretic heat of fusion of the particular polymer in a fully crystalline state (100%). Consequently, a high degree of crystallinity involves a high heat of fusion for the particular polymer type/grade.

The investigated polymer types (abbreviation) and grades are summarized in Table 5.1Table 5.1 along with their melt flow rate, melt volume rate or viscosity number (as taken from the material data sheets and distinguishable by the given unit: g/10 min = melt flow rate; cm³/10 min = melt volume rate; cm³/g = viscosity number) and their thermo-physical properties (heat of crystallization ΔH_C, crystallization peak temperature T_C, heat of fusion ΔH_M, melting peak temperature T_{Mpeak}) as determined by DSC. on a DSC 1 (Mettler Toledo, Greifensee, CH). The specimens were taken from the granules and the sample weight ranged between 5 mg and 10 mg. 40 µl aluminum crucibles were used. After an equilibration time of 5 min at the starting temperature T_{start} (at least 50 °C below the first expected thermo-physical effect [35]), the samples were heated under nitrogen atmosphere from T_{start} to T_{end} (30 °C above T_{Mpeak}) and cooled to T_{start} by applying a constant heating rate of 10 K/min and -10 K/min, respectively. After another equilibration time of 5 min at T_{start}, the samples were heated a second time from T_{start} to T_{end} by applying a constant heating rate of 10 K/min. ΔH_C, T_{Cpeak} and the extrapolated crystallization onset and end temperatures T_{Con} and T_{Cend} were evaluated from the cooling curves. ΔH_M, T_{Mpeak} and the extrapolated melting onset and end temperatures T_{Mon} and T_{Mend} were evaluated from the second heating. The evaluations were done according to ISO 11357-2. In general, one DSC-measurement was conducted for each polymer grade. Two to three measurements were conducted for polymer grades of primary interest due to high ΔH_M or high T_{Mpeak}. In this case, the evaluated values in Table 5.1 are highlighted in grey and the presented data represent the average of those measurements. A schematic thermogram of the melting process of a polymer which undergoes thermo-oxidative degradation at temperatures far above the melting range is presented in Figure 5.1a. The area of the melting peak equals ΔH_M and represents the heat storage capacity of the polymer. The melting peak temperature T_{Mpeak} and the extrapolated melting onset and endset temperatures T_{Mon} and T_{Mend} indicate the melting characteristics of the polymer. According to that Figure 5.1b depicts schematically the stored thermal energy as a function of temperature.
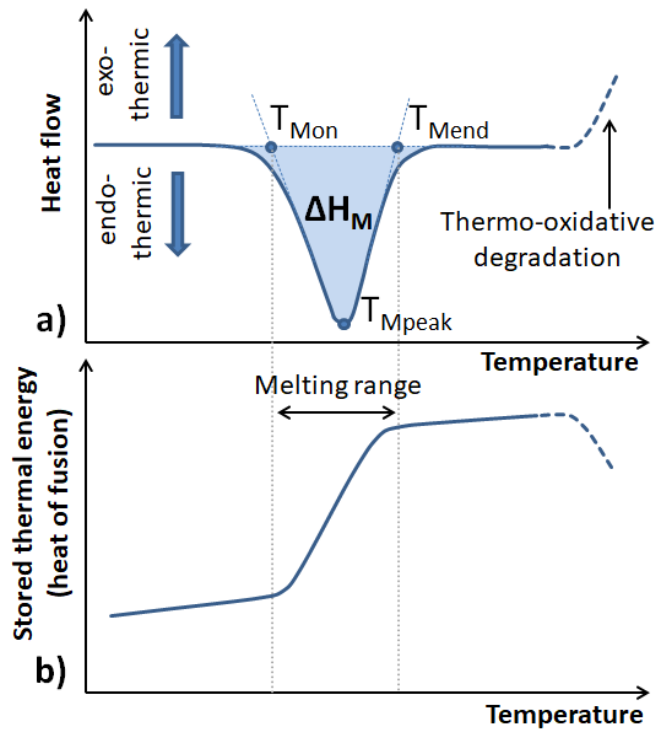
Figure 5.1: a) schematic DSC-thermogram of the melting process of a semi-crystalline polymer: T_{Mpeak}, T_{Mon} and T_{Mend} are the melting peak temperature, the extrapolated melting onset and endset temperature, respectively; b) schematic of the stored thermal energy (heat of fusion) of the material over the temperature.

Table 5.1: Investigated semi-crystalline polymer types (abbreviation) and grades along with the melt flow/the melt volume rate with the according testing parameters or the viscosity number (as taken from the material data sheet) and ΔH_C (heat of crystallization), T_{Cpeak} (crystallization peak temperature), ΔH_M (heat of fusion) and T_{Mpeak} (melting peak temperature) as determined via DSC by applying a cooling and heating rate of -10 K/min and 10 K/min, respectively.

Polymer type (abbreviation)	Polymer grade	Melt flow rate/ melt volume rate/ viscosity number (testing parameters)	ΔH_C [J/g]	T_{Cpeak} [°C]	T_{Con}/ T_{Cend} [°C]	ΔH_M [J/g]	T_{Mpeak} [°C]	T_{Mon}/ T_{Mend} [°C]
Polyethylene glycol (PEG)	PEG1	-	182 ± 0	34 ± 0	41 ± 0/ 28 ± 1	183 ± 1	58 ± 0	56 ± 0/ 65 ± 0
	PEG2	-	176 ± 1	40 ± 1	43 ± 1/ 36 ± 1	177 ± 1	64 ± 0	60 ± 0/ 69 ± 0
	PEG3	-	169	45	48/ 40	168	65	61/ 71
	PEG4	-	163	44	47/ 39	164	65	61/ 70
	PEG5	-	164	41	44/ 37	164	64	60/ 69
	PEG6	-	125	47	50/ 40	126	67	59/ 73

Polyethylene – linear low density (LLDPE)	LLDPE1	6.6 g/10 min (190 °C, 2.16 kg)	110 ± 5	104 ± 0	108 ± 0/ 35 ± 1	111 ± 6	124 ± 0	62 ± 6/ 128 ± 0
Polyethylene - high density (HDPE)	HDPE1	0.85 g/10 min (190 °C, 2.16 kg)	222	116	120/ 106	222	135	124/ 143
	HDPE2	4 g/10 min (190 °C, 2.16 kg)	226 ± 2	117 ± 0	119 ± 0/ 108 ± 0	226 ± 1	134 ± 0	125 ± 0/ 141 ± 0
	HDPE3	8 g/10 min (190 °C, 2.16 kg)	235 ± 10	118 ± 0	120 ± 0/ 110 ± 0	233 ± 8	134 ± 0	126 ± 0/ 141 ± 0
	HDPE4	8 g/10 min (190 °C, 2.16 kg)	239 ± 5	118 ± 0	120 ± 0/ 109 ± 0	239 ± 4	133 ± 0	126 ± 0/ 141 ± 0
	HDPE5	0.7 g/10 min (190 °C, 2.16 kg)	228 ± 8	118 ± 0	120 ± 0/ 108 ± 1	228 ± 6	133 ± 0	124 ± 0/ 140 ± 0
	HDPE6	0.7 g/10 min (190 °C, 2.16 kg)	232 ± 2	119 ± 0	120 ± 0/ 108 ± 0	234 ± 2	132 ± 0	124 ± 1/ 139 ± 1
	HDPE7	12 g/10 min (190 °C, 2.16 kg)	226 ± 4	118 ± 0	119 ± 0/ 108 ± 0	224 ± 5	135 ± 1	125 ± 2/ 142 ± 1
	HDPE8	1.5 g/10 min (190 °C, 2.16 kg)	211	117	118/ 109	215	130	121/ 135
	HDPE9	4 g/10 min (190 °C, 2.16 kg)	201 ± 5	114 ± 0	117 ± 0/ 105 ± 0	205 ± 4	131 ± 1	121 ± 0/ 138 ± 0
	HDPE10	8 g/10 min (190 °C, 2.16 kg)	239 ± 8	119 ± 0	118 ± 4/ 114 ± 4	239 ± 3	133 ± 1	125 ± 0/ 139 ± 1
	HDPE11	8 g/10 min (190 °C, 2.16 kg)	239 ± 1	118 ± 0	120 ± 0/ 110 ± 0	237 ± 1	133 ± 0	126 ± 0/ 139 ± 1
	HDPE12	7.6 g/10 min (190 °C, 2.16 kg)	225 ± 2	118 ± 0	120 ± 0/ 108 ± 0	226 ± 3	133 ± 0	122 ± 1/ 140 ± 0
	HDPE13	25 g/10 min (190 °C, 2.16 kg)	204 ± 2	117 ± 0	120 ± 0/ 110 ± 1	206 ± 3	134 ± 1	125 ± 0/ 140 ± 1
	HDPE14	0.8 g/10 min (190 °C, 2.16 kg)	236 ± 2	119 ± 0	121 ± 0/ 108 ± 2	235 ± 1	133 ± 0	124 ± 0/ 141 ± 1
Polyethylene - ultra-high molecular weight (UHMWPE)	UHMWPE 1	-	149 ± 10	118 ± 01	122 ± 1/ 111 ± 1	151 ± 7	133 ± 0	62 ± 6/ 128 ± 0
	UHMWPE 2	-	200 ± 6	119 ± 1	122 ± 1/ 111 ± 1	204 ± 3	132 ± 0	121 ± 1/ 136 ± 0
Polylactide (PLA)	PLA1	6 g/10 min (210 °C, 2.16 kg)	0	-	-	<1	153	147/ 159
	PLA2	-	0	-	-	<1	167	161/ 174
Poly-propylene (PP)	PP1	25 g/10 min (230 °C, 2.16 kg)	111	122	127/ 117	114	163	141/ 169
	PP2	15 g/10 min (230 °C, 2.16 kg)	102	129	132/ 123	102	166	144/ 171
	PP3	3.5 g/10 min (230 °C, 2.16 kg)	93 ± 1	117 ± 1	120 ± 0/ 111 ± 1	93 ± 1	166 ± 0	152 ± 1/ 171 ± 0
	PP4	6.5 g/10 min (230 °C, 2.16 kg)	115	128	130/ 120	122	167	145/ 175
	PP5	20 g/10 min (230 °C, 2.16 kg)	114 ± 5	129 ± 0	133 ± 0/ 122 ± 0	116 ± 6	167 ± 0	145 ± 1/ 174 ± 0
	PP6	20 g/10 min (230 °C, 2.16 kg)	114	125	132/ 115	115	166	144/ 173

Polyoxy-methylene-copolymer (POM-C)	POM-C1	12 cm³/10 min (190 °C, 2.16 kg)	186 ± 7	146 ± 0	149 ± 0/ 138 ± 0	180 ± 16	167 ± 0	162 ± 0/ 175 ± 0
	POM-C2	-	180 ± 4	148 ± 1	151 ± 1/ 138 ± 3	176 ± 6	168 ± 1	159 ± 1/ 174 ± 1
	POM-C3	12 cm³/10 min (190 °C, 2.16 kg)	182 ± 10	150 ± 1	151 ± 0/ 142 ± 0	187 ± 6	171 ± 0	166 ± 0/ 178 ± 0
	POM-C4	39 cm³/10 min (190 °C, 2.16 kg)	185 ± 4	148 ± 1	149 ± 0/ 140 ± 2	187 ± 5	166 ± 1	162 ± 0/ 173 ± 3
	POM-C5	8 cm³/10 min (190 °C, 2.16 kg)	173 ± 3	146 ± 0	148 ± 0/ 138 ± 0	177 ± 0	168 ± 0	161 ± 0/ 174 ± 0
	POM-C6	-	191 ± 8	147 ± 0	152 ± 0/ 139 ± 0	193 ± 6	175 ± 0	168 ± 0/ 183 ± 0
	POM-C7	9 g/10 min (190 °C, 2.16 kg)	167	145	147/ 137	180	164	159/ 172
	POM-C8	8 cm³/10 min (190 °C, 2.16 kg)	181 ± 0	146 ± 0	148 ± 0/ 137 ± 1	181 ± 1	167 ± 0	161 ± 0/ 173 ± 0
	POM-C9	11 cm³/10 min (190 °C, 2.16 kg)	184 ± 2	148 ± 0	150 ± 0/ 141 ± 0	186 ± 1	169 ± 0	163 ± 0/ 175 ± 0
	POM-C10	11 cm³/10 min (190 °C, 2.16 kg)	186 ± 8	146 ± 1	149 ± 0/ 138 ± 1	189 ± 8	167 ± 0	161 ± 1/ 174 ± 1
Polyhydroxy butyrate (PHB)	PHB1	10 g/10 min (180 °C/5 kg)	67	119	123/ 112	77	170	152/ 175
Polyoxy-methylene - homo-polymer (POM-H)	POM-H1	-	191	148	151/ 141	192	175	169/ 182
	POM-H2	2 cm³/10 min (190 °C, 2.16 kg)	182	148	151/ 137	185	179	170/ 188
	POM-H3	21 cm³/10 min (190 °C, 2.16 kg)	188	148	151/ 140	190	175	170/ 183
	POM-H4	13 cm³/10 min (190 °C, 2.16 kg)	200 ± 0	148 ± 0	152 ± 0/ 140 ± 1	200 ± 0	176 ± 0	170 ± 0/ 184 ± 1
	POM-H5	2 cm³/10 min (190 °C, 2.16 kg)	191 ± 2	148 ± 0	151 ± 0/ 140 ± 0	194 ± 3	178 ± 0	170 ± 0/ 185 ± 1
Polyamide 12 (PA12)	PA12-1	-	55	145	150/ 140	58	178	165/ 183
Polyamide 10.10 (PA 10.10)	PA10.10-1	-	80	172	178/ 163	83	202	159/ 206
Polyamide 6.10/6.6 (PA 6.10/6.6)	PA6.10/6.6-1	-	59	138	146/ 133	44	203	188/ 208
Polyamide 6.12 (PA 6.12)	PA6.12-1	-	67	180	186/ 174	69	214	166/ 218
Polyamide 6 (PA 6)	PA6-1	146-151 cm³/g (96% H_2SO_4)	78	172	182/ 163	76	221	208/ 225
	PA6-2	165 cm³/g	66	174	182/ 166	55	221	207/ 226
	PA6-3	165 cm³/g	63	173	182/ 166	62	221	208/ 225
	PA6-4	145 cm³/g	86 ± 3	193 ± 1	197 ± 1/ 183 ± 2	97 ± 2	219 ± 1	206 ± 2/ 226 ± 1
	PA6-5	-	77	185	189/ 179	76	221	204/ 226
	PA6-6	-	49	187	190/ 182	57	220	190/ 224
Polyamide 6.10 (PA 6.10)	PA6.10-1	-	58	177	186/ 168	54	222	209/ 226
	PA6.10-2	150 cm³/g	91 ± 2	194 ± 0	196 ± 0/ 188 ± 0	90 ± 2	222 ± 0	214 ± 0/ 226 ± 0
Polybutylene terephthalate (PBT)	PBT-1	105 ml/g	52	176	198/ 168	40	223	215/ 226
	PBT-2	130 cm³/g	54	183	191/ 177	40	222	215/ 225

Polytri-methylene terephthalate (PTT)	PTT-1	-	59	196	201/191	63	228	221/232
Polyamide 4.10 (PA 4.10)	PA4.10-1	-	67	224	227/219	67	246	231/250
	PA4.10-2	150 cm³/g	71	228	234/222	69	246	231/250
	PA4.10-3	210 cm³/g	63	223	228/217	63	245	230/250
Polyethylene terephthalate (PET)	PET-1	-	38	190	216/133	27	251	234/259
Polyamide 6.6 (PA 6.6)	PA6.6-1	-	64	230	234/224	75	261	243/265
	PA6.6-2	150 cm³/g	86 ± 1	233 ± 1	237 ± 3/230 ± 4	86 ± 4	262 ± 0	250 ± 0/266 ± 0
	PA6.6-3	150 cm³/g	47	217	228/211	67	261	217/265
Polystyrene – syndiotactic (sPS)	sPS-1	-	-	-	-	29	274	259/280
Polyamide 4.6 (PA 4.6)	PA4.6-1	185 cm³/g	85	259	262/250	109	291	280/298
	PA4.6-2	220 cm³/g	88 ± 1	259 ± 1	263 ± 0/253 ± 1	111 ± 2	288 ± 1	279 ± 1/294 ± 1
Polyphtha-lamide 6T/6 (PA 6T/6)	PA6T/6-1	130 cm³/g	35	269	278/248	39	300	201/320

In Figure 5.2 the melting temperature ranges and ΔH_M of the investigated polymer types are compared schematically: the given melting temperature range of each polymer type reflects the temperature range between the lowest detected T_{Mon} and the highest detected T_{Mend} of any polymer of the according polymer type since this is assumed to better represent the possible application temperature range than T_{Mpeak}. In general, the polymer types (PEG, PE, PP and POM) with rather low melting temperature ranges (53°C to 188°C) exhibited the highest ΔH_M (93 J/g to 239 J/g). Polyamides, polyesters (PHB, PBT, PTT and PET) and sPS with higher melting temperature ranges (115 °C to 320 °C), exhibited a significantly lower ΔH_M (15 J/g to 111 J/g) than PEG, PE, PP and POM (both examined PLA types are not listed in Figure 5.2 because their ΔH_M was lower than 1 J/g). Based on the above mentioned selection criteria (high ΔH_M and different melting temperature ranges), PEG, PE, PP and POM (high ΔH_M) and PA (higher melting temperature range) were identified as most suitable polymeric PCM. The applicability of PEG as PCM has already been examined profoundly [11,13,14,17,20,22-28]. The melting temperature range of PP is almost congruent with POM (which exhibits higher ΔH_M) and the degradation behavior of PP is assumed to be comparable to the one of PE. Thus, the focus for the following application-oriented stability investigations is kept on PE, POM and PA.
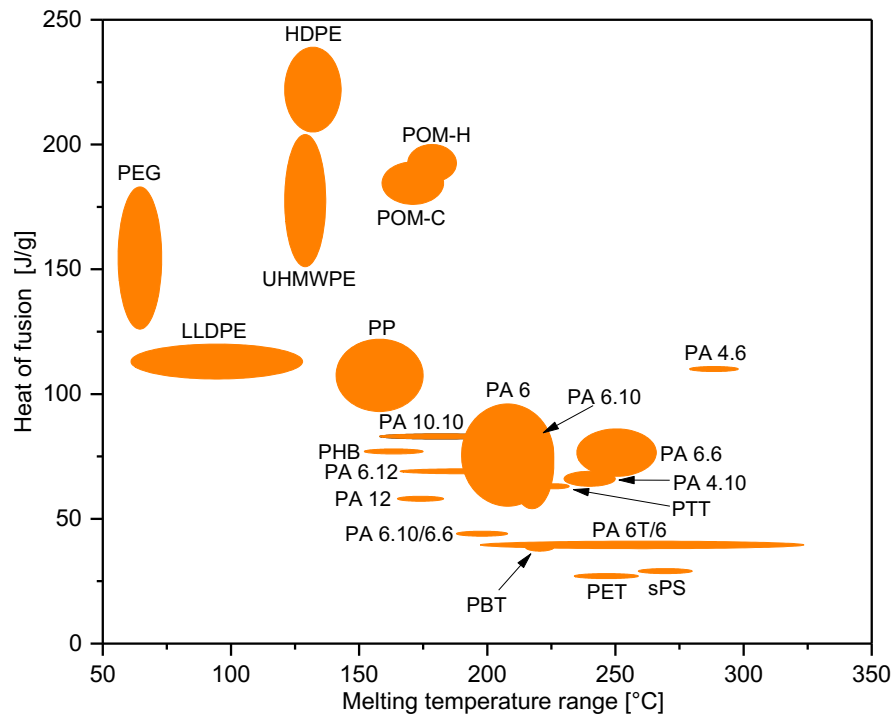
Figure 5.2: Overview of the melting behavior of examined semi-crystalline polymers generated via DSC when priorly cooled with -10 K/min and heated with 10 K/min. The melting temperature range of each polymer type reflects the temperature range between the lowest T_{Mon} and the higher T_{Mend} of any polymer of the according polymer type.

5.5. Application-oriented stability investigations

In Figure 5.3a, a schematic of the effective thermal loads on a PCM during its application is given. The PCM's temperature evolution over the time is depicted. The PCM is heated above its melting temperature to charge it and held at this temperature. To release the stored energy, the PCM is cooled below its crystallization temperature to discharge it and below the crystallization temperature until charged again. Abhat [36] introduced thermal cycling (Figure 5.3b) as suitable exposure type for stability investigations on PCMs. This exposure type is especially crucial for salt hydrates. Due to incongruent melting (the dehydration of the salt hydrate equals melting thermodynamically) and resulting differences in density, phase segregation occurs after various thermal cycles which decreases the storage capacity [2]. Whereas polymeric materials are not susceptible to phase segregation, they are susceptible inter alia to degradation upon thermal and thermo-oxidative loads. Associated alterations of the polymer's morphology can also affect the storage capacity. Consequently the thermal energy input and not the phase change per se constitutes the highest load on a polymeric PCM. Thus, the

stability investigations within the present study covered both, thermal cycling (schematic given in Figure 5.3b) and the application of a static thermal load above the material's melting temperature (schematic given in Figure 5.3c). The static thermal loads represent the isothermal segments between the charging and the discharging of the PCM.
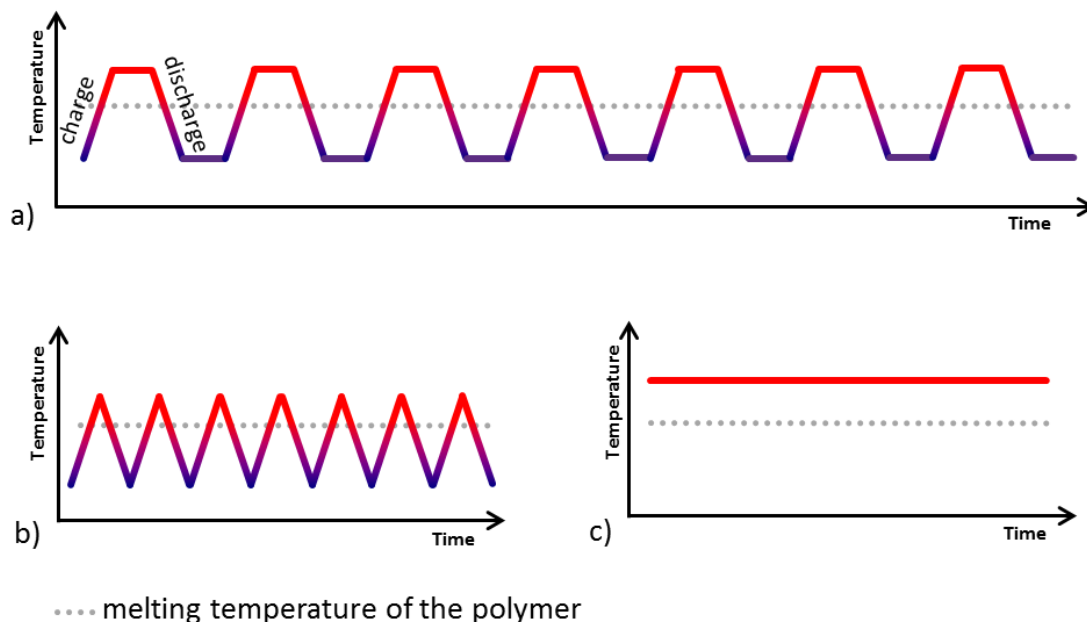

Figure 5.3: a) effective thermal load on a PCM; PCM temperature evolution over time during b) thermal cycling and c) static thermal exposure above the melting temperature.

5.5.1. Experimental

The materials for the application-oriented stability investigations were chosen based on the selection criteria discussed in 5.4, i.e. maximum ΔH_M and differing melting temperature ranges (for different fields of application). The identified polymers types of primary interest were PE and POM due to their high ΔH_M and different polyamides due to their higher melting temperature ranges. The selected polymer grades (HDPE, POM-H, POM-C, PA 4.6 and PA 6) and the applied exposure parameters are listed in Table 5.2. The short-term stability investigations were done to assess the polymers' sensitivity towards degradation and to identify the prevalent degradation mechanisms in order to optimize the polymer's long-term stability for the desired application as PCM. The granules for the thermal cycling were directly taken from the (vacuum-) sealed bags and were used as received without any pretreatment. In order to avoid hydrolysis the PA 6 granules were predried for 4 h at 80 °C in a vacuum oven VD23MI (Binder GmbH,

Tuttlingen, DE) prior to the exposure to static thermal load. HDPE and POM-C granules were exposed to static thermal load without predrying.

Table 5.2: The polymer grade, $T_{ThCstart}$ (starting temperature of the thermal cycle), T_{ThCend} (end temperature of the thermal cycle), number of the applied thermal cycles, T_{Stat} (exposure temperature of static thermal load) and maximum static exposure time of the application-oriented stability investigations.

Polymer grade	Thermal cycling				Static thermal load	
	$T_{ThCstart}$ [°C]	T_{ThCend} [°C]	Cycle quantity	Atmosphere	T_{Stat} [°C]	Max. exposure time [h]
HDPE7	105	150	500	Nitrogen	160	360
POM-H3	100	190	100	Nitrogen	-	-
POM-C5	100	190	500	Nitrogen	190	360
PA4.6-1	225	305	300	Nitrogen	-	-
PA6-4	153	230	500	Nitrogen	250	360

The thermal cycling enclosed the melting and crystallization peaks of the polymer (Figure 5.3b) and was done under nitrogen atmosphere on a DSC1 (Mettler Toledo, Greifensee, CH). A sample of 10 mg was taken from the polymer granules and placed in a 40 µl aluminum crucible. The thermal cycling consisted of two phases. First the sample was heated from ambient temperature to the start temperature of the thermal cycle $T_{ThCstart}$ with a constant heating rate of 10 K/min. After a short equilibration time of 1 min, the sample was heated to the end temperature of the thermal cycle T_{ThCend} with a constant heating rate of 10 K/min. After a short equilibration time of 1 min, the sample was then cooled to $T_{ThCstart}$ with a constant cooling rate of -10 K/min to complete the thermal cycle ($T_{ThCstart}$ and T_{ThCend} are listed in Table 5.2). After selected cycles, the thermo-physical properties of the PCM were determined according to the procedure described in 5.4. $T_{ThCstart}$, T_{ThCend} and the number of applied thermal cycles are listed in Table 5.2.

The materials for the exposure to static thermal load above the polymer's melting temperature (Figure 5.3Figurec) were selected based on the results from the thermal cycling. Thus, HDPE, PA 6 and POM-C were chosen.

About 100 g of granules of HDPE and PA 6 were placed in large aluminum crucibles (ø=80 mm; h=25 mm) in a convection oven Heraeus® TK 6060 (Thermo Fisher Scientific Inc., Waltham, US) in air. The static exposure temperature T_{Stat} ($\approx T_{Mpeak}$ + 30 °C of the according polymer grade) and the maximum exposure time of the static thermal loads are listed in Table 5.2. The sampling was done after 120 h, 240 h and 360 h. After cooling at

ambient temperature, the specimen's weight was determined. The specimens exhibited a rather cylindrical shape with a diameter of 80 mm according to the aluminum crucible. The height however varied between 15 and 22 mm due to uneven shrinkage during the cooling. The cylindrical HDPE and PA 6 specimens were cut in half with a specimen saw Diadisc 500 (MUTRONIC Praezisionsgeraetebau GmbH & Co.KG, Rieden am Forggensee, DE). Large microtome slides with a thickness of 500 µm were extracted parallel to the specimen surface with a rotary microtome Reichert Jung (Leica Microsystems GmbH, Wetzlar, DE). Samples for DSC measurements were extracted carefully with a blade from these surface microtome slides and from the specimen bottom. The sample weight ranged between 5 and 6 mg. The thermo-physical properties of the statically exposed specimens were determined by means of DSC according to the procedure described in 5.4. The presented data represent the average of three measurements. The morphological characteristics of the exposed specimens were investigated in detail by means of Fourier-transform infrared (FTIR) spectroscopy. FTIR was applied on the surface and on the bottom of the cylindrical specimens. Therefore, a piece of the specimen center with the dimensions of 8 mm * 20 mm * the specimen height (which was about 15 mm in the specimen center) was extracted. The surface of the specimen bulk which was used for the FTIR measurements was smoothed and flattened with a rotary microtome RM2255 (Leica Microsystems GmbH, Wetzlar, DE). FTIR spectra were recorded with a fully automated stand-alone FTIR microscope Lumos (Bruker Corporation, Billerica, US) in Attenuated Total Reflection (ATR) mode with a germanium crystal at a resolution of 4 cm^{-1} with a total of 64 scans. The spectra were recorded in the wavelength range between 4000 cm^{-1} and 600 cm^{-1}. Three spectra of each specimen surface were recorded in distances of several mm. Three spectra of the specimen bulk were recorded: the first one was recorded in the middle of the bulk specimen (ca. 8 mm underneath the surface), the second was recorded 3 mm further towards the bottom and the third was recorded another 3 mm further towards the bottom (2 mm above the specimen bottom). The last spectra will be used as representative spectrum and will be referred to as the spectrum of the "specimen bottom". Spectra of the non-exposed materials were recorded from as-received polymer granules.

About 100 g of granules of POM-C were placed in large aluminum crucibles (ø=80 mm; h=25 mm) and also in sealed cylindrical metal containers (ø=60 mm; h=140 mm) in order to impede depolymerisation to formaldehyde and the accompanied loss of storage capacity. Both set-ups were placed in a convection oven Heraeus® TK 6060 (Thermo Fisher Scientific Inc., Waltham,

US) in air. The static exposure temperature T_{Stat} ($\approx T_{Mpeak}$ + 30 °C of the according polymer type) and the maximum exposure time of the static thermal loads are listed in Table 5.2. The sampling was done after 8 h, 16 h, 24 h and 32 h for the POM-C in the aluminum crucible and after 120 h, 240 h and 360 h for the POM-C in the sealed metal container. After cooling at ambient temperature, the specimen's weight was determined. After 120 h of exposure in the sealed metal container, DSC-samples were taken from the specimen surface and DSC-measurements were conducted according to the procedure described in chapter 2. After 360 h of exposure, the specimen was liquid at ambient temperature. Both specimens were analyzed by means of FTIR spectroscopy. The FTIR spectra of the specimens of 120 h (spectrum recorded from the specimen surface) and 360 h of exposure were recorded with a FTIR-spectrometer Vertex 70 (Bruker Corporation, Billerica, US). The spectra were recorded in ATR mode with a germanium crystal at a resolution of 4 cm^{-1} with a total of 64 scans in the wavelength range between 4000 cm^{-1} and 400 cm^{-1}. The liquid specimen was additionally analyzed via Gas Chromatography Mass Spectroscopy (GC-MS) with GCMS-QP2010 Plus (Shimadzu Corp., Kyoto, JP) which was equipped with an auto injector AOC-20i. The GC-MS was provided with a Optima-5-Accent-0.25 µm fused silica capillary column. The liquid specimen was diluted 1:1 with dichloromethane. The testing parameters of the GC-MS measurement are given in Table 5.3.

Table 5.3: Testing parameters of the GC-MS measurement. Gas chromatography: injection temperature, injection mode, split ratio, start temperature, heating rate, end temperature, sample volume. Mass spectroscopy: ion source temperature, interface temperature, solvent cut time and acquisition mode.

Gas chromatography		Mass spectroscopy	
Injection temperature	180 °C	Ion source temperature	300 °C
Injection mode	Split	Interface temperature	300 °C
Split ratio	1.0	Solvent cut time	0 min
Start temperature	60 °C – 4 min	Acquisition mode	Scan (m/z 41 – m/z 600)
Heating rate	180 °C – 7 min		
End temperature	10 °C/min		
Sample volume	1.5 µl		

5.5.2. Results and discussion

5.5.2.1. HDPE

In Figure 5.4 the effect of thermal cycling in nitrogen atmosphere on ΔH_M and the sample weight of HDPE is depicted. After 500 thermal cycles in nitrogen atmosphere, the thermo-physical properties (ΔH_M and melting temperature range) and the weight of the polymer were not altered.
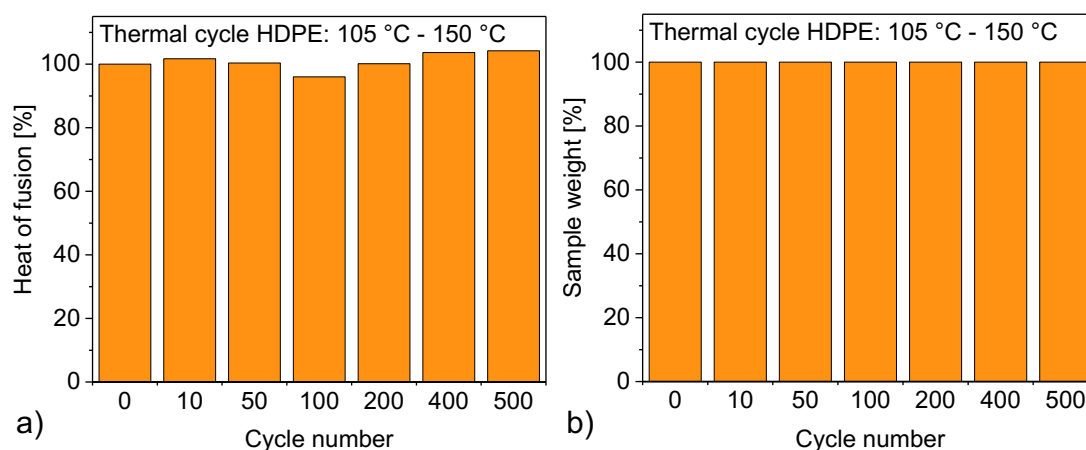

Figure 5.4: .Thermal cycling was applied on the HDPE in nitrogen atmosphere in the DSC: a) the heat of fusion and b) the sample weight for different numbers of thermal cycles. The thermo-physical properties and the sample weight remained unaffected after 500 thermal cycles.

In Figure 5.5 cross-sections of the HDPE specimens which were exposed to static thermal load at 160 °C in air are presented. The static thermal load yielded a discoloration of the specimen surface, whereas the specimen bulk seemed to be unaffected. The discoloration indicated thermo-oxidative degradation. The extent of surface discoloration increased with increasing exposure time. On the surface of the specimen which was exposed for 360 h, dark spots were ascertained. These were attributed to acidic catalyst residues which acted as aging accelerators [22]. Hydrotalcite-based antacids, calcium stearate and zinc stearate are usually applied as acid scavengers for the stabilization of commercially available polyolefins to overcome this accelerating effect of catalyst residues [23].

Figure 5.5: Cross sections of the HDPE specimens after 120 h, 240 h and 360 h of static thermal exposure at 160 °C in air. The extent of discoloration increased with increasing exposure time. Dark spots on the surface were attributed to accelerated aging caused by catalyst residues.

In Figure 5.6 the ΔH_M at the top and the bottom of the HDPE specimens which were exposed to static thermal load at 160 °C for various times are presented. ΔH_M of the specimen surface decreased from 224 J/g to 73 J/g (33 %), 71 J/g (32 %) and 53 J/g (27 %) after 120 h, 240 h and 360 h of exposure, respectively. The melting temperature range changed significantly (125 °C-142 °C for the unexposed HDPE; -2 °C-88 °C after 360 h of static thermal load at 160 °C). On the specimen bottom, ΔH_M and the melting temperature range were unaffected by the exposure to static thermal load. Also the sample weight remained unchanged after 360 h of exposure to static thermal load at 160 °C.
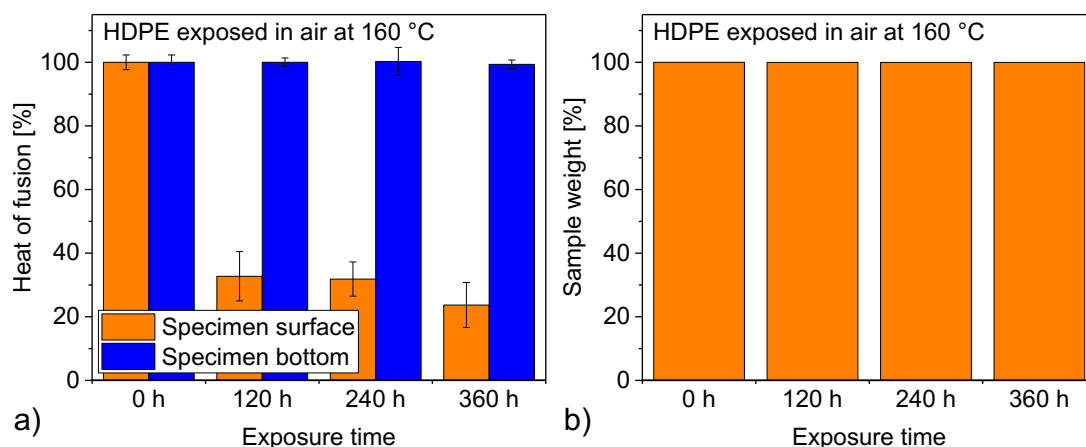

Figure 5.6: A static thermal load of 160 °C was applied on the HDPE in air: a) the heat of fusion (ΔH_M) of the HDPE specimens after various exposure times; samples were taken from the specimen surface and the specimen bottom; ΔH_M of the specimen surface was strongly affected by thermo-oxidative degradation, whereas ΔH_M of the specimen bottom remained unaffected. b) the sample weight of the HDPE specimens after various exposure times; it remained unchanged.

FTIR spectra recorded from the surface of the exposed HDPE specimens could not be normalized due to the high extent of aging where all absorption

bands of the spectra were affected. However, because of the identical specimen preparation and the automated procedure of the ATR crystal (internal pressure control), a qualitative comparison between the spectra was still possible. FTIR spectra of the unexposed granule and the specimen bulk were normalized with the absorption band at 2850 cm^{-1}, which represents the CH$_2$-stretching vibration [24]. The exposure to static thermal load did not alter the IR absorbance at the bottom of the HDPE specimen. This spectrum is therefore not displayed. The spectrum recorded from the unexposed granule and representative spectra recorded from the surface of specimens exposed to static thermal load of 160 °C at various times are displayed in Figure 5.7. Compared to the unexposed granule, an increase of the absorption band at 3404 cm^{-1}, which represents the stretching vibration of hydroperoxides, an increase of the absorption bands in the wavenumber range from ~1780 cm^{-1} to 1700 cm^{-1}, which represent the stretching vibrations of carbonyl groups, an increase of the absorption band at 1171 cm^{-1}, which represents the C-O-stretching vibration of the ester and an increase in the absorption bands in the wavenumber range from ca. 970 cm^{-1} to 880 cm^{-1}, which represent the deformation vibrations of unsaturated compounds, a decrease of the absorption bands at 2915 cm^{-1} and 2850 cm^{-1}, which represent the CH$_2$-stretching vibrations and changes in the absorption bands in the wavenumber range from ca. 1480 cm^{-1} to 1200 cm^{-1}, which represent the CH$_2$-deformation vibrations, were ascertained [24-28] at the specimen surface. These findings were in good agreement with the thermo-oxidative degradation mechanism and the resulting oxidation products for PE given in [26].

The absorption band at 3404 cm^{-1} (hydroperoxides) increased until 120 h of exposure at 160 °C and decreased after 240 h which was attributed to the unstable character of hydroperoxides. The decrease of the absorption bands at 2915 cm^{-1} and 2850 cm^{-1} (CH$_2$) was attributed to the degradation of the HDPE backbone which indicated a high extent of thermo-oxidative degradation. The change of the absorption bands of carbonyl vibrations (1777 cm^{-1}, 1734/1731 cm^{-1}, 1712 cm^{-1}) is depicted in more detail in Figure 5.8. As described in [26,27], the thermo-oxidative degradation of PE yields inter alia lactones (1777 cm^{-1}), esters/aldehydes (1734/1731 cm^{-1}), which are rather difficult to distinguish with a spectral resolution of 4 cm^{-1}, and carboxylic acids (1712 cm^{-1}) as oxidation products. Most likely, the broad absorption band between 1780 cm^{-1} and 1700 cm^{-1} represents an overlap of these oxidation products. Except for the specimen exposed for 120 h at 160 °C, the main absorption band of carbonyl groups was the one at 1734/1731 cm^{-1} which corresponds either to the formed ester or the formed

aldehyde groups. This absorption band was probably mainly caused by the ester groups because a second absorption band at 1171 cm^{-1} (Figure 5.7), which represents the C-O stretching vibration of esters, was ascertained. Both absorption bands which correspond to the ester groups increased with increasing exposure time. The broad absorption band between 1700 cm^{-1} and 1600 cm^{-1} resulted from the overlapping of several absorption bands. According to [26,27], the absorption bands correspond to unsaturated compounds (the presence of these unsaturated compounds was further proved by the increase of the absorption bands in the wavenumber range from ~ 970 cm^{-1} to 880 cm^{-1}, which represent the deformation vibrations of the unsaturated compounds). However, these compounds proved to be thermally less stable than the simultaneously formed carbonyl groups (lactones, esters, aldehydes and carboxylic acids) as this broad absorption band decreased after 120 h of exposure at 160 °C. The oxygen attack during radical oxidation (which finally leads to the formation of the carbonyl groups) occurs at the methylene units with thermo-labile defects such as vinyls for PE [26]. The activation-energy of the according C-H bonds is lowered due to the inductive effect of the unsaturated group and the H-atom can be abstracted more easily (first step of the thermo-oxidation). Therefore, the initial content of unsaturated groups in PE exhibits a great impact on the oxidation rate of PE [26,29].
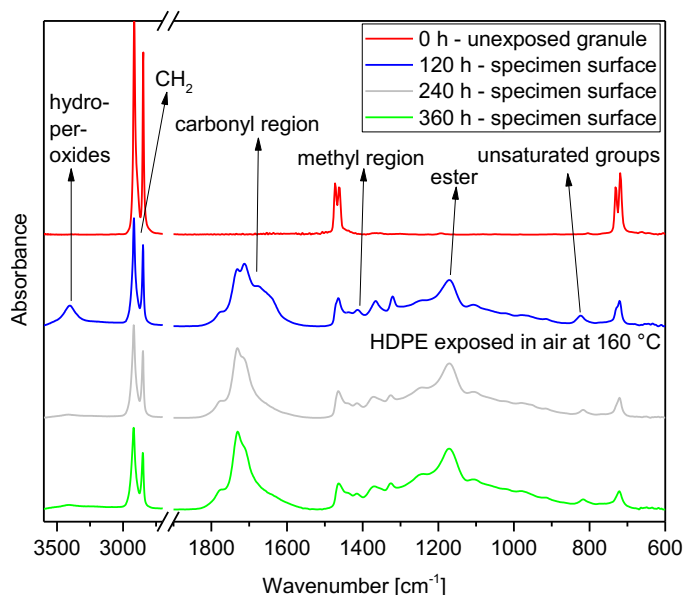

Figure 5.7: FTIR spectra from the HDPE specimens prior and after the exposure to static thermal load of 160 °C at various times. Oxidation products (hydroperoxides, carbonyl groups and unsaturated groups) and a deterioration of the HDPE backbone due to thermo-oxidation were ascertained.

In Figure 5.8 also the absorption bands which correspond to the CH_2-bending vibrations of the crystalline (1474 cm^{-1}) and the amorphous phase (1464 cm^{-1}) [25] of the PE specimens exposed to 160 °C for various times are depicted. The absorption band which represents the crystalline phase, decreased with increasing exposure time. To a smaller extent also the absorption band which represents the amorphous phase decreased with increasing exposure time (probably due to the high extent of degradation). This was in good agreement with the loss of ΔH_M as shown in Figure 5.6 where ΔH_M was decreased to 27 % after 360 h of exposure to static thermal load at 160 °C. However, an increase in ΔH_M is typically observed at the beginning of the thermo-oxidation due to higher chain mobility caused by chain scission [27]. In the present study, however, this step in thermo-oxidation could not be detected probably due to the comparably high exposure temperatures above T_{Mpeak} and/or the long exposure times (minimum exposure time of 120 h) and the accompanied fast degradation of the HDPE. The resulting high extent thermo-oxidative degradation is indicated by the degradation of the CH_2-backbone (decrease of the absorption bands at 2915 cm^{-1} and 2850 cm^{-1}, which represent the CH_2-stretching vibrations).
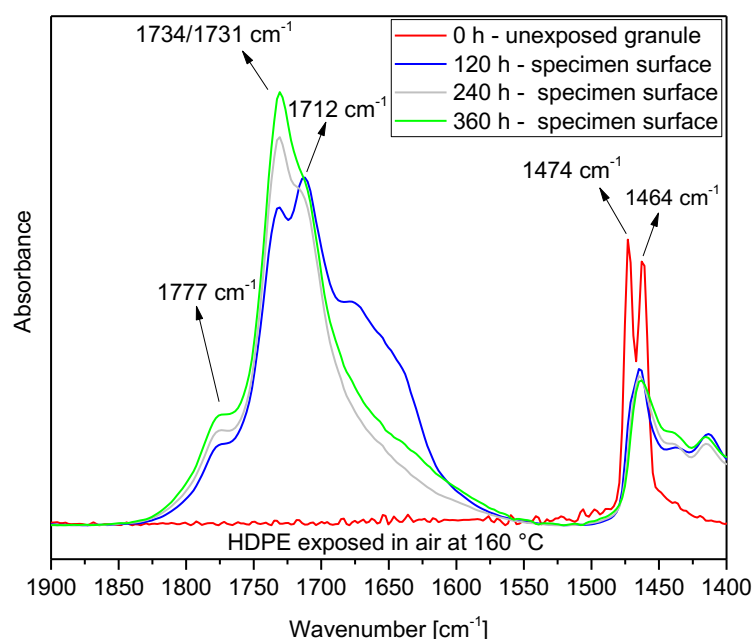

Figure 5.8: FTIR spectra of the HDPE specimens prior and after the exposure to static thermal load at 160 °C in air after various exposure times. The absorption bands, which represent the stretching vibrations of different carbonyl groups (ca. 1780-1710 cm^{-1}) and the absorption bands, which represent the CH_2-bending vibration of the crystalline and amorphous (1474 cm^{-1} and 1464 cm^{-1}) phase were changed due to thermo-oxidation.

The discoloration differences within the respective HDPE specimens (Figure 5.5) as well as the DSC- and FTIR investigations (Figure 5.6 and Figure 5.7) revealed that thermo-oxidative degradation was only present at the specimen surface. This was attributed to diffusion limited oxidation (DLO). Due to DLO, an oxidation profile in depth develops due to the balance of the oxidation rate and the oxygen diffusion rate of the polymer [30,31]. The highest extent of oxidation takes place at the surface and then the oxidation rapidly decreases non-linearly when going deeper into the specimen bulk. The specimen surface therefore acted as "oxygen scavenger" for the specimen bulk. This further indicates that the surface undergoes thermo-oxidative degradation whereas the specimen bulk undergoes at most a thermal-induced degradation. However, the thermo-physical characteristics of the specimen bulk were not affected by the exposure to static thermal load. Therefore almost the entire storage capacity was maintained which revealed a great potential of HDPE as polymeric PCM. However, due to the combination of thermo-oxidative and thermal aging mechanisms caused by DLO and the bulky specimen dimensions, further application-oriented stability investigations should be addressed in future studies in order to predict the overall long-term stability.

5.5.2.2. POM

In Figure 5.9 the effect of thermal cycling in nitrogen atmosphere on ΔH_M and the sample weight of POM-H and of POM-C are depicted. After 50 thermal cycles, a significant decrease in ΔH_M and the sample weight was ascertained for the investigated POM-H. After 100 exposure thermal cycles, the crucible was empty, which indicates a complete degradation of the polymer.

Kern and Chedron [32] identified five degradation mechanisms for POM-H: depolymerisation, auto-oxidative chain scission, degradation due to secondary products of the auto-oxidation, thermal degradation and hydrolysis and acidolysis. The main degradation mechanism, however, is the depolymerisation to the gaseous formaldehyde [33] as shown in Figure 5.10. The depolymerisation starts at the thermo-labile hemiacetal end group which is a remnant of the monomer (formaldehyde or trioxane). It then propagates along the polymer chain ("unzipping" of the polymer). Via the "end-capping" of the labile hemiacetal hydroxyl end groups (acetylization), POM-H becomes more stable and can be processed [22]. However, also random chain scission occurs during thermal degradation [33]. The depolymerisation starts at the newly formed chain end (which is not acetylized) and propagates along the polymer chain. This explains the rapid decrease in ΔH_M and the sample weight of the investigated POM-H grade after 50 thermal cycles.

Consequently POM-H is not suitable as PCM and was therefore not exposed to static thermal load above its melting temperature.
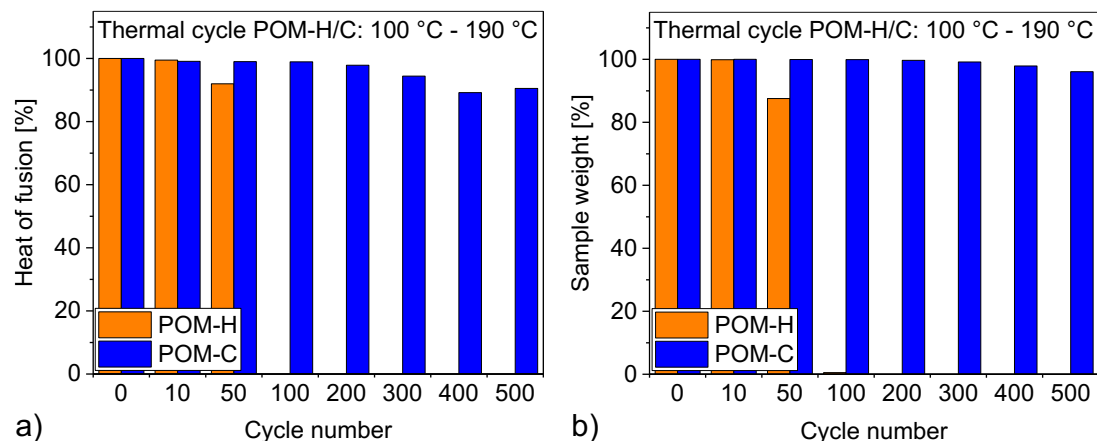

Figure 5.9: Thermal cycling was applied on the POM-H and on the POM-C in nitrogen atmosphere in the DSC: a) the heat of fusion and b) the sample weight over the cycle number. Whereas the POM-H did not prove to be thermally stable (complete loss of heat of fusion and sample weight after 100 thermal cycles), the thermo-physical properties and the sample weight of the POM-C were only changed moderately after 500 cycles.
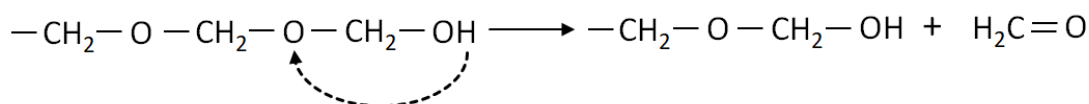

Figure 5.10: Main degradation mechanism of POM-H: depolymerisation to formaldehyde. The degradation starts at the labile hemiacetal hydroxyl end group and propagates along the polymer chain. It is therefore referred to as "unzipping".

For the investigated POM-C grade, only a minor decrease in ΔH_M of (-10 %; 180 J/g for the unexposed sample; 163 J/g after 500 thermal cycles) and in the sample weight of (-4 %; 9.78 mg for the unexposed sample; 9.39 mg after 500 thermal cycles) was detected after 500 thermal cycles in nitrogen atmosphere. This is in good agreement with the work of Kern [34] who showed that degradation mechanisms which occur in POM-H, also occur in POM-C but to a smaller extent. In contrast to the POM-H, POM-C is polymerized with a small amount of a second monomer which contains adjacent –C–C– bonds [35]. Usually cyclic ethers like ethylene oxide, 1,3-dioxolane or 1,3-dioxepane are used as comonomers [36]. In case of random

chain scission, the depolymerisation propagates only until reaching a –C–C– bond. Therefore, the investigated POM-C grade was more stable during the thermal cycling than the POM-H grade. During the thermal degradation of POM-C, the major degradation product is gaseous formaldehyde, which is highly carcinogen. Moreover, to a much smaller extent carbon dioxide, fragments of formic acid, trioxane and methoxy oligomers are formed [36]. To observe the extent of depolymerisation an exposure to static thermal load at 190 °C was applied in steps of 8 h. In Figure 5.11a, the sample weight of the POM-C specimens after various exposure times is presented. The sample weight decreased steadily with increasing exposure time. After 32 h of exposure at 190 °C in air, the sample weight was reduced by 1.07 %. In Figure 5.11b, a picture of the melted specimen after 32 h of exposure to static thermal load at 190 °C in air is given. On the specimen surface, numerous bubbles were present, which were attributed to gaseous degradation products.
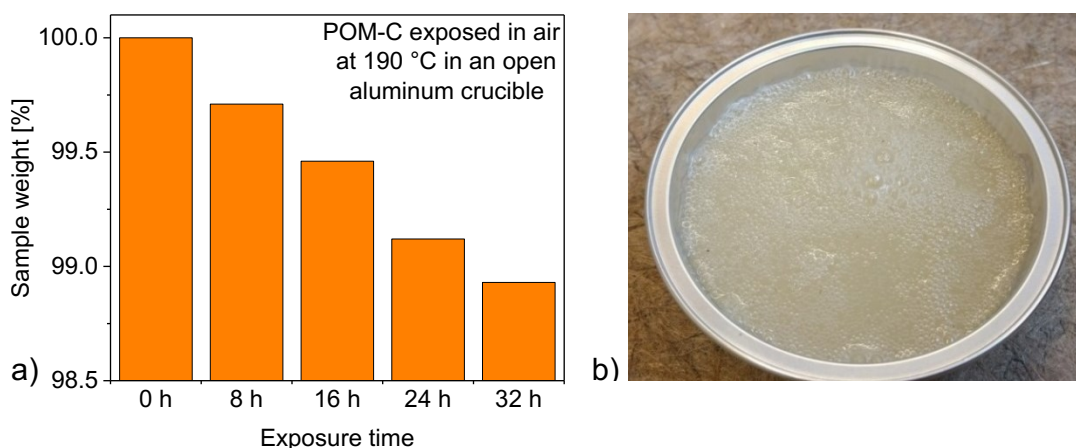

Figure 5.11: A static thermal load of 190 °C was applied on the POM-C specimens in an open aluminum crucible in air: a) the sample weight of the POM-C specimen after various exposure times. The sample weight was reduced steadily with increasing exposure times due to depolymerisation of the POM-C to formaldehyde by 1.07 % after 32 h of exposure. b) The melted POM-C specimen after 32 h of exposure. Gaseous degradation products caused the bubbles at the specimen surface.

In order to potentially prevent depolymerisation and the accompanied loss of storage capacity, the POM-C grade was exposed in a sealed metal container to establish a closed environment. After 120 h of exposure to static thermal load at 190 °C, the sample weight was reduced by only 0.04 % (in the open aluminum crucible the specimen weight was reduced by 0.29 % after 8 h of

exposure). The sample showed a moderate discoloration which was equally spread within the specimen. However, ΔH_M remained unchanged. Also the recorded FTIR spectra did not reveal any changes (representative spectrum given in Figure 5.12a) of the molecular structure. After 360 h of exposure, however, the sample weight was reduced by 0.49 % and the specimen represented a fluid after cooling to ambient temperature. Furthermore, a distinct discoloration to dark brown had taken place. Instantaneously after opening the sealed metal container, the liquid specimen bubbled and gas escaped. After a couple of hours, the bubbling stopped. A representative FTIR spectrum recorded from the liquid specimen is given in Figure 5.12a. It differs strongly from the FTIR spectra recorded from the unexposed granule and the specimen exposed for 120 h which are also displayed in Figure 5.12a. The GC-MS diagram of the fluid is depicted in Figure 5.12b. The numerous peaks indicate numerous degradation products. Referring to the NIST Standard Reference Database, three peaks were correlated to a composition with an accordance greater than 90 % (chemical structures are indicated in Figure 5.12b). These were bis(2-hydroxyethyl) ether, methyl methoxyacetate and ethane, 1-methoxy-2-(methoxymethoxy)-1-methoxy-2-(methoxymethoxy) ethane. The correlations suggest that the main characteristic chemical groups present in the degradation products are acetal groups, carbonyl groups, ether groups, ester groups, hydroxyl (alcohol) groups and CH_2-groups. These findings were are in good agreement with the FTIR spectra, where a broad absorption band in the wavenumber range from $3700~cm^{-1}$ to $3000~cm^{-1}$, which represents the OH-stretching vibration, several absorption bands in the wavenumber range from $3000~cm^{-1}$ to $2700~cm^{-1}$, which represent the CH_2-stretching vibrations, a broad absorption band in the wavenumber range from $1800~cm^{-1}$ to $1600~cm^{-1}$, which represents the stretching vibrations of the carbonyl groups, and several sharp absorption bands in the wavenumber range from $1200~cm^{-1}$ to $900~cm^{-1}$, which represent CO-stretching vibrations of the acetal, alcohol, ether and ester groups, were ascertained [24]. However, a quantitative analysis of the degradation products was not conducted. Nonetheless, the FTIR- and GC-MS measurements revealed that only short fragments of the initial polymer chains were present after the exposure to static thermal load at 190 °C (which explains the liquid character of the specimen). Therefore chain scission must have occurred. In the presence of air, formaldehyde oxidizes to carbon dioxide, water and formic acid. As POM is sensible towards acidolysis, the formic acid probably accelerated the degradation of the POM-C as described by Blyumenfield et al. [37].
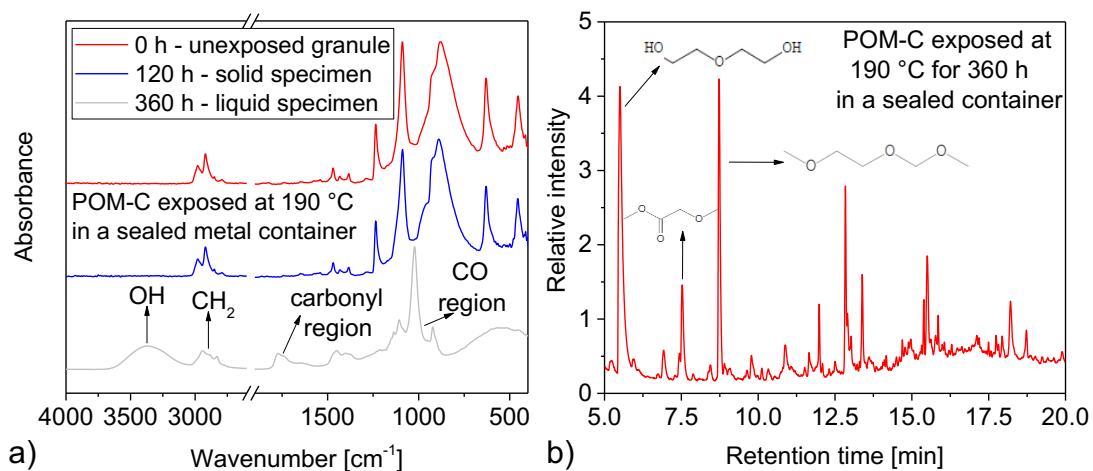
Figure 5.12: a) FTIR spectra from the POM-C specimens prior and after the exposure to static thermal load of 190 °C in a sealed metal container at various exposure times. After 360 h of exposure, the specimen was liquid at ambient temperature and strongly discolored. b) GCMS diagram of the specimen after 360 h of exposure. Numerous different substances are present as indicated by the numerous peaks. Three peaks were correlated to the compositions as given in the chemical structures.

Even though, the main degradation mechanism of POM-C (i. e. depolymerisation) was impeded via the application of a sealed exposure container and the thermo-physical characteristics of the POM-C grade did not change until 120 h of exposure, the polymer did not prove to be stable for longer exposure times as its polymer chains were fragmented down to numerous smaller organic compositions due to chain scission. Therefore, the POM-C is no candidate polymeric PCM.

5.5.2.3. PA 4.6 and PA 6

In Figure 5.13 the effect of thermal cycling in nitrogen atmosphere on ΔH_M and the sample weight of PA 4.6 and PA 6 are depicted. The measurements were stopped after 300 thermal cycles for the investigated PA 4.6 grade due to the significant decrease of ΔH_M and the sample weight. ΔH_M decreased steadily with increasing thermal cycles down to 18 % of the initial ΔH_M (109 J/g for the unexposed sample; 20 J/g after 300 thermal cycles). The sample weight was reduced to 70 % (10.65 mg for the unexposed sample; 7.45 mg after 300 thermal cycles). Moreover, the melting temperature range was reduced remarkably (280 °C-298 °C for the unexposed sample; 166 °C-227 °C after 300 thermal cycles).
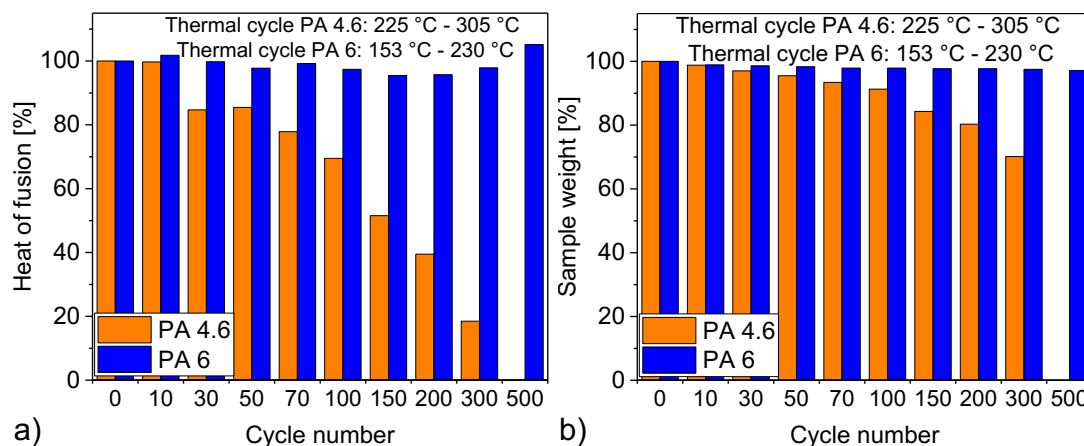
Figure 5.13: Thermal cycling was applied on the PA 4.6 and on the PA 6 in nitrogen in the DSC: a) the heat of fusion and b) the sample weight over the cycle number. Whereas the PA 4.6 did not prove to be thermally stable, the thermo-physical properties and the sample weight of the PA 6 remained rather unaffected for the 500 thermal cycles.

The changes in thermo-physical properties of PA 4.6 were attributed to thermal degradation. During the thermal degradation of aliphatic polyamides of the diacid-diamine type (only little scientific literature is available specifically about the thermal degradation of PA 4.6), intramolecular back-biting and hydrogen transfer lead to scission of the C-N bond [38]. However, also crosslinking is reported as degradation mechanism for aliphatic polyamides. Peebles and Huffman proposed a crosslinking mechanism for PA 6.6 [39] (schematic given in Figure 5.14). A decrease in crystallinity was observed for PA 6.6 during its thermal degradation and it was attributed to crosslinking by Hollande and Hay [38]. Therefore, the detected decrease in ΔH_M of the investigated PA 4.6 grade was also attributed to crosslinking.
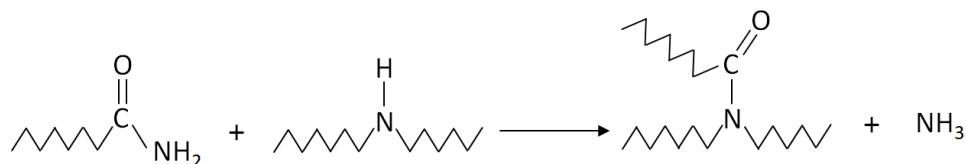

Figure 5.14: Crosslinking mechanism of PA 6.6 as proposed by Peebles and Huffman [39].

The detected weight loss indicated the occurrence of gaseous degradation products during the thermal degradation. This was in good agreement with the work of Pramoda et al. [40] and Herrera et al. [41] who identified H_2O, CO_2, NH_3, HCN and several olefinic compounds as evolving gases during the

thermal degradation of aliphatic polyamides. Since the investigated PA 4.6 grade did not prove to be thermally stable during the applied thermal cycling, and consequently is not suitable as PCM, the material was not exposed to static thermal load above its melting temperature.

For the investigated PA 6 grade, a moderate increase in ΔH_M between 300 and 500 cycles was observed. This was attributed to a higher chain mobility and an accompanied increased crystallizability caused by chain scission during thermal degradation and was also observed for PA 6 by Holland and Hay [38] during the exposure to static thermal load at 280 °C. The thermal cycling did not affect the melting temperature range of the investigated PA 6 grade. Interestingly, the sample exhibited a distinct brown discoloration after 500 thermal cycles.

In Figure 5.15 cross-sections of the PA 6 specimens which were exposed to static thermal load at 250°C in air are presented. The static thermal load yielded a discoloration (initial granulate color white), whereas the effect was stronger pronounced on the surface than within the bulk. Moreover, the sample surface exhibited several cracks. However, no effect of the exposure time on these effects was ascertained. Merely the sample which was exposed for 360 h showed an additional cavity underneath the surface. According to literature, the discoloration indicates a thermo-oxidative material degradation [42,43].
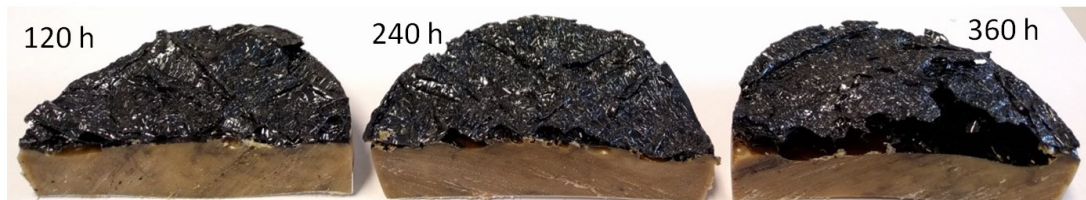

Figure 5.15: Cross sections of the PA 6 specimens after 120 h, 240 h and 360 h of static thermal exposure at 250 °C in air. The discoloration was stronger pronounced on the specimen surface and several cracks appeared. The specimen which was exposed for 360 h showed a cavity underneath the strongly degraded surface.

In Figure 5.16 the ΔH_M at the surface and the bottom of the PA 6 specimens which were exposed to static thermal load at 250 °C for various times are presented. The exposure to static thermal loads causes a distinct deterioration of the crystalline morphology of the specimen surface (ΔH_M is no longer detectable). On the specimen bottom, ΔH_M decreased merely slightly (around 9 %) after 120 h of exposure and remained rather constant after longer exposure times. The melting temperature range changed moderately (207 °C-226 °C for the unexposed sample; 198 °C-220 °C after

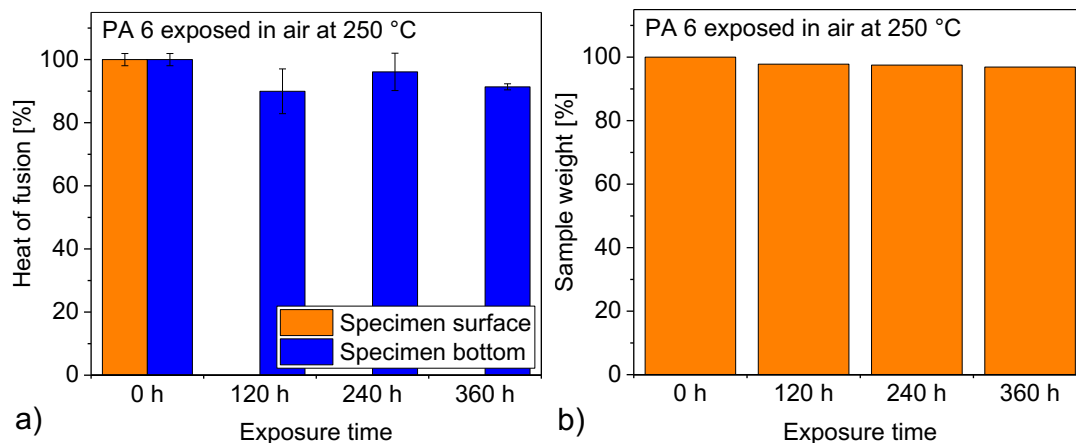360 h of static thermal load at 250 °C). The overall sample weight decreased by 3.1 % after 360 h of exposure.

Figure 5.161: A static thermal load of 250 °C was applied on PA 6 in air: a) the heat of fusion (ΔH_M) of the PA 6 specimens after various exposure times. Samples were taken from the specimen surface and the specimen bottom. ΔH_M of the specimen surface was completely lost by thermo-oxidative degradation, whereas ΔH_M of the specimen bottom was only reduced by 9 % after 120 h of exposure to static thermal load. b) the sample weight of the PA 6 specimens after various exposure times. After 360 h of exposure, the sample weight was reduced by 3.1 %.

FTIR spectra recorded from the specimen surface did not show sharp and typical absorption bands, but rather broad overlapping absorption bands ranging over up to 2000 cm^{-1}. This indicated an extensive material degradation. Hence, the spectra are not displayed. Representative FTIR spectra which were recorded from the specimen bottom are displayed in Figure 5.17. The PA 6 spectra were normalized with the absorption band at 1462 cm^{-1}, which corresponds to the CH_2 scissors vibration since this band is not sensitive to oxidation [30,42]. Compared to the unexposed PA 6, a moderate increase in the absorption bands in the wavenumber range from 1780 cm^{-1} to 1700 cm^{-1}, which represent the stretching vibrations of carbonyl groups [42], an increase in the absorption band at 688 cm^{-1}, which represents the COOH deformation vibration [44], changes in the absorption bands in the wavenumber ranges from 1480-1360 cm^{-1} and 975-850 cm^{-1}, which represent the CH_2-/amide-scissors and wag vibrations [45-47] and the CO-NH in plane vibrations of the crystalline α- and γ-phase [48], were ascertained.
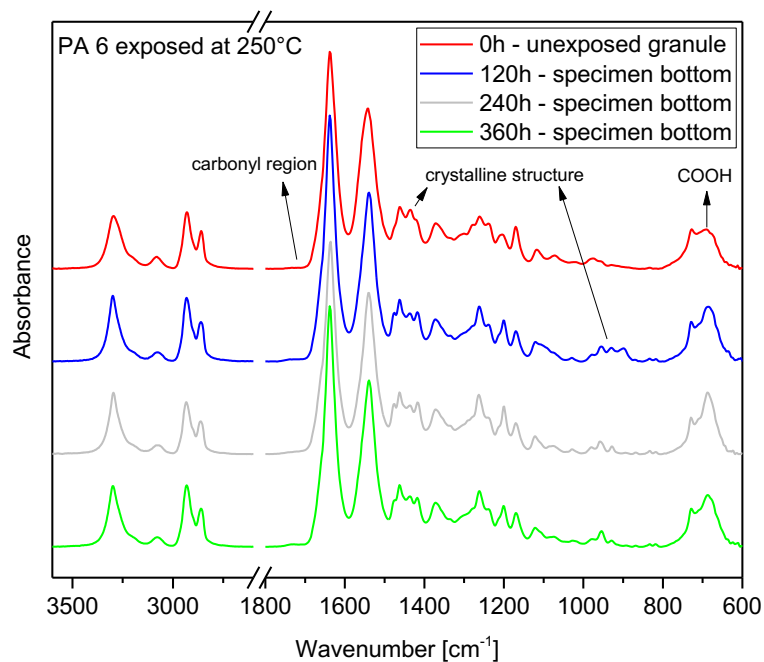
Figure 5.17: FTIR spectra of the PA 6 specimens prior and after the exposure to static thermal load of 250 °C in air at various exposure times. Spectra were recorded from the specimen bottom. Oxidation products (hydroperoxides and carbonyl groups) due to thermo-oxidation and differences in the crystalline phases due to differences in the thermal history of the polymer were ascertained.

The change of the absorption bands of carbonyl vibrations is depicted in more detail in Figure 5.18a. The thermo-oxidative degradation of PA 6 yields inter alia carboxylic acids (1750 cm^{-1}), esters (1735 cm^{-1}), aldehydes (1725 cm^{-1}) and ketones (1715 cm^{-1}) as oxidation products [30,42]. Most likely, the broad absorption band between 1780 cm^{-1} and 1700 cm^{-1} represents an overlap of these oxidation products. As shown by Dong et al. [42], also COOH groups represent possible oxidation products. This was in good agreement with the increase of the absorption band at 688 cm^{-1}, which represents the COOH-deformation vibration [44]. Simultaneously, the absorption band which corresponds to the OH-stretching vibration at ~ 3330 cm^{-1} should therefore be increased [24]. However, it was most likely overlapped by the significant absorption band at 3300 cm^{-1} which represents the N-H stretching vibration [24]. Thus, the two absorption bands could not be distinguished.
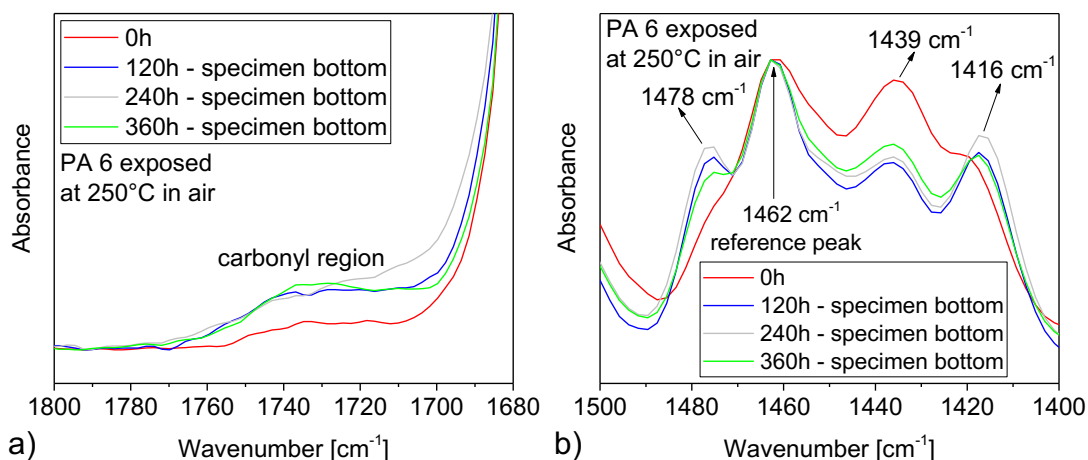
Figure 5.18: FTIR spectra of the PA 6 specimen prior and after the exposure to static thermal load at 250 °C in air: a) absorption bands in the carbonyl region (ca. 1760-1710 cm^{-1}); b) absorption bands in the methyl region corresponding to different crystalline phases (ca. 1480 -1400 cm^{-1}).

The oxygen attack during radical oxidation (which finally leads to the formation of the carbonyl groups) is selective and occurs mainly at the α-methylene [49] which is the methylene group next to the amide group (PA 6 possesses five methylene units between the amide and carbonyl group as indicated in Figure 5.19). This is attributable to the destabilizing role of the neighboring, electronegative nitrogen atom which reduces the activation energy of the C-H bond. Due to this selective oxygen attack at the α-methylene, the methylene groups of PA are less stable against thermo-oxidative degradation when compared to the methylene groups of PE. Furthermore, α-amino hydroperoxides possess high instability which is also linked to the inductive effect of nitrogen. This results in the absence of an induction period during the thermo-oxidation of aliphatic polyamides [49]. Simultaneously, the amide group causes the appealing high melting temperature range because it enables the formation of hydrogen bonds.
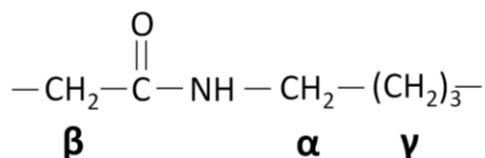

Figure 5.19: Repeating unit of PA 6. The methylene units exhibit different reactivities towards thermo-oxidation and are therefore labelled with α through γ. The oxygen attack during radical oxidation occurs mainly at the α-methylene.

In order to display the changes in the crystalline morphology of the investigated PA 6 grade upon exposure to static thermal load, FTIR spectra of the spectral region between 1500 cm^{-1} and 1400 cm^{-1} are displayed in more detail in Figure 5.18b. In general, two different crystalline structures of PA 6 usually coexist, i.e. the α-phase and the γ-phase. The γ-phase, however, is unstable and under equilibrium conditions and at ambient temperature, the crystalline structure consists only of the α-form [47]. The spectra show an increase of the absorption bands at 1478 cm^{-1} and 1416 cm^{-1}, which correspond to the α-phase CH_2 scissors vibration [45]. Simultaneously, the spectra show a decrease of the absorption band at 1439 cm^{-1}, which corresponds to the γ-phase CH_2 scissors vibration [46]. This indicated that the crystalline morphology of the specimen bulk (when cooled at ambient temperature) consisted more of the stable α-form than the unexposed granule. However, with increasing exposure time these differences in the absorption bands of the exposed and unexposed PA6, which represent the α- and γ-phase, decreased again. This indicated a continuing alteration in the crystalline morphology for the exposed PA6 specimen with increasing exposure time. Most likely, the alteration in the crystalline morphology resulted from the thermo-oxidative degradation of the polymer.

The extent of thermo-oxidative degradation was more pronounced on the specimen surface than within the bulk of the PA 6 specimen as proved by the loss of ΔH_M (Figure 5.16a) and the IR-inactivity (FTIR) on the surface. This indicated the thermo-oxidative aging phenomenon of DLO for the PA 6 specimens. The impact of DLO on the thermo-oxidation mechanism of PA 6 was examined by Gijsman et al. [30]. They investigated the influence of temperature on DLO profiles of PA 6 plaques with a thickness of up to 500 µm. At the maximum exposure temperature (180 °C), the oxidation depth was found to be ~150 µm. It did not further increase between 2 h until 16 h of exposure (maximum exposure time). Therefore, an oxidation depth close to 150 µm was expected for the present study. Interestingly, oxidation products were also detected 13 mm underneath the surface which is nearly a hundred times deeper than what Gisjman et al. discovered. The applied exposure conditions of the present study were harsher than the exposure conditions applied by Gisjman et al. (up to 360 h at 250 °C vs. up to 16 h at 180 °C). Furthermore, at 250 °C crystallites, which usually hinder oxygen diffusion into the specimen (oxygen permeates only through the amorphous phase of the polymer [22]), are in a melted state. However, one must question the applicability of DLO for the exposed PA 6 specimens of the present study because of the major differences in the maximum oxidation depths for PA 6

(13000 µm after 120 h at 250 °C for the present study vs. 150 µm after 16 h at 180 °C for [30]). Two further observations disprove the impeccable applicability of DLO for the exposed PA 6 specimens:

1. Unequally distributed discoloration patterns in the PA 6 specimen bulk: in Figure a darker discoloration of the specimen surface compared to specimen bulk was ascertained and attributed to DLO (darker discoloration = higher extent of degradation on specimen surface). However, also darker streaks were distributed unequally in the specimen bulk which cannot be explained with DLO.

2. No continuous oxidation profile from the specimen surface down to the specimen bottom: as mentioned in the preceding paragraph, an oxidation profile from the specimen surface into the specimen bulk develops due to DLO. In the present work, three spectra were recorded from each specimen starting at the specimen center and going towards the specimen bottom. According to DLO, the extent of oxidation should have declined in this order. However, this was not the case.

Therefore we suspected that another aging phenomenon additionally to DLO took place simultaneously. The molecules which caused these darker streaks must have been degraded thermo-oxidatively at the specimen surface at some point. Considering that the exposure temperature was higher than the melting temperature range of the PA 6, the specimen exhibited movability due to its melted state. Therefore, we suspected that some kind of movement of the polymer melt took place during the exposure which resulted from the combination of a minor temperature gradient in the oven and natural convection within the melted PA 6 specimen. The degraded molecules of the streaks were first thermo-oxidatively degraded at the specimen surface (and/or when cracks appeared) and were then moved into the specimen bulk due to this melt movement. Further experiments will be conducted in order to prove this hypothesis.

Nonetheless, the application-oriented stability investigations of PA 6 revealed only minor changes in the thermo-physical properties of the specimen bulk and in the specimen weight during the exposure to the static thermal load of 250 °C for up to 360 h and the majority of the polymer's storage capacity was maintained. The stability investigations therefore revealed a great potential of PA 6 as polymeric PCM. However, the combination of a high melting temperature range and a low thermo-oxidative stability (caused by the destabilizing effect of the nitrogen) minimizes the application temperature range of the polymer as PCM as depicted in Figure 5.1b. Due to the

combination of thermo-oxidative and thermal aging mechanisms caused by DLO and the fact that the specimens exhibit melt movability and surface cracking, further application-oriented stability investigations should be addressed in future studies in order to predict the overall long-term stability of PA 6.

5.6. Economic aspects of polymers as PCM

According to 5.5 HDPE and PA 6 are the most promising polymeric PCM. Additionally, 5.4 revealed the potential of PP as polymeric PCM. These polymers are widely used in the industry and show broad commercial availability. Due to their high volume use, also recyclates of these polymers are available on a regular basis. As indicated by the preceding investigations, only thermo-physical properties matter for PCM (mechanical and optical properties can be neglected). Therefore, the recyclates of HDPE, PP and PA 6 show also great potential as PCM especially in terms of economic efficiency since they typically are cheaper than the new material. In order to compare the economic efficiency of polymeric PCM from new polymer and polymeric recyclates, the storage price *SP* in €/kWh was calculated according to equation (2)

$$SP = \frac{P_M * 3600}{\Delta H_{\varnothing M}} \tag{2}$$

with P_M as the material price in €/kg and $\Delta H_{\varnothing M}$ in J/g as the heat of fusion representing the storage capacity. P_M of the new polymers and the recyclates was averaged from the price reports from April 2017 through March 2018 from Plastics Information Europe (https://pieweb.plasteurope.com). For $\Delta H_{\varnothing M}$ of the new polymers, the average value of the according polymer group was calculated from all the examined polymer grades of the group. Considering moderate thermal damage via reprocessing and thus a possible decrease of ΔH_M of the recyclates, $\Delta H_{\varnothing M}$ of the recyclates was estimated conservatively to be 90 % of the according new polymer type. The data and assumptions for the calculation of SP are listed in Table 5.4. The material designation (e.g. "rHDPE inj. moulding, grade black") was taken exactly as it appeared in the price report.

Table 5.4: The material, the designation of the material as taken from PIEWEB, the P_M (the material price) and $\Delta H_{øM}$ (the heat of fusion) as taken for the calculation of the storage price (SP) given in equation (2). The prices were taken from Plastics Information Europe (https://pieweb.plasteurope.com) from the price reports from April 2017 to March 2018. $\Delta H_{øM}$ for the new polymers was taken from the material selection in 5.4 and $\Delta H_{øM}$ for the recyclates was estimated conservatively to be 90 % of $\Delta H_{øM}$ of the according new polymer type.

Material	New polymers			Recyclates		
	Designation on PIEWEB	P_M [€/kg]	$\Delta H_{øM}$ [J/g]	Designation on PIEWEB	P_M [€/kg]	$\Delta H_{øM}$ [J/g]
HDPE	HDPE injection moulding	1.468 ± 0.010	226 ± 11	rHDPE inj. moulding, grade black	0.965 ± 0.002	204 ± 10
PP	PP homo-polymer, injection	1.338 ± 0.037	110 ± 10	rPP homo black	0.893 ± 0.002	99 ± 9
PA 6	PA 6 natural	3.209 ± 0.049	70 ± 14	rPA 6 black	2.500 ± 0.061	63 ± 13

In Figure 5.20 the SP of the different polymer types are given (the variation was calculated according to the Gaussian error propagation) and large differences in the SP between the polymer types were found. The new HDPE represented the cheapest storage material with a SP of 23 €/kWh. This resulted from the combination of an outstandingly high ΔH_M and the very low P_M of about 1.5 €/kg. The SP of the new PP was found to be 44 €/kWh, respectively. The new PA 6 represented the most expensive storage material with 164 €/kWh. Naturally, for all polymer types, the SP was decreased by applying recyclates. The SP for HDPE was reduced by 26 % to 17 €/kWh. For PP, a relative SP reduction of 27 % down to 32 €/kWh was obtained by applying a recyclate. By applying recyclate instead of new polymer, the SP of PA 6 was reduced only by a smaller extent of 13 % to 142 €/kWh. However, the lowered SP of the recyclates of PP and PA 6 could not compete neither with the SP of the new HDPE (24 €/kWh) nor with the SP of the HDPE recyclate (17 €/kWh). Thus, HDPE is the most economically efficient polymeric PCM.
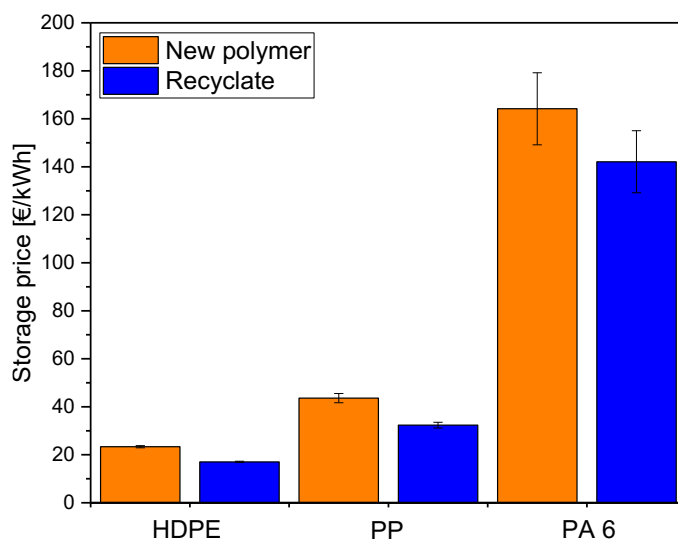
Figure 5.20: Estimation of the storage price (SP) in €/kWh of new polymers and recyclates as PCM. HDPE was by far the cheapest phase change material (PCM) and not even the SP of the recyclates could compete with the SP of the new (and more expensive) HDPE. PA 6 was by far the most expensive PCM.

5.7.   Summary and outlook

In this study, more than 70 semi-crystalline polymer grades were tested in regard of their applicability as phase change materials (PCM). Selection criteria were a maximum heat of fusion (ΔH_M), which represents the storage capacity, and different melting temperature ranges as indication for the application temperature range. These storage-relevant properties were determined via Differential Scanning Calorimetry (DSC). Application-oriented stability investigations were applied on the most suitable polymer grades to investigate their thermal and thermo-oxidative stability. The application-oriented stability investigations consisted of thermal cycling and static thermal loads above the polymer's melting temperature range. Finally, the economic efficiency of new polymers and recyclates as polymeric PCM was assessed.

Large differences in the storage capacity and melting temperature ranges were identified between the investigated polymer grades. The polymers with the greatest potential as PCM (maximum ΔH_M at different melting temperature ranges) were high density polyethylene (HDPE), polypropylene (PP), the polyoxymethylene homopolymer and copolymer (POM-H and POM-C), polyamide 6 and 4.6 (PA 4.6 and PA 6). These polymers (except PP) were used for application-oriented stability investigations. Whereas the storage capacity was strongly reduced for POM-H and PA 4.6 during the

thermal cycling, the thermo-physical properties of HDPE, POM-C and the PA 6 remained mostly unchanged. Therefore, these polymers were additionally exposed to a static thermal load in air at 160 °C, 190 °C and 250 °C for up to 360 h, respectively. Whereas the POM-C did not prove to stable upon the static thermal exposure, the majority of the storage capacity of the HDPE and PA 6 specimens was maintained as only the specimen surface was highly degraded. This was attributed to diffusion-limited oxidation (DLO). Thus, HDPE and PA 6 were identified as suitable polymeric PCM. The calculation of the storage price of the new polymers and recyclates as polymeric PCM, however, identified HDPE as the cheapest and PA 6 as the most expensive polymeric PCM.

The present study revealed a high potential of polymeric materials as PCM in general. However, different exposure and aging phenomena (i.e. DLO, melt movability, surface cracking), which occur during the exposure above the polymer's melting temperature, complicate the life time prediction of polymeric PCM. In the present study, only short-term stability investigations were conducted. Long-term stability investigations need to be carried out to further analyze the thermal and thermo-oxidative stability and hence the application-relevant long-term stability of polymeric PCM. Additional stabilization against thermal and thermo-oxidative degradation might be necessary.

5.8. Acknowledgements

5.9. References

[1]   A. Jamekhorshid, S.M. Sadrameli, M. Farid, A review of microencapsulation methods of phase change materials (PCMs) as

a thermal energy storage (TES) medium, Renewable and Sustainable Energy Reviews 31 (2014) 531–542.

[2]   A. Sharma, V.V. Tyagi, C.R. Chen, D. Buddhi, Review on thermal energy storage with phase change materials and applications, Renewable and Sustainable Energy Reviews 13 (2) (2009) 318–345.

[3]   K. Pielichowska, K. Pielichowski, Phase change materials for thermal energy storage, Progress in Materials Science 65 (2014) 67–123.

[4]   S. Peng, A. Fuchs, R.A. Wirtz, Polymeric phase change composites for thermal energy storage, J. Appl. Polym. Sci. 93 (3) (2004) 1240–1251.

[5]   B. Zalba, J.M. Marín, L.F. Cabeza, H. Mehling, Review on thermal energy storage with phase change: Materials, heat transfer analysis and applications, Applied Thermal Engineering 23 (3) (2003) 251–283.

[6]   S. Khare, M. Dell'Amico, C. Knight, S. McGarry, Selection of materials for high temperature latent heat energy storage, Sol Energ Mat Sol C 107 (2012) 20–27.

[7]   M.M. Kenisarin, High-temperature phase change materials for thermal energy storage, Renewable and Sustainable Energy Reviews 14 (3) (2010) 955–970.

[8]   K. Tumirah, M.Z. Hussein, Z. Zulkarnain, R. Rafeadah, Nano-encapsulated organic phase change material based on copolymer nanocomposites for thermal energy storage, Energy 66 (2014) 881–890.

[9]   Q. Yan, L. Li, D. Shen, Thermal properties of shape-stabilized paraffin used for wallboard, International Journal of Sustainable Energy 29 (2) (2010) 87–95.

[10]   C. van Do, T.T.T. Nguyen, J.S. Park, Fabrication of polyethylene glycol/polyvinylidene fluoride core/shell nanofibers via melt electrospinning and their characteristics, Sol Energ Mat Sol C 104 (2012) 131–139.

[11]   A. Sarı, C. Alkan, A. Biçer, Synthesis and thermal properties of polystyrene-graft-PEG copolymers as new kinds of solid–solid phase change materials for thermal energy storage, Materials Chemistry and Physics 133 (1) (2012) 87–94.

[12]   K. Resch-Fauster, M. Feuchter, Thermo-physical characteristics, mechanical performance and long-term stability of high temperature latent heat storages based on paraffin-polymer compounds, Thermochim Acta 663 (2018) 34–45.

[13]   K. Pielichowski, Thermal energy storage systems based on poly(vinyl chloride) blends, Eur Polym J 35 (1) (1999) 27–34.

[14]   K. Pielichowski, K. Flejtuch, Recent developments in polymeric phase change materials for energy storage: Poly(ethylene oxide)/stearic acid blends, Polym. Adv. Technol. 16 (2-3) (2005) 127–132.

[15]   I. Krupa, G. Miková, A.S. Luyt, Phase change materials based on low-density polyethylene/paraffin wax blends, Eur Polym J 43 (11) (2007) 4695–4705.

[16]   Y. Cai, C. Gao, X. Xu, Z. Fu, X. Fei, Y. Zhao, Q. Chen, X. Liu, Q. Wei, G. He, H. Fong, Electrospun ultrafine composite fibers consisting of lauric acid and polyamide 6 as form-stable phase change materials for storage and retrieval of solar thermal energy, Sol Energ Mat Sol C 103 (2012) 53–61.

[17]   C. Alkan, A. Sari, O. Uzun, Poly(ethylene glycol)/acrylic polymer blends for latent heat thermal energy storage, AIChE J. 52 (9) (2006) 3310–3314.

[18] C. Alkan, K. Kaya, A. Sarı, Preparation, Thermal Properties and Thermal Reliability of Form-Stable Paraffin/Polypropylene Composite for Thermal Energy Storage, J Polym Environ 17 (4) (2009) 254–258.

[19] Y. Cai, Q. Wei, F. Huang, S. Lin, F. Chen, W. Gao, Thermal stability, latent heat and flame retardant properties of the thermal energy storage phase change materials based on paraffin/high density polyethylene composites, Renewable Energy 34 (10) (2009) 2117–2123.

[20] Y. Jiang, E. Ding, G. Li, Study on transition characteristics of PEG/CDA solid–solid phase change materials, Polymer 43 (1) (2002) 117–122.

[21] X. Huang, G. Alva, L. Liu, G. Fang, Microstructure and thermal properties of cetyl alcohol/high density polyethylene composite phase change materials with carbon fiber as shape-stabilized thermal storage materials, Applied Energy 200 (2017) 19–27.

[22] Y. Fang, H. Kang, W. Wang, H. Liu, X. Gao, Study on polyethylene glycol/epoxy resin composite as a form-stable phase change material, Energy Conversion and Management 51 (12) (2010) 2757–2761.

[23] H. Li, G.-Y. Fang, Experimental Investigation on the Characteristics of Polyethylene Glycol/Cement Composites as Thermal Energy Storage Materials, Chem. Eng. Technol. 33 (10) (2010) 1650–1654.

[24] C. Chen, L. Wang, Y. Huang, Crosslinking of the electrospun polyethylene glycol/cellulose acetate composite fibers as shape-stabilized phase change materials, Materials Letters 63 (5) (2009) 569–571.

[25]   C. Alkan, E. Günther, S. Hiebler, Ö.F. Ensari, D. Kahraman, Polyurethanes as solid–solid phase change materials for thermal energy storage, Solar Energy 86 (6) (2012) 1761–1769.

[26]   S. Sundararajan, A.B. Samui, P.S. Kulkarni, Shape-stabilized poly(ethylene glycol) (PEG)-cellulose acetate blend preparation with superior PEG loading via microwave-assisted blending, Solar Energy 144 (2017) 32–39.

[27]   A. Sari, C. Alkan, A. Karaipekli, O. Uzun, Poly(ethylene glycol)/poly(methyl methacrylate) blends as novel form-stable phase-change materials for thermal energy storage, J. Appl. Polym. Sci. 30 (2009) n/a-n/a.

[28]   K. Pielichowski, K. Flejtuch, Differential scanning calorimetry studies on poly(ethylene glycol) with different molecular weights for thermal energy storage materials, Polym. Adv. Technol. 13 (10-12) (2002) 690–696.

[29]   Kamimoto, M., Abe, Y., Sawata, S., Tani, T., & Ozawa, T., Latent thermal storage unit using form-stable high density polyethylene: Part I: performance of the storage unit, Journal of solar energy engineering 108 (4) (1986) 282–289.

[30]   H. Inaba, Z. Li, Thermal energy storage characteristics of a latent heat storage vessel packed with surface cross-linked, form-stabilized, high-density polyethylene pellets by boiling phenomenon, Heat Trans. Asian Res. 28 (8) (1999) 649–663.

[31]   C. Yang, M.E. Navarro, B. Zhao, G. Leng, G. Xu, L. Wang, Y. Jin, Y. Ding, Thermal conductivity enhancement of recycled high density polyethylene as a storage media for latent heat thermal energy storage, Sol Energ Mat Sol C 152 (2016) 103–110.

[32]   C. Zauner, F. Hengstberger, M. Etzel, D. Lager, R. Hofmann, H. Walter, Durability of a fin-tube latent heat storage using high density

82

polyethylene as PCM, IOP Conf. Ser.: Mater. Sci. Eng. 251 (2017) 12123.

[33]   C. Zauner, F. Hengstberger, M. Etzel, D. Lager, R. Hofmann, H. Walter, Experimental characterization and simulation of a fin-tube latent heat storage using high density polyethylene as PCM, Applied Energy 179 (2016) 237–246.

[34]   I.O. Salyer, J.E. Davison, Thermal-energy storage in crosslinked pellets of high-density polythylene for home heating and cooling via off-peak electric power utilization, J. Appl. Polym. Sci. 28 (9) (1983) 2903–2924.

[35]   G.W. Ehrenstein, G. Riedel, P. Trawiel, Thermal analysis of plastics: Theory and practice, Hanser, Munich, 2004.

[36]   A. Abhat, Low temperature latent heat thermal energy storage: Heat storage materials, Solar Energy 30 (4) (1983) 313–332.

Part IV.

Long-term stability of polymeric phase-change materials

6.   Introduction to publication 2

Publication 1 revealed the potential of high-density polyethylene (HDPE), polypropylene, polyamide 6 (PA 6) and their recyclates as they exhibit high heats of fusion and a variance of melting temperatures. When applied as phase-change materials (PCM), these polymers can therefore cover a broad application temperature range from approximately 100 °C to 250 °C. The thermal and thermo-oxidative stability of the HDPE and the PA 6 was proved by cyclic testing in a Differential Scanning Calorimeter (DSC) in inert atmosphere up to 500 cycles and by the exposure to static thermal load in air in the melt state for up to 360 h (estimating one cycle to take 8 h, the applied thermal loads equaled 45 cycles). However, many latent heat storages are used on a diurnal base [1] which implies that the contained PCM undergoes approximately 300 charging and discharging cycles during only one year. The executed stability tests can therefore only be regarded as short-term stability tests as several years of application are expected for latent heat storages so that the initial investment costs eventually amortize by reducing the energy costs.

The exposure to static thermal loads resulted in a pronounced superficial degradation of the samples as shown in publication 1. Nonetheless, this exposure type rather resembled application-related conditions over the thermal cycles in a DSC as bulky specimens were exposed and atmospheric oxygen was present. Thus, the exposure to static thermal load is refined by expanding the exposure temperatures and adjusting the dimensions of the exposure containers in order to examine the long-term applicability of polymeric PCM. For this purpose HDPE is selected as the most promising PCM in terms of the highest heat of fusion. Application-relevant thermo-physical properties of the entire volume are monitored for exposure times of up to approximately 7200 h in air in the melt state (which equals 900 cycles or 3 years of application according to the estimation above). The investigations focus on understanding the occurring aging mechanisms to further optimize HDPE for the application as PCM.

As the application of polymers as PCM establishes a severe environment for the polymer and as its long-term stability has not been addressed in detail yet in the scientific literature, several HDPE grades containing differing stabilizer systems against thermo-oxidation are exposed along with the neat HDPE for investigating their long-term stability. In general, these stabilizers interfere with the free-radical reactions that induce polymer chain cleavage during thermo-oxidation [2]. According to their mechanism on slowing down or stopping these chain-breaking reactions, they can be categorized into primary and secondary antioxidants (AO). Primary AO consume free radicals by donating a hydrogen atom in order to make the radical species stable again [2]. Different types of primary AO are available including hindered phenols, hindered amine stabilizers and chemical species based on lactones or hydroxylamines [2]. Secondary AO reduce the unstable hydroperoxides which are formed during thermo-oxidation into stable alcohols [3]. They comprise phosphite- and thioester-based AO [2,3]. Depending on the service temperature, the field of application and the presence of other additives in the polymer, a variety of different AO systems at different filler loadings is typically applied in polymer industry. For the long-term stability investigations, AO with long-term efficiency are chosen. Their impact on HDPE's degradation behavior and their benefits are evaluated in publication 2.

Besides the publication shown in the following, a contribution in terms of an oral presentation has been made by the author in this field and is given in the following:

Conference contribution: H. Weingrill, K. Resch-Fauster, T. Lucyshyn, C. Zauner.; "Polymers as phase-change materials and application-oriented stability investigations", Danube Vltava Sava Polymer Meeting, Vienna, AT, 2017

6.1. References

[1]   İ. Dinçer, M.A. Rosen, Thermal energy storage: Systems and applications, 2nd ed., Wiley, Hoboken, N.J, 2011.

[2]   M. Tolinski, Additives for Polyolefins: Getting the Most out of Polypropylene, Polyethylene and TPO, 2nd ed., Elsevier Science, Burlington, 2015.

[3]   H. Zweifel, Stabilization of Polymeric Materials, Springer, Berlin, Heidelberg, 1998.

7. Publication 2

7.1. Bibliographic information

- Title: High-density polyethylene as phase-change material: long-term stability and aging

- Authors:

  - Helena Weingrill[1,2]

  - Katharina Resch-Fauster[1]

  - Thomas Lucyshyn[2]

  - Christoph Zauner[3]

- Affiliation:

  1. Materials Science and Testing of Polymers, Montanuniversitaet Leoben, Otto-Gloeckel-Strasse 2, 8700 Leoben, Austria

  2. Polymer Processing, Montanuniversitaet Leoben, Otto-Gloeckel-Strasse 2, 8700 Leoben, Austria

  3. Austrian Institute of Technology, Giefinggasse 2, 1020 Vienna, Austria

- Periodical: Polymer Testing

Statement with regard to this publication: The manuscript presented here is an adapted accepted manuscript in order to fit the formatting of the thesis and does not necessarily reflect exactly the actually published version.

7.2.　　Abstract

Bulky HDPE specimens containing different stabilization systems are exposed in air for up to 7200 h in the melt state to investigate the HDPE's applicability as phase change material (PCM). Their thermo-oxidative stability is investigated. The maintenance of the storage capacity (heat of fusion) and the HDPE's degradation behavior is monitored via Differential Scanning Calorimetry (DSC). Different aging phenomena of the thermo-oxidative exposure are investigated in more detail by means of Fourier-transform infrared spectroscopy (FTIR) and polarized light microscopy (PLM). Only a small loss in the storage capacity upon thermo-oxidative exposure is detected. Therefore, HDPE proves to be a candidate material for polymeric PCM.

7.3.　　Introduction

High-density polyethylene (HDPE) with a melting temperature of ~135 °C exhibits an outstandingly high heat of fusion of up to 240 J/g [1]. Along with its toxicological safety, commercial availability and low price, this makes HDPE an interesting phase change material (PCM) in principal. However, the long-term stability and aging of HDPE under PCM-relevant conditions is highly complex and has not yet been addressed in detail in the scientific literature so far as it has rather been used as encapsulating material than as PCM per se [2]. Only thermal cycling [3–5] (i.e. consecutive melting/freezing cycles) as proposed by Abhat [6] has been applied and no change in the HDPE's properties was observed. Above HDPE's melting temperature (i.e. in the charged state), however, the combination of (atmospheric) oxygen and the lack of its crystalline morphology in the melt state (which usually hinders oxygen diffusion into the polymer bulk [7]) results in a very aggressive environment for the polymer. Therefore, the thermo-oxidative long-term stability at temperatures far above the melting temperature is probably the most crucial application-relevant parameter. The thermo-oxidative stability of polymers in the melt state is in general determined via the following two types of testing: Oxidation Induction Time and Temperature (isothermal and dynamic OIT) measurements in a Differential Scanning Calorimeter (DSC)

according to ISO 11357-6 and/or combined shear and high temperature tests to imitate processing. For the second type of testing, the HDPE is heated above its melting temperature and shear is applied upon it via an open mixer, a torque rheometer or several consecutive extrusion rounds [8–12]. However, both types of testing are not applicable for the prediction of the long-term stability of HDPE as polymeric PCM where large bulky samples (as opposed to the OIT measurements) are present and no shear is applied upon them (shear induces chain scission and thereby accelerates aging by the generation of radicals [9]). The typically bulky specimen size of polymeric PCM results in diffusion limited oxidation (DLO) during the thermo-oxidation which causes a higher extent of oxidation at the specimen surface when compared to the extent of oxidation in the specimen bulk [13,14]. Therefore, a combination of a thermal and a thermo-oxidative environment is present during the use of HDPE as polymeric PCM. The present study aims at comprehensively investigating the long-term stability of HDPE upon the combination of thermal and thermo-oxidative loads in order to predict the applicability of HDPE as PCM. Bulky specimens are exposed to temperatures far above the melting temperature range for up to 7214 h. The HDPE is used as received and also additionally stabilized against thermo-oxidation with two different types of stabilizers. The occurring aging mechanisms and the progress of material degradation are analyzed in detail and their effects on the polymer's supermolecular morphology and heat of fusion (i.e. the polymer's heat storage capacity) are revealed.

7.4. Experimental

7.4.1. Materials

The commercially available high-density polyethylene (HDPE) grade Bormed^{TM} HE9621-PH with a melt flow rate of 12 g/10 min (2.16 kg, 190 °C) was generously provided by Borealis GmbH (Linz, AT) and used as received (basic stabilization system - no further information provided) and also additionally stabilized with two antioxidants at different weight ratios. The antioxidants were generously provided by Lanxess AG (Cologne, DE). The first antioxidant VULKANOX® HS/LG belongs to the group of Hindered Amine Stabilizers (HAS) and will be referred to as TMQ (from 2,2,4-trimethyl-1,2-dihydroquinoline). The second antioxidant VULKANOX® MB2 belongs to the group of benzimidazoles and was applied as a protector for the TMQ. It will be referred to as MBI (from 4/5-methyl-2-mercaptobenzimidazole). These types of stabilizers were applied due to their long-term efficiency [15] which was found to be a characteristic feature of HAS [16,17]. TMQ was delivered

in granular form and MBI was delivered in powder form. Both were used as received.

The compounding of HDPE with the two different stabilizers (concentrations between 0.5 wt.-% and 2 wt.-%) was done on a co-rotating twin screw compounder (Werner & Pfleiderer GmbH, Dinkelsbühl, DE) with an L/D ratio of 38 and equipped with 6 control zones, a gravimetric dosing unit, side feeding, vacuum degassing, a cool bath and strand pelletizing. The temperature of the six control zones was set to 150 °C and the mass feed rate was set to 12 kg/h. For those compounds containing only the TMQ, the HDPE and the TMQ granules were dry blended and compounded to granules. For those compounds containing TMQ and MBI, a master batch with 18 wt.-% of MB and 82 wt.-% of HDPE was compounded in a first step. The granules of the master batch were dry blended with the HDPE and the TMQ granules and then compounded to the according weight ratios in a second step. The incorporated weight ratios and compound names which are used in the following are given in Table 7.1. The stabilizer contents partly exceed typical levels (up to 0.5 wt.-% for HDPE [18]) since a completely amorphous melt state during the exposure to static thermal loads along with a higher solubility of the stabilizer in the HDPE matrix were present.

Table 7.1: Applied materials: the HDPE Bormed^{TM} HE9621-PH was used as received (PE-S0) and additionally stabilized with the two stabilizers VULKANOX® HS/LG (TMQ) (delivered in granulate form) and the VULKANOX® MB2 (MBI) (delivered in powder form) at the given weight ratios (PE-S1 – PE-S4).

Polymer grade	Stabilizer		Polymer compound
	VULKANOX ® HS/LG (TMQ) [wt.-%]	VULKANOX ® MB2 (MBI) [wt.-%]	
Bormed^{TM} HE9621-PH	-	-	PE-S0
	0.5	-	PE-S1
	0.25	0.25	PE-S2
	0.5	0.5	PE-S3
	1	1	PE-S4

7.4.2. Exposure parameters and specimen preparation

The thermo-oxidative stability was tested by storing the different HDPE samples in cylindrical glass containers (h= 110 mm; inner ø= 72 mm) in convection ovens Heraeus® TK 6060 (Thermo Fisher Scientific Inc.,

Waltham, US) in air at 160 °C and 180 °C. The position of the glass containers was changed weekly in order to compensate temperature gradients in the convection oven. The large aperture of the glass container was chosen to ease oxygen diffusion into the specimen bulk. Sampling was done in monthly intervals after 765 h, 1440 h, 2139 h, 2851 h, 3625 h, 7200 h and after 790 h, 1459 h, 2155 h, 2854 h, 3651, 7214 h at 160 °C and 180 °C, respectively. The specimens will be referred to as material-exposure temperature-exposure time. For example, PE-S0-160°C-765h refers to the PE-S0 which was exposed for 765 h at 160 °C. After the given exposure times, the glass containers were removed from the convection oven and freely cooled at ambient temperature. In order to impede uneven shrinkage, a metal cylinder with a weight of 2 kg was placed on the specimen top during cooling (a polytetrafluoroethylene sheet was placed in between to prevent adhesion). After cooling, the cylindrical specimens (approx. dimensions: h = 80 mm; inner ø = 65 mm) were taken out from the glass containers and cut vertically into semi-cylinders with a specimen saw Diadisc 500 (MUTRONIC Praezisionsgeraetebau GmbH & Co.KG, Rieden am Forggensee, DE). The specimens displayed differences in their optical appearance as described in more detail in 7.5.2. In order to determine averaged characteristics of the whole specimen volume (in addition to local material characteristics), a homogenization procedure was applied on one of the semi-cylinders. A "homogenization device" was applied. It consisted of two aluminum crucibles (ø=80 mm; h=25 mm) aligned vertically and separated by a placeholder tube which was formed out of a perforated grid as given in Figure 7.1a.
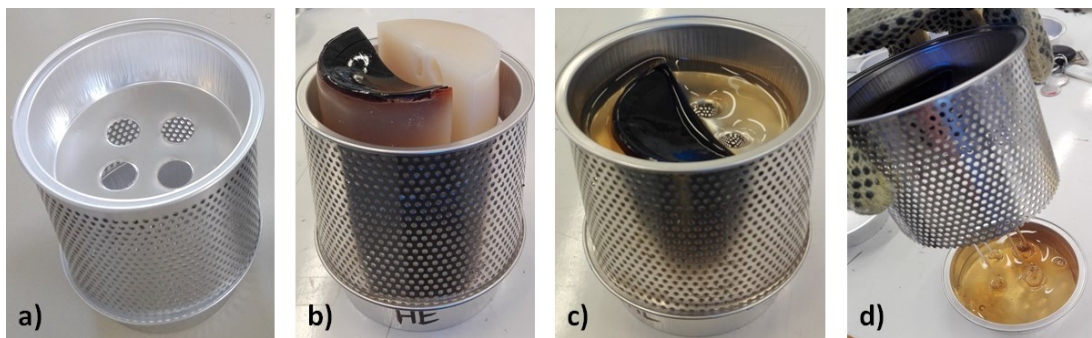

Figure 7.1: Homogenization procedure: a) homogenization device consisting of two aluminum crucibles aligned vertically and separated by a placeholder; b) semi-cylindrical specimen cut in half and placed on the upper aluminum crucible with the punched holes before the homogenization procedure; c) immobile specimen part after 1.5 h at 200 °C in the upper aluminum crucible; d) mobile specimen part after 1.5 h at 200°C collected in the lower crucible.

The upper aluminum crucible had 4 punched holes (ø = 12 mm) centrically distributed. One semi-cylindrical specimen part of every specimen was first cut horizontally into two smaller semi-cylinders as depicted in Figure 7.2a. The two pieces were placed on the homogenization device as depicted in Figureb. The homogenization device with the cut semi-cylinders was placed in a convection oven Heraeus® TK 6060 (Thermo Fisher Scientific Inc., Waltham, US) in air at 200 °C for 1.5 h (minimum time required to melt the entire specimen). After 1.5 h at 200 °C, the specimen parts were completely melted and collected by the lower aluminum crucible. The surface of certain specimens had degraded to such an extent that it remained solid after 1.5 h at 200 °C and it did not flow through the punched holes (Figurec). It will be referred to as the "immobile specimen part" in the following. The immobile specimen part could thereby be separated from the rest of the specimen. The immobile specimen part consisted of a very brittle surface and a ductile transition layer (transition between completely immobile and meltable) at the bottom. The lower crucible with the contained melted specimen was then placed on a heating plate (200 °C) and the melted specimen part was stirred manually for 5 min with a spatula for homogenization. Afterwards it was cooled in the aluminum crucible at ambient temperature. Both, the weight of the mobile specimen part m_{mob} and of the immobile specimen part m_{immob} were determined after the homogenization.

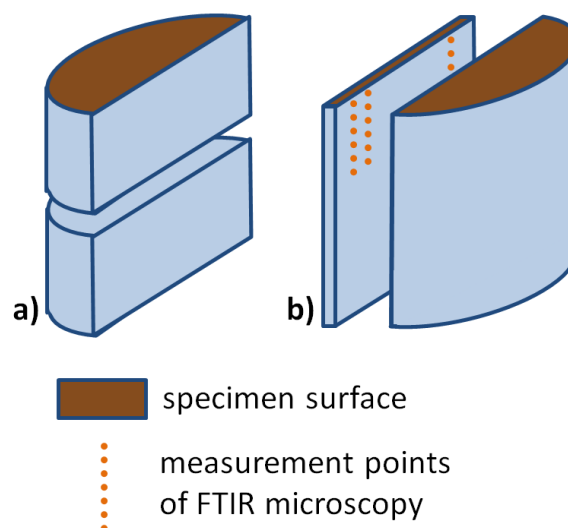specimen surface

measurement points
of FTIR microscopy

Figure 7.2: Cooled and cut specimen: a) the semi-cylinder used for the homogenization and the DSC-measurements to determine the representative heat of fusion of the whole volume of the exposed specimen; b) the semi-cylinder of which a plate with a thickness of 8 mm was extracted for the FTIR microscopy.

7.4.3. Characterization of material degradation

The thermo-physical properties of the different types of HDPE were determined on a Differential Scanning Calorimeter (DSC) DSC 1 (Mettler Toledo, Greifensee, CH). Samples for DSC-measurements were taken from the cooled mobile part and the immobile specimen part if present and the sample weight ranged between 4 mg and 6 mg. 40 µl aluminum crucibles with a perforated lid were used. After an equilibration time of 5 min at 0 °C, the samples were heated under nitrogen atmosphere to 160 °C and cooled to 0 °C by applying a constant heating rate of 10 K/min and -10 K/min, respectively. After another equilibration time of 5 min at 0 °C, the samples were heated a second time to 160 °C by applying a constant heating rate of 10 K/min. The heat of fusion ΔH_M and the peak melting temperature T_{Mpeak} were evaluated from the second heating. The evaluations were done according to ISO 11357-2. The presented data represent the average of three to five measurements for the mobile specimen part and of two measurements of the immobile specimen parts. The heat of fusion of the whole specimen ΔH_{Mwhole} was calculated according to Equation (1),

$$\Delta H_{Mwhole} = \Delta H_{Mmob} * \frac{m_{mob}}{m_{mob}+m_{immob}} + \Delta H_{Mimmob} * \frac{m_{immob}}{m_{mob}+m_{immob}} \quad (1)$$

with ΔH_{Mmob} as the heat of fusion of the mobile specimen part, m_{mob} as the weight of mobile specimen part, ΔH_{Mimmob} as the heat of fusion of the immobile specimen part and m_{immob} as the weight of immobile specimen part.

The Oxidation Induction Temperature (dynamic OIT) of the different types of HDPE was determined on a DSC 822e (Mettler Toledo, Greifensee, CH) for every second sample (after 1440 h, 2851 h and 7200 h at 160 °C and after 1459 h, 2854 h and 7214 h at 180 °C). Samples were taken from the mobile specimen part and the sample weight was 10 mg. Open 40 µl aluminum crucibles were used. The sample was heated under air atmosphere from ambient temperature until an exothermic curve indicating the thermo-oxidative degradation was recorded by applying a constant heating rate of 10 K/min. The oxidation induction temperature T_{ox} was evaluated according to ISO 11357-6. The presented data represent the average of two measurements. The dynamic OIT measurements will be referred to as OIT measurements.

The morphological characteristics of the specimens were investigated in detail by means of Fourier-transform infrared (FTIR) spectroscopy and

polarized light microscopy (PLM). For the FTIR measurements, plates with a thickness of 8 mm were cut parallel to the longitudinal axis from the semi-cylindrical specimens with a specimen saw Diadisc 500 (MUTRONIC Praezisionsgeraetebau GmbH & Co.KG, Rieden am Forggensee, DE) as depicted in Figure 7.2b. FTIR spectra were recorded with a fully automated stand-alone FTIR microscope Lumos (Bruker Corporation, Billerica, US) in Attenuated Total Reflection (ATR) mode with a germanium crystal (refractive index n=4) at a resolution of 4 cm^{-1} with a total of 64 scans. The spectra were recorded in the wavelength range between 4000 cm^{-1} and 600 cm^{-1}. On the one hand, three spectra of each specimen surface were recorded in distances of several mm from the specimen plates. In order to investigate the degradation/oxidation propagation into the bulk, FTIR was also implemented in stepwise measurements from the surface into the bulk parallel to the longitudinal axis of the semi-cylindrical specimens (orange dotted line in Figure 7.2b) on the other hand. The first FTIR spectrum was recorded 200 μm underneath the specimen surface and following steps of 500 μm into the specimen bulk. FTIR spectra were recorded until no difference compared to the spectrum recorded from the unexposed specimen was detected. This was done three times on every specimen plate (8 mm) in a distance of at least 5 mm to at most 15 mm from the specimen edge. It was applied on the non-additionally stabilized PE-S0 and the additionally stabilized PE-S3 specimens as the PE-S3 proved to be the most efficient stabilizer system according to DSC measurements. FTIR spectra of the unexposed materials were recorded from as-received polymer granules for PE-S0 and from the granules after compounding for PE-S3.

For the PLM, microtome sections of the PE-S0 and PE-S3 after 765 h, 2851 h, 3625 h and 7200 h of exposure at 160 °C and after 790 h, 3651 h and 7214 h of exposure at 180 °C with a thickness 20 μm were extracted with a rotary microtome RM2255 (Leica Microsystems GmbH, Wetzlar, DE) from the surface region of the mobile specimen part or if present, from the immobile specimen part. All microtome sections (mobile specimen part and immobile specimen parts) were embedded in immersion oil and placed between two microscope object carriers of glass. A light microscope BX51 (Olympus, Tokyo, JP) equipped with a retardation plate and an objective with a magnification of 50 was applied for the image recording.

7.5. Thermal and thermo-oxidative stability

7.5.1. Oxidation induction temperature

In Figure 7.3 the effect of static thermal exposure at 160 °C and 180 °C in air on T_{OX} is depicted for the different investigated HDPE types. T_{OX} of the unexposed HDPE types increased with increasing stabilizer content (PE-S0: 0 wt.-%, 237 °C; PE-S4: 2 wt.-%, 280 °C). The increase in T_{OX} by the incorporation of HAS is typically due to the formation of nitroxyl radicals which act as alkyl radical scavengers [16,19] and thereby delay the thermo-oxidation of the polymer. When looking at T_{OX} of PE-S1 and PE-S2 which were both additionally stabilized with a total of 0.5 wt. -%, one can clearly see that T_{OX} of PE-S2 (containing TMQ and MBI as additional stabilizers) exceeded T_{OX} of PE-S1 (containing only the TMQ as additional stabilizer). Thus, the combined incorporation of TMQ and MBI exhibited synergistic effects and the focus of the present study was therefore kept on stabilizer systems containing both stabilizers (PE-S2 – PE-S4).

After the exposure in air the range of T_{OX} decreased for all HDPE types from 280 °C – 237 °C to 267 °C – 214 °C when exposed at 160 °C and to 257 °C – 212 °C when exposed at 180 °C. Interestingly, PE-S3 proved to be more efficient at 180 °C than at 160 °C as its T_{OX} decreased to smaller extent at the higher exposure temperature for the majority of the specimens. It will therefore be used for the material and specimen morphology investigations in 7.5.2. Decreases in T_{OX} correlate in general with decreases in the stabilizer effectiveness which are caused by chemical consumption or degradation of the stabilizer, stabilizer migration ("blooming" effect) and physical evaporation [20,21]. Nonetheless, after 7200 h of exposure at 160 °C and 7214 h of exposure at 180 °C, T_{OX} of all additionally stabilized HDPE types was still higher than T_{OX} of the non-additionally stabilized PE. Thus, the stabilizer was still effective even after the longest exposure times.
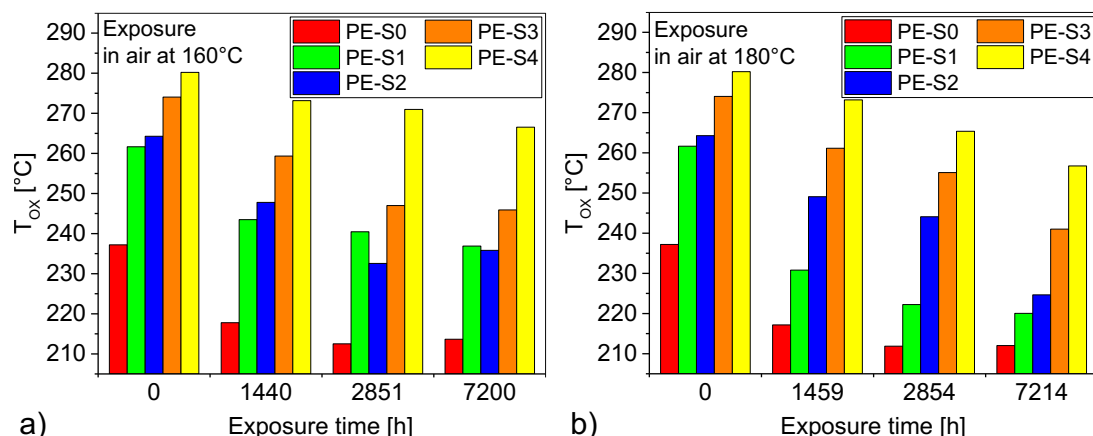
Figure 7.3: Oxidation Induction Temperature (T_{OX}) of PE-S0-PE-S4 when exposed in air at a) 160 °C and b) 180 °C. T_{OX} decreased with increasing exposure temperature for all materials.

7.5.2.   Material degradation and specimen morphology

In Figure 7.4 the cross sections of the PE-S0 through PE-S4 specimens after 765 h of exposure to static thermal load at 160 °C and after 790 h of exposure to static thermal load at 180 °C are displayed. All specimens exhibited a distinct discoloration on the surface. Additionally unevenly distributed discoloration patterns in the specimen bulk which resembled helically arrangements were ascertained for all stabilized HDPE types (except for PE-S1 at 180 °C). Within the stabilized HDPE types, larger and more blurry discoloration patterns were found for the PE-S2 through PE-S4 after the exposure to 160 °C (Figure 7.4b to e), whereas more defined streaks were found for PE-S2 through PE-S4 after the exposure to 180 °C (Figure 7.4h to j).

The FTIR spectra recorded from the surface of the non-additionally stabilized PE-S0 exposed after different exposure times at 160 °C are given in Figure 7.5a. The FTIR spectra of the specimen surfaces were significantly affected by the exposure to heat and all absorption bands changed. Therefore normalization was not possible. However, because of the identical specimen preparation and the automated procedure of the ATR crystal (internal pressure control), a qualitative comparison between the spectra was still possible. Compared to the spectra recorded from the surface of the unexposed PE-S0 granule, an increase of the absorption bands in the wavenumber range from 1780 cm^{-1} to 1700 cm^{-1}, which represent the stretching vibrations of carbonyl groups, an increase of the absorption band at 1171 cm^{-1}, which represents the C-O-stretching vibration of the ester and

100

an increase in the absorption bands in the wavenumber range from ca. 970 cm^{-1} to 880 cm^{-1}, which represent the deformation vibrations of unsaturated compounds, whereas a decrease of the absorption bands at 2915 cm^{-1} and 2850 cm^{-1}, which represent the CH_2-stretching vibrations, and changes in the absorption bands in the wavenumber range from ca. 1480 cm^{-1} to 1200 cm^{-1}, which represent the CH_2-deformation vibrations, were ascertained [22-29] for the spectra recorded from the surfaces of the non-additionally stabilized PE-S0 specimens until exposure times of up to 2851 h.
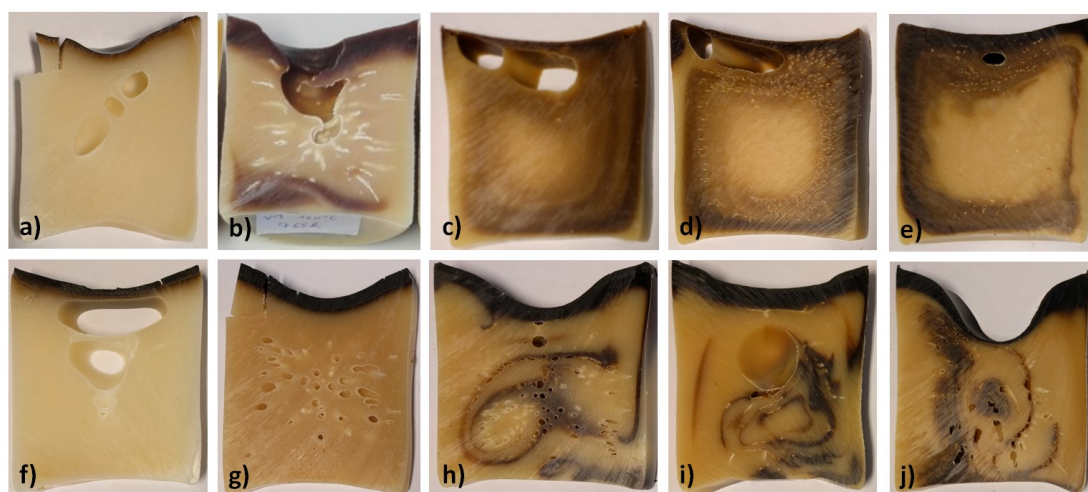

Figure 7.4: Cross sections of the PE-S0 - PE-S4 after 765 h of exposure to static thermal load at 160 °C: a) PE-S0, b) PE-S1, c) PE-S2, d) PE-S3, e) PE-S4 and after 790 h of exposure to static thermal load at 180 °C: f) PE-S0, g) PE-S1, h) PE-S2, i) PE-S3, j) PE-S4. The surface of all HDPE types exhibited distinct discoloration. The additionally stabilized PE-S1 - PE-S4 (b)-e) and g)-j)) exhibited unevenly distributed discoloration patterns in the specimen bulk.

The detected changes in the IR absorption bands are in good agreement with the thermo-oxidative degradation mechanism and the resulting oxidation products for PE given in [29,30]. After 3625 h and 7200 h of exposure at 160 °C, however, no IR-active groups were left on the surface as seen on the lower two spectra in Figure 7.5a. Thus, an extensive thermo-oxidative material degradation had taken place on the specimen surface as the oxidation products were further decomposed to IR-inactive carbon products. The degradation mechanism of the non-additionally stabilized specimens exposed at 180°C and the additionally stabilized specimens were similar. For the non-additionally stabilized HDPE exposed at 180 °C, IR-active groups were no longer detectable already after 2854 h of exposure. As expected, the higher exposure temperature accelerated the thermo-oxidative material degradation on the surface of the non-additionally stabilized PE-S0. The

incorporation of the additional stabilizers yielded a delay in thermo-oxidative degradation as IR-active groups were still detectable after 7200 h of exposure at 160 °C and after 7214 h of exposure at 180 °C for all additionally-stabilized HDPE types.
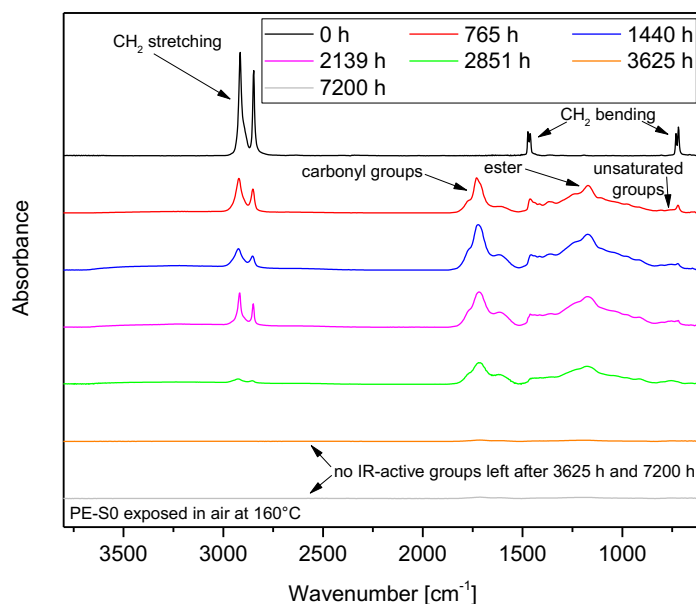

Figure 7.5: FTIR spectra recorded from the surface of the PE-S0 specimens when exposed to static thermal load in air at 160 °C after different exposure times. After 3625 h of exposure, no IR-active groups were left on the specimen surface due the extensive thermo-oxidative degradation.

In Figure 7.6a, the FTIR spectra recorded stepwise from the surface into the bulk of the PE-S0-160°C-765h are presented exemplarily for all specimens. In accordance with DLO, the absorption bands, which represent the carbonyl groups (1780 cm^{-1} – 1700 cm^{-1}) and therefore the extent of oxidation, decreased by going further into the bulk. These absorption bands were used to describe the oxidation penetration depth (OPD) into the bulk of each specimen. An "oxidation threshold" (grey dashed line) of an absorbance of 0.005 was chosen to describe the OPD because this was the minimum absorbance which could explicitly be identified as an absorption band within the noise of the spectrum. The measurement position in regard to the specimen surface of the last FTIR measurement which yielded an absorption band above the oxidation threshold was then taken as the OPD. No changes in the FTIR spectra underneath the OPD were detected. Thus, only oxidative degradation but not thermal degradation of the material occurred during the applied thermal loads. This was in good agreement with Thermogravimetric

Analysis measurements in inert atmosphere where the thermal degradation of polyethylene occurs only above 300 °C [31,32].
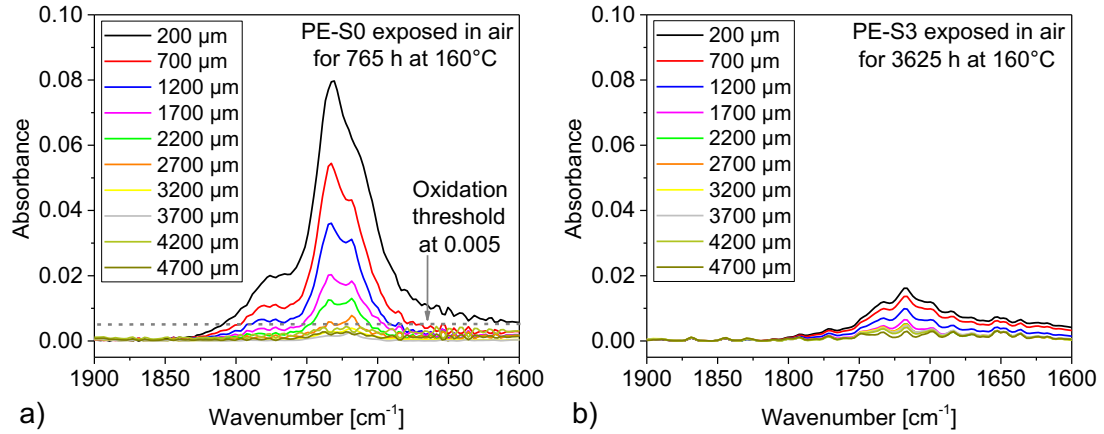

Figure 7.6: FTIR spectra recorded from the bulk of a) the PE-S0 specimen after 765 h of exposure to static thermal load at 160 °C and of b) the PE-S3 specimen after 3625 h of exposure to static thermal load. The extent of oxidation decreased by going further into the specimen bulk as described by diffusion limited oxidation (DLO). Both specimens exhibited a similar oxidation penetration depth. However, the extent of oxidation as given by the absorbance of the carbonyl groups differed strongly.

Representatively for all the investigated HDPE specimens, the OPDs of the non-additionally stabilized PE-S0 and the additionally stabilized PE-S3 after exposure times up to 7200 h at 160 °C and 7214 h at 180 °C are displayed in Figurea and b. For a better comprehension and a better reading flow, the PE-S0 will simply be called the non-additionally stabilized PE and PE-S3 will be called the additionally stabilized PE until the end of chapter 7.5.2.

For the non-additionally stabilized PE specimens, the evolution of the OPDs over the exposure time was nearly congruent for both exposure temperatures. It increased from 3030 µm to 4370 µm (160 °C; 765 h – 7200 h) and from 2870 µm to 4200 µm (180 °C; 790 h – 7214 h). For the additionally stabilized PE specimens exposed at 160 °C, an oxidation was first detected after 3625 h (OPD = 3075 µm). Thus the incorporated stabilizer delayed oxidation. After 7200 h its OPD had increased to 6200 µm. At the higher exposure temperature of 180 °C, however, an oxidation was already detected after 790 h and the OPD stayed rather constant within the data scattering until an exposure of 3651 h (OPD = 700 µm to 1870 µm). After 7214 h, its OPD had increased to 5030 µm. Therefore, the incorporated stabilizer was less efficient at the higher exposure temperature of 180 °C than at 160 °C until exposed for 3651 h/3625 h, but more efficient at longer

exposure times. Compared to the non-additionally stabilized PE, however, the stabilization lost its effect after 7200 h/7214 h when the OPDs of the additionally stabilized PE (160°C: 6200 µm; 180 °C: 5030 µm) exceeded the OPDs of the non-additionally stabilized PE (160°C: 4370 µm; 180 °C: 4200 µm).

If an oxidation in the specimen bulk was detected, also an immobile specimen part at the specimen surface was present in the exposed specimen. However, the immobile specimen parts from the non-additionally stabilized PE-S0 proved to be a lot more brittle (formation of cracks) as opposed to the immobile specimen parts of the additionally-stabilized PE types which were rather ductile. The non-additionally stabilized PE-S0-160°C-765h and the additionally stabilized PE-S3-160°C-3625h exhibited similar OPDs (3030 µm vs. 3070 µm). However, the extent of oxidation was smaller for the additionally stabilized PE-S3 as given in Figure 7.6b. Thus, a smaller extent of oxidation yielded a more ductile immobile specimen part.
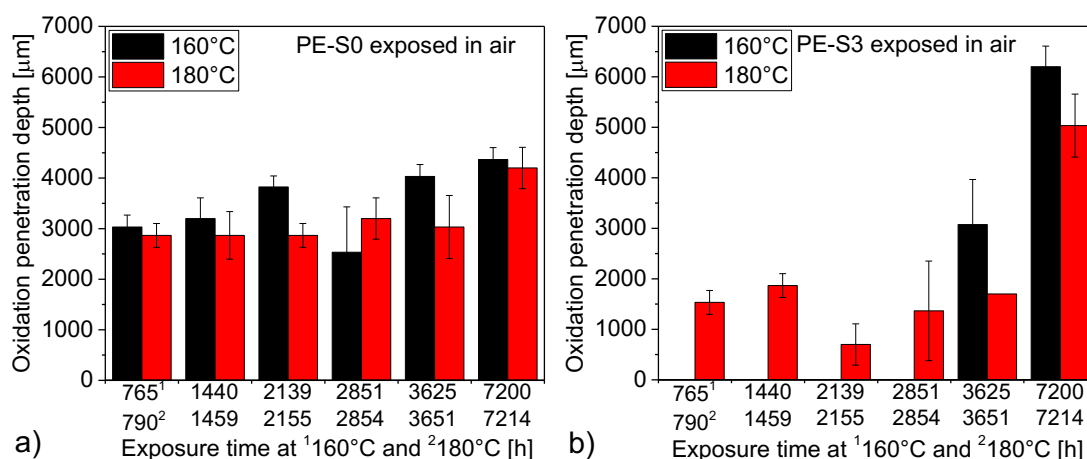

Figure 7.7: Oxidation penetration depth (OPD) as measured via FTIR microscopy after different exposure times: a) the non-additionally stabilized PE-S0 exhibited similar OPDs independent from the exposure temperature; b) the additionally stabilized PE-S3 exhibited differing OPDs in regard to the exposure temperature. Whereas the oxidation was delayed for PE-S3 compared to the PE-S0, a higher OPD was reached after 7200 h of exposure at 160 °C and 7214 h of exposure at 180 °C.

As no oxidation products were ascertained in the recorded FTIR spectra of the additionally stabilized PE, the unevenly distributed discolored specimen patterns within the specimen bulk (Figure 7.4d) do not represent an oxidation of the PE. Representative OIT thermograms given in Figure 7.8 reveal a difference of 19 °C in T_{OX} between the non-discolored specimen part (T_{OX} = 268 °C; light blue line) and the distinctly discolored specimen part (T_{OX} = 249 °C; orange dashed line). Thus, the stabilizing effect of the antioxidant was lowered in the discolored-specimen part. As stated by [19], transformation products of the aromatic amines of HAS can lead to a discoloration of the substrate. However, these transformation products could probably not be detected via the FTIR measurements because the stabilizer content was below the detection limit of the FTIR spectroscope. Therefore, about 2 g of both stabilizers were exposed in air at 160 °C and 180 °C for 24 h in aluminum crucibles (ø=80 mm; h=25 mm). Representatively for both exposure temperatures, pictures of the stabilizers before and after the exposure at 160 °C are given in Figure 7.9a and b, respectively. Whereas the color of MBI only changed slightly, the color of TMQ changed distinctly from light brown to dark brown indicating that the discoloration of the specimen bulk was mainly caused by a temperature-induced coloration of the TMQ. Moreover, a weight decrease during the exposure of the stabilizers occurred. After 24 h at 160 °C and 180 °C, 16.2 % and 18.6 % of the TMQ and 0.9 % and 5.5 % of the MBI had evaporated, respectively. Even though the stabilizers were surrounded by the polymer during the applied stability investigations, it is likely that the stabilizers evaporated as well through the surface of the exposed specimen. In Figure 7.10 the FTIR-spectra recorded from the stabilizers before and after the exposure in air at 160 °C are given. Both spectra were normalized with the absorption bands at 2866 cm^{-1} (TMQ) and 2870 cm^{-1} (MBI), which represent the CH$_2$-stretching vibration [27]. Compared to the spectra recorded from the unexposed stabilizers, an increase of the absorption bands in the wavenumber range from 1780 cm^{-1} to 1700 cm^{-1}, which represent the stretching vibrations of carbonyl groups for both stabilizers were ascertained inter alia. This confirms a thermo-oxidative degradation of the stabilizer. Thus the detected decrease in T_{OX} for the discolored specimen part was caused by a degradation of both stabilizers and the physical evaporation mainly of the TMQ.
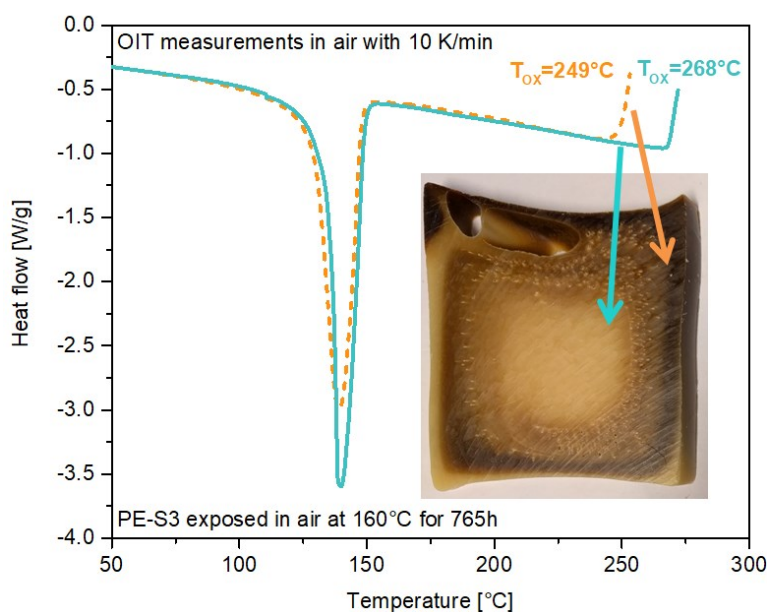
Figure 7.8: Representative thermograms of the OIT measurements of the non-discolored specimen part (pink line) and the distinctly discolored specimen part (blue dashed line). The cross section of the PE-S3-160°C-765h specimen from which the samples were taken is given in the graph. T_{OX} was lower by 19 °C for the discolored specimen part which was attributed to the chemical consumption of the stabilizer.
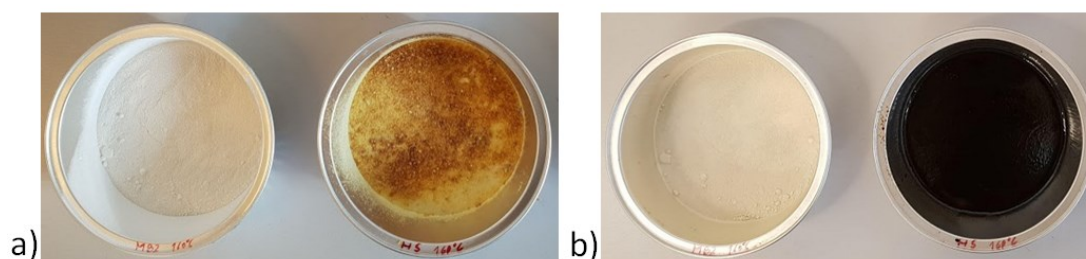

Figure 7.9: Photographs of the stabilizers MBI (left) and TMQ (right) exposed in air at 160 °C: a) before the exposure; b) after 24 h of exposure. A distinct color change occurred after the exposure for the TMQ.
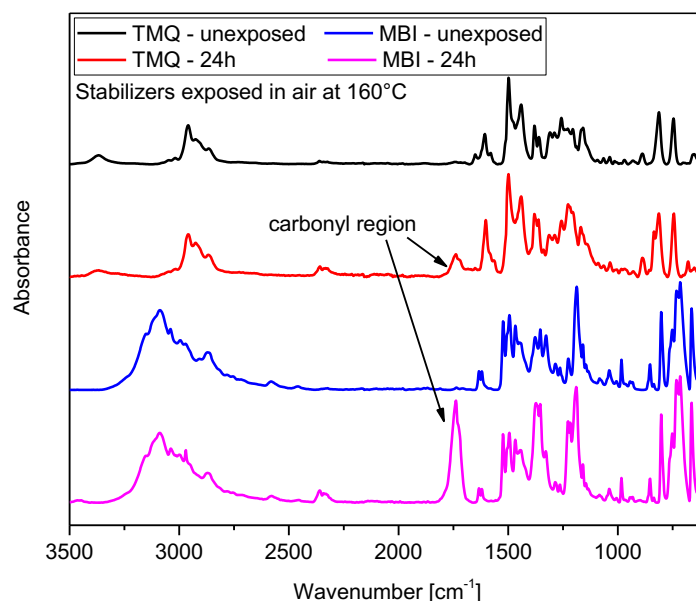
Figure 7.10: FTIR spectra of the stabilizers TMQ and MBI before and after exposure in air at 160°C. Both stabilizers showed an increase of the absorption band in the carbonyl region (1780 cm^{-1} - 1700 cm^{-1})

Naturally, the thermo-oxidative degradation caused significant changes in the crystalline morphology of the additionally stabilized PE specimens as deducible from the PLM micrographs and from FTIR measurements recorded from 700 µm (spectra were normalized) underneath the surface (Figure 7.11 and Figure 7.12a). After 2851 h of exposure at 160 °C, a fine and regular crystalline superstructure was detected (Figure 11a). It was attributed to the non-oxidized condition as no absorption band in the carbonyl region (1780 cm^{-1} – 1700 cm^{-1}) was detected. After 3625 h of exposure at 160 °C (Figure 11b) a less fine and irregular crystalline superstructure was ascertained and an absorption peak in the carbonyl region indicated the oxidized condition of the specimen. Simultaneously, the absorption band at 1474 cm^{-1}, which represents the bending vibration of the crystalline phase [26], and the absorption band at 1764 cm^{-1}, which represents the bending vibration of the amorphous phase [26], decreased compared to the non-oxidized specimen. At the higher exposure temperature of 180 °C, an amorphous superstructure was found right underneath the specimen surface additionally to the less fine and irregular crystalline superstructure (Figure 11c). This was in good agreement with the recorded FTIR spectra where a larger absorption peak in carbonyl region (indicating a higher extent of oxidation), an absorption band at 1464 cm^{-1}, which represents the bending vibration of the amorphous phase [26], but no absorption band at 1474 cm^{-1} (crystalline phase) were found. Condensed, the larger the absorption band in

the carbonyl region, the higher the extent of oxidation and the smaller the absorption band at 1474 cm^{-1} (crystalline phase). Thus, the oxidation of the material destroyed the crystalline superstructure of the PE gradually during the exposure to air. This is further proved by the DSC measurements as displayed in Figure 7.12b, where ΔH_M decreased from 213 J/g for the non-oxidized PE (mobile specimen) to 184 J/g and to 174 J/g for the oxidized PE (immobile specimen part) when exposed at 160°C and at 180°C, respectively. Its altered crystalline structure also shifted T_{Mpeak} towards lower temperatures from 134 °C for the non-oxidized PE to 131 °C and to 130°C for the oxidized PE at 160°C and at 180°C, respectively, and changed the shape of the melting peak. These two findings indicated that a decrease and/or irregularities in the crystallite size occurred due to the thermo-oxidative degradation.
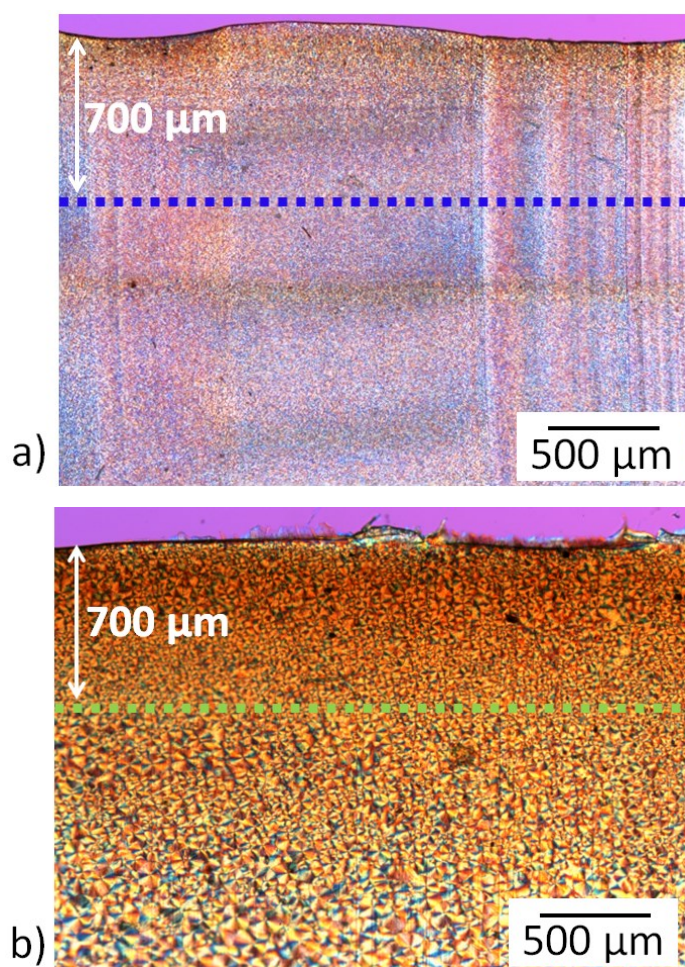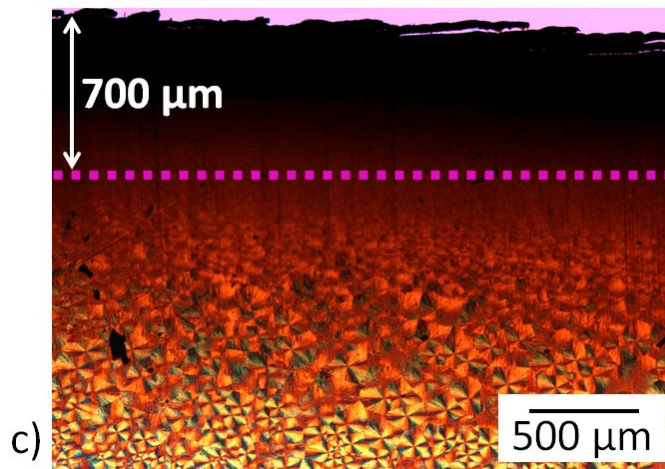
Figure 7.11: PLM micrographs of: a) the non-oxidized PE-S3-160°C-2851h (mobile specimen) ; b) the oxidized PE-S3-160°C-3625h (immobile specimen part); c) the oxidized PE-S3-180°C-3651h (immobile specimen part). The significant changes in the crystalline morphology after 3625 h of exposure at 160 °C and 3651 h at 180 °C were attributed to oxidation.
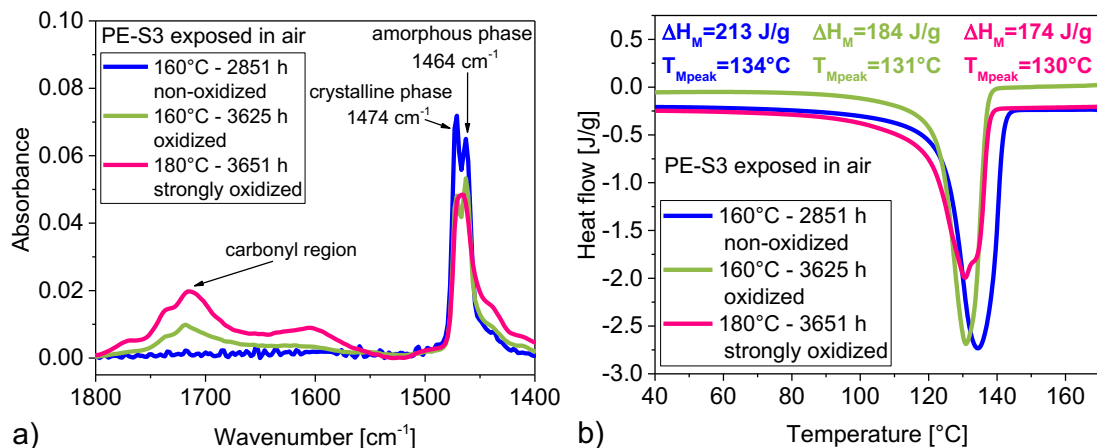

Figure 7.12: a) FTIR spectra and b) DSC thermograms of the non-oxidized PE-S3-160°C-2851h (mobile specimen) and the oxidized PE-S3-3625h (immobile specimen part) and the strongly oxidized PE-S3-3651h (immobile specimen part) presented in blue, green and pink, respectively. The decrease in the heat of fusion ΔH_M was attributed to the extent of oxidation.

7.5.3.   Heat of fusion

In Figure 7.13 the effect of static thermal exposure at 160 °C and 180 °C in air on ΔH_{Mwhole} and ΔH_{Mmob} of PE-S0 through PE-S4 is depicted. The opaque columns display ΔH_{Mwhole} whereas the transparent columns display ΔH_{Mmob}. If no immobile specimen part was ascertained after the homogenization

procedure, the opaque and transparent columns are congruent since the entire specimen had maintained its meltability. The rather high data scatter originated from material fluctuations and the measurement uncertainty of the applied DSC device. After 765 h of exposure at 160 °C and 790 h of exposure at 180 °C, a minor decrease in ΔH_{Mwhole} for all investigated HDPE types was detected. After longer exposure times, however, ΔH_{Mmob} and ΔH_{Mwhole} stayed rather constant in the range from 198 J/g to 234 J/g and from 192 J/g to 227 J/g, respectively. Consequently, the exposure decreased ΔH_{Mwhole} by maximum 15%. This decrease in storage capacity has to be considered in the design of the storage for the final application.
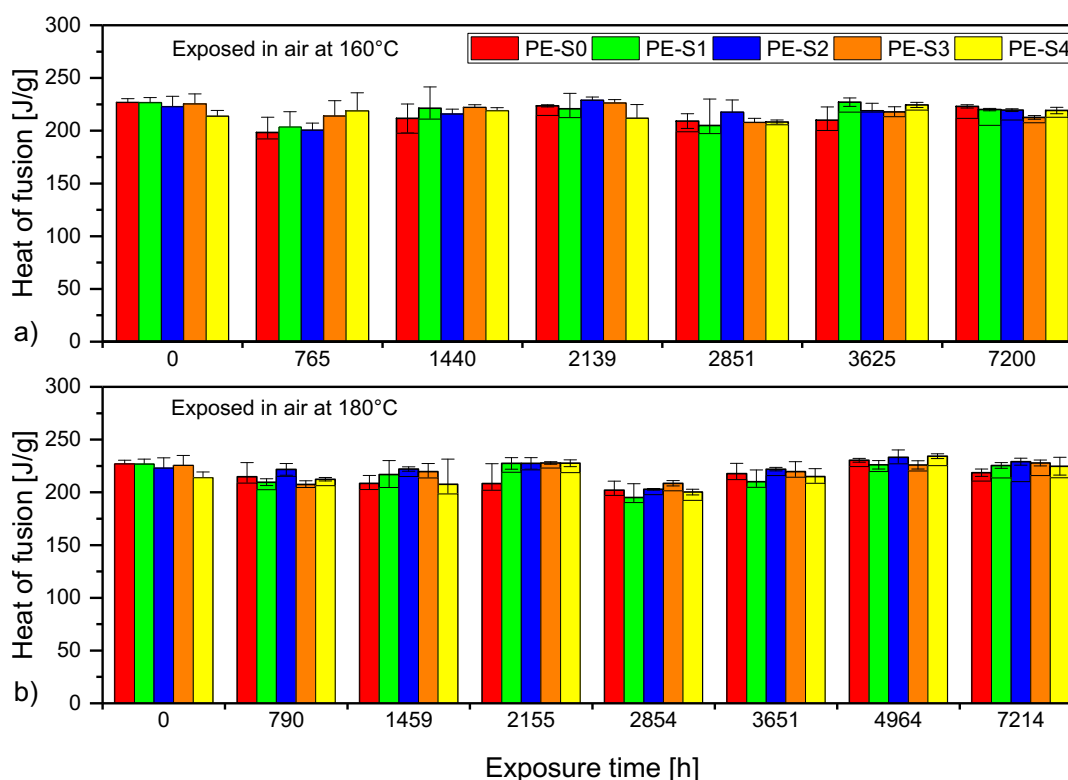

Figure 7.13: The heat of fusion of PE-S0-PE-S4 when stored in air at a) at 160 °C and b) at 180 °C. The opaque columns represent the heat of fusion of the whole volume (ΔH_{Mwhole}). The transparent columns represent the heat of fusion of the mobile specimen part (ΔH_{Mmob}). Only minor losses of the heat of fusion were detected after the applied thermo-oxidative loads.

7.6. Stability and aging phenomena

The characterization of the exposed HDPE specimens revealed two thermo-oxidative aging phenomena, the first one being the unevenly distributed discoloration patterns in the specimen bulk of the additionally stabilized specimens PE-S1 - PE-S4 (Figure 7.4). They were mainly caused by the

110

thermo-oxidative degradation of the TMQ (Figure 7.9 and Figure 7.10). Therefore the discolored specimen parts in the bulk were at the surface at some point when their color was changed. They were then moved into the specimen bulk leaving the tracks of their movement as indicated by the yellow arrows in Figure 7.14a. The melt movement was caused by small temperature gradients in the convection oven and the movability of the melted specimens which resulted in a natural convection within the specimen bulk causing the helically pattern.

For the non-additionally stabilized PE, no discoloration patterns in the specimen bulk were found. This was due to an immediate immobilization of the surface after 765 h/790 h of exposure because of the lack of an additional stabilizer. This hindered the degraded specimen surface to be part of the melt movement (Figure 7.14b). Thus, the strongly-oxidized immobile specimen surface of the non-additionally stabilized PE acted as a "sacrificial" protective layer for the specimen bulk against thermo-oxidative degradation.
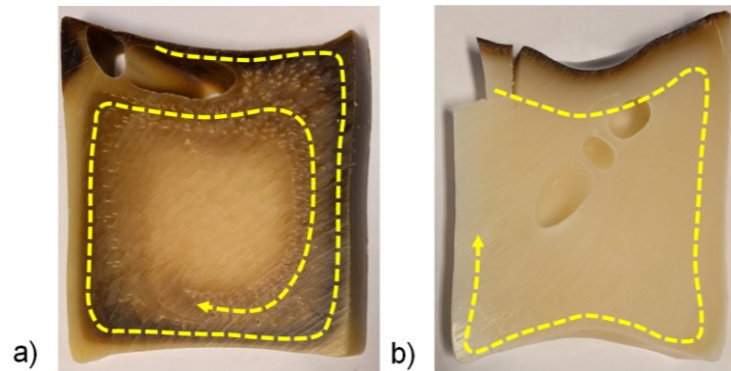

Figure 7.14: Direction of the melt movement during the static exposure due to the combination of small temperature gradients in the convection ovens and melt movability. a) PE-S3-160°C-765h: the additional stabilization delayed oxidation and an immobilization of the specimen surface. It was therefore moved into the specimen bulk by natural convection resulting in the discoloration patterns. b) PE-S0-160°C-765h: the specimen surface was immobilized immediately, lost its melt movability and was therefore not moved into the specimen bulk by natural convection.

The second thermo-oxidative aging phenomenon was the larger final OPDs of the additionally stabilized PE over the OPDs of the non-additionally stabilized PE and the larger final OPD for the additionally stabilized PE at the lower exposure temperature of 160 °C than at the higher exposure temperature of 180 °C (Figure 7.7a and b). The additional stabilization of the PE did not only delay the oxidation but also the immobilization of the specimen surface and the formation of a protective layer for the specimen

bulk. Thus, the OPD was increased by the delay in oxidation/immobilization for the additionally stabilized PE. Only once the stabilizer effectiveness decreased, the oxidation set in in the specimen. However, as the stabilizer had not yet lost its full effectiveness, a lower extent of oxidation in the immobile specimen part was ascertained (Figure 6b) which proved to be a less effective protective layer against thermo-oxidation. This resulted in a larger final OPD of the additionally stabilized PE (both exposure temperatures) over the non-additionally stabilized PE and in a larger final OPD of the additionally stabilized PE when exposed at 160 °C compared to when exposed at 180 °C.

Whereas the oxidation of the non-additionally stabilized PE seemed to be very clear (immediate oxidation at the specimen surface accompanied by discoloration and immobilization, loss of ΔH_M due to destruction of the crystalline morphology), the oxidation phenomena of the additionally stabilized PE proved to be more complex as discussed in the preceding paragraphs. They are chronically put into order in the following:

1. The additional stabilizer is degraded and evaporates physically, its effectiveness is decreased and discoloration occurs at the specimen surface (Figure Figure 7.8). No change in the crystalline structure of the polymer occurs (Figure 7.11a) and ΔH_M remains unchanged as no oxidation of polymer occurs. The specimen surface is still moveable and the distribution of the discolored specimen part from the surface into specimen bulk takes places due to natural convection.
2. The stabilizer is mostly degraded and/or evaporated and its effectiveness decreases further. The oxidation sets in (Figure 7.7b) causing a change in the crystalline structure when the polymer is cooled (Figure 7.11b) and a decrease in ΔH_M (Figure 7.12b). The specimen surface is immobile. The melt movement still takes place, but the immobile specimen part at the surface is not included anymore.
3. The effectiveness of the stabilizer is completely lost due to degradation and physical evaporation. A high extent of oxidation of the polymer is present which is accompanied by a total loss of the crystalline superstructure (Figure 7.12a). The affected specimen part turns completely amorphous (Figure 7.11c).

Condensed, regarding the application of PE as PCM the incorporation of an additional stabilization seems to be rather counterproductive: the immediate immobilization of the specimen surface acted as a protective layer for the specimen bulk and thus maintained the molecular and supermolecular

structure to the greatest possible extent. However, the surface of the non-additionally stabilized PE specimen exhibited cracks after higher exposure times. The sealed immobile surface was not intact anymore. Therefore, atmospheric oxygen could again diffuse into the specimen. This might have caused the non-steady increase in OPD for the non-additionally stabilized PE after 7200 h of exposure at 180 °C. However, this was not detected when exposed at 160 °C.

7.7.   Conclusion and outlook

The present study demonstrated that the specimen dimensions of polymeric phase change materials (PCM) are crucial as they determine the surface through which the atmospheric oxygen can diffuse into the polymer bulk. The diffused oxygen initiates oxidation which further results in a loss in ΔH_M und thus the storage capacity. A small surface in regard to the total volume is therefore desirable for polymeric PCM. Nonetheless, the majority of the storage capacity was maintained during the applied thermal loads for all high-density polyethylene (HDPE) types. Thus HDPE proves to be a promising/applicable polymeric PCM.

7.8.   Acknowledgements

7.9.   References

[1]   H.M. Weingrill, K. Resch-Fauster, C. Zauner, Applicability of Polymeric Materials as Phase Change Materials, Macromol. Mater. Eng. 31 (2018) 1800355.

[2]   I. Krupa, Z. Nógellová, Z. Špitalský, I. Janigová, B. Boh, B. Sumiga, A. Kleinová, M. Karkri, M.A. AlMaadeed, Phase change materials based on high-density polyethylene filled with microencapsulated paraffin wax, Energy Conversion and Management 87 (2014) 400–409.

[3]   C. Yang, M.E. Navarro, B. Zhao, G. Leng, G. Xu, L. Wang, Y. Jin, Y. Ding, Thermal conductivity enhancement of recycled high density polyethylene as a storage media for latent heat thermal energy storage, Sol Energ Mat Sol C 152 (2016) 103–110.

[4]   I.O. Salyer, J.E. Davison, Thermal-energy storage in crosslinked pellets of high-density polythylene for home heating and cooling via off-peak electric power utilization, J. Appl. Polym. Sci. 28 (9) (1983) 2903–2924.

[5]   C. Zauner, F. Hengstberger, M. Etzel, D. Lager, R. Hofmann, H. Walter, Durability of a fin-tube latent heat storage using high density polyethylene as PCM, IOP Conf. Ser.: Mater. Sci. Eng. 251 (2017) 12123.

[6]   A. Abhat, Low temperature latent heat thermal energy storage: Heat storage materials, Solar Energy 30 (4) (1983) 313–332.

[7]   C. Krebs, K.W. Leu (Eds.), Langzeitverhalten von Thermoplasten: Alterungsverhalten und Chemikalienbeständigkeit, Hanser, München, 1999.

[8]   F. Gugumus, Physico-chemical aspects of polyethylene processing in an open mixer 4. Comparison of PE-LLD and PE-HD with PE-LD, Polym Degrad Stabil 68 (2) (2000) 219–229.

[9]   A.A. Cuadri, J.E. Martín-Alfonso, The effect of thermal and thermo-oxidative degradation conditions on rheological, chemical and thermal properties of HDPE, Polym Degrad Stabil 141 (2017) 11–18.

[10]   P. Oblak, J. Gonzalez-Gutierrez, B. Zupančič, A. Aulova, I. Emri, Processability and mechanical properties of extensively recycled high density polyethylene, Polym Degrad Stabil 114 (2015) 133–145.

[11]   E.M. Hoàng, N.S. Allen, C.M. Liauw, E. Fontán, P. Lafuente, The thermo-oxidative degradation of metallocene polyethylenes: Part 2: Thermal oxidation in the melt state, Polym Degrad Stabil 91 (6) (2006) 1363–1372.

[12]   A.A. Mendes, A.M. Cunha, C.A. Bernardo, Study of the degradation mechanisms of polyethylene during reprocessing, Polym Degrad Stabil 96 (6) (2011) 1125–1133.

[13]   G.C. Furneaux, K.J. Ledbury, A. Davis, Photo-oxidation of thick polymer samples—Part I: The variation of photo-oxidation with depth in naturally and artificially weathered low density polyethylene, Polym Degrad Stabil 3 (6) (1981) 431–442.

[14]   A. Quintana, M.C. Celina, Overview of DLO modeling and approaches to predict heterogeneous oxidative polymer degradation, Polym Degrad Stabil 149 (2018) 173–191.

[15]   E. Richaud, X. Colin, C. Monchy-Leroy, L. Audouin, J. Verdu, Polyethylene stabilization against thermal oxidation by a trimethylquinoleine oligomer, Polym Degrad Stabil 94 (3) (2009) 410–420.

[16]   G.W. Ehrenstein, S. Pongratz, Resistance and stability of polymers, Hanser, München, 2013.

[17]   P. Gijsman, The mechanism of action of hindered amine stabilizers (HAS) as long-term heat stabilizers, Polym Degrad Stabil 43 (2) (1994) 171–176.

[18]   M. Tolinski, Additives for Polyolefins: Getting the Most out of Polypropylene, Polyethylene and TPO, 2nd ed., Elsevier Science, Burlington, 2015.

[19]   H. Zweifel, Stabilization of Polymeric Materials, Springer, Berlin, Heidelberg, 1998.

[20]   E. Richaud, Kinetic modelling of phenols consumption during polyethylene thermal oxidation, Eur Polym J 49 (8) (2013) 2223–2232.

[21]   C.W. Klampfl, M. Himmelsbach, Advances in the determination of hindered amine light stabilizers - A review, Anal. Chim. Acta 933 (2016) 10–22.

[22]   Y.-C. Hsu, R.W. Truss, B. Laycock, M.P. Weir, T.M. Nicholson, C.J. Garvey, P.J. Halley, The effect of comonomer concentration and

distribution on the photo-oxidative degradation of linear low density polyethylene films, Polymer 119 (2017) 66–75.

[23]   L. Costa, M.P. Luda, L. Trossarelli, Ultra high molecular weight polyethylene—II. Thermal- and photo-oxidation, Polym Degrad Stabil 58 (1-2) (1997) 41–54.

[24]   M.C. Antunes, J.A. Agnelli, A.S. Babetto, B.C. Bonse, S.H. Bettini, Correlating different techniques in the thermooxidative degradation monitoring of high-density polyethylene containing pro-degradant and antioxidants, Polymer Testing 69 (2018) 182–187.

[25]   Q. Liu, H. Yang, J. Zhao, S. Liu, L. Xia, P. Hu, Y. Lv, Y. Huang, M. Kong, G. Li, Acceleratory and inhibitory effects of uniaxial tensile stress on the photo-oxidation of polyethylene: Dependence of stress, time duration and temperature, Polymer 148 (2018) 316–329.

[26]   P. Pages, F. Carrasco, J. Saurina, X. Colom, FTIR and DSC study of HDPE structural changes and mechanical properties variation when exposed to weathering aging during Canadian winter, J. Appl. Polym. Sci. 60 (2) (1996) 153–159.

[27]   H. Günzler, H.-U. Gremlich, IR-Spektroskopie: Eine Einführung, 4th ed., Wiley; Wiley-VCH, Hoboken, NJ, Weinheim, 2003.

[28]   M.U. de La Orden, J.M. Montes, J. Martínez Urreaga, A. Bento, M.R. Ribeiro, E. Pérez, M.L. Cerrada, Thermo and photo-oxidation of functionalized metallocene high density polyethylene: Effect of hydrophilic groups, Polym Degrad Stabil 111 (2015) 78–88.

[29]   M. Gardette, A. Perthue, J.-L. Gardette, T. Janecska, E. Földes, B. Pukánszky, S. Therias, Photo- and thermal-oxidation of polyethylene: Comparison of mechanisms and influence of unsaturation content, Polym Degrad Stabil 98 (11) (2013) 2383–2390.

[30]   W. Zhu, G. Zhang, B. Liu, T.M. Chung, Polyethylene containing antioxidant moieties exhibiting high thermal-oxidative stability for high temperature applications, Polymer 146 (2018) 101–108.

[31]   P. Pereira, L. Fernandes, H. Gaspar, G. Bernardo, Melt processed polyethylene/fullerene nanocomposites with highly improved thermo-oxidative stability, Polymer Testing 45 (2015) 124–131.

[32]   J. Gong, R. Niu, N. Tian, X. Chen, X. Wen, J. Liu, Z. Sun, E. Mijowska, T. Tang, Combination of fumed silica with carbon black for simultaneously improving the thermal stability, flame retardancy and mechanical properties of polyethylene, Polymer 55 (13) (2014) 2998–3007.

Part V.

Functionalized polymeric phase-change materials

8.   Introduction to publication 3

In publication 1 and 2 the applicability of neat polymers as phase-change materials (PCM) in latent heat storages was proven in terms of their high storage capacity, different application temperatures and their ability to maintain these material characteristics during application-relevant conditions. However, the low inherent thermal conductivity (TC) of semi-crystalline polymers in the approximate range from 0.3-0.6 W/(mK) [1] inhibits fast heat transfer rates and decelerates the discharging and charging procedure of the latent heat storage. A higher TC of polymeric PCM would therefore significantly improve the well-functioning of the latent heat storage and thereby enhance the competitiveness of polymeric PCM against existing PCM.

The low TC of polymers has already been addressed in the scientific literature as higher conductivities are necessary for all applications that require enhanced thermal management such as electronic packaging or printed circuit boards [1,2]. For these applications, the TC could be increased by up to several hundred percent via the incorporation of highly conductive particles [1]. For PCM, however, the incorporation of particles comes along with a reduction in the storage capacity as the fillers do typically not undergo a phase transition in the application temperature range of the PCM. Thus, available fillers for enhancing the TC which are also economically reasonable need to be screened for an efficient TC enhancement of polymeric PCM.

The exact TC of a PCM is essential for an appropriate design of the latent heat storage as the heat transfer rate depends inter alia on the heat exchange surface between the heat transfer fluid and the PCM as well as on their TC. The TC of the compound is a function of the TC of the polymer and the filler [2]. As stated above, the TC of semi-crystalline polymers are comparably rather similar whereas the intrinsic TC of the available fillers for enhancing their TC (metals, carbon-based materials, ceramic fillers [2]) range from 6 W/(mK) for carbon black to up to 7000 W/(mK) for single-walled carbon nanotubes [1]. This results in differences in the enhancement of the TC depending on the filler type. Furthermore, the filler shape, size, size

distribution, processing, specimen preparation resulting in different filler orientations and filler surface treatment [3-7] as well as the applied measurement method [8] may also affect the TC of compounds. Thus, in order to execute reliable TC measurements, the impacts on TC need to be investigated in detail prior to the necessary filler screening. Publication 3 identifies and analyses those impacts for 20 polymeric materials (two neat polymers, 18 compounds). Their TC is determined with different commercially available devices and their morphology is investigated in detail. The identified impacts can thereby be categorized into material- and technology-induced ones.

Besides the publication shown in the following, contributions in terms of oral presentations have been made by the author in this field and are given in the following:

Conference contribution: H. Weingrill, W. Hohenauer, K. Resch-Fauster, L. Gnegeler, C. Zauner.; "Thermal conductivity of polymeric materials – finding the appropriate measurement system", 3rd International Conference on thermophysical and mechanical Properties of Advanced Materials, Izmir, TR, 2016

Conference contribution: H. Weingrill; "Thermal conductivity of polymeric materials", Look and feel like metals, but design flexibility of plastics: New aspects of polymers and metal-polymer composites, Slovenj Gradec, SI, 2018

8.1. References

[1]   N. Mehra, L. Mu, T. Ji, X. Yang, J. Kong, J. Gu, J. Zhu, Thermal transport in polymeric materials and across composite interfaces, Applied Materials Today 12 (2018) 92–130.

[2]   H. Chen, V.V. Ginzburg, J. Yang, Y. Yang, W. Liu, Y. Huang, L. Du, B. Chen, Thermal conductivity of polymer-based composites: Fundamentals and applications, Prog Polym Sci 59 (2016) 41–85.

[3]   K. Wattanakul, H. Manuspiya, N. Yanumet, Thermal conductivity and mechanical properties of BN-filled epoxy composite: Effects of

filler content, mixing conditions, and BN agglomerate size, J Compos Mater 45 (19) (2011) 1967–1980.

[4]   H.J. Ahn, Y.J. Eoh, S.D. Park, E.S. Kim, Thermal conductivity of polymer composites with oriented boron nitride, Thermochim Acta 590 (2014) 138–144.

[5]   S. Ganguli, A.K. Roy, D.P. Anderson, Improved thermal conductivity for chemically functionalized exfoliated graphite/epoxy composites, Carbon 46 (5) (2008) 806–817.

[6]   B. Debelak, K. Lafdi, Use of exfoliated graphite filler to enhance polymer physical properties, Carbon 45 (9) (2007) 1727–1734.

[7]   H.S. Tekce, D. Kumlutas, I.H. Tavman, Effect of Particle Shape on Thermal Conductivity of Copper Reinforced Polymer Composites, J Reinf Plast Comp 26 (1) (2007) 113–121.

[8]   W.N. dos Santos, Thermal properties of polymers by non-steady-state techniques, Polym Test 26 (4) (2007) 556–566

.

9. Publication 3

9.1. Bibliographic information

- Title: Analyzing thermal conductivity of polyethylene-based compounds filled with copper

- Authors:
  - Helena Weingrill[1,2]
  - Wolfgang Hohenauer[3]
  - Katharina Resch-Fauster[1]
  - Christoph Zauner[3]

- Affiliation:

  1. Materials Science and Testing of Polymers, Montanuniversitaet Leoben, Otto-Gloeckel-Strasse 2, 8700 Leoben, Austria

  2. Polymer Processing, Montanuniversitaet Leoben, Otto-Gloeckel-Strasse 2, 8700 Leoben, Austria

  3. Austrian Institute of Technology, Giefinggasse 2, 1020 Vienna, Austria

- Periodical: Macromolecular Materials and Engineering

9.2.   Abstract

The thermal conductivity (TC) of different polymeric materials is measured via four commercially available testing devices: TPS2500S by Hot Disk (Hot Disk), Transient Hot Bridge (THB) by Linseis, the Laser Flash Analysis (LFA) by NETZSCH and the DTC-300 by TA Instruments. The investigated materials include high-density polyethylene (HDPE) and linear low-density polyethylene (LLDPE) which are analyzed as received and after being compounded with copper particles. The filler geometry and ratio are varied systematically. Major differences in the TC generated by the different measurement methods are revealed and analyzed in detail. Moreover, material-induced impacts on the TC as well as technology-induced impacts on the TC are outlined comprehensively.

9.3.   Introduction

Polymeric materials exhibit rather low thermal conductivity (TC) in the range from 0.01 to 0.5 W/(mK) [1,2] due to the lack of free-moving electrons. However, their TC can be enhanced by the incorporation of particles which exhibit high TC (compounding). Polymers with enhanced TC are typically used for LED devices, electronic packaging, batteries and solar applications [3] to improve their thermal management. The enhancement of TC can be achieved via the incorporation of the following three main groups of fillers: metal powders (e.g. aluminum, copper or nickel) [4-10] carbon additives (e.g. graphite, graphene, carbon nanotubes or carbon black) [11-24] and mineral fillers (e.g. boron nitride, aluminum nitride or talcum) [18,25-31]. Moreover, hybrid filler systems have been in the focus of investigations [28,32-37] trying to evoke synergistic effects by mixing the above mentioned filler types. Since the fillers are available in different geometries, sizes and surface modifications, much work already covered the effect of varying filler size or shape [4-6,16-19,21,25,28] and specimen preparation (including filler and matrix pretreatment, blending procedure and type of molding) [11,14,15,17, 25-28,34,38-40] on the TC. The TC of polymers can thereby be increased by several hundred percent. Nevertheless, the TC enhancements presented in the scientific literature differ significantly. The scientists apply different

measurement instruments based on varying measurement principles to determine the TC. Only two studies were found that examine a possible impact of the applied measurement device on either the thermal diffusivity (proportional to TC) [41] or on the TC of the polymeric materials [42]. Both studies compare the results generated by the Laser Flash Analysis (LFA) and the Hot Wire technique. If available, also literature results were added to the comparative work. However, this was only done with unfilled polymers whereas compounds have not been tested in spite of their important role in thermal management as mentioned above. Zhao and co-workers [20] published a sound overview on TC of carbon additive-filled compounds based on their own results and on several other publications. In this overview the utilized measurement system was indicated to the according result. This indicates that a possible impact of the applied measurement system on the detected TC was considered. However, to the best of our knowledge, this aspect has not been investigated systematically and comprehensively yet. Thus, the present study aims at examining the impact of the measurement system on the TC of unfilled polymers and of polymeric compounds. It specifically focuses on evaluating material-induced and measurement technology-induced effects on the TC. For this purpose, high-density polyethylene and linear low-density polyethylene were used as unfilled polymers and matrix materials for the compounds. Copper particles with different shapes were added to the polyethylene matrices with filler loadings of 10, 30 and 50 wt%. The applied TC measurement techniques cover four commercially available devices (Hot Disk, Transient Hot Bridge (THB), LFA, DTC-300).

9.4. Experimental section

9.4.1. Materials

Two commercially available semi-crystalline polyethylene types (one high-density polyethylene (HDPE) and one linear low-density polyethylene (LLDPE)) were used. Both types were synthesized via solution polymerization and Ziegler-Natta catalysts. Their melting temperature, density, melt flow rate and degree of crystallinity (as deduced from Differential Scanning Calorimetry (DSC) measurements and described in 9.4.3) are given in Table 9.1.

Table 9.1: Melting temperature, density, melt flow rate and the degree of crystallinity of the applied polyethylene types. The first three characteristics were taken from the manufacturer's material data sheet and determined via ISO 11357-3, ISO 1183 and ISO 1133, respectively. The degree of crystallinity was determined in this study.

Polymer type	Melting temperature [°C]	Density at 23 °C [g/cm³]	Melt flow rate (190 °C/2.16 kg) [g/10 min]	Degree of crystallinity [%]
HDPE	134	0.966	25	≈ 80
LLDPE	124	0.919	6.6	≈ 45

To enhance the thermal conductivity of the polymers three different types of copper particles were used. They were used as received without any further surface treatment or functionalization. The copper particles possess a purity ≥99.9 %. They differ in shape, size and specific surface as summarized in Table 9.2 and depicted in the SEM image given in Figure 9.1 (specimen preparation and experimental setup described in 9.4.3). To describe a compound, the matrix material will be stated first, followed by a "/" and the copper type, followed by a "/" and the contained wt% in the last place. For instance, the HDPE-based compound containing 50 wt% of C1 will be called HDPE/C1/50.

Table 9.2: Shape, size and specific surface of the applied filler/copper types as taken from the manufacturer's data sheet.

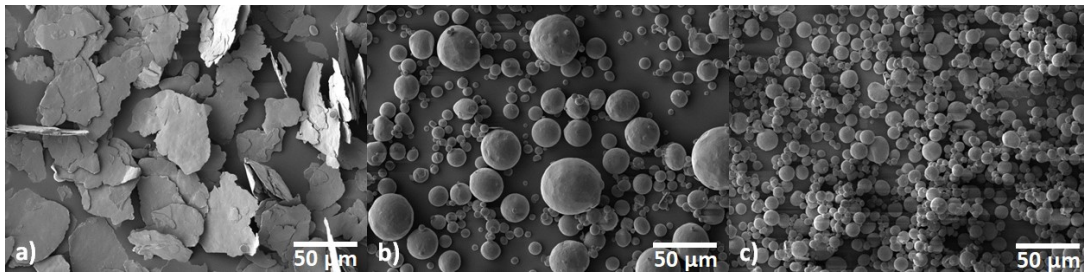| Copper type	Shape	Size [μm]	Specific surface [cm²/g]
C1	Platelet	> 45	4300
C2	Sphere (broad size distribution)	< 63	250
C3	Sphere (narrow size distribution)	< 15	650

Figure 9.1: SE-SEM micrographs of the copper particles exhibiting their different shape, size and size distribution – a) C1 – platelets and a particle size > 45 µm b) C2 – spheres with a broad size distribution and a particle size < 63 µm c) C3 – spheres with a narrow size distribution and a particle size < 15 µm.

9.4.2.　Specimen preparation

The copper particles were blended into each of the polyethylene matrices at filler loadings of 10, 30 and 50 wt% using a compounding extruder. This resulted in a total of 20 polymeric materials (two unfilled polymers and 18 copper compounds). The compounding process was done at GEBA Kunststofftechnik GmbH & Co KG (St. Veit, AT). The granules of the compounds and the unfilled polymers were used to produce plates with a thickness of 1 mm or 4 mm which were used for carrying out experimental tests. A vacuum press P 200 PV (Dr. Collin GmbH, Ebersberg, DE) was used. The compression molding parameters are summarized in Table 9.3.

Table 9.3: Compression molding parameters.

Pressing segment	Temperature [°C]	Time (4 mm/1 mm) [min]	Pressure [bar]
1	200	20/5	0
2	200	5/3	16
3	200	3/2	23
4	200	1/1	39
5	30	10/10	39

After compression molding, the plates with a thickness of 4 mm were cut with a specimen saw Diadisc 500 (MUTRONIC Praezisionsgeraetebau GmbH & Co.KG, Rieden am Forggensee, DE) into 160 mm * 80 mm plates for the Hot Disk and the Transient Hot Bridge (THB) measurements (measurement

devices are explained in the following section). After the Hot Disk and THB measurements were executed, disk-like specimens with a diameter of 50 mm were taken from the used Hot Disk and THB specimens (4 mm-plates) by a hydraulic workshop press of 20 t (Erba GmbH, Vienna, AT) for the DTC measurements. For the Laser Flash Analysis (LFA) and the Differential Scanning Calorimetry (DSC) measurements (in order to determine the specific heat capacity), the plates with a thickness of 1 mm were punched manually with a hollow puncher (Hilka Tools, Chessington, UK) into disk-like specimens with diameters of 12.7 mm and 5 mm respectively. Afterwards the specimens were deburred with fine sandpaper.

9.4.3. Analysis of specimen morphology

The filler loading was determined by Thermogravimetrical Analysis (TGA) on a TGA/DSC 1 (Mettler Toledo GmbH, Greifensee, CH). The samples were taken from the plates with a thickness of 4 mm and the weight was 10 mg. 70 µl alumina crucibles were used. After an equilibration time of 10 min at 25 °C, the samples were heated under nitrogen atmosphere (in order to prevent oxidation of copper) from 25 °C to 600 °C by applying a constant heating rate of 20 °C/min. Polymer pyrolysis took place between 400 °C and 530 °C. Therefore, the sample weights at 100 °C (m_{100}) and 550 °C (m_{550}) was used to calculate the filler loading f in wt% as presented in equation (1)

$$f = \frac{m_{550}}{m_{100}} * 100\% \tag{1}$$

The presented data represent the average of three measurements.

The polymer's degree of crystallinity was determined by DSC on a DSC 1 (Mettler Toledo, Greifensee, CH). The specimens were taken from the plates with a thickness of 4 mm (unfilled polymers and compounds) and the weight was 7 mg. 40 µl aluminum crucibles were used. After an equilibration time of 5 min at 0 °C, the samples were heated under nitrogen atmosphere from 0 °C to 160 °C and cooled down to 0 °C by applying a constant heating and cooling rate of 10 °C/min and -10 °C/min, respectively. Evaluations were done on thermograms from the heating according to ISO 11357-3. The degree of crystallinity k was calculated as presented in equation (2)

$$k = \frac{\Delta H_m}{\Delta H_m^0} * 100\% \tag{2}$$

with ΔH_m as the polymer's heat of fusion in J/g and ΔH_{m0} as the heat of fusion of a 100% crystalline polymer (ΔH_{m0} of polyethylene was assumed to be 293 J/g [43]). The measured heat of fusion of the compounds was

weighted for the weight fraction of the polymeric material as deduced from TGA. The presented data represent the average of three measurements.

The morphology of the different materials and compounds was investigated by Scanning Electron Microscopy (SEM) on a Tescan-Vega-II (TESCAN, Brno, CZ). The copper particles were sprinkled on an adhesive carrier and sputtered with gold with a sputter coater SCD005 (BalTec Maschinenbau AG, Pfäffikon, CH). An electrical voltage of 5 kV was applied and images were recorded in secondary electron (SE) mode. Micrographs of the cross sections of the specimens containing copper particles were prepared by grinding and polishing with a grinder Phoenix Beta (Buehler, Lake Bluff, IL, US) and the abrasive papers with varying roughness CarbiMetTM SiC P600, P1200, P2500 and P4000 (Buehler, Lake Bluff, IL, US) were used. Afterwards the compounds were sputtered with gold as described above. The specimen surfaces of the compounds were aligned parallel to the horizontal edges of each micrograph. An electrical voltage of 25 kV was applied and images were recorded in back-scattering electron (BSE) mode. Selected specimens were cooled in liquid nitrogen and ruptured in an impact pendulum to investigate the matrix-filler-bonding of the compounds. The fractured surface was sputtered with gold as described above. An electrical voltage of 5 kV was applied and images were recorded in the secondary electron (SE) mode.

9.4.4.   Thermal conductivity measurements

Four different commercially available thermal conductivity measurement devices were applied in this study and will be explained here shortly. Furthermore, the applied measurement parameters are explained in detail. All experiments were conducted at room temperature.

9.4.4.1. TPS 2500S by Hot Disk AB (Gothenborg, SE)

The TPS 2500S uses a non-steady-state model which is based on the standardized transient plane heat source technique (ISO 22007-2:2015) and similar to the before mentioned Hot Wire technique applied in [41,42]. In this work, this measurement method will be referred to as the Hot Disk. A sensor made of a double spiral nickel wire which is surrounded by a protecting insulation is placed between two specimen plates with flat surfaces as shown in Figure 9.2a. During the measurement a current is sent through the nickel wire. The current evokes a raise in temperature of the wire itself and of the surrounding material. The temperature raise evokes a quantifiable change of the electrical resistance within the nickel wire. This change depends on the thermo-physical properties of the specimen material. Through the known

power input and the temperature raise (measured via the change in electrical resistance), the thermal conductivity, thermal diffusivity and the specific heat are evaluated via solving complex thermal conductivity equations [44]. The equations are based on the physical dimensions of the sensor and by assuming infinite specimen dimensions and a concentric circle alignment of the nickel wire. A temperature raise of about 1 K is recommended for proper evaluation. The power output and the measurement time must be chosen prior to each measurement the measurement module. Different measurement modules take the morphological aspects of the specimens into account like an isotropic morphology (generates an overall TC), an anisotropic morphology (generates an axial and a radial TC) or stack-like specimens. It is an absolute technique which does not require calibration. Within the present study, the sensor type 7577 was used, which exhibits Kapton insulation and a wire radius of 2 mm. At least six measurements were conducted for each sample, whereas the sensor position was changed for each measurement to generate a statistical mean of the specimen's TC. For all materials the isotropic measurement module was applied. The anisotropic measurement module was additionally implemented for the compounds containing C1 particles. The power output and the measurement time were adjusted according to the applied material in order to reach the recommended temperature raise of 1 K and ranged between 0.03 - 0.1 W and 1-10 sec, respectively.
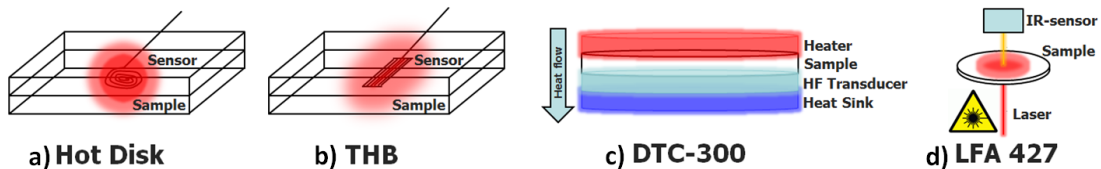

Figure 9.2: Schematic measurement set-ups a) Hot Disk b) THB c) DTC-300 d) LFA 427.

9.4.4.2. Transient Hot Bridge by Linseis (Selb, DE)

The Transient Hot Bridge operates on a similar principle as the Hot Disk (and the Hot Wire technique). Solely the wire in the sensor is aligned in a parallel pattern instead of a concentric pattern which causes different heat propagation within the specimen as given in a schematic in Figure 9.2b. In contrast to the Hot Disk only one measurement module is available. The THB can be calibrated prior to each measurement with different standards of known TC. The apparatus was calibrated with two materials of known TC (poly (methyl methacrylate) (PMMA) and BK7 (a highly pure borosilicate glass)) and LLDPE of which the TC was generated beforehand via a LFA

measurement. The sensor type THB6K77 was used for the present study. Several measurements were conducted for each sample, whereas the sensor position was changed for each measurement. The applied current was set to 75 mA and the measurement time ranged between 10 - 15 sec.

9.4.4.3. DTC-300 by TA Instruments (New Castle, US)

The DTC-300 offers a steady-state technique to measure TC by applying the ASTM E1530 guarded heat flow meter test method. The process of TC determination will be explained in more detail for this method since it is not as widely used as the other applied methods. A disk-like shaped specimen is placed within a cylindrical stack consisting of a top heater and its plate, the specimen itself, a heat flow transducer, a bottom heater and a heat sink as depicted in Figure 9.3. T_u, T_m and T_l represent the measured temperature of the placed thermocouples. The stack is placed in an oven to easily set the experiment temperature. A defined compressive load is applied on the stack to hold the measurement set-up in place. An axial temperature gradient is then established between the top heater and the heat sink which results in a constant heat flux through the specimen. The constant heat flux is equal to the heat flux through the heat flux transducer.
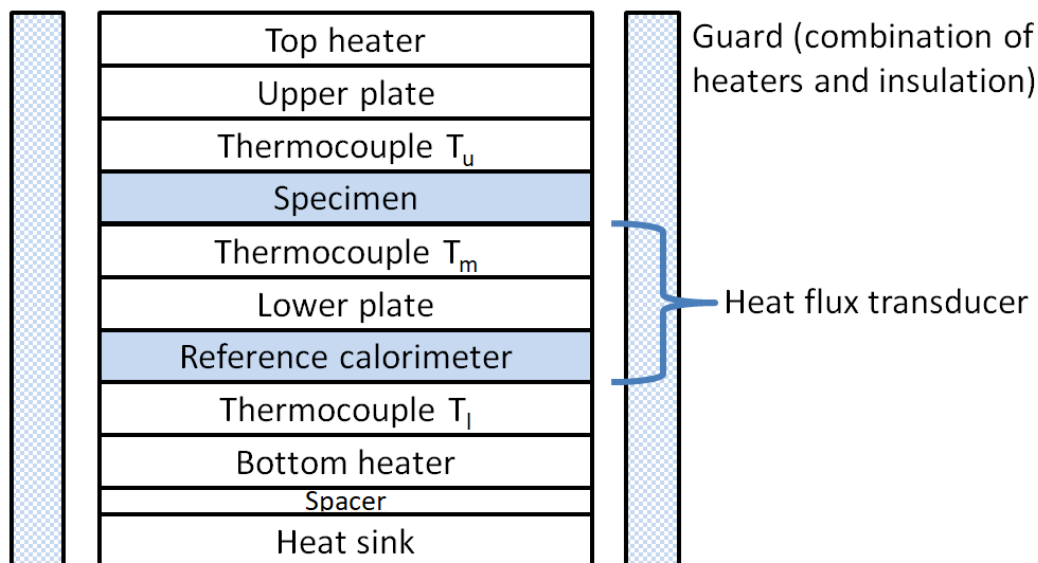

Figure 9.3: Schematic of the DTC-300 experimental set-up [45].

The Fourier heat flow equation can be applied to the specimen because of the constant heat flow as in equation (3),

$$R = \frac{T_u - T_m}{Q} - R_{int} \qquad (3)$$

132

with R as the thermal resistance of the test specimen, T_u as the upper plate surface temperature, T_m as the lower plate surface temperature, Q as the heat flux through the test specimen and R_{int} as the total thermal resistance of the interface between the specimen and the surface plates. The thermal resistance of the test specimen R is further defined as in equation (4),

$$R = \frac{d}{\lambda} \tag{4}$$

with d as the specimen thickness and λ as the TC. Q can be determined by measuring the temperature difference through the reference calorimeter as defined in equation (5)

$$Q = N(T_m - T_l) \tag{5}$$

with N as the reference calorimeter heat transfer coefficient, T_m to the lower plate surface temperature and T_l to the bottom heater surface temperature. Inserting equation (5) into equation (3) yields equation (6)

$$R = \frac{1}{N} * \frac{T_u - T_m}{T_m - T_l} - R_{int} \tag{6}$$

with $(T_u$-$T_m)$ as the temperature difference across the specimen and $(T_m$-$T_l)$ as the temperature difference across the reference calorimeter. Equation (6) demonstrates the linear relationship between R and temperature differences across the specimen $(T_u$-$T_m)$ and the reference calorimeter $(T_m$-$T_l)$ with $1/N$ as the slope and R_{int} as the y-axis intersection. Therefore, $1/N$ and -R_{int} can be determined via calibration with specimens of known thermal resistance when measured at varied temperature differences as depicted in Figure 9.4.
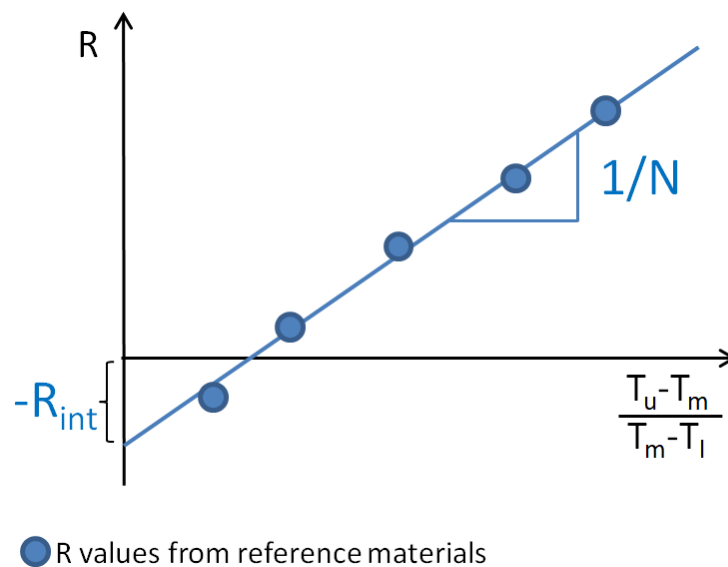

○ R values from reference materials

Figure 9.4: DTC calibration process.

Thus, *R* of any unknown specimen can be determined. The TC can then be evaluated simply by entering the specimen thickness into the MODEL 2022 DATA ANALYSIS SOFTWARE (Anter Corporation, Pittsburgh, US). Two specimens for each material were tested twice. Thus, the presented data represent the average of four measurements.

9.4.4.4. Laser Flash Analysis 427 & DSC 204 F1 by NETZSCH (Selb, DE)

The LFA is a non-steady technique where the material's thermal diffusivity is evaluated. A laser beam hits one side of a disk-like shaped specimen which causes an increase in the specimen's temperature (energy pulse). The specimen's temperature is detected on the opposite surface via an infrared (IR)-sensor. The experimental set-up is given in Figure 9.2d. A typical temperature rise that is expected to be observed on the opposite side of the specimen is demonstrated in Figure 9.5.
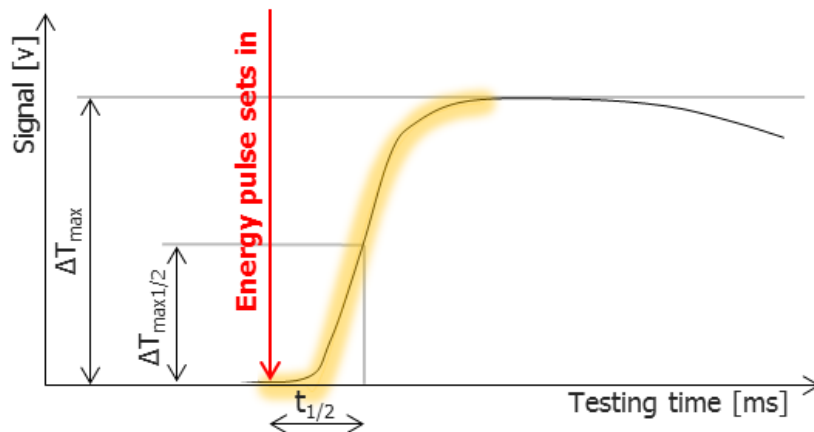

Figure 9.5: Detected signal during LFA experiment representing the temperature rise of the specimen during a Laser Flash Analysis experiment.

The thermal conductivity was determined according to equation (7),

$$\lambda = a \cdot \rho \cdot c_p \tag{7}$$

with *a* as the thermal diffusivity, *ρ* as the density and c_p as the specific heat of the material. The density of each material was determined at room temperature by measuring the physical dimensions of 6 different LFA specimens with a digital caliper and weighing them. The detected densities were compared to the theoretic ones as described in 9.5.1. After the determination of their density, the specimens were coated with colloidal graphite for LFA experiments in order to overcome the IR-transmittance of the polymeric material. The specific heat was determined via a NETZSCH

DSC 204 F1 by using sapphire as a standard. Three specimens were used for each material and several measurements were conducted on each specimen.

9.5. Results and discussion

9.5.1. Specimen morphology

The filler loading, the degree of crystallinity and the density of the different material types are summarized in Table 9.4. The theoretic density ρ_{theo} was determined according to equation (8),

$$\rho_{theo} = \frac{100}{\frac{100-\varphi_{Cu}}{\rho_{PE}} + \frac{\varphi_{Cu}}{\rho_{Cu}}} \tag{8}$$

with ρ_{PE} as the density of PE (deduced from the material data sheet, listed in Table 9.1), ρ_{Cu} as the density of copper which was assumed to be 8.94 g/cm³ [46] and ρ_{Cu} as the weight fraction of copper.

Table 9.4: Theoretic and detected filler loadings and densities as well as the degree of crystallinity of the investigated samples. The actual filler loading was detected by TGA measurements. The actual degree of crystallinity was deduced from DSC measurements (first heating curve). The actual density was determined by measuring the physical dimensions of the samples and by weighing them.

Polymer type	Filler type	Filler loading [wt%]		Degree of crystallinity [%]	Density [g/cm³]	
		Theoretic	Detected		Theoretic	Detected
HDPE	**-**	**-**	**-**	**80 ± 0.4**	**0.966**	**0.966 ± 0.005**
HDPE	C1	10	8.4 ± 0.21	82 ± 0.1	1.061	1.033 ± 0.005
		30	29.9 ± 0.34	78 ± 1.8	1.319	1.297 ± 0.003
		50	50.1 ± 0.24	80 ± 0.9	1.743	1.738 ± 0.019
	C2	10	9.5 ± 0.28	78 ± 2.2	1.061	1.057 ± 0.006
		30	28.2 ± 0.14	79 ± 1.8	1.319	1.289 ± 0.001
		50	49.7 ± 0.26	78 ± 2.8	1.743	1.682 ± 0.112
	C3	10	13.5 ± 0.52	80 ± 0.6	1.061	1.086 ± 0.004
		30	31.3 ± 0.18	81 ± 1.9	1.319	1.333 ± 0.006
		50	49.5 ± 0.19	79 ± 2.1	1.743	1.728 ± 0.011

				45 ± 0.8	0.916	0.929 ± 0.003
LLDPE	**-**	**-**	**-**	**45 ± 0.8**	**0.916**	**0.929 ± 0.003**
LLDPE	C1	10	8.8 ± 0.06	42 ± 1.2	1.020	1.002 ± 0.008
		30	27.7 ± 0.16	43 ± 1.8	1.270	1.222 ± 0.005
		50	50.7 ± 0.31	43 ± 0.7	1.683	1.680 ± 0.011
	C2	10	10.5 ± 0.22	44 ± 1.1	1.020	1.021 ± 0.005
		30	28.2 ± 0.20	43 ± 0.2	1.270	1.227 ± 0.006
		50	49.3 ± 0.45	42 ± 1.2	1.683	1.660 ± 0.007
	C3	10	12.0 ± 2.17	42 ± 0.8	1.020	1.023 ± 0.007
		30	30.9 ± 0.83	44 ± 1.1	1.270	1.258 ± 0.010
		50	48.3 ± 0.42	46 ± 0.3	1.683	1.612 ± 0.013

The detected filler loadings and densities were in good agreement with the theoretic values. The degrees of crystallinity of the unfilled HDPE and LLDPE were 80 % and 45 %, respectively. The degree of crystallinity of HDPE did not change significantly by the addition of copper particles for all compounds. The degree of crystallinity was highest for HDPE/C1/10 with 82 % and lowest for HDPE/C2/10 and HDPE/C2/50 with 78 %. Except for LLDPE/C3/50, the degree of crystallinity of LLDPE was decreased by the addition of copper particles. However, no distinct relationship between the filler geometry or the filler concentration and the decrease in the degree of crystallinity was ascertainable. The degree of crystallinity was lowest for LLDPE/C1/10, LLDPE/C2/50 and LLDPE/C3/10 with 42 % which gave a relative decrease of the degree of crystallinity of 7 %.

In order to display the filler distribution, in Figure 9.6 representative BSE-SEM micrographs of different LLDPE-based compounds with a filler loading of 30 wt% are depicted exemplarily. The filler particles were distributed evenly without agglomerates throughout the specimens of the LLDPE- and HDPE-based compounds (micrographs with larger magnifications were taken but are not shown here).
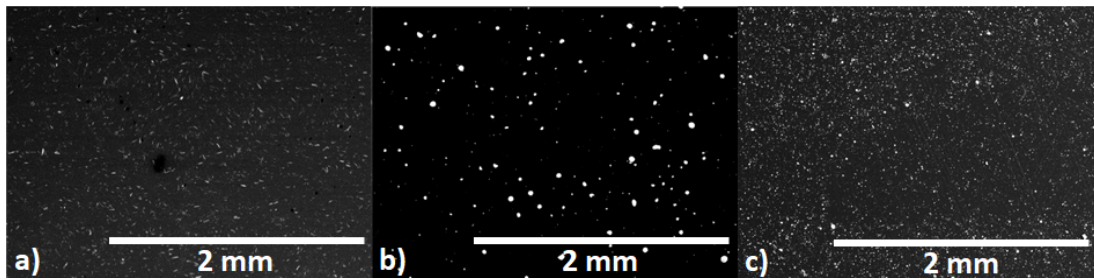
Figure 9.6: Representative BSE-SEM micrographs of the cross sections of the specimens containing copper particles: a) LLDPE/C1/30 4mm-plate b) LLDPE/C2/30 4mm-plate c) LLDPE/C3/30 4 mm-plate.

SEM images revealed the absence of voids for the great majority of samples which correlates with the excellent agreement between the theoretic and the detected material densities (see Table 9.4). Merely, for samples HDPE/C1/30 and LLDPE/C1/50 voids were observed by means of SEM. However, also for these samples the theoretic and the detected densities coincided. Thus, the quantity of voids must be rather low. Interestingly, the voids were only detected in samples containing C1 particles. This was attributed to the comparably high specific surface of the C1 particles (4300 cm²/g vs. 250 cm²/g and 650 cm²/g for the C2 and C3 particles, respectively). The incorporation of the C1 particles caused the material to become form-stable even above its melting temperature (the material had lost its flowability in the melted state without any externally applied force). This hampered the material's processability during the compression molding significantly.

For all specimens formulated with C1 particles an orientation of the platelets parallel to the specimen surface was detected. This is shown exemplarily in the BSE-SEM micrograph of the specimen with a thickness of 1 mm of HDPE/C1/10 in Figure 9.7. For the specimens with a thickness of 4 mm, the parallel orientation was mainly present close to the specimen surface. This is probably due to the processing of the specimen. A schematic of the compression molding process is depicted in Figure 9.8. About 40 bar of pressure were applied via parallel plates to the polymer melt. The melt was first moved in the same direction as the plates move but was eventually also moved parallel to plates to fill the mold. This is indicated via the yellow arrows in Figure 9.8. The C1 particles therefore aligned parallel to the flow direction of the polymer melt. The orientation was less pronounced for the specimens with a thickness of 4 mm because the larger gap between the plates left more room for melt circulation.
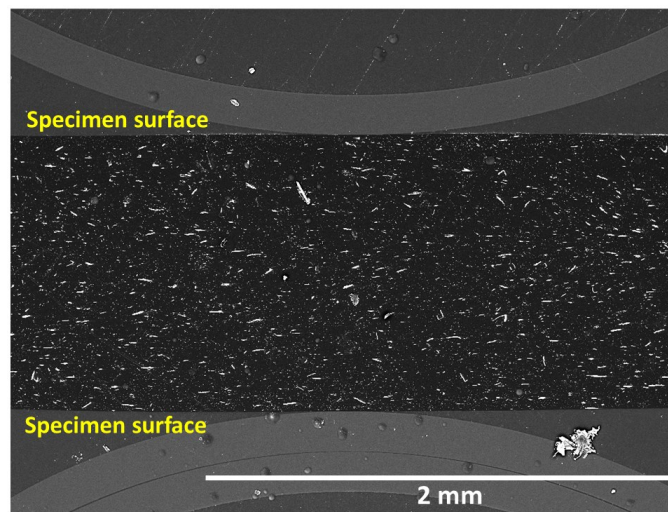
Figure 9.7: BSE-SEM micrograph of the 1 mm – specimen of HDPE/C1/10: orientation of the copper platelets parallel to the specimen surface.
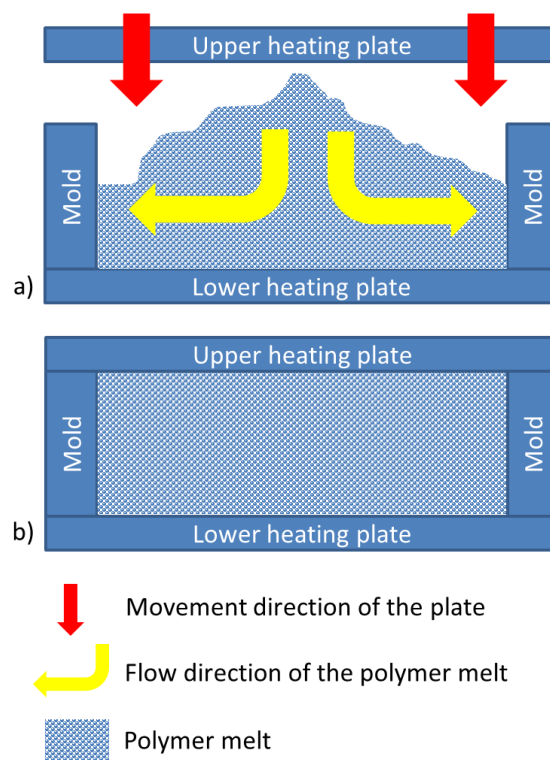

Figure 9.8: Schematic of the set-up during the compression molding process: a) the polymer melt is compression molded into the mold; b) the mold is filled with the polymer melt.

9.5.2.   Thermal conductivity

In Figure 9.9 and Figure 9.10 the TC of HDPE- and LLDPE-based compounds as detected by the various measurement devices are displayed, respectively. The lines in the background indicate the TC of the unfilled polymer. The BK7 as calibration standard and the Radiation model for evaluation were chosen out of the different options for calibration (THB) and evaluation (LFA) (details are given in 9.5.2.2.). In the following material-induced and technology-induced impacts on the TC are discussed in detail.
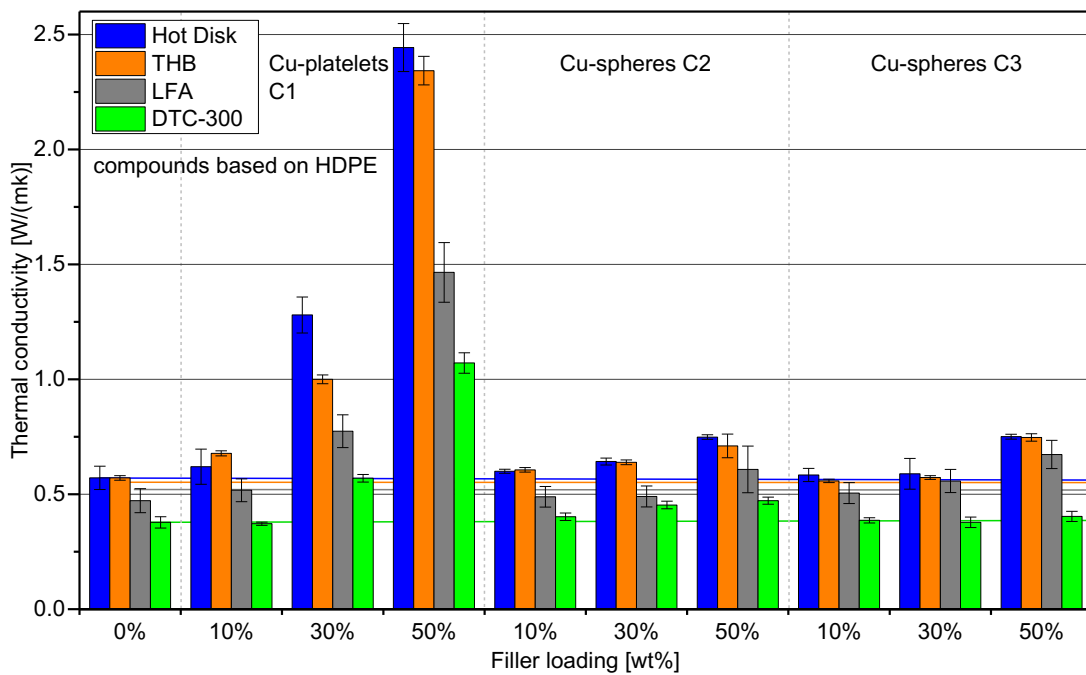

Figure 9.9: Effect of the filler geometry and concentration on the TC of HDPE-based compounds as determined by Hot Disk (isotropic measurement module), THB (BK7 calibration), LFA (Radiation evaluation model) and DTC-300.
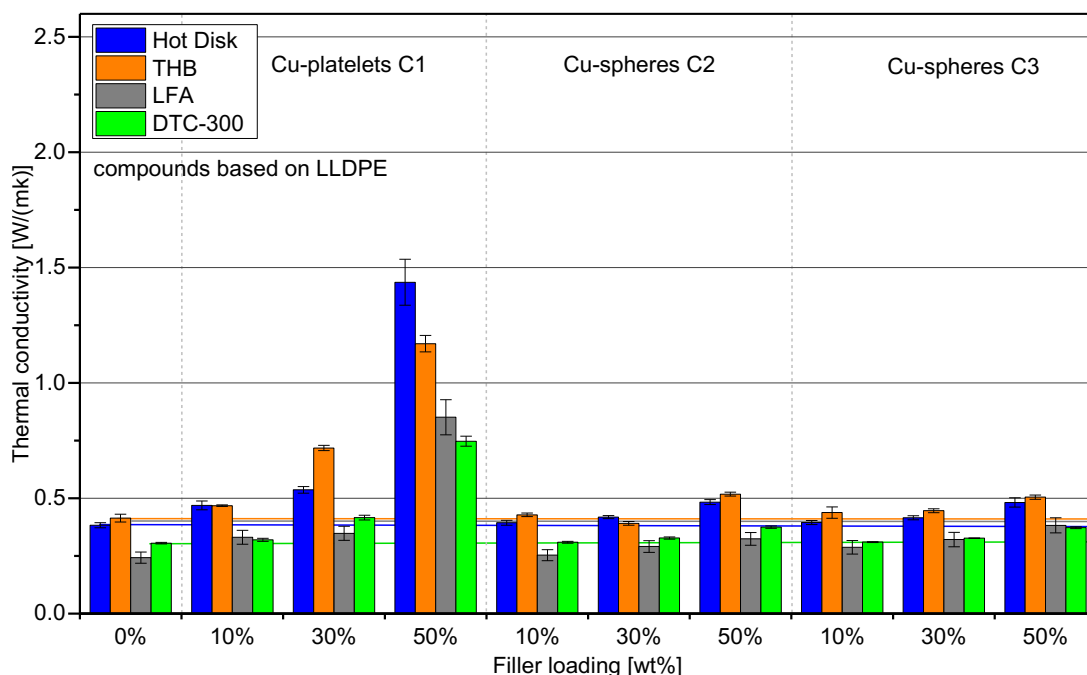
Figure 9.10: Effect of the filler geometry and concentration on the TC of LLDPE-based compounds as determined by Hot Disk (isotropic measurement module), THB (BK7 calibration), LFA (Radiation evaluation model) and DTC-300

9.5.2.1. Material-induced impacts on TC

The TC of HDPE and LLDPE ranged between 0.38 W/(mK) and 0.57 W/(mK) and 0.31 W/(mK) and 0.41 W/(mK), respectively, depending on the applied measurement device. The higher TC of HDPE over LLDPE was attributed to its higher degree of crystallinity (Table 1). Higher crystallinity yields higher TC since phonons which are mainly responsible for heat conduction in polymers can travel more easily through the material along the crystalline structure without being scattered at obstacles in amorphous regions [1,2]. The addition of copper yielded an increase in TC for the polymers. The incorporation of C1 particles induced the largest increase for HDPE-based and LLDPE-based compounds. This was ascribed to the geometry of the highly conductive particles within the matrix with low TC. The high aspect ratio of the C1 particles shortened the distance between the copper particles more efficiently than C2 and C3 particles did at the same filler loadings (spherical particles yield an aspect ratio of only 1). This enhanced the thermal energy transport through the material. The effect of the filler geometry on the TC corresponds to findings from Tekce et al. [8]. They incorporated copper in the form of

140

fibers, platelets and spheres into a polyamide matrix. The most efficient enhancement of TC was observed for platelet-shaped particles.

The TC increased with increasing filler concentration whereas the TC of HDPE-based compounds (50 wt%: 0.40 – 2.44 W/(mK)) exceeded the values of LLDPE-based compounds (50 wt%: 0.33 – 1.44 W/(mK)). If a crystalline phase is located next to a copper particle, the heat can propagate more easily through the compound than if an amorphous phase is located next to a copper particle. Consequently, HDPE's higher degree of crystallinity (k_{HDPE}=80 % vs. k_{LLDPE}=45 %) increases the probability for all HDPE-based compounds that a crystalline phase is located next to a copper particle and that heat propagates more easily through the compound. The largest difference in TC (2.44 W/(mK) vs. 1.44 W/(mK)) was detected between HDPE/C1/50 and LLDPE/C1/50 (platelets). Interestingly, the differences were smaller for C2- and C3-reinforced compounds (spherical particles). Thus, the large difference in TC for C1-reinforced compounds was attributed to a combination of differences in the degree of crystallinity and to the orientation of the platelets whereas the smaller differences in TC for the C2- and C3-reinforced compounds were mainly attributed to the differences in the degree of crystallinity. The compound's TC was therefore normalized to its relative TC enhancement according to equation (9)

$$\text{Relative TC enhancement} = \frac{\lambda_C - \lambda_{PE}}{\lambda_{PE}} \cdot 100\% \qquad (9)$$

with λ_C as the compound TC and λ_{PE} as the matrix TC. The results are shown in Figure 9.11. Irrespective of the applied measurement device, the TC of HDPE-based compounds increased steadily. This was not observed for the LLDPE-based compounds (although the filler loadings of the HDPE-based and LLDPE-based compounds are equal (compare Table 4)): irrespective of the applied measurement device, the TC did not increase significantly between filler loadings of 10 and 30 wt%. A further increase in the filler concentration to 50 wt% yielded a distinct increase in the TC.
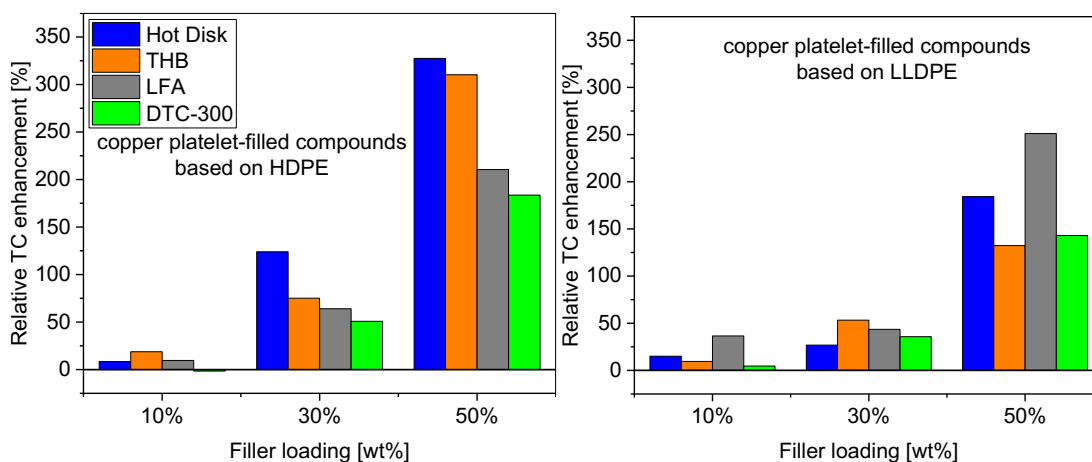
Figure 9.11: Relative TC enhancement as determined by Hot Disk (isotropic measurement module), THB (BK7 calibration), LFA (Radiation evaluation model) and DTC-300 at various filler loadings for C1-filled compounds (left: compounds based on HDPE, right: compounds based on LLDPE)

High magnification SE-SEM micrographs of the cryogenic fracture surfaces of HDPE/C1/50 and LLDPE/C1/50 are presented in Figure 9.12a and b, respectively. Fibrils and unsmooth surface regions indicate the polymer matrix. For the HDPE/C1/50, the matrix polymer still adhered to some of the C1 particles after the fracture as indicated by the red arrows. This was not the case for LLDPE/C1/50. All C1 particles on the fractured surface of the LLDPE-based compounds were polymer-free. Thus, the lower relative TC enhancement of the C1 particles in the LLDPE was attributable to a worse matrix-filler-bonding. The worse matrix-filler-bonding acted as an obstacle for the heat propagation.
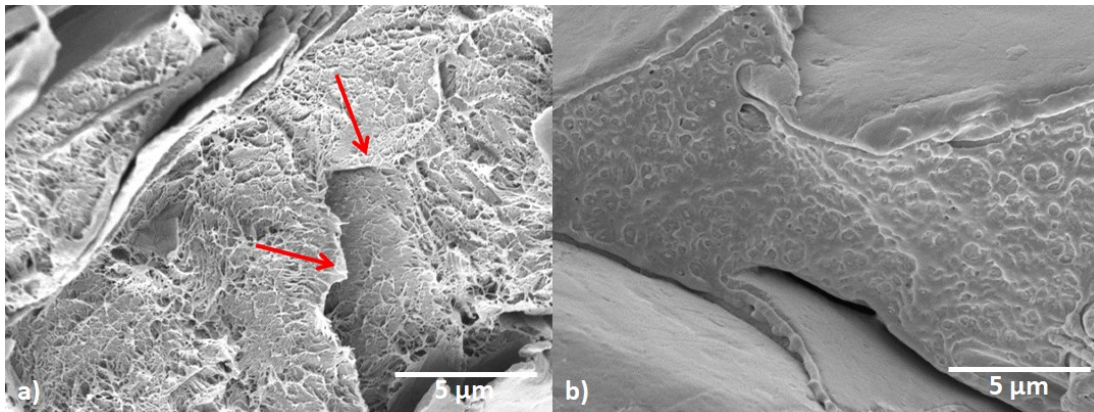
Figure 9.12: SE-SEM micrographs of the cryogenic surface fractures of a) HDPE/C1/50 and b) LLDPE/C1/50. The red arrows point at the copper particles edges where the HDPE matrix still adheres to them as seen by the fibrils and the unsmooth surface. For the LLDPE-based compounds, there were mainly no matrix residues left on the copper particles. This indicated a worse matrix-filler-bonding and resulted in a smaller relative TC enhancement of the LLDPE-based compounds over the HDPE-based compounds.

C2 and C3 particles exhibited a spherical geometry. In HDPE-based compounds these particles provoked a rather moderate increase in TC. For the HDPE-based compounds filled with C2 and C3 particles, the TC ranged from 0.40 to 0.75 W/(mK) and from 0.39 to 0.75 W/mK, respectively. The obtained results were in good agreement with [47] where copper particles were also blended into an HDPE matrix. For the LLDPE-based compounds filled with C2 and C3, the TC ranged from 0.31 to 0.52 W/(mK) and from 0.31 to 0.51 W/(mK). The TC of most LLDPE-based compounds was enhanced only after adding 30 wt% of copper spheres. This was also found by He et al. [48] where spherical copper particles were used to enhance the TC of polyoxymethylene. In that study a distinct increase in TC was observed only after adding more than 10 wt% of copper particles. Irrespective of the differences in the size distribution of C2 and C3 particles, no significant differences in the increase in TC were found for HDPE-based and LLDPE-based compounds.

Despite of the high TC of copper of 401 W/(mK) [46] and filler loadings up to 50 wt%, the TC of the compounds was increased only moderately. This was attributed to the differences in the density between the components (ρ_{cu}=8.94 g/cm^3, ρ_{HDPE}=0.966 g/cm^3 and ρ_{LLDPE}=0.919 g/cm^3). A filler loading of 50 wt% equals a filler loading of 10 vol%. Vol% indicates the unity for TC enhancement since it reflects the spatial presence of the filler particles in a compound. It indicates the available space of highly conducting particles in

the insulating matrix and therefore the ease of heat passing through the bulk material by using this available conductive space as transfer routes.

9.5.2.2. Technology-induced impacts on TC

In general, the highest values for TC were obtained by applying the Hot Disk, followed by THB, LFA and DTC. Dos Santos [42] compared LFA and the Hot Wire technique (which is similar to the Hot Disk and THB method). In that study, HDPE and LDPE were tested among other polymers. For both polyethylene types, the Hot Wire technique yielded higher values for TC than LFA. This is in agreement with the present study if the Hot Disk is considered as the Hot Wire equivalent.

The largest differences between the various measurement systems were observed for the compounds containing C1 particles (maximum and minimum for HDPE/C1/50: $TC_{HotDisk}=2.44$ W/(mK) and $TC_{DTC}=1.07$ W/(mK), respectively). Hot Disk and THB are both based on the above mentioned Hot Wire technique. They are closely related methods especially when it comes to the measurement direction. Hot Disk and THB detected the three-dimensional TC (3D-TC) as indicated via the hollow arrows in Figure 13. This was proved by the similarity of the TC values of the unfilled polymer (e.g. HDPE: $TC_{HotDisk}=0.57$ W/(mK) and $TC_{THB}=0.57$ W/(mK)) and also of the compounds (e.g. HDPE/C1/50: $TC_{HotDisk}=2.44$ W/(mK) and $TC_{THB}=2.34$ W/(mK)). In contrast to that, DTC and LFA only detected the one-dimensional TC (1D-TC) as shown via the hollow arrows in Figure 9.13.

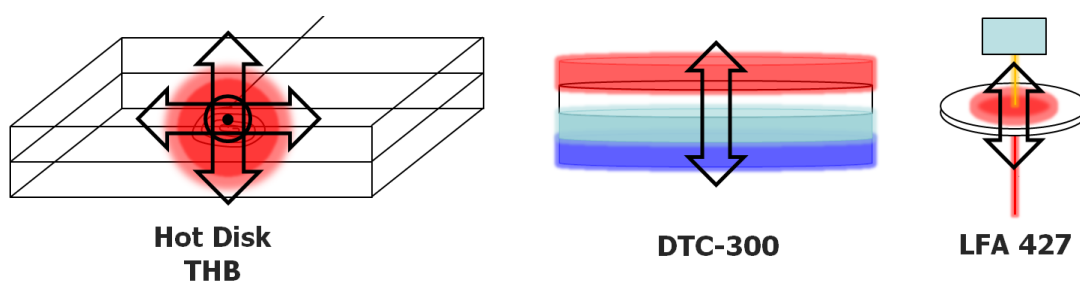**Hot Disk THB** **DTC-300** **LFA 427**

Figure 9.13: Measurement directions indicated by hollow arrows of the applied measurement devices. Hot Disk and THB detect 3D-TC, DTC and LFA detect 1D-TC

The anisotropic measurement module of the Hot Disk revealed the large differences between the 3D-detecting devices (Hot Disk and THB) and the 1D-detecting devices (DTC and LFA). In Figure 9.14 the TC of the C1-filled compounds as determined by Hot Disk measurements are presented. A differentiation between axial, isotropic and radial TC (i.e. direction of aligned copper platelets) was done. For these compounds, irrespective of the filler

144

concentration, the radial TC exceeded the isotropic TC, which exceeded the axial TC. The measurements proved the parallel orientation of the C1 particles as mentioned earlier and shown in Figure 9.7. The heat can travel more easily in the direction of the alignment of the C1 particles (radial direction). However, this was only detectable by Hot Disk and THB since only the three-dimensional TC includes the enhanced radial TC. Therefore the differences in TC were caused by the different dimensional detection possibilities of the measurement devices (e.g. HDPE: TC_{LFA}=0.52 W/(mK) and TC_{DTC}=0.38 W/(mK) and HDPE/C1/50: TC_{LFA}=1.48 W/(mK) and TC_{DTC}=1.07 W/(mK)).
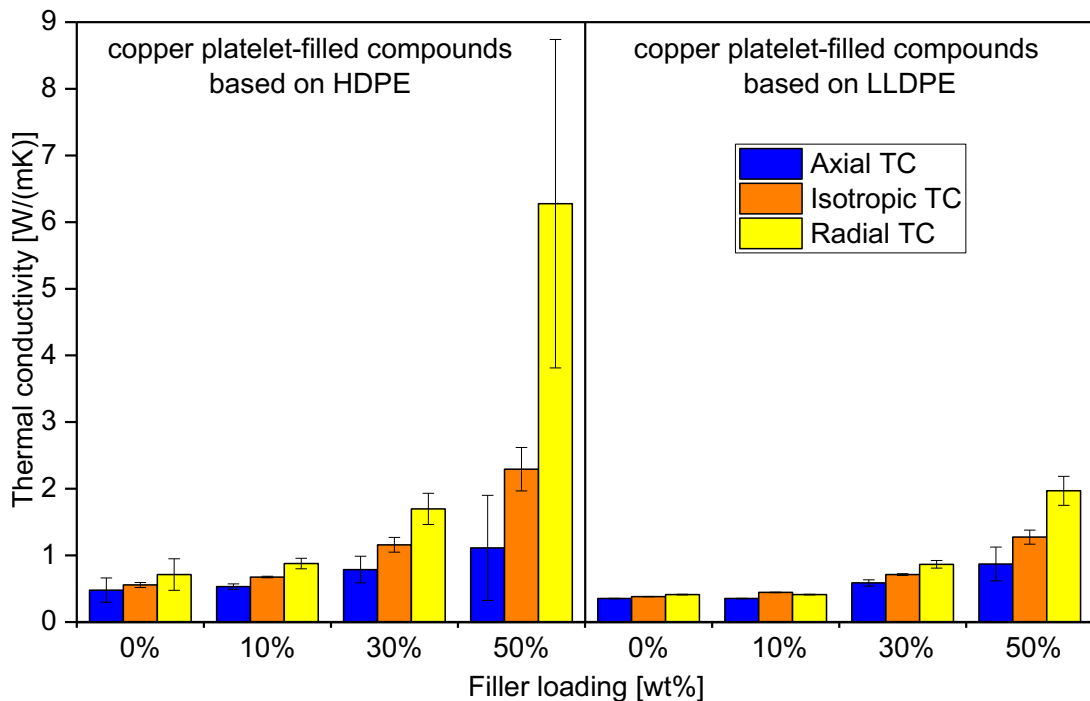

Figure 9.14: Anisotropic and isotropic Hot Disk-measurements of C1-filled compounds at various filler loadings. The differences in the axial, isotropic and radial TC values revealed the anisotropic material character

The differences between the various measurement directions increased with increasing filler loading. The largest difference between axial and radial TC occurred for HDPE/C1/50 with TC_{axial}=1.11 W/(mK) and TC_{radial}=6.28 W/(mK). The more C1 particles that were present in the specimen, the more particles were aligned and the more the radial TC was increased with regard to the axial TC.

Since the radial TC exceeded the isotropic TC which exceeded the axial TC, the anisotropic measurement module also revealed an alignment of the crystalline features of the unfilled polymer somewhat parallel to the specimen surface. The effect was stronger pronounced for HDPE than for LLDPE which was attributed to the higher degree of crystallinity of HDPE.

In Figure 9.15 the axial TC as determined by Hot Disk and LFA (evaluated with the Radiation model) are compared. The values for TC were in good agreement for the majority of the C1-filled compounds. This further emphasizes the large impact of the measurement direction on the detected TC value.
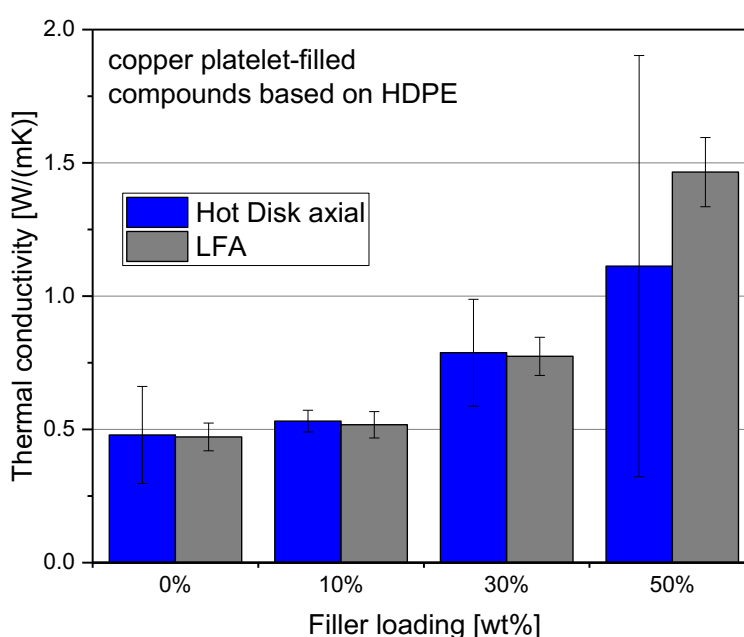

Figure 9.15: TC as determined by Hot Disk (anisotropic measurement module) and LFA (Radiation evaluation model) at various filler loadings of C1-filled compounds (left: compounds based on HDPE, right: compounds based on LLDPE)

No anisotropic evaluation module is available for the THB. However, this measurement device can be calibrated with different standards which may affect the detected TC. In Figure 9.16 the TC determined by THB which was calibrated by either LLDPE, PMMA or BK7 are compared. For all three calibrations, the effects of the matrix polymer or the filler shape correspond to the findings as discussed above. Irrespective of the applied filler type and concentration, the lowest TC was obtained by applying the LLDPE calibration and the highest TC was obtained by applying the BK7 calibration. These differences in the TC values were attributed to the differences in the TC of the calibration standards ($TC_{LFA-LLDPE}$=0.242 W/(mK); TC_{PMMA}=0.194 W/(mK);

TC_{BK7}=1.12 W/(mK). A suitable calibration standard possesses similar behavior as the specimen with regard to the measured property. This means that the closer the TC of the calibration standard is to the measured TC, the more suitable the calibration standard is. As mentioned above, the Hot Disk and the THB are closely related measurement techniques. Therefore the range of TC values determined via Hot Disk (from $TC_{HotDisk-LLDPE}$=0.38 W/(mK) to $TC_{HotDisk-HDPE/C1/50}$=2.44 W/(mK)) was taken for the choice of the calibration standard. $TC_{LFA-LLDPE}$ and TC_{PMMA} are already lower than the minimum $TC_{HotDisk}$. TC_{BK7} lies in between the $TC_{HotDisk}$ range. Therefore, BK7 was chosen as the most suitable calibration standard also for comparison purposes (i.e. Figure 9.9 and Figure 9.10).
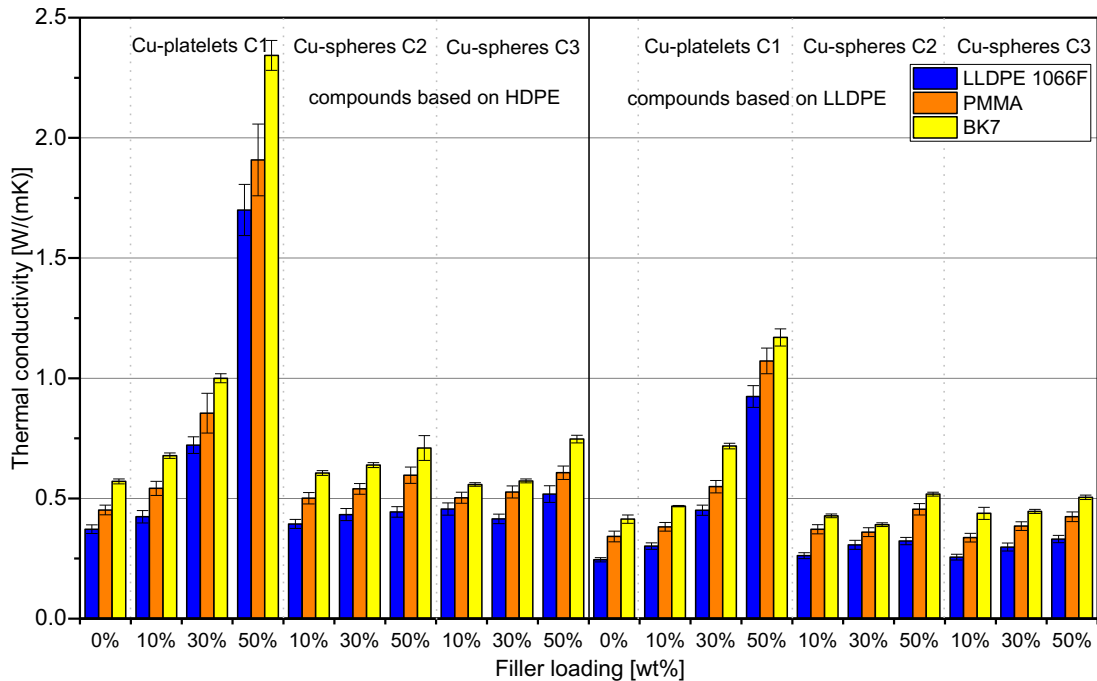

Figure 9.16: TC of the THB-measurements (left: HDPE-based compounds; right: LLDPE-based compounds) at various filler loadings when calibrated with three different calibration standards (LLDPE, PMMA, BK7)

In Figure 9.17 the effects of the evaluation model on the TC as determined by LFA are compared. In general, the TC was lower for the Radiation model than for the Conduction model. During the measurements, heat conduction and heat radiation (in the form of radiation losses) were detected. The Radiation model differentiated between those two thermal transport mechanisms. Only the heat conduction was taken into account to generate thermal diffusivity. The Conduction model, however, did not differentiate

between the two thermal transport mechanisms and therefore the TC for the Conduction model was higher. Because of the detected radiation losses, the Radiation model was chosen for the comparative graphs in Figure 9 and Figure 9.10.
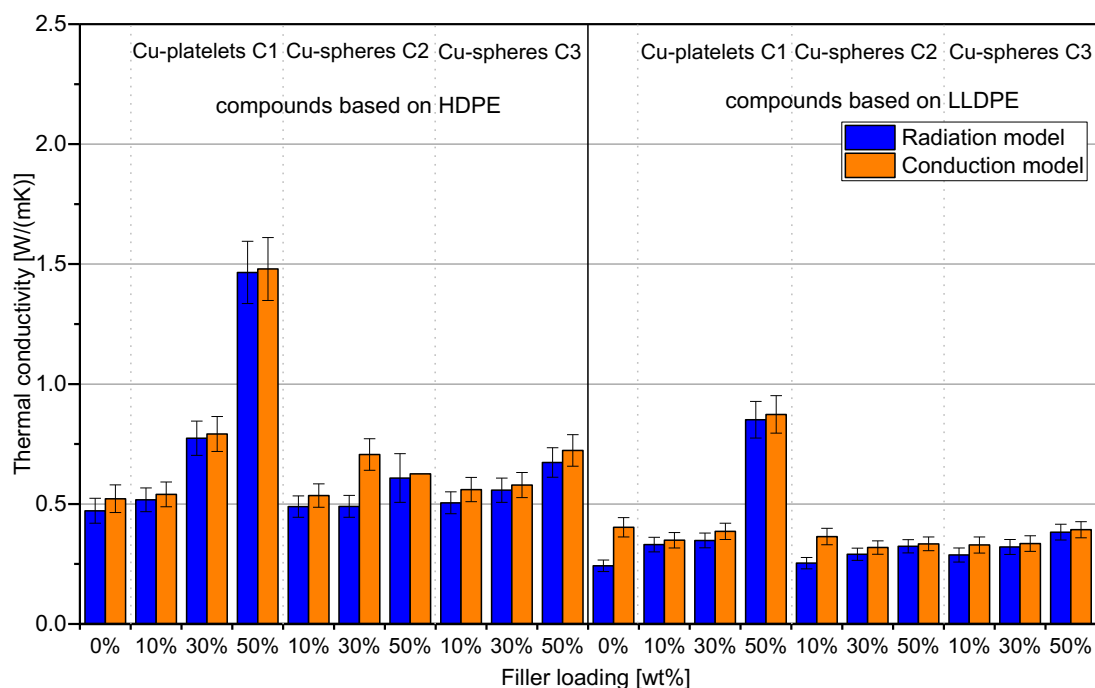

Figure 9.17: TC of the LFA-measurements (left: HDPE-based compounds; right: LLDPE-based compounds) at various filler loadings evaluated via the Radiation or the Conduction model

The TC increased with increasing filler loading for all HDPE-based compounds irrespective of the applied evaluation model. However, this was not the case for the LLDPE-based compounds which were evaluated by the Conduction model. The effect of the evaluation model on the TC enhancement of LLDPE-based compounds is therefore displayed in Figure 9.18. By applying the Radiation model, the TC increased with increasing filler concentration for all three types of compounds as expected. Interestingly, by applying the Conduction model, the TC decreased with increasing filler concentration for all three types of compounds. Merely for the samples containing 50 wt% of C1 particles an increase in the TC was detected as those particles proved to be the most efficient ones for the enhancement in TC. The decrease in TC of C2- and C3-filled compounds was attributed to the initially lower TC of the unfilled LLDPE. The Radiation model generated a TC of 0.24 W/(mK), whereas the Conduction model generated a TC of 0.40 W/(mK). The TC of the polymer matrix λ_{PE} was present in every

calculated relative TC enhancement according to equation (9), and thus yielded the differences in the relative TC enhancement.
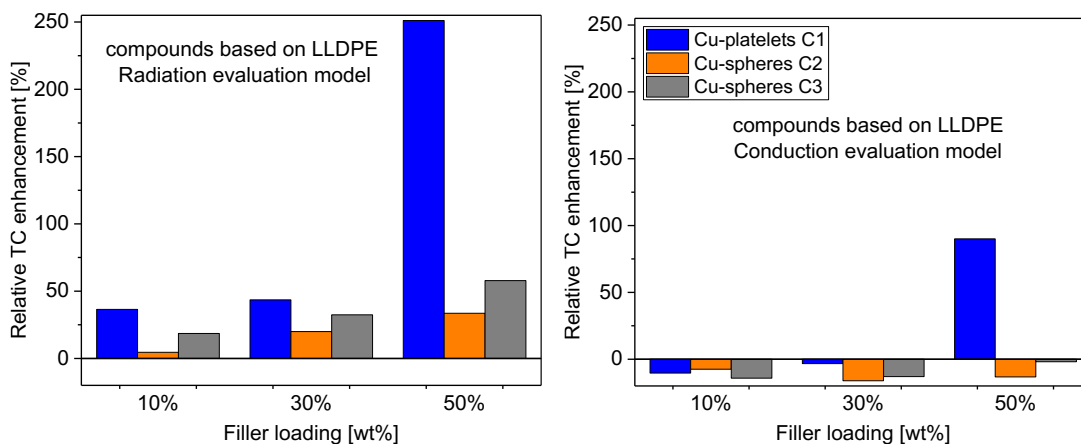

Figure 9.18: Relative TC enhancement measured via LFA 427 (left: the Radiation model was applied for evaluation, right: the Conduction model was applied for evaluation) of LLDPE-based compounds at various filler loadings

9.6.   Summary and conclusion

In this study the thermal conductivity (TC) of 20 polymeric materials in the form of compression molded plates was analyzed. 2 unfilled polymers (HDPE and LLDPE) and 18 compounds (HDPE and LLDPE were used as matrix materials) filled with three different copper particles (platelets, large and small spheres) at filler loadings of 10 – 50 wt% were investigated. The TC was determined via four different measurement devices: the Hot Disk (the isotropic and anisotropic measurement modules were applied), the Transient Hot Bridge (LLDPE, PMMA and BK7 as calibration standards were applied), the Laser Flash Analysis (Conduction and Radiation model for evaluation were applied) and the DTC. The filler loadings of the compounds were examined via Thermogravimetrical Analysis (TGA). The degree of crystallinity and the crystallization behavior of all materials were examined via Differential Scanning Calorimetry (DSC). The specimen morphology was analyzed via Scanning Electron Microscopy (SEM).

The results clearly demonstrate that the determination of the TC of polymeric materials is a highly complex field. Generally, the different measurement devices yielded different values for the TC of the very same materials. Consequently, the exact TC ranges of the investigated polymers remain an open question. Hot Disk/Transient Hot Bridge measurements yielded the highest TC values and Laser Flash Analysis/DTC the lowest ones. The

differences were mainly attributed to the combination of the partially anisotropic character of the specimens and the different dimensional detection possibilities of the measurement devices (three-dimensional for Hot Disk/Transient Hot Bridge vs. one-dimensional for Laser Flash Analysis/DTC).

Three major conclusions can be drawn:

1) Morphological understanding of the specimens is crucial in order to interpret the results correctly but also to choose the adequate measurement device and to tailor the testing parameters to the sample morphology (Hot Disk offers variable measurement modules, THB an adjustable calibration and the LFA different evaluation models). The testing parameters of DTC may not be varied, which is on the one hand advantageous regarding reproducibility, but also impedes the consideration of anisotropic material characteristics.

2) For comparison purposes or for material development it is essential to use the same measurement device and to apply the same testing parameters.

3) The measurement devices applying a non-steady state model for measuring TC (Hot Disk, Transient Hot Bridge, Laser Flash Analysis) proved to be less time consuming than the DTC which applied a steady state model. Nonetheless, one has to consider that three different measurements are necessary for the determining TC via Laser Flash Analysis.

9.7.   Acknowledgements

9.8.   References

[1]   G. Menges, E. Haberstroh, W. Michaeli, E. Schmachtenberg, Menges Werkstoffkunde Kunststoffe, 1st ed., Carl Hanser Fachbuchverlag, s.l., 2014.

[2]   T.A. Osswald, E. Baur, S. Brinkmann, K. Oberbach, E. Schmachtenberg, International Plastics Handbook, Carl Hanser Verlag GmbH & Co. KG, München, 2006.

[3]   H. Chen, V.V. Ginzburg, J. Yang, Y. Yang, W. Liu, Y. Huang, L. Du, B. Chen, Thermal conductivity of polymer-based composites: Fundamentals and applications, Prog Polym Sci 59 (2016) 41–85.

[4]   Mamunya, Y. P., Davydenko, V. V., Pissis, P., & Lebedev, E. V., Electrical and thermal conductivity of polymers filled with metal powders, Eur Polym J 38 (9) (2002) 1887–1897.

[5]   A. Boudenne, L. Ibos, E. Géhin, M. Fois, J.C. Majesté, Anomalous behavior of thermal conductivity and diffusivity in polymeric materials filled with metallic particles, J Mater Sci 40 (16) (2005) 4163–4167.

[6]   A. Boudenne, L. Ibos, M. Fois, J.C. Majesté, E. Géhin, Electrical and thermal behavior of polypropylene filled with copper particles, Compos Part A-Appl S 36 (11) (2005) 1545–1554.

[7]   I. Krupa, A. Boudenne, L. Ibos, Thermophysical properties of polyethylene filled with metal coated polyamide particles, Eur Polym J 43 (6) (2007) 2443–2452.

[8]   H.S. Tekce, D. Kumlutas, I.H. Tavman, Effect of Particle Shape on Thermal Conductivity of Copper Reinforced Polymer Composites, J Reinf Plast Comp 26 (1) (2007) 113–121.

[9]   A.S. Luyt, J.A. Molefi, H. Krump, Thermal, mechanical and electrical properties of copper powder filled low-density and linear low-density polyethylene composites, Polym Degrad Stabil 91 (7) (2006) 1629–1636.

[10]   Rusu, M., Sofian, N., & Rusu, D, Mechanical and thermal properties of zinc powder filled high density polyethylene composites., Polym Test 20 (4) (2001) 409–417.

[11]   H. Ji, D.P. Sellan, M.T. Pettes, X. Kong, J. Ji, L. Shi, R.S. Ruoff, Enhanced thermal conductivity of phase change materials with ultrathin-graphite foams for thermal energy storage, Energy Environ. Sci. 7 (3) (2014) 1185.

[12]   C. Yang, M.E. Navarro, B. Zhao, G. Leng, G. Xu, L. Wang, Y. Jin, Y. Ding, Thermal conductivity enhancement of recycled high density polyethylene as a storage media for latent heat thermal energy storage, Sol Energ Mat Sol C 152 (2016) 103–110.

[13]   I. Krupa, I. Novák, I. Chodák, Electrically and thermally conductive polyethylene/graphite composites and their mechanical properties, Synthetic Metals 145 (2-3) (2004) 245–252.

[14]   X. Zhao, L. Ye, Study on the thermal conductive polyoxymethylene/graphite composites, J. Appl. Polym. Sci. (2008) NA-NA.

[15]   M.-T. Hung, O. Choi, Y.S. Ju, H.T. Hahn, Heat conduction in graphite-nanoplatelet-reinforced polymer nanocomposites, Appl. Phys. Lett. 89 (2) (2006) 23117.

[16]   I. Krupa, I. Chodák, Physical properties of thermoplastic/graphite composites, Eur Polym J 37 (11) (2001) 2159–2168.

[17]   A. Moisala, Q. Li, I.A. Kinloch, A.H. Windle, Thermal and electrical conductivity of single- and multi-walled carbon nanotube-epoxy composites, Compos Sci Technol 66 (10) (2006) 1285–1288.

[18]   X. Lu, G. Xu, Thermally conductive polymer composites for electronic packaging, J. Appl. Polym. Sci. 65 (13) (1997) 2733–2738.

[19]   K. Kalaitzidou, H. Fukushima, L.T. Drzal, Multifunctional polypropylene composites produced by incorporation of exfoliated graphite nanoplatelets, Carbon 45 (7) (2007) 1446–1452.

[20]   Y.-H. Zhao, Z.-K. Wu, S.-L. Bai, Study on thermal properties of graphene foam/graphene sheets filled polymer composites, Compos Part A-Appl S 72 (2015) 200–206.

[21]   B. Debelak, K. Lafdi, Use of exfoliated graphite filler to enhance polymer physical properties, Carbon 45 (9) (2007) 1727–1734.

[22]   R.J. Kuriger, M.K. Alam, THERMAL CONDUCTIVITY OF THERMOPLASTIC COMPOSITES WITH SUBMICROMETER CARBON FIBERS, Exp Heat Transfer 15 (1) (2002) 19–30.

[23]   Jinhong Yu, Xingyi Huang, Chao Wu, Pingkai Jiang, Permittivity, thermal conductivity and thermal stability of poly(vinylidene fluoride)/graphene nanocomposites, IEEE Trans. Dielect. Electr. Insul. 18 (2) (2011) 478–484.

[24]   S.H. Song, K.H. Park, B.H. Kim, Y.W. Choi, G.H. Jun, D.J. Lee, B.-S. Kong, K.-W. Paik, S. Jeon, Enhanced thermal conductivity of epoxy-graphene composites by using non-oxidized graphene flakes with non-covalent functionalization, Adv Mater 25 (5) (2013) 732–737.

[25]   G.-W. Lee, M. Park, J. Kim, J.I. Lee, H.G. Yoon, Enhanced thermal conductivity of polymer composites filled with hybrid filler, Compos Part A-Appl S 37 (5) (2006) 727–734.

[26]   S. Yu, P. Hing, X. Hu, Thermal conductivity of polystyrene–aluminum nitride composite, Compos Part A-Appl S 33 (2) (2002) 289–292.

[27]   S.A. Putnam, D.G. Cahill, B.J. Ash, L.S. Schadler, High-precision thermal conductivity measurements as a probe of polymer/nanoparticle interfaces, J. Appl. Phys. 94 (10) (2003) 6785.

[28]   Y. Xu, D. Chung, C. Mroz, Thermally conducting aluminum nitride polymer-matrix composites, Compos Part A-Appl S 32 (12) (2001) 1749–1757.

[29]   R.F. Hill, P.H. Supancic, Thermal Conductivity of Platelet-Filled Polymer Composites, J Am Ceram S 85 (4) (2002) 851–857.

[30]   G. Droval, J.-F. Feller, P. Salagnac, P. Glouannec, Thermal conductivity enhancement of electrically insulating syndiotactic poly(styrene) matrix for diphasic conductive polymer composites, Polym. Adv. Technol. 17 (9-10) (2006) 732–745.

[31]   2009 IEEE Electrical Insulation Conference (EIC) (Ed.), Thermal Behaviour of Epoxy Resin Filled with High Thermal Conductivity Nanopowders.

[32]   Y.-H. Zhao, Y.-F. Zhang, Z.-K. Wu, S.-L. Bai, Synergic enhancement of thermal properties of polymer composites by

graphene foam and carbon black, Compost Part B-Eng 84 (2016) 52–58.

[33]   S. Ghose, K.A. Watson, D.C. Working, J.W. Connell, J.G. Smith, Y.P. Sun, Thermal conductivity of ethylene vinyl acetate copolymer/nanofiller blends, Compos Sci Technol 68 (7-8) (2008) 1843–1853.

[34]   W. Zhou, S. Qi, Q. An, H. Zhao, N. Liu, Thermal conductivity of boron nitride reinforced polyethylene composites, Mater Res Bull 42 (10) (2007) 1863–1873.

[35]   M. Karkri, L. Ibos, B. Garnier, Comparison of experimental and simulated effective thermal conductivity of polymer matrix filled with metallic spheres: Thermal contact resistance and particle size effect, J Compos Mater 49 (24) (2015) 3017–3030.

[36]   H. Liem, H.S. Choy, Superior thermal conductivity of polymer nanocomposites by using graphene and boron nitride as fillers, Solid State Commun 163 (2013) 41–45.

[37]   V. Goyal, A.A. Balandin, Thermal properties of the hybrid graphene-metal nano-micro-composites: Applications in thermal interface materials, Appl. Phys. Lett. 100 (7) (2012) 73113.

[38]   K. Wattanakul, H. Manuspiya, N. Yanumet, Thermal conductivity and mechanical properties of BN-filled epoxy composite: Effects of filler content, mixing conditions, and BN agglomerate size, J Compos Mater 45 (19) (2011) 1967–1980.

[39]   M. Hu, J. Feng, K.M. Ng, Thermally conductive PP/AlN composites with a 3-D segregated structure, Compos Sci Technol 110 (2015) 26–34.

[40]   Y. Agari, A. Ueda, S. Nagai, Thermal conductivities of composites in several types of dispersion systems, J. Appl. Polym. Sci. 42 (6) (1991) 1665–1669.

[41]   W. Nunes dos Santos, P. Mummery, A. Wallwork, Thermal diffusivity of polymers by the laser flash technique, Polym Test 24 (5) (2005) 628–634.

[42]   W.N. dos Santos, Thermal properties of polymers by non-steady-state techniques, Polym Test 26 (4) (2007) 556–566.

[43]   D.W. van Krevelen, K.t. Nijenhuis, Properties of polymers: Their correlation with chemical structure ; their numerical estimation and prediction from additive group contributions, 4th ed., Elsevier, Amsterdam, 2009.

[44]   Y. He, Rapid thermal conductivity measurement with a hot disk sensor, Thermochim Acta 436 (1-2) (2005) 122–129.

[45]   Anter Corporation, Manual DTC-300: Operation and SOFTWARE Unitherm 2022, 3rd ed., 2010.

[46]   B.E. Langner, Understanding copper: Technologies, markets, business, 1st ed., B. E. Langner, Winsen, Glockenheide 11, 2011.

[47]   I.H. Tavman, Thermal and mechanical properties of copper powder filled poly (ethylene) composites, Powder Technol 91 (1) (1997) 63–67.

[48]   J. He, L. Zhang, C. Li, Thermal conductivity and tribological properties of POM-Cu composites, Polym Eng Sci 50 (11) (2010) 2153–2159.

10.   Introduction to publication 4

The enhancement of the thermal conductivity (TC) of polymeric phase-change materials (PCM) is a necessary step to pave the way for their market maturity. This can be achieved inter alia via the incorporation of highly conductive particles into the PCM [1–3]. However, as particles tend to interact with the polymeric matrix in compounds, the application relevant-characteristics such as the storage capacity, their melting and crystallization behavior and especially their ability to maintain these may be affected [4–8]. Therefore, the long-term stability of PCM compounds needs to be addressed additionally to the investigation of the long-term stability of the neat polymeric PCM presented in publication 2.

As manifold filler types are available for enhancing the TC of polymers [1,2], a screening of fillers which are selected based on the results of a sound literature research was executed prior to the long-term stability investigations of the polymeric compounds. This required step in the development of polymeric PCM with enhanced TC is described in the following.

10.1.   Development of polymeric phase-change materials with enhanced thermal conductivity

Publication 3 revealed the highly complex procedure of measuring the TC of polymeric materials. Major discrepancies in the TC of up 1.37 W/(mK) for the very same material were detected via different measurement devices. Nevertheless, the same tendencies of the TC enhancement were revealed by each measurement device. This pointed out that the available measurement methods can be applied for the development of a material as long as only one method is utilized. Out of the tested devices, the Hot Disk was chosen for the filler screening due to its fast and simple handling and the available measurement modules that can be adapted to the condition of the specimen (isotropic, anisotropic, stack-like).

10.1.1. Filler screening

The commercially available high-density polyethylene (HDPE) Bormed™ HE9621-PH (Borealis GmbH, Linz, AT) with a density of 0.964 kg/m³ and a melt flow rate of 12 g/10 min (2.16 kg, 190 °C) was used as matrix polymer for the compounding. Nine different fillers were added to the HDPE matrix with filler ratios of 10 vol%, 20 vol% and 30 vol%. The applied filler types including their filler name, the manufacturer, the particle size, the density (the latter two were deduced from the manufacturer's material data sheet), the TC and the shape are presented in Table 10.1. The compounds will be referred to as "abbreviation - filler loading". For example, the compound containing 20 vol% of boron nitride will be called BN-20.

Table 10.1: Filler type (abbreviation) including its exact name, the manufacturer, the mean particle size, the density (the latter two were deduced from the manufacturer's material data sheet), the thermal conductivity and the shape.

Filler type (abbreviation)	Filler name	Manufacturer	Particle size [μm]	Density [g/cm³]	Thermal conductivity [W/(mK)]	Shape
Aluminum (A)	AS81	Ecka Granules (Fürth, DE)	< 200	2.7	204 [9]	Irregular, spherical-like
Aluminum (AP)	Non-leafing METALLIC 7814	Benda Lutz GmbH (Nussdorf o. d. Traisen, AT)	35 - 45	2.7	204 [9]	Platelet
Boron nitride (BN)	Cooling Filler Agglomerates Typ 50	3M (Maplewood, US)	50	2.3	2 - 400 [10] depending on the crystalline orientation	Platelet
Carbon fibers (CF)	Sigrafil® C10 M150 UNS	SGL Carbon (Wiesbaden, DE)	150	1.8	5 – 58 [11]	Fibers
Copper (C)	MP 6100	Ecka Granules (Fürth, DE)	> 45	8.9	401 [12]	Platelet
Expanded graphite (EG)	Sigratherm® GFG 1200	SGL Carbon (Wiesbaden, DE)	1200	2.2	Up to 3000 [13] depending on the crystalline orientation	Platelet
Micaceous iron ore (MX)	MIOX 100/200	Kärntner Montanindustrie GmbH (Wolfsberg, AT)	100 - 200	5.3	17 [14]	Platelet
Natural graphite (G)	1:1 blend from Silbergrafit 96 and Grafit 1496	Grafitbergbau Kaisersberg GmbH (St. Stefan bei Leoben, AT)	< 75 / 5 - 6	2.2	208 [15] depending on the crystalline orientation	Platelet
Zinc (Z)	Z 2031	Benda Lutz GmbH (Nussdorf ob der Traisen, AT)	10	7.1	112 [16]	Platelet

The compounds were fabricated on a co-rotating twin screw compounder (Werner & Pfleiderer, Dinkelsbühl, DE) with an L/D ratio of 38 and equipped with six control zones, a gravimetric dosing unit, side feeding, vacuum degassing, a cool bath and strand pelletizing. The temperatures of the six control zones were set to 140 °C, 180°C, 190°C, 190°C, 190°C, 190°C and the mass feed rate was set to 6 kg/h. The fillers were added to the compounder via the side feeding. The granules of the neat HDPE and the compounds were then compression molded on a vacuum press P 200 PV (Dr. Collin GmbH, Ebersberg, DE) into plates of 160 * 160 * 8 mm for 30 min at 195 °C with a pressure ramp from 0 to 39 bar. The plates were then cooled for 15 min at 30 °C at 39 bar. After the compression molding, the plates were cut into half with a specimen saw Diadisc 5200 (MUTRONIC Praezisionsgeraetebau GmbH & Co. KG, Rieden am Forggensee, DE) into plates with the dimensions of 80 * 160 * 8 mm.

A TPS 2500S by Hot Disk AB (Gothenborg, SE) was used to determine the TC of the compounds. It will simply be referred to as Hot Disk. The TC was measured at ambient temperature in the isotropic measurement module with two different sensors. The Kapton sensor 7577 with a radius of the embedded Nickel double spiral of 2 mm was used for all compounds expect for the compounds containing 10 vol% or more of expanded graphite. For those compounds, the Kapton sensor 5501 with a radius of the embedded Nickel double spiral of 6.4 mm was applied as it was not possible to conduct reasonable measurements with the smaller sensor. The presented data represent the average of at least seven measurements. After each measurement, the sensor was moved to a different measurement position in between the two specimen plates.

The TC of the neat HDPE and the HDPE-based compounds with filler loadings up to 30 vol% is displayed in Figure 10.1a. The lines that connect the experimentally generated values do not represent a function, but are implemented to guide the eye. The TC increased for all compounds with increasing filler loading. However, the maximum TC of the compounds (at a filler loading of 30 vol%) varied. The TCs of A-30, CF-30, MX-30 and Z-30 differed only slightly and HDPE's initial TC of 0.56 W/(mK) was enhanced to approximately 1 W/(mK). The TCs for AP-30, BN-30, C-30, EG-30 and G-30, on the other hand, were significantly higher and laid in between approximately 3 to 21 W/(mK). Several impacts on the TC of polymeric compounds have been identified so far and typically overlap for the compound's final TC [1–3]. In general, it depends on the filler's and matrix's characteristics and their interaction. As the matrix was identical for all

compounds, the large differences in the TC enhancements could largely be attributed to the significant differences in the intrinsic TC of the individual fillers as given in Table 10.1. Along with their low efficiency in enhancing HDPE's TC (TC_{MX-30} = 1.73 W/(mK); TC_{CF-30} = 1.22 W/(mK)), micaceous iron ore and carbon fibers exhibit also the lowest intrinsic TCs with 17 W/(mK) and 5 – 58 W/(mK), respectively. On the other hand, the fillers enhancing HDPE's TC more efficiently from 3 up to 21 W/(mK) (aluminum platelets, boron nitride, copper, (expanded) graphite)), also possess higher intrinsic TCs in the approx. range from 200 to 3000 W/(mK) (Table 10.1). Interestingly, the intrinsic TCs of zinc and the irregularly-shaped, spherical-like aluminum particles (TC_Z = 112 W/(mK); TC_A = 208 W/(mK)) are substantially higher than the intrinsic TC of micaceous iron ore and carbon fibers (TC_{MX} = 17 W/(mK); TC_{CF} = 5-58 W/(mK)). Nonetheless, their incorporation into the HDPE matrix shows similar low efficiency in regard to the compound's final TC (TC_{Z-30} = 1.63 W/(mK); TC_{A-30} = 1.54 W/(mK)). Burger et al. categorized the various impacts on a polymeric compound's TC into processing (dispersion, filler alignment/networking), filler functionalization, filler/matrix interface and sizes/aspect ratios [3]. The first two coincide for all compounds as they were processed identically and the fillers were not functionalized. However, the filler sizes and aspect ratios (determined by their shape) and thus the filler/matrix interface vary for each filler type (Table 10.1). The incorporated zinc particles exhibit comparably small particles with an average particle size of 10 µm. Its polymer/filler interface is therefore relatively large and thus, its interfacial thermal resistance increased by an augmented phonon-boundary scattering which lowers the material's TC [1,3]. The difference in the TC enhancement between the compounds containing the irregularly, spherical-like aluminum particles (TC_{A-30} = 1.54 W/(mK)) and the aluminum platelets (TC_{AP-30} = 4.38 W/(mK)) was ascribed to their different aspect ratios. The first-mentioned particles possess an aspect ratio close to 1 whereas the platelets' aspect ratio is higher. The latter helps to form conductive pathways through the insulating polymeric matrix at lower filler loadings and increases the compound's TC more efficiently [17].

At the lowest filler level of 10 vol%, copper, expanded graphite and aluminum platelets proved to be the most efficient fillers with TCs of 2.49 W/(mK), 6.01 W/(mK) and 1.19 W/(mK), respectively. Therefore, their Oxidation Induction Temperature T_{OX} was determined on a DSC 822e (Mettler Toledo, Greifensee, CH) additionally to the TC measurements. The samples were taken from the granules and a sample weight of 10 mg was used. Open 40 µl aluminum crucibles were applied. The samples were heated from 23 °C in air

atmosphere until an exothermic curve indicating the thermo-oxidative degradation was recorded with a heating rate of 10 °C/min. T_{OX} was evaluated according to ISO 11357-6. The presented data represent the average of two measurements.
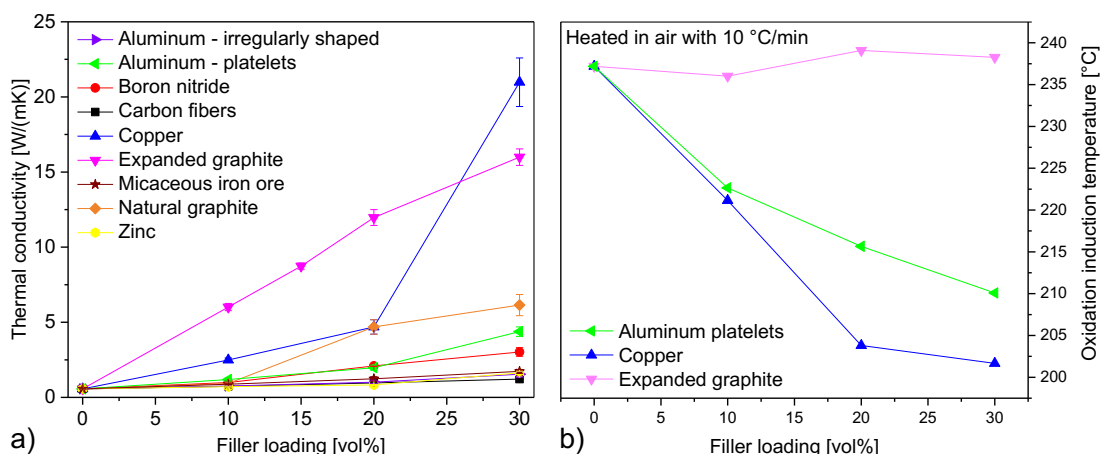

Figure 10.1: a) the thermal conductivity of the neat HDPE and HDPE-based compounds containing different filler particles with filler loadings up to 30 vol%. At 10 vol%, the expanded graphite, the copper and the aluminum platelets enhanced the thermal conductivity of the HDPE the most efficient. b) the oxidation induction temperatures T_{OX} as deduced from DSC measurements of the compounds containing aluminum platelets, copper and expanded graphite as filler. Both metallic filler decreased T_{OX} over the neat HDPE whereas the expanded graphite increased it.

In Figure 10.1b T_{OX} of the compounds containing the above mentioned filler particles at various filler loadings are depicted. Whereas T_{OX} for the compounds with expanded graphite as filler did not change in regard to the neat HDPE and stayed rather constant ($T_{OX-HDPE}$ = 237 °C; $T_{OX-EGmin}$ = 236 °C; $T_{OX-EGmax}$ = 239 °C), T_{OX} for the compounds containing aluminum platelets and copper decreased with increasing filler loading ($T_{OX-APmin}$ = 210 °C; $T_{OX-Kmin}$ = 202 °C). A decrease in the thermo-oxidative stability of HDPE caused by the presence of different metal ions was also reported by Gorghiu et al. where copper accelerated the thermo-oxidation of HDPE to a higher extent than aluminum out of the tested metals [8]. Metal ions typically catalyze the decomposition of peroxides which promotes polymer degradation due to the generation of free radicals [8,18]. Therefore, the focus for further optimization was put on expanded graphite as filler for enhancing the TC as the TC of EG-10 also exceeds by far the TC of AP-10 and C-10.

10.1.2. Optimization of compounds filled with expanded graphite

The same HDPE grade was used for the optimization of the compounds filled with expanded graphite. The already tested GFG 1200 and additional expanded graphite types were tested at a filler ratio of 15 vol% for comparison purposes. All tested expanded graphite types along with their manufacturer and particle size are given in Table 10.2. The density, the TC and the shape of the fillers did not change and can be taken from Table 10.1. The compounds were fabricated and their TC was determined as described in 10.1.1.

Table 10.2: The name, the manufacturer and the particle size (as deduced from the manufacturer's material data sheets) of the tested expanded graphite types for optimization.

Expanded graphite name	Manufacturer	Particle size [µm]
Sigratherm® GFG 130	SGL Carbon (Wiesbaden, DE)	130
Sigratherm® GFG 600		600
Sigratherm® GFG 1000 HD		1000
Sigratherm® GFG 1200		1200
Exo 5	Grafitbergbau Kaisersberg GmbH (St. Stefan bei Leoben, AT)	3 - 5
TIMREX® C-Therm 011	IMERYS (Paris, FR)	> 85

In Figure 10.2a the TC of HDPE-based compounds containing different types of expanded graphite with a filler loading 15 vol% is displayed. The expanded graphite types GFG 600 and GFG 1200 increased the TC of the HDPE the most efficient with TCs of 9.06 W/(mK) and 8.74 W/(mK), respectively. Both TC values exceeded by far the target of improving the functioning of the LHS with a TC of 1.5 W/(mK) [19]. Thus, the focus was kept on decreasing the filler loading of the GFG 600 and GFG 1200 to meet the TC targets on the one hand and to increase the storage capacity of the compounds to the highest possible extent on the other hand.

For the optimization of the two selected expanded graphite types, two different compounding procedures (i.e. direct processing and compounding via masterbatch) were applied to investigate a possible impact. The same co-rotating compounder set to the same parameters as in 10.1.1 was used for the direct compounding. This was only possible for filler loadings above

162

3 vol% due to the lower limit of the gravimetric dosing unit. For the processing via masterbatch, a compound with a filler loading of 18 vol% was fabricated in a first compounding round. It was then dry blended with the HDPE for dilution to the according filler loadings indicated in Table 10.3 and processed in a second compounding round. Filler loadings down to 1 vol% were possible. The same compounder and the same parameters as in 10.1.1 were applied for both compounding rounds.
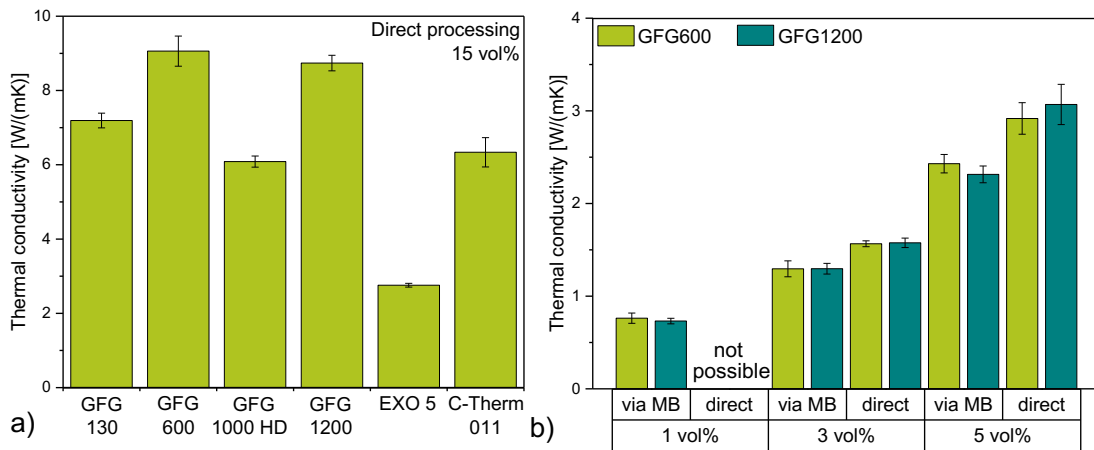

Figure 10.2: a) the thermal conductivity of HDPE-based compounds containing 15 vol% of different types of expanded graphite. The GFG 600 and GFG 1200 increase the thermal conductivity the most efficient; b) the thermal conductivity of HDPE-based compounds containing GFG 600 and GFG 1200 as filler at lower filler loadings (via MB = processing via masterbatch; direct = direct processing).

Table 10.3: Expanded graphite type, filler loadings and the according processing type for the optimization of the compounds.

Expanded graphite name	Filler loadings [vol%]	Processing type
Sigratherm® GFG 600	1,3 and 5	Via masterbatch
Sigratherm® GFG 600	3 and 5	Direct processing
Sigratherm® GFG 1200	1,3 and 5	Via masterbatch
Sigratherm® GFG 1200	3 and 5	Direct processing

In Figure 10.2b the TCs of the HDPE-based compounds containing GFG 600 and GFG 1200 and processed differently are given for filler loadings of 1 vol%, 3 vol% and 5 vol%. With increasing filler loading the TC increased for

all compounds as expected. Interestingly, the TC was enhanced more efficiently for the compounds which were processed directly. For those containing 3 vol% of GFG 600 and GFG 1200, similar TCs of 1.57 W/(mK) and 1.58 W/(mK) were achieved, respectively. As opposed to that, TCs of 1.29 W/(mK) and 1.30 W/(mK) were detected for the compounds containing 3 vol% of GFG 600 and GFG 1200 which were processed via masterbatch. The same tendency was seen for the compounds with filler loadings of 5 vol%: 3.06 W/(mK) and 2.92 W/(mK) for directly processed compounds containing GFG 600 and GFG 1200 and 2.43 W/(mK) and 2.31 W/(mK) for the compounds containing GFG 600 and GFG 1200 which were processed via masterbatch.

Due to the dependence of the compound's TC on the processing method, the compounds containing 1 – 5 vol% of the expanded graphite types GFG 600 and GFG 1200 were investigated in more detail with a light microscope BX51 (Olympus, Tokyio, JP). For this purpose, microtome sections with a thickness of 20 μm were extracted with a rotary microtome (Leica Microsystems GmbH, Wetzlar, DE) from the compression molded plates. The microtome sections were embedded in immersion oil and placed between two microscope object carriers made out of glass and investigated in transmitting light mode with a magnification of 100. Representative for all compounds, images of the microtome sections taken from the compounds containing 3 vol% of GFG 1200 which were processed via masterbatch and directly, are displayed in Figure 10.3a and b. The processing via masterbatch yielded smaller filler particles than the direct processing. Graphite is made up of several individual carbon layers which are held together only by weak Van der Waals bonds. Upon external force such as the shear during compounding, the carbon layers may separate easily. Therefore, the smaller particles were ascribed to the shear sensitivity of the expanded graphite and the additional compounding round. This further resulted in a comparably large interfacial area between the particles and the surrounding HDPE matrix which led to an increased phonon-boundary scattering and thus to a smaller TC [2,20]. Moreover, large particles tend to form conductive pathways more easily as they start to touch each other at lower filler loadings. Interestingly, the initial differences in the mean particle size (600 μm vs. 1200 μm, Table 10.2) did not significantly affect the TC enhancement. It seems that the compounding procedure shredded the varying particle sizes of the GFG 600 and the GFG 1200 to the same size as similarly sized expanded graphite particles were found during the morphological investigations (not all images displayed here).
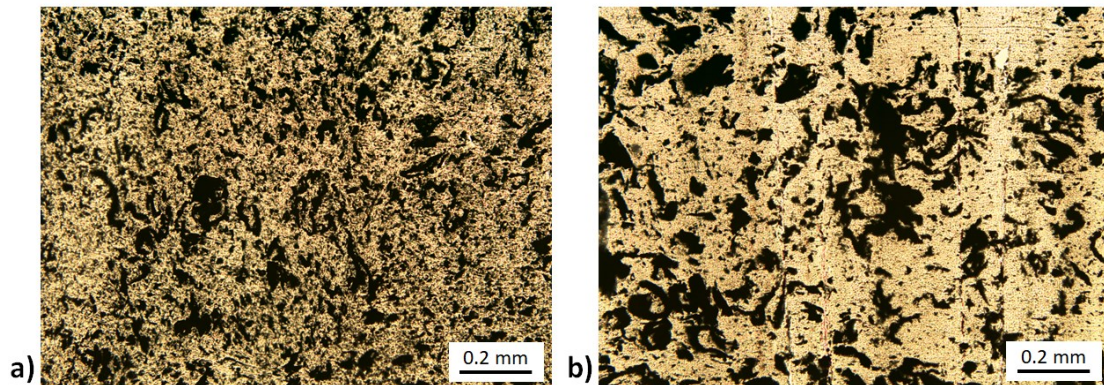
164

Figure 10.3: Images of the microtome sections of the compounds containing 3 vol% of GFG 1200: a) the compound was processed via masterbatch; b) the compound was processed directly. The finer filler distribution of a) was caused by the additional processing round as the expanded graphite particles was sheared a second time.

The directly processed compounds with a filler loading of 3 vol% and all compounds with a filler loading of 5 vol% met the TC target of 1.5 W/(mK) [19]. However, the flowability of the granules was significantly affected by the incorporation of the expanded graphite particles. To investigate their ability to fill the storage tank without air inclusions during melting, about 100 g of the granules were poured in aluminum crucibles (Ø = 80 mm; h = 25 mm) and heated in convection ovens Heraeus® TK 6060 (Thermo Fisher Scientific Inc., Waltham, US) at 180 °C for 8 h and then cooled freely at ambient temperature. Representative for all compounds, the cross sections of the cooled specimens of the directly processed compounds containing 3 vol% and 5 vol% of GFG 1200 are displayed in Figure 10.4a and b. The compounds with 5 vol% exhibited such a reduced flowability that voids were still present in the bulk of the specimen after the exposure in the convection ovens (Figure 10.4b). Thus, the directly processed compounds containing 3 vol% of GFG 600 and GFG 1200 proved to the most suitable polymeric PCM with enhanced TC out of the tested materials.
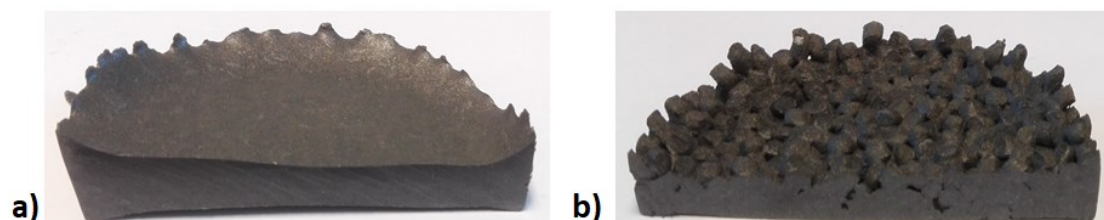

Figure 10.4: Cross sections of the cooled specimens of the HDPE-based compounds: a) directly processed compound containing 3 vol% of GFG 1200; b) directly processed compound containing 5 vol% of GFG 1200.

10.1.3. Conclusion and compound long-term stability investigations

The filler screening identified aluminum platelets, copper and expanded graphite as the most efficient fillers for enhancing the TC of HDPE. The particle type and filler loading for the compounds containing expanded graphite were further optimized. Compounds which were processed directly and contained 3 vol% of GFG 600 and GFG 1200 proved to be most suitable as polymeric PCM with enhanced TC. Nevertheless, aluminum is the metal with the least accelerating effect on the thermo-oxidation of HDPE [8]. It therefore remains an interesting filler for enhancing the TC of HDPE applied as PCM as well.

During the filler screening, it was further shown that the incorporated fillers do not only affect the material's TC but also its short-term thermo-oxidative stability. This implies that also the material's long-term stability may be altered. Therefore, a detailed investigation of the application-relevant long-term stability of the compounds - as already done for the neat HDPE - is conducted. For this purpose, the two compounds AP-10 and the directly processed one containing 3 vol% of GFG 600 are selected. Identical exposure parameters and investigation methods as for the neat HDPE are chosen for comparison purposes (publication 2). Furthermore, the maintenance of the isotropic material character is observed (particle positions are variable during the compound's exposure in the melt state) which is essential for a uniform heat transfer throughout the PCM. The results are presented in publication 4 in the following.

10.2. References

[1]   N. Mehra, L. Mu, T. Ji, X. Yang, J. Kong, J. Gu, J. Zhu, Thermal transport in polymeric materials and across composite interfaces, Applied Materials Today 12 (2018) 92–130.

[2]   H. Chen, V.V. Ginzburg, J. Yang, Y. Yang, W. Liu, Y. Huang, L. Du, B. Chen, Thermal conductivity of polymer-based composites: Fundamentals and applications, Prog Polym Sci 59 (2016) 41–85.

[3]   N. Burger, A. Laachachi, M. Ferriol, M. Lutz, V. Toniazzo, D. Ruch, Review of thermal conductivity in composites: Mechanisms, parameters and theory, Prog Polym Sci 61 (2016) 1–28.

[4]   A.S. Luyt, J.A. Molefi, H. Krump, Thermal, mechanical and electrical properties of copper powder filled low-density and linear low-density polyethylene composites, Polym Degrad Stabil 91 (7) (2006) 1629–1636.

[5]   Rusu, M., Sofian, N., & Rusu, D, Mechanical and thermal properties of zinc powder filled high density polyethylene composites., Polym Test 20 (4) (2001) 409–417.

[6]   A.K. Pandey, K. Singh, K.K. Kar, Thermo-mechanical properties of graphite-reinforced high-density polyethylene composites and its structure–property corelationship, J Compos Mater 51 (12) (2016) 1769–1782.

[7]   E. Tarani, Z. Terzopoulou, D.N. Bikiaris, T. Kyratsi, K. Chrissafis, G. Vourlias, Thermal conductivity and degradation behavior of HDPE/graphene nanocomposites, J Therm Anal Calorim 129 (3) (2017) 1715–1726.

[8]   L.M. Gorghiu, S. Jipa, T. Zaharescu, R. Setnescu, I. Mihalcea, The effect of metals on thermal degradation of polyethylenes, Polym Degrad Stabil 84 (1) (2004) 7–11.

[9]   I.H. Tavman, Thermal and mechanical properties of aluminum powder-filled high-density polyethylene composites, J. Appl. Polym. Sci. 62 (12) (1996) 2161–2167.

[10]   R.F. Hill, P.H. Supancic, Thermal Conductivity of Platelet-Filled Polymer Composites, J Am Ceram S 85 (4) (2002) 851–857.

[11]   T. Yamane, S. Katayama, M. Todoki, I. Hatta, The measurements of Thermal Conductivity of Carbon Fibers, in: T.W. Tong (Ed.), Thermal conductivity 22, Technomic Pub. Co, Lancaster, Penn., 1994, p. 313.

[12]   B.E. Langner, Understanding copper: Technologies, markets, business, 1st ed., B. E. Langner, Winsen, Glockenheide 11, 2011.

[13]   H. Fukushima, L.T. Drzal, B.P. Rook, M.J. Rich, Thermal conductivity of exfoliated graphite nanocomposites, J Therm Anal Calorim 85 (1) (2006) 235–238.

[14]   J. Severin, P. Jund, Thermal conductivity calculation in anisotropic crystals by molecular dynamics: Application to α-Fe2O3, J. Chem. Phys. 146 (5) (2017) 54505.

[15]   I. Krupa, I. Chodák, Physical properties of thermoplastic/graphite composites, Eur Polym J 37 (11) (2001) 2159–2168.

[16]   N.M. Sofian, M. Rusu, R. Neagu, E. Neagu, Metal Powder-Filled Polyethylene Composites. V. Thermal Properties, Journal of Thermoplastic Composite Materials 14 (1) (2001) 20–33.

[17]   H.S. Tekce, D. Kumlutas, I.H. Tavman, Effect of Particle Shape on Thermal Conductivity of Copper Reinforced Polymer Composites, J Reinf Plast Comp 26 (1) (2007) 113–121.

[18]   M. Tolinski, Additives for Polyolefins: Getting the Most out of Polypropylene, Polyethylene and TPO, 2nd ed., Elsevier Science, Burlington, 2015.

[19]   Christoph Zauner, Private correspondence, 2017.

[20]   N. Tsutsumi, N. Takeuchi, T. Kiyotsukuri, Measurement of thermal diffusivity of filler-polymide composites by flash radiometry, J. Polym. Sci. B Polym. Phys. 29 (9) (1991) 1085–1093.

11.   Publication 4

11.1.   Bibliographic information

- Title: Thermally conductive high-density polyethylene as novel phase-change material: application and long-term stability

- Authors:
    - Helena Weingrill[1,2]
    - Katharina Resch-Fauster[1]
    - Thomas Lucyshyn[2]
    - Christoph Zauner[3]

- Affiliation:

    1. Materials Science and Testing of Polymers, Montanuniversitaet Leoben, Otto-Gloeckel-Strasse 2, 8700 Leoben, Austria

    2. Polymer Processing, Montanuniversitaet Leoben, Otto-Gloeckel-Strasse 2, 8700 Leoben, Austria

    3. Austrian Institute of Technology, Giefinggasse 2, 1020 Vienna, Austria

- Periodical: Journal of Applied Polymer Science

- Status: Submitted

Statement with regard to this publication: The manuscript presented here is an adapted accepted manuscript in order to fit the formatting of the thesis and does not necessarily reflect exactly the actually published version.

11.2.   Abstract

The long-term stability of thermally conductive high-density polyethylene (HDPE)-based compounds as phase-change material (PCM) is investigated. For this purpose, bulky specimens are stored in air for up to 7289 h in the melt state to investigate the compounds' long-term stability as PCM. Their thermo-oxidative/thermal stability and their ability to maintain the isotropic material character (homogeneous distribution of the incorporated particles) is investigated. The compounds' degradation behavior is monitored via Fourier-transform infrared spectroscopy (FTIR) and the maintenance of the homogeneous filler distribution is examined via a combined Differential Scanning Calorimetry (DSC)/Thermal Gravimetric Analysis (TGA) mapping of each exposed specimen. The storage capacity decreases minimally after 7289 h of exposure. Furthermore, the incorporated filler particles enhance the thermo-oxidative stability of HDPE as PCM. Consequently, thermally conductive HDPE is a highly interesting PCM.

11.3.   Introduction

High-density polyethylene (HDPE) is an interesting novel phase-change material (PCM) for thermal energy storages (TES). It meets three major requirements for TES materials [1]: low-cost, a high heat of fusion (i.e. the energy density) and an outstanding stability when exposed above its melting temperature in storage-like conditions [2,3]. However, as for other low-temperature PCMs (e.g. paraffins, fatty acids, esters), HDPE's thermal conductivity (TC) is low and in the approximate range of 0.3 - 0.5 W/(mK) [4,5]. This results in a slow thermal response when applied as PCM which may inhibit a complete melting of the PCM if the time for charging is limited. To avoid such an underuse of the thermal energy storage, a higher TC can be obtained via compounding highly conductive particles into the PCM [6,7]. The incorporation of carbon-based fillers (e.g. expanded graphite, graphene, carbon nanotubes, carbon fibers), metal fillers (e.g. aluminum, copper, steel, zinc) and ceramic fillers (e.g. aluminum nitride, boron nitride, talc) has been extensively studied for enhancing the thermal conductivity of polymers and TC enhancements of several hundred percent were obtained [8-15].

170

However, two aspects have to be considered when a polymeric compound with enhanced thermal conductivity is applied as PCM:

1.) As the particles interact with the surrounding matrix, not only the compound's TC is enhanced but simultaneously storage-relevant properties such as the polymer's melting and crystallization behavior (which determine the operating temperature of the PCM), the heat of fusion (storage capacity) and the degradation behavior (thermal stability) [16-21] may be affected.

2.) The polymeric compound exhibits melt movability in the charged state [2]. Thus, the positions of the incorporated particles in the polymeric matrix are variable. For a well-functioning of the TES, however, isotropic properties in terms of a homogeneous distribution of particles throughout the PCM must be present at all times to ensure uniform heat transfer (physical stability) [1].

Therefore, the long-term stability of a polymeric PCM compound includes its thermo-oxidative/thermal stability as given by its degradation behavior (chemical stability) and its ability to maintain its homogeneous filler distribution.

Yang et al. [5] proved the short-term thermal stability of recycled HDPE/graphite compounds for 10 consecutive heating and cooling cycles in a Differential Scanning Calorimeter (DSC). However, as HDPE is a rather novel polymeric material for PCM [3,22], no data for the long-term stability of its compounds is available in the scientific literature so far. Thus, the present study aims at investigating the long-term stability of polymeric PCM compounds. For this purpose, bulky specimens of HDPE-based compounds containing either expanded graphite or aluminum particles were exposed to static thermal loads in air for up to 7289 h.

11.4.   Experimental

11.4.1.   Materials

The high-density polyethylene (HDPE) Bormed^{TM} HE9621-PH (Borealis GmbH, Linz, AT) with a density of 0.964 kg/m³ and a melt flow rate of 12 g/10 min (2.16 kg, 190 °C) was used for compounding. The HDPE grade was chosen as it exhibited an outstanding high heat of fusion and was already tested as PCM [2]. Also, other HDPE grades have been tested as PCM [3,22], but the selected grade possesses the lowest viscosity among the tested grades. It is thus assumed that it exhibits a high sensitivity towards phase segregation and the most severe conditions could be established by the use of this low-viscosity grade. It will be referred to as PE in the following.

The PE was used as received for the compounding. To enhance the thermal conductivity, expanded graphite Sigratherm® GFG 600 from SGL Carbon SE (Wiesbaden, DE) and aluminum particles Metallic 7814 from Benda Lutz GmbH (Nussdorf ob der Traisen, AT) were compounded into the PE, respectively. The particles were used as received without any further surface treatment and functionalization. In Figure 11.1 micrographs of the incorporated particles which were recorded in secondary electron (SE) mode via scanning electron microscopy (SEM) are displayed (experimental procedure see 11.4.3). The fillers' average particle size, specific surface, density as taken from the manufacturer's material data sheet and their shape are given in Table 11.1.

Table 11.1: Filler and its abbreviation, and its average particle size, specific surface, density as taken from the manufacturer's material data sheet and the filler's shape.

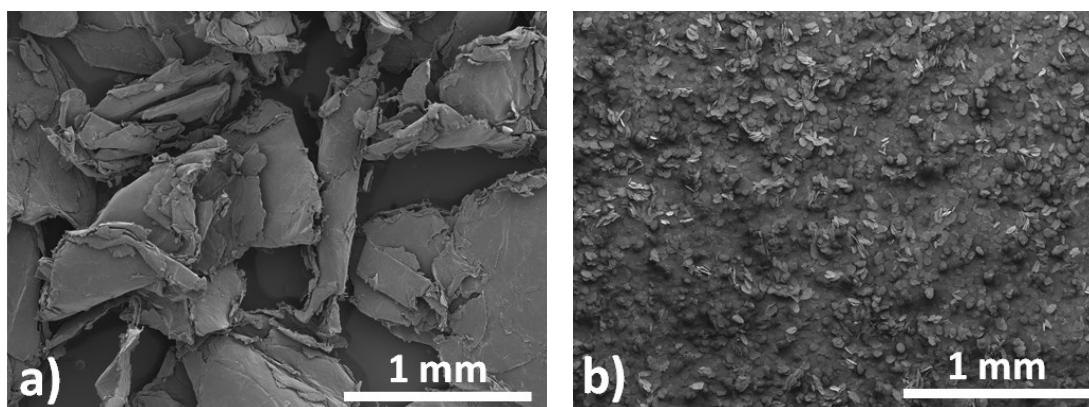| Filler	Filler abbreviation	Average particle size [µm]	Specific surface [m²/g]	Density [kg/m³]	Shape
Sigratherm® GFG 600	Expanded graphite (EG)	600	18-20	2.2	Flakes
Metallic 7814	Aluminum (A)	40	1.29	2.7	Flakes

Figure 11.1: SE-SEM micrographs of the: a) expanded graphite and b) aluminum particles which were incorporated into the HDPE matrices to enhance the thermal conductivity.

The compounding of the PE with the different fillers was executed on a co-rotating twin screw compounder (Werner & Pfleiderer GmbH, Dinkelsbühl, DE) with an L/D ratio of 38 and equipped with 6 control zones, a gravimetric dosing unit, side feeding, vacuum degassing, a cool bath and strand pelletizing. The temperatures of the six control zones were set to 140 °C,

180 °C, 190 °C, 190 °C, 190 °C, 190 °C and the mass feed rate was set to 6 kg/h. The fillers were added to the compounder via the side feeding.

The incorporation of expanded graphite and aluminum enhances the thermal conductivity (TC) with different efficiency. Thus, the filler loadings of the compounds were chosen so that both compounds exhibited similar TC to achieve a similar thermal response during charging and discharging of the thermal energy storage. Their TC was determined at ambient temperature in preliminary measurements via a TPS 2500S (Hot Disk AB, Gothenborg, SE) on compression molded plates (pressed for 30 min at 195 °C with a pressure ramp from 0 to 39 bar, cooled for 15 min at 30 °C at 39 bar) with the dimensions of 80 mm * 160 mm * 5 mm. The given TC represents the average of 7 measurements. A more detailed description of the measurement procedure can be found in [23]. The polymer grade, the fillers, the filler loading in vol% and in wt%, the thermal conductivity and the compound names are given in Table 11.2.

Table 11.2: The polymer grade, the filler, the filler loading in vol% and wt%, their thermal conductivity and the name of the compounds.

Polymer grade	Filler	Filler loading [vol%]	Filler loading [wt%]	Thermal conductivity [W/(mK)]	Compound name
Bormed™ HE9621-PH	Expanded graphite Sigratherm® GFG 600	3	7	1.57	PE-EG
	Aluminum Metallic 7814	10	25	1.19	PE-Al

11.4.2. Exposure to static thermal load

The long-term stability was tested by storing the PE-based compounds in cylindrical glass containers (h= 110 mm; inner ø= 72 mm) in convection ovens Heraeus® TK 6060 (Thermo Fisher Scientific Inc., Waltham, US) in air at 180 °C. The position of the glass containers was changed weekly in order to equalize temperature gradients in the convection oven. Sampling was done after 24 h ("zero samples"), 739 h, 3600 h and 7289 h. The glass containers were removed from the convection oven and freely cooled at ambient temperature after the given exposure times. In order to impede warpage, a metal cylinder with a weight of 2 kg was placed on the specimen top during cooling (a polytetrafluoroethylene sheet in between prevented adhesion). After cooling, the cylindrical specimens (approx. dimensions: h = 80 mm; ø = 65 mm) were removed from the glass containers. They were

then cut vertically into semi-cylindrical specimens with a specimen saw Diadisc 5200 (MUTRONIC Praezisionsgeraetebau GmbH & Co.KG, Rieden am Forggensee, DE) as depicted in Figure 11.2a.
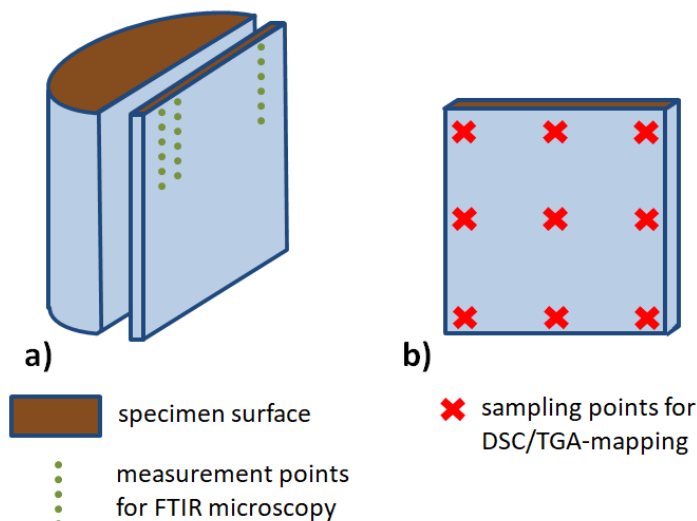

Figure 11.2: The exposed cylindrical specimens were cooled and cut into two semi-cylinders and a plate with a thickness of 8 mm for FTIR microscopy and the DSC/TGA-mapping: a) FTIR spectra were recorded with steps of 200 µm from the surface into the specimen bulk; b) samples for the combined DSC/TGA-mapping of the specimens were extracted underneath the specimen surface("upper area"), in the specimen center ("center") and at the specimen bottom ("bottom").

11.4.3.   Characterization of the PE-compounds

11.4.3.1. Compound morphology and thermo-physical properties

The morphology of the compounds was investigated via SEM on a Tescan-Vega-II (TESCAN, Brno, CZ). Micrographs of the cross sections of the zero samples and the exposed samples were prepared by cutting out a rectangular piece (approximately 10 mm * 10 mm * 4 mm) of the center and/or the bottom of one semi-cylinder. Afterwards the rectangular pieces were sputtered with gold with a sputter coater SCD005 (BalTec Maschinenbau AG, Pfäffikon, CH). An electrical voltage of 20-30 kV was applied and images were recorded in back-scattering electron (BSE) mode.

The viscosity of the compounds at 180 °C was determined via rotational testing on a rheometer MCR 502 TwinDrive (Anton Paar GmbH, Graz, AT) in the shear rate range from 0.001 s^{-1} to 5 s^{-1} with a parallel plate geometry (Ø = 25 mm). Samples (h = 2 mm; Ø = 25 mm) were prepared via compression molding on a vacuum press P 200 PV (Dr. Collin GmbH, Ebersberg, DE) at

195 °C. The plates were pressed for 15 min at 195 °C with a pressure ramp from 0 to 39 bar and then cooled for 10 min at 30 °C and 39 bar.

The melting and crystallization characteristics of the neat PE and the PE-based compounds were determined via combined Differential Scanning Calorimetry (DSC) and Thermogravimetrical Analysis (TGA). A power compensation calorimeter DSC8000 (PerkinElmer, Waltham, US) was applied for the DSC measurements. Samples were taken from the unexposed granules of the neat polymer and the compounds. The sample weight was 10 mg and 50 µl aluminum crucibles with a perforated lid were used. After an equilibration time of 5 min at 0 °C, the samples were heated under nitrogen atmosphere to 160 °C and cooled to 0 °C by applying a constant heating rate of 10 °C/min and -10 °C/min, respectively. After another equilibration time of 5 min at 0 °C, the samples were heated a second time to 160 °C by applying a constant heating rate of 10 °C/min. The peak crystallization temperature T_C and the extrapolated crystallization onset and endset temperatures T_{Con}/T_{Cend} were evaluated from the cooling curves. The heat of fusion ΔH_M, the peak melting temperature T_M and the extrapolated melting onset and endset temperatures T_{Mon}/T_{Mend} were evaluated from the second heating. The evaluations were done according to ISO 11357. The presented data represent the average of two to three measurements (depending on the variance of the results). The measured heat of fusion of the compounds is given as $\Delta H_{M,PCM}$ and as $\Delta H_{M,corr}$ for which $\Delta H_{M,PCM}$ was corrected for the polymeric weight fraction as deduced from consecutive TGA (only the polymeric matrix in the compound contributes to the heat of fusion; combined DSC/TGA - procedure in accordance with [24]). For this purpose, the DSC samples were transferred from the DSC crucibles to 70 µl alumina TGA crucibles. The TGA measurements were done on a TGA/DSC 1 (Mettler Toledo GmbH, Greifensee, CH). After an equilibration time of 10 min at 25 °C, the samples were heated under nitrogen atmosphere from 25 °C to 600 °C by deploying a constant heating rate of 20 °C/min. Polymer pyrolysis took place between 400 °C and 530 °C. Therefore, the sample weights at 100 °C (m_{100}) and 550 °C (m_{550}) was used to calculate the filler loading f in wt% according to equation (1).

$$f = \frac{m_{550}}{m_{100}} * 100\% \qquad (1)$$

$\Delta H_{M,corr}$ could then be calculated according to equation (2).

$$\Delta H_{M,corr} = \frac{\Delta H_{M,PCM}}{1 - \frac{f}{100}} \qquad (2)$$

Additionally, the Oxidation Induction Temperature (dynamic OIT) of the neat PE and the PE-compounds (unexposed granules) was determined on a DSC 1 (Mettler Toledo, Greifensee, CH). The sample weight was 10 mg and open 40 µl aluminum crucibles were used. After an equilibration time of 5 min at 25 °C under nitrogen atmosphere, the sample was heated under oxygen atmosphere from 25 °C until an exothermic curve indicating the thermo-oxidative degradation was recorded. The heating rate was 10 °C/min. The Oxidation Induction Temperature T_{OX} was evaluated according to ISO 11357-6. The presented data represent the average of two measurements. The dynamic OIT measurements will be referred to as OIT measurements.

11.4.3.2. Degradation behavior and filler distribution

The degradation behavior of the exposed specimens was examined in detail via Fourier-transform infrared (FTIR) spectroscopy. Plates with a height of 8 mm were cut in parallel direction to the longitudinal axis from the semi-cylindrical specimens with a specimen saw Diadisc 500 (MUTRONIC Praezisionsgeraetebau GmbH & Co.KG, Rieden am Forggensee, DE) as displayed in Figure 11.2a. A fully automated stand-alone FTIR microscope Lumos (Bruker Corporation, Billerica, US) was used. The FTIR spectra were recorded in Attenuated Total Reflection (ATR) mode with a germanium crystal (refractive index n=4) with a total of 64 scans, at a resolution of 4 cm^{-1} and in the wavelength range from 4000 cm^{-1} to 600 cm^{-1}. In order to investigate the thermo-oxidative degradation propagation from the specimen surface into the bulk, FTIR spectra were recorded stepwise in this direction on the plates (green dotted line in Figure 11.2a). The first FTIR spectrum was measured 200 µm underneath the specimen surface followed by consecutive steps of 200 µm into the specimen bulk. FTIR spectra were recorded until the spectra from the unexposed and the exposed specimen coincided. This was done three times for each exposed specimen in a distance of at least 5 mm from the specimen edge.

The compounds' filler distribution (physical stability) was investigated via a combined DSC/TGA-mapping of the exposed specimens. The combined DSC/TGA-measurements were executed as described in 11.4.3.1 and the filler loading and $\Delta H_{M,PCM}$ were evaluated. Three samples were extracted from the upper area of the specimen right underneath its surface, the specimen center and the specimen bottom from the plate with a thickness of 8 mm as depicted in Figure 11.2b. The samples from underneath the specimen surface were extracted at least 5 mm below the surface to ensure not to test thermo-oxidatively degraded material. The average of the three measurements of each row ("upper area", "center", "bottom") was calculated.

176

11.5. Results

11.5.1. Characterization of polymeric PCM-compounds

In Figure 11.3 BSE-SEM micrographs of the center of the zero samples of PE-EG and PE-Al are displayed representatively for all compounds. The filler particles were distributed homogeneously in the zero samples. Thus, a uniform heat transfer can be expected throughout the specimens.
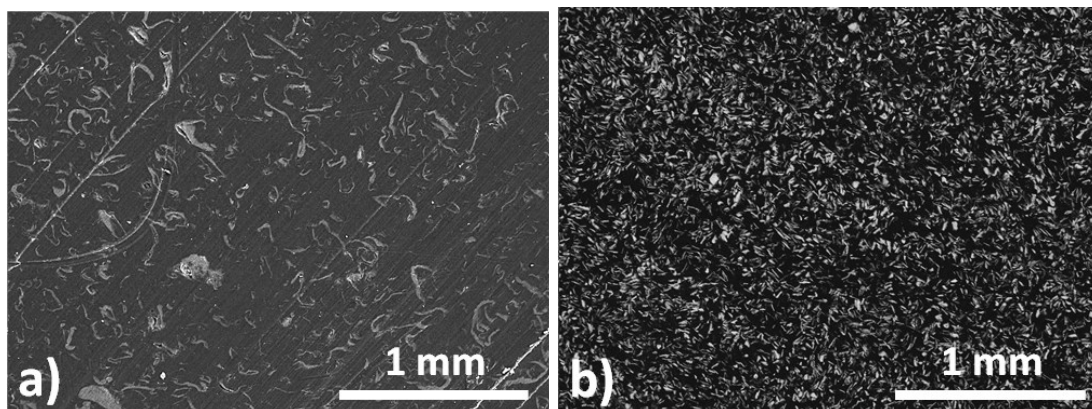

Figure 11.3: BSE-SEM micrographs of the zero samples of a) PE-EG and b) PE-Al. The particles were distributed homogeneously throughout the specimens which resulted in a uniform heat transfer.

In Figure 11.4 the viscosity η of the neat PE and the PE-compounds is given as a function of the shear rate. During the charging of the PCM, the polymer melts without any external force application besides gravitation. In this case, shear rates in the range of ≤ 0.1 s^{-1} are present [25]. By adding expanded graphite and aluminum particles, η is increased for both compound types due to internal friction between the fillers and the fillers and the polymers [26]. At a shear rate of 0.01 s^{-1}, η of the neat PE was increased from $1.5*10^3$ Pa.s to $1.3*10^4$ Pa.s and $2.8*10^3$ Pa.s for the PE-EG and PE-Al, respectively. Thus, PE-EG possessed a higher η than PE-Al despite the smaller filler loading of 3 vol%. Hence, the internal friction is increased stronger by EG than by Al particles. This was attributed to the frayed and fanned out shape of the EG particles. It facilitated entanglements of the particles among each other and between the particles and the polymer chains. Additionally, some polymer chains probably reached into the individual carbon layers of the particles leading to increased interaction between the EG particles and the polymeric matrix compared to the interaction within the PE-Al. Nonetheless, the compounds exhibited sufficient flowability as the bulky zero samples were void-free (Figure 11.3). This is essential for the application as the polymer

PCM compound is poured in the form of granules into the storage container. Thus, no losses in the storage capacity due to air inclusions are expected.
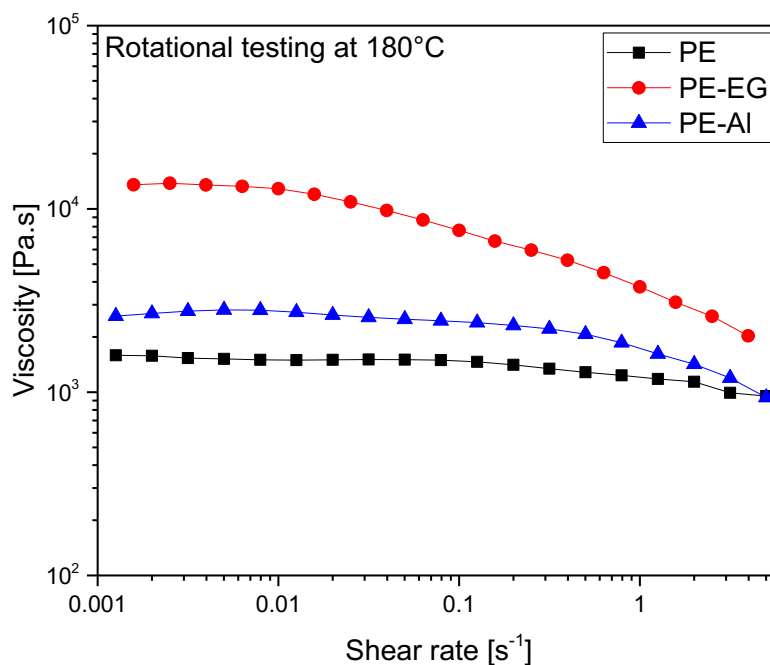

Figure 11.4: The viscosity of the neat PE and the PE-compounds as a function of the shear rate. The viscosity of the materials increased by the incorporation of the expanded graphite and aluminum particles.

The melting peak temperature T_M, the extrapolated melting onset and endset temperatures T_{Mon}/T_{Mend}, the crystallization peak temperature T_C, the extrapolated melting onset and endset temperatures T_{Con}/T_{Cend}, the heat of fusion $\Delta H_{M,PCM}$ and $\Delta H_{M,corr}$ as deduced from the combined DSC- and TGA-measurements and the oxidation onset temperature T_{OX} of the unexposed granules of the neat PE and the PE-compounds are given along with their standard deviations in Table 11.3.

The thermograms of the cooling and the second heating of PE, PE-EG and PE-Al are depicted in Figure 11.5a and b, respectively. The incorporation of fillers affects the crystallization process of the PE. For both compounds, the crystallization process was shifted to a higher temperature range compared to the neat PE. T_C increased from 116.8 °C for the neat PE to 119.4 °C for both compounds and T_{Conset}/$T_{Cendset}$ increased from 120.3 °C/110.5 °C to 123.7 °C/114.2 °C and 122.0 °C/113.3 °C for PE-EG and PE-Al, respectively. Thus, the filler particles acted as nucleating sights for the PE chains during the crystallization process and thereby enabled crystallization at higher temperatures. Compared to the neat PE, the cooling curve of PE-EG exhibited two additional small crystallization peaks at 129.2 °C and 135.1 °C

(detailed view in Figure 11.5a) whereas the crystallization peak at 129.2 °C was more pronounced. This phenomenon was also discovered by Weng et al. [27]. They ascribed it to a promoted crystallization of the PE lying in between the individual stacked carbon layers of the expanded graphite. T_M and T_{Mon}/T_{Mend} were affected little by the incorporation of aluminum and expanded graphite as filler. Overall, the phase transitions (crystallization and melting) of the PE and thereby the charging and discharging temperature of the phase change-material are not significantly affected by the applied filler types.

Table 11.3: Thermo-physical characteristics of the neat PE and the PE-compounds as determined via DSC: the melting peak temperature (T_M), the extrapolated melting onset and endset temperatures (T_{Mon} and T_{Mend}), the crystallization peak temperature (T_C), the extrapolated crystallization onset and endset temperatures (T_{Con} and T_{Cend}), the heat of fusion $\Delta H_{M,PCM}$ and the heat of fusion which was corrected for the polymeric weight fraction of the compounds $\Delta H_{M,corr}$ and the oxidation onset temperature T_{OX} of the unexposed neat PE and the PE-compounds.

Material	T_M [°C]	T_{Mon} [°C]/ T_{Mend} [°C]	T_C [°C]	T_{Con} [°C]/ T_{Cend} [°C]	$\Delta H_{M,PCM}$ [J/g]	$\Delta H_{M,corr}$ [J/g]	T_{OX} [°C]
PE	136.8 ± 0.4	127.0 ± 0.9/ 139.5 ± 1.8	116.8 ± 0.2	120.3 ± 0.3/ 110.5 ± 0.2	227.2 ± 0.5	-	232.5 ± 1.9
PE-EG	136.8 ± 0.4	126.6 ± 0.2/ 139.4 ± 0.7	119.4 ± 0.1	123.7 ± 0.1/ 114.2 ± 0.5	215.2 ± 0.8	230.8 ± 1.2	229.7 ± 0.5
PE-Al	136.0 ± 0.7	126.0 ± 0.8/ 138.8 ± 0.8	119.0 ± 0.6	122.0 ± 0.5/ 113.3 ± 0.0	169.3 ± 2.6	228.6 ± 0.8	220.5 ± 0.6

As the fillers did not undergo a phase transition during the melting of the compounds, only PE contributed to the compound's heat of fusion. $\Delta H_{M,PCM}$ therefore decreased from 227.2 J/g for the neat PE to 215.2 J/g and to 169.3 J/g for PE-EG and PE-Al, respectively. The differences in the decrease of $\Delta H_{M,PCM}$ are due to the different filler loadings (PE-EG: 7 wt%, PE-Al: 25 wt%; - both deduced from TGA measurements). $\Delta H_{M,corr}$ of the compounds was not affected by the fillers. This means that even though the crystallization behavior of the compounds differed from the one of the neat PE, the overall crystallinity of the PE did not change by the incorporation of the fillers.
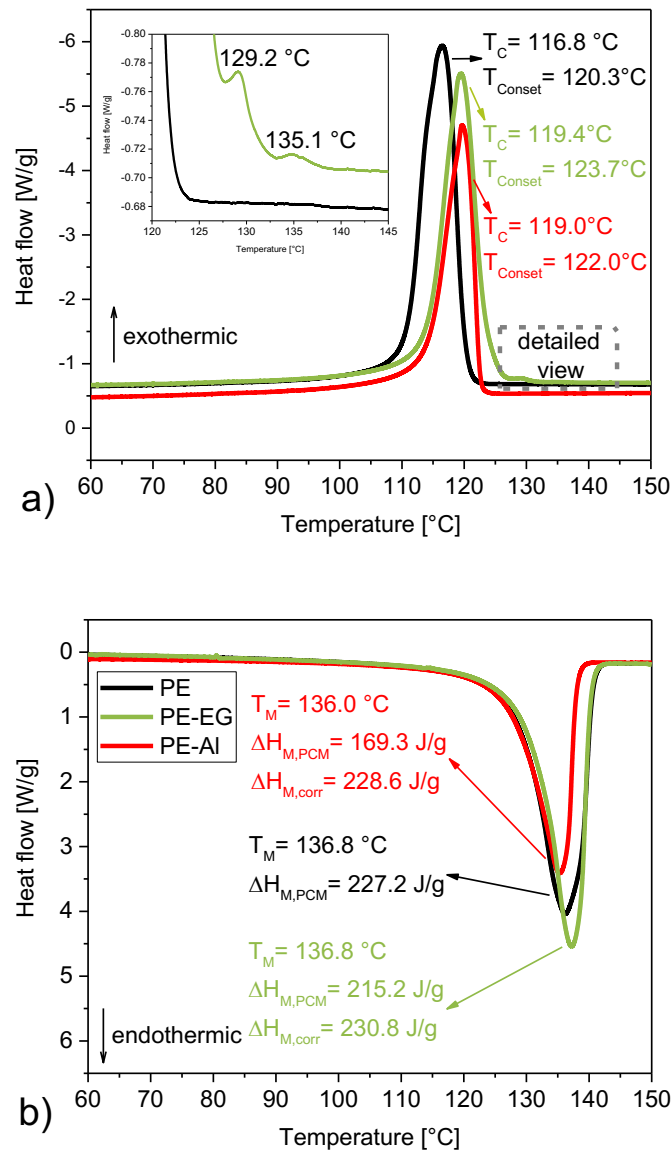
Figure 11.5: Representative thermograms of the neat PE and PE-based compounds: a) the cooling curve with a detailed view of the multiple crystallization peaks of PE-EG; b) the melting curve. The incorporation of both filler particle types impacts the crystallization and melting behavior of the HDPE moderately.

11.5.2. Long-term stability

In Figure 11.6 the cross sections of the specimens of the neat PE after 7214 h [2] and of PE-Al and PE-EG after 7289h of exposure to static thermal load at 180 °C are displayed. The specimens of the neat PE and PE-Al exhibited a distinct discoloration at the specimen surface. A change in the optical appearance was also detected at the specimen surface for the PE-

EG. However, due to its inherent black color a more detailed description of this change in appearance is not possible.
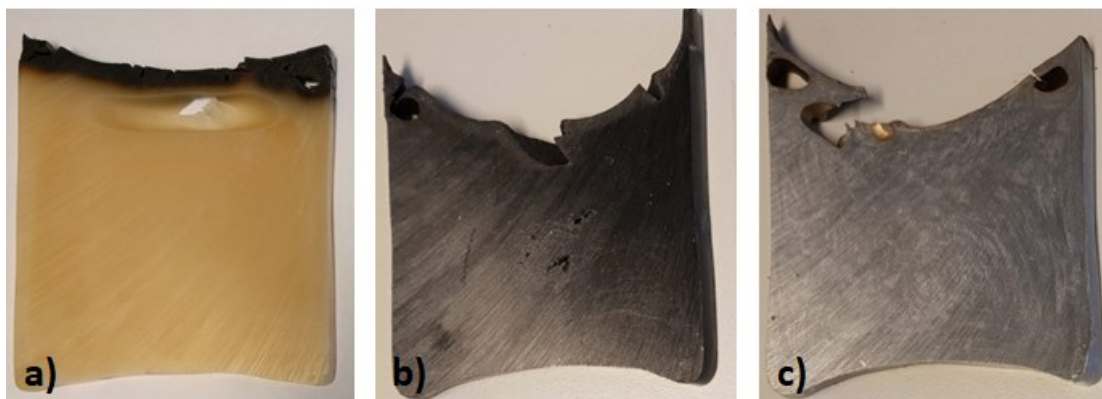

Figure 11.6: Cross sections of: a) the neat PE after 7214 h of exposure to static thermal load at 180 °C; b) PE-EG after 7289 h of exposure to static thermal load at 180 °C; c) PE-Al after 7289 h of exposure to static thermal load at 180 °C.

11.5.2.1. Degradation behavior

The FTIR spectra recorded from the center of the specimens of PE-EG and PE-Al after 24 h of exposure to 180 °C ("zero samples") and from the first measurement point underneath the specimen surface (200 µm) after 7289 h of exposure to 180 °C are presented in Figure 11.7a. Additionally, the FTIR spectra recorded from the specimens of the neat PE after 7214 h of exposure at 180 °C are displayed for comparison purposes (data taken from [2]). The FTIR spectra of the zero samples and the exposed specimens exhibited significant differences. All absorption bands were affected after 7289 h of exposure and thus, normalization was not possible. However, the identical specimen preparation and the automated procedure of the ATR crystal (internal pressure control) allowed a qualitative comparison of the different spectra. Similar degradation products were detected for the compounds and the neat PE which is discussed in more detail in [2]. Consequently, the incorporated filler particles did not affect the degradation mechanism of the neat PE. Nonetheless, two detected changes in the recorded spectra are worth mentioning as they will be used for further discussion: changes in the wavenumber range from ca. 750 cm^{-1} to 700 cm^{-1} and from ca. 1480 cm^{-1} to 1200 cm^{-1}, which represent the CH_2-bending vibrations, and an increase of the absorption bands in the wavenumber range from ca. 1780 cm^{-1} to 1700 cm^{-1}, which represent the stretching vibrations of carbonyl groups [28,29].
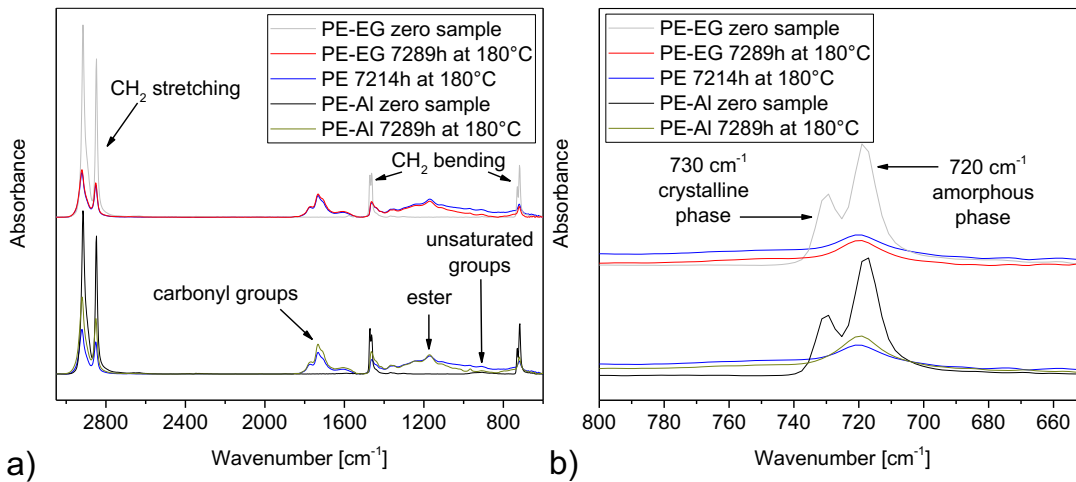
Figure 11.7: a) FTIR spectra recorded from the center of the zero samples and 200 μm underneath the surface of the PE-EG and PE-Al after 7289 h of exposure to 180 °C and of the neat PE after 7214 h of exposure at 180 °C; b) detailed view of the absorption bands which represent the CH_2-bending vibrations of the crystalline phase (730 cm^{-1}) and the amorphous phase (720 cm^{-1}). For the exposed samples (neat PE, PE-EG and PE-Al), the absorption band at 730 cm^{-1} vanished as the crystalline structure was destroyed due to thermo-oxidative degradation.

In Figure 11.7b a detailed view of the absorption bands at 730 cm^{-1} and 720 cm^{-1} which represent the CH_2-bending vibrations of the crystalline and the amorphous phase [29] are displayed. The absorption band of the crystalline phase vanished due to the thermo-oxidative degradation of the PE. Thus, the material turned amorphous during the exposure and its $\Delta H_{M,PCM}$ was decreased or even lost entirely. The thermo-oxidative degradation therefore affects the storage capacity of the thermal energy storage. In order to assess the loss of storage capacity due to exposure, the oxidation penetration depth (OPD) from the surface into the bulk was determined for each specimen. For this purpose, an absorbance of 0.005 of the absorption bands in the wavenumber range between 1780 cm^{-1} and 1700 cm^{-1} (carbonyl groups) was chosen as "oxidation threshold" to find the OPD of each material. This was the smallest detectable absorbance within the noise of the spectrum. The distance between the specimen surface and the last measurement position which yielded an absorption band above the oxidation threshold was taken as OPD.

The OPDs of the specimens of the neat PE [2] and the PE-based compounds after exposure times of up to 7289 h at 180 °C are displayed in Figure 11.8. For all materials, the OPD increased with increasing exposure time. For the neat PE, an OPD of 2870 µm, 3030 µm and 4200 µm was detected after 790 h, 3656 h and 7214 h of exposure, respectively. For the PE-EG and the PE-Al, an OPD of 1630 µm, 2600 µm and 3000 µm and of 730 µm, 600 µm and 1030 µm, was detected after comparable exposure times (736 h, 3600 h and 7289 h), respectively.
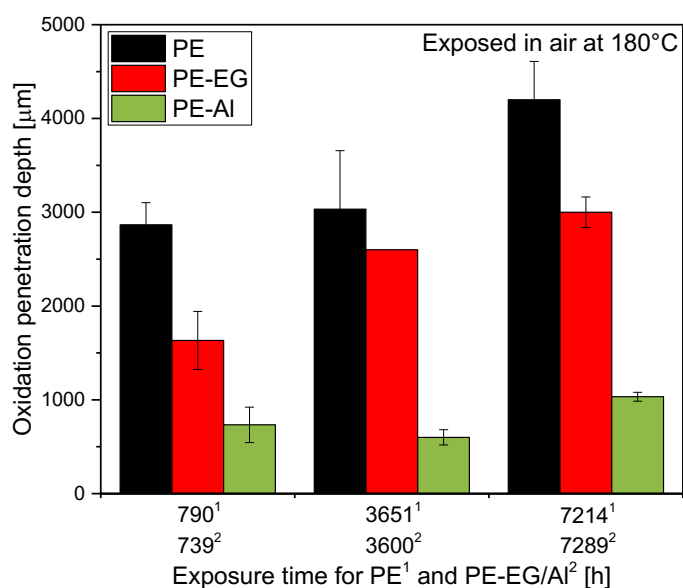

Figure 11.8: Oxidation penetration depth (OPD) of the neat PE [2], PE-EG and PE-Al as measured via FTIR microscopy after different exposure times. The OPD increased with increasing exposure time for both compounds. The incorporation of TC enhancing particles reduced the OPD as the particles acted as oxygen diffusion barrier.

The OPD was significantly reduced by the incorporation of the fillers which suggested an enhanced thermo-oxidative stability of the compounds over the neat PE. As opposed to that, both compounds exhibited a lower thermo-oxidative stability than the neat PE as deducible from T_{OX} (Table 11.3): $T_{OX,PE}$= 232.5 °C; $T_{OX,PE-EG}$= 229.7 °C; $T_{OX,PE-Al}$= 220.5 °C. In general, fillers tend to interact with the surrounding matrix and affect its thermo-oxidative degradation behavior as determined via different methods [21,24,30,31]. In the present study, T_{OX} identified the temperature at which oxidation first took place, whereas the OPD reflected the propagation of oxidation after a given time at a constant temperature. Thus, two factors, i.e. oxygen diffusion into the bulk material and its thermo-oxidative stability are decisive for OPD. Oxygen diffusion was most likely hampered by the incorporation of the fillers

(both fillers exhibited higher density than the neat PE (Table 11.1)) which outweighed the decreased thermo-oxidative stability as deduced from OIT. The differences in OPD between the PE-Al and the PE-EG resulted from the higher filler loading (smaller particles) of the PE-Al as more obstacles decelerated oxygen diffusion. Nonetheless the majority of the storage capacity of the bulky specimens was maintained after the applied thermal loads considering the height of the specimens of approx. 50 mm and the maximum detected OPD of 3 mm.

11.5.2.2. Maintenance of homogeneous filler distribution

In Figure 11.9 the $\Delta H_{M,PCM}$ and the filler loading as deduced from the combined DSC/TGA-mapping of the zero samples and the specimens exposed to static thermal load for 7289 h at 180 °C are displayed. As no horizontal gradient of $\Delta H_{M,PCM}$ and the filler loading was detected across the specimens, the average results for each row of the mapping ("upper area", "center", "bottom") are presented.

$\Delta H_{M,PCM}$ was constant throughout each specimen (detected minor differences were within the measurement uncertainty of the DSC). The average $\Delta H_{M,PCM}$ (average of all 3 rows) were 212.3 J/g and 172.3 J/g of each zero sample and 214.2 J/g and 170.0 J/g of each exposed specimen for the PE-EG and the PE-Al, respectively. Thus no thermal degradation had taken place outside the detected OPD and the storage capacity of the non-oxidized specimen part was fully maintained.

Minor differences in the filler loading of the zero samples (left column group in Figure 11.9) were within an acceptable variation range (≤0.3 wt%) which probably resulted from the compounding process. This was in good agreement with the homogeneous filler distribution seen in the BSE-SEM micrographs of the zero samples (Figure 11.3). The average filler loadings of the entire zero samples (average of all 3 rows) for PE-EG and PE-Al were 7.0 % and 24.6 wt%, respectively. After an exposure to static thermal load for 7289 h at 180 °C, the PE-EG specimen exhibited a slightly increased filler loading of 7.9 wt% at the bottom. This indicated that a small amount of particles had sunk during the exposure due to sedimentation as the density of the EG particles (2.2 g/cm³) exceeded the density of PE (0.964 g/cm³ at ambient temperature, lower at higher temperatures). Diminutive changes in the filler loading of the entire volume of the specimen except the bottom part added up to the small increase of 0.9 wt% of the filler loading at the bottom of the specimen. However, these diminutive changes were probably too small to be detected in the sampling points in the upper area and the center of the

184

specimen as those filler loadings stayed constant at 6.9 wt% and 7 wt%, respectively. The filler loadings of the exposed PE-Al specimen stayed constant at 24.6 wt%, 24.5 wt% and 24.4 wt% at the upper area, the center and the bottom of the specimen, respectively. Thus, sedimentation did not take place in the exposed PE-Al specimen.
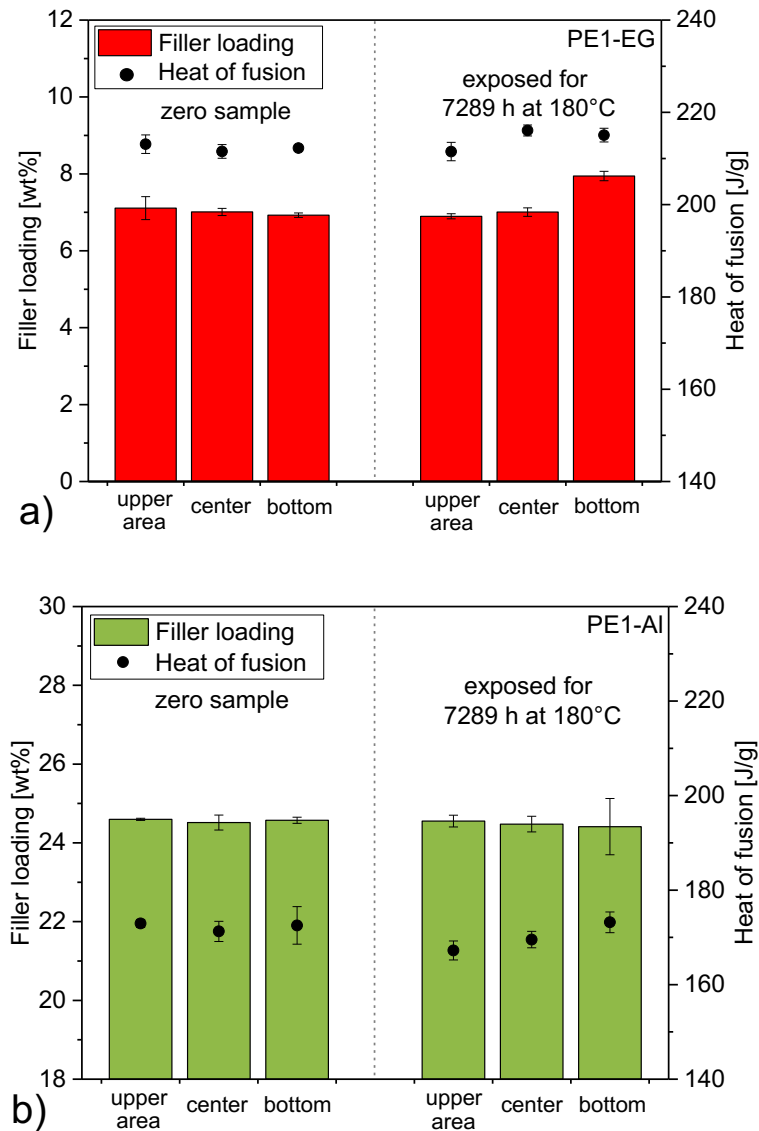

Figure 11.9: Filler loading and the heat of fusion $\Delta H_{M,PCM}$ as detected from the combined DSC/TGA-mapping of the exposed specimens. The columns are put in order according to the position of the sample extraction from the specimen: a) PE-EG; b) PE-Al. The filler particles were distributed homogeneously before the exposure. A small increase in the filler loading was detected at the bottom of the exposed PE-EG specimen, no changes were detected for the exposed PE-Al specimen.

Even though PE-EG exhibited a higher η than PE-Al (η_{PE-EG}= 1.3*10^4 Pa.s; η_{PE-Al}=2.8*10^3 Pa.s at 0.01 s^{-1} and 180 °C), sedimentation was only detected for PE-EG. In general, sedimentation depends upon η of the surrounding fluid (i.e. the neat PE in the present study) and the properties of the incorporated particles [25]. In colloidal dispersions (particles sizes < 1 μm), sedimentation only takes place if the particle size exceeds a critical diameter and the particles can therefore not be moved by Brownian motion [32]. Even though the compounds cannot be characterized as colloidal dispersions as the incorporated particles are larger than 1 μm (Table 11.1), the smaller aluminum particles (40 μm) seem to lie below a similar critical particle size that decelerated or even hampered sedimentation during the applied thermal loads. However, the larger mean particle size of 600 μm of the EG particles might have therefore led to sedimentation of the EG particles. Furthermore, they had more available polymer volume to sink into over the aluminum particles (PE-EG possessed a lower filler loading than PE-Al). The sinking aluminum particles on the other hand encountered more particles which acted as obstacles for sedimentation. Sedimenation was thereby probably impeded. Hence, the filler particle shape and the filler loading seem to be crucial for sedimentation.

To further investigate the sedimentation behavior of the PE-EG during the exposure at 180 °C, a cylindrical glass container (h= 110 mm; inner ø= 72 mm) was first filled with neat PE up to three quarters of the volume and melted at 180 °C in a vacuum drying oven VD23MI (Binder GmbH, Tuttlingen, DE). One layer of PE-EG compound was added and the rest of the container was filled with neat PE and melted in the same convection oven as used for the exposure (Figure 11.10a: after 2 h of exposure at 180 °C). The melted compound layer started to slowly sink within two hours. The sedimentation of the PE-EG layer during the first 8 h can be seen in Figure 11.10. Interestingly, the particles within the compound did not sink individually, but the compound layer stayed largely intact. This indicates that the polymer chains still entangle the filler particles as coming from the compounding process and hamper them to sink individually. The polymer chains cannot easily untangle them as the filler particles increase internal friction [26] which further helps to maintain an intact compound layer within the neat PE. This suggests that a certain fixation of the filler particles in the compound layer within the PE matrix was present. This further implies that a fixation was also present throughout the exposed PE-EG specimens. This might have contributed to the rather small sedimenation of the EG particles after an exposure of 7289 h.

Nonetheless, considering the even distribution of the particles at the specimen bottom (no orientations or agglomerates, Figure 11.11), a sufficiently uniform heat transfer throughout the PE-EG specimen can still be expected after the applied exposure of 7289 h. Furthermore, the polymeric PCM compound is not continuously used in the melt state but undergoes consecutive melting and crystallization cycles during the real application. Thus, particle sedimentation is delayed whenever the PCM is in the solid state. This renders a change in thermal conductivity more unlikely. Hence, both compounds exhibit appropriate physical stability as PCM.
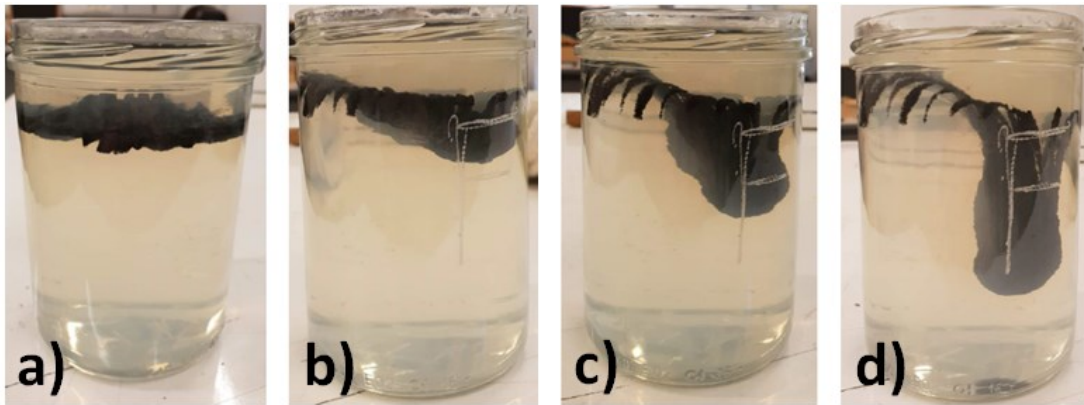

Figure 11.10: Sedimentation behavior of PE-EG layer in neat PE at 180 °C after: a) 2 h; b) 4 h; c) 6 h; d) 8 h. The particles within the compound do not sediment individually but the compound layer stayed mostly intact.
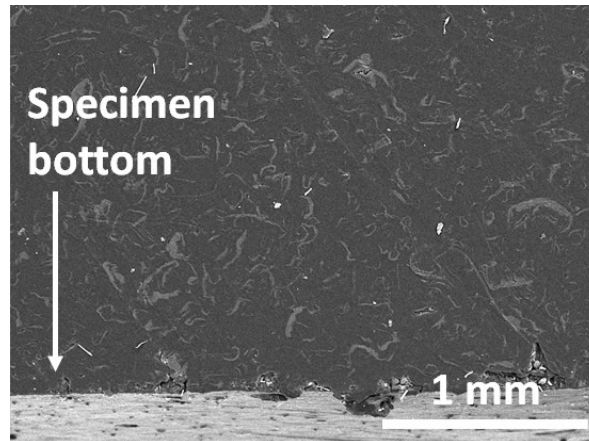

Figure 11.11: BSE-SEM-micrograph of the bottom of the PE-EG specimen after an exposure of 7289 h at 180 °C where a slightly higher filler loading was detected. However, the particles were distributed evenly within the specimens. Thus a uniform heat transfer throughout the specimens was present.

11.6.   Conclusion and outlook

Thermally conductive high-density polyethylene (HDPE) proves to be an advanced phase-change material (PCM) with increased thermo-oxidative stability over the neat HDPE. It is capable of maintaining its homogeneous filler distribution after an exposure to static thermal load in the melt state for up to 7289 h. If segregation of the filler particles and the surrounding HDPE matrix occurs the heat transfer rates are not affected due to its minmal extent. This confirms the applicability of the compounds as novel polymeric PCM. Nonetheless, the incorporation of particles results in a reduced storage capacity over the unfilled HDPE. Therefore, further work needs to focus on optimizing the filler loading in order to find the optimum balance between a thermal conductivity for a sufficiently fast heat transfer rate and the necessary storage capacity for a well-functioning of the thermal energy storage.

11.7.   Acknowledgements

11.8.   References

[1]   Z. Ge, Y. Li, D. Li, Z. Sun, Y. Jin, C. Liu, C. Li, G. Leng, Y. Ding, Thermal energy storage: Challenges and the role of particle technology, Particuology 15 (2014) 2–8.

[2]   H.M. Weingrill, K. Resch-Fauster, T. Lucyshyn, C. Zauner, High-density polyethylene as phase-change material: Long-term stability and aging, Polym Test 76 (2019) 433–442.

[3]   H.M. Weingrill, K. Resch-Fauster, C. Zauner, Applicability of Polymeric Materials as Phase Change Materials, Macromol. Mater. Eng. 31 (2018) 1800355.

[4]   T.A. Osswald, E. Baur, S. Brinkmann, K. Oberbach, E. Schmachtenberg, International Plastics Handbook, Carl Hanser Verlag GmbH & Co. KG, München, 2006.

[5]   C. Yang, M.E. Navarro, B. Zhao, G. Leng, G. Xu, L. Wang, Y. Jin, Y. Ding, Thermal conductivity enhancement of recycled high density polyethylene as a storage media for latent heat thermal energy storage, Sol Energ Mat Sol C 152 (2016) 103–110.

[6]   Y. Lin, Y. Jia, G. Alva, G. Fang, Review on thermal conductivity enhancement, thermal properties and applications of phase change materials in thermal energy storage, Renewable and Sustainable Energy Reviews 82 (2018) 2730–2742.

[7]   L. Fan, J.M. Khodadadi, Thermal conductivity enhancement of phase change materials for thermal energy storage: A review, Renewable and Sustainable Energy Reviews 15 (1) (2011) 24–46.

[8]   Mamunya, Y. P., Davydenko, V. V., Pissis, P., & Lebedev, E. V., Electrical and thermal conductivity of polymers filled with metal powders, Eur Polym J 38 (9) (2002) 1887–1897.

[9]   R.F. Hill, P.H. Supancic, Thermal Conductivity of Platelet-Filled Polymer Composites, J Am Ceram S 85 (4) (2002) 851–857.

[10]   A. Boudenne, L. Ibos, E. Géhin, M. Fois, J.C. Majesté, Anomalous behavior of thermal conductivity and diffusivity in polymeric materials filled with metallic particles, J Mater Sci 40 (16) (2005) 4163–4167.

[11]   G.-W. Lee, M. Park, J. Kim, J.I. Lee, H.G. Yoon, Enhanced thermal conductivity of polymer composites filled with hybrid filler, Compos Part A-Appl S 37 (5) (2006) 727–734.

[12]   I.H. Tavman, Thermal and mechanical properties of aluminum powder-filled high-density polyethylene composites, J. Appl. Polym. Sci. 62 (12) (1996) 2161–2167.

[13]   I.H. Tavman, Thermal and mechanical properties of copper powder filled poly (ethylene) composites, Powder Technol 91 (1) (1997) 63–67.

[14]   K. Wattanakul, H. Manuspiya, N. Yanumet, Thermal conductivity and mechanical properties of BN-filled epoxy composite: Effects of filler content, mixing conditions, and BN agglomerate size, J Compos Mater 45 (19) (2011) 1967–1980.

[15]   D. Kumlutas, Thermal conductivity of particle filled polyethylene composite materials, Compos Sci Technol 63 (1) (2003) 113–117.

[16]   A.S. Luyt, J.A. Molefi, H. Krump, Thermal, mechanical and electrical properties of copper powder filled low-density and linear low-density polyethylene composites, Polym Degrad Stabil 91 (7) (2006) 1629–1636.

[17]   Rusu, M., Sofian, N., & Rusu, D, Mechanical and thermal properties of zinc powder filled high density polyethylene composites., Polym Test 20 (4) (2001) 409–417.

[18]   Jinhong Yu, Xingyi Huang, Chao Wu, Pingkai Jiang, Permittivity, thermal conductivity and thermal stability of poly(vinylidene fluoride)/graphene nanocomposites, IEEE Trans. Dielect. Electr. Insul. 18 (2) (2011) 478–484.

[19]   A.K. Pandey, K. Singh, K.K. Kar, Thermo-mechanical properties of graphite-reinforced high-density polyethylene composites and its structure–property corelationship, J Compos Mater 51 (12) (2016) 1769–1782.

[20]   E. Tarani, Z. Terzopoulou, D.N. Bikiaris, T. Kyratsi, K. Chrissafis, G. Vourlias, Thermal conductivity and degradation behavior of HDPE/graphene nanocomposites, J Therm Anal Calorim 129 (3) (2017) 1715–1726.

[21]   L.M. Gorghiu, S. Jipa, T. Zaharescu, R. Setnescu, I. Mihalcea, The effect of metals on thermal degradation of polyethylenes, Polym Degrad Stabil 84 (1) (2004) 7–11.

[22]   C. Zauner, F. Hengstberger, M. Etzel, D. Lager, R. Hofmann, H. Walter, Durability of a fin-tube latent heat storage using high density polyethylene as PCM, IOP Conf. Ser.: Mater. Sci. Eng. 251 (2017) 12123.

[23]   H. Weingrill, W. Hohenauer, K. Resch-Fauster, C. Zauner, Analyzing Thermal Conductivity of Polyethylene-Based Compounds Filled with Copper, Macromol. Mater. Eng. 59 (2019) 1800644.

[24]   G.W. Ehrenstein, G. Riedel, P. Trawiel, Thermal analysis of plastics: Theory and practice, Hanser, Munich, 2004.

[25]   T. Mezger, Das Rheologie-Handbuch: Für Anwender von Rotations- und Oszillations-Rheometern, 4th ed., Vincentz Network, Hannover, 2012.

190

[26] H. Chen, V.V. Ginzburg, J. Yang, Y. Yang, W. Liu, Y. Huang, L. Du, B. Chen, Thermal conductivity of polymer-based composites: Fundamentals and applications, Prog Polym Sci 59 (2016) 41–85.

[27] W.-G. Weng, G.-H. Chen, D.-J. Wu, W.-L. Yan, HDPE/expanded graphite electrically conducting composite, Composite Interfaces 11 (2) (2004) 131–143.

[28] M.U. de La Orden, J.M. Montes, J. Martínez Urreaga, A. Bento, M.R. Ribeiro, E. Pérez, M.L. Cerrada, Thermo and photo-oxidation of functionalized metallocene high density polyethylene: Effect of hydrophilic groups, Polym Degrad Stabil 111 (2015) 78–88.

[29] P. Pags, F. Carrasco, J. Saurina, X. Colom, FTIR and DSC study of HDPE structural changes and mechanical properties variation when exposed to weathering aging during Canadian winter, J. Appl. Polym. Sci. 60 (2) (1996) 153–159.

[30] V.M. Khumalo, J. Karger-Kocsis, R. Thomann, Polyethylene/synthetic boehmite alumina nanocomposites: Structure, thermal and rheological properties, Express Polym. Lett. 4 (5) (2010) 264–274.

[31] S. Yang, S. Bai, Q. Wang, Morphology, mechanical and thermal oxidative aging properties of HDPE composites reinforced by nonmetals recycled from waste printed circuit boards, Waste Manag. 57 (2016) 168–175.

[32] D.H. Everett, Basic principles of colloid science, Royal Society of Chemistry, London, 2010.

Part VI.

Summary, conclusions and outlook

Summary

Latent heat storages (LHS) with phase-change materials (PCM) as storage media can be applied to close the gap between energy demand and supply and to increase energy efficiency thereby. Manifold PCM out of different material classes already exist, but they all face several challenges during their application. Interestingly, polymers have been mainly neglected for this purpose. Within this thesis, the applicability of semi-crystalline polymers as PCM was investigated. The first approach included a broad material selection process for which more than 70 different semi-crystalline polymer grades were tested. Their application-relevant thermo-physical properties such as the heat of fusion (i.e. storage capacity of the PCM) and their melting and crystallization behavior (i.e. the charging and discharging characteristics of the PCM) were investigated in detail by means of Differential Scanning Calorimetry (DSC). The tested polymers comprised mainly polyolefins, polyoxymethylenes (POM), polyamides (PA) and polyesters. Out of the tested polymer groups polyethylenes (PE), polypropylenes (PP), PA 6 and PA 4.6 as well as their recyclates were identified as potential polymeric PCM. However, also their thermal and thermo-oxidative stability needed to be investigated as it reflects the polymer's ability to maintain the above mentioned decisive material characteristics. For this purpose, application-relevant testing in the form of cyclic thermal loads in a DSC and thermal static loads on bulky specimens in air were applied on selected polymer grades. The cyclic thermal loads proved to be less aggressive and were therefore used a preliminary testing for the thermal static loads in air. For this second type of exposure, a high-density polyethylene (HDPE) grade, a copolymer of POM (POM-C) and a PA 6 grade were exposed in cylindrical containers at approximately 30 °C above their melting temperature for 15 days. After the applied thermal loads, thermo-oxidative degradation was detected only the specimen surface which was ascribed to diffusion-limited oxidation (the atmospheric oxygen could not diffuse into the specimen bulk). The storage capacity of the exposed specimens of the HDPE and PA 6 was therefore only reduced to a minimal extent. For the POM-C, however, the thermo-oxidative degradation caused multiple chain cleavage and the

polymer degraded to a mixture of low-molecular substances (which were fluid at ambient temperature). It therefore did not prove to be suitable as PCM. Nonetheless, HDPE, PP and PA 6 can cover an approximate temperature range from 100 °C to 250°C as polymeric PCM due to their different melting temperatures.

Estimating one thermal cycle to take 8 h, the applied thermal loads of 15 days (=360 h) only equaled 45 cycles and were therefore considered as short-term stability investigations. For the consecutive long-term stability investigations, the exposure parameters were refined (exposure 30 °C and 50 °C above the melting temperature and bulkier specimen dimensions) to better imitate the conditions during the application as PCM for exposure times up to 10 months (= 7200 h which equal approximately 900 cycles). The most promising polymeric PCM HDPE was exposed along with additionally stabilized HDPE grades. Hindered amine stabilizers (HAS) were applied at different concentrations as additional stabilization against thermo-oxidative degradation. The oxidation-induction temperature of all HDPE grades was monitored during the applied thermal loads and it decreased for all HDPE grades with increasing exposure time. This was ascribed to a combination of physical evaporation and chemical consumption of the contained stabilizer systems. The long-term stability investigations further revealed the challenges that occur for polymers when applied in the melt sate. A constant melt movement within the exposed specimens was detected which was caused by natural convection. Consequently, the positions of the polymeric chains changed throughout the exposure. Depending on the exposure temperature and applied stabilizer system, the surface of the exposed specimen was eventually immobilized due to thermo-oxidative degradation and was therefore excluded from this continuous melt movement. Polarization light microscopy (PLM) and Fourier Transform Infrared spectroscopy (FTIR) unveiled the changes in the crystalline morphology of the immobilized specimen surface. With increasing extent of oxidation, the fine crystalline structure first turned to a less fine crystalline structure and eventually to a completely amorphous one. The loss of the crystalline structure due to thermo-oxidation correlated with a loss in the storage capacity. Therefore, the oxidation penetration depth (OPD) from the specimen surface into the bulk was determined by the extent of carbonyl content to estimate the total loss in storage capacity due to the exposure in air in the melt state. Interestingly, the OPD of the additionally stabilized HDPE grades eventually exceeded the OPD of the non-additionally stabilized HDPE. The immediate immobilization of the non-additionally stabilized HDPE seemed to act as barrier for further oxygen diffusion into the specimen bulk.

Thus, an additional stabilization proved to not be necessary for the application of HDPE as PCM. Nevertheless, the majority of the storage capacity of the exposed specimens was maintained as the thermo-oxidatively degraded specimen part presented only a fractional amount of the entire specimen volume (as deduced from the OPD measurements). Consequently, the HDPE is a highly interesting polymeric PCM.

After the long-term stability of the HDPE as polymeric PCM was demonstrated, its inherent low thermal conductivity (TC) was addressed via the incorporation of highly conductive particles. The outcome of a sound literature review indicated a great available variety of filler particles for enhancing the TC of polymers. The incorporation of those particles typically comes along with a reduction in the storage capacity as they do not contribute to the storage capacity of the material (their phase transitions lay in general outside the application temperature of polymeric PCM). Thus, a filler screening was necessary to identify the most efficient fillers. However, the sound literature review also revealed multiple impact factors on the TC of polymeric compounds. These arise inter alia from differences in the compound fabrication and specimen preparation, from varying filler particle shape and size, its surface treatment and also from the measurement method. Thus, a comparative study of HDPE and linear-low density polyethylene (LLDPE) containing differently shaped copper particles (platelets and two types of spheres) was conducted in order to find the appropriate measurement method for polymeric compounds and to conduct reliable TC measurements. Four commercially available measurement methods were utilized for the determination of the fabricated compounds and the neat polymers which implemented either steady state or transient measurement principles. Within the comparative study, large discrepancies in the TC for the very same materials were found. Complementary morphological investigations via Scanning Electron Microscopy (SEM) helped to ascribe them to differences in the detection possibilities of the present specimen conditions (orientation of filler particles and crystalline structure) via the applied measurement methods. Nevertheless, the same tendencies in regard to the TC enhancement were detected for each of the methods.

The measurement method which exhibited the most possibilities to adapt to the specimen conditions i.e. the Hot disk method was chosen for the consecutive filler screening. Out of the three available filler groups for enhancing the TC of polymers (carbon-based fillers, ceramics and metals), nine were chosen based on an extensive literature review and incorporated in the HDPE matrix at filler loadings up to 30 vol%. Aluminum, copper and

expanded graphite particles proved to be the most efficient fillers at low filler loadings. However, the TC of the compounds which contained the expanded graphite exceeded by far the TC of the other two compound types. Furthermore, the expanded graphite did not lower the oxidation induction temperature and therefore the short-term thermo-oxidative stability of the fabricated compounds over the neat HDPE (as opposed to the aluminum and copper particles). Thus, multiple types of expanded graphite and differing compounding procedures were evaluated to find the optimum balance between a TC for a sufficiently fast heat transfer rate and the minimal loss in the storage capacity.

In general, incorporated particles tend to interact with the surrounding polymeric matrix as it was shown by a reduced flowability of the expanded graphite compounds and a lowered oxidation induction temperature of the compounds containing metal fillers over the neat HDPE. Thus, in order to prove the applicability of the polymeric compounds applied as PCM, their application-relevant thermo-physical properties as well as their long-term stability needed to be examined additionally to the already conducted long-term stability investigations of the neat HDPE. The compounds' long-term stability included also their ability to maintain a homogeneous filler distribution (the positions of the filler particles are variable in the melt state) to guarantee a uniform heat transfer throughout the PCM. For this purpose, compounds containing expanded graphite and aluminum were exposed under identical conditions as the neat HDPE in the melt state for up to 10 months. Their melting and crystallization behavior was affected only little by the incorporation of the fillers. However, both compounds exhibited an increased viscosity over the neat HDPE which resulted in a reduced flowability (a certain degree of flowability is necessary for the compound to fill the storage tank without air inclusions). This was ascribed to an increased internal friction between the filler particles and filler particles and the polymer chains. On the other hand, the increased internal friction contributed most likely to the maintenance of the homogeneous filler distribution throughout the applied thermal loads. Especially the larger expanded graphite particles seemed to have created a filler network that impeded sedimentation for the most part. Furthermore, the compounds showed an increased thermo-oxidative stability over the neat HDPE as their exposed specimens exhibited a comparably lower OPD after the applied thermal loads. The incorporated particles were assumed to have acted as oxygen barrier which hampered oxygen diffusion into the specimen bulk and thereby the initiation of thermo-oxidative degradation. Both investigated compounds therefore proved to be suitable polymeric PCM with enhanced TC.

Conclusions and outlook

The results which are presented in this thesis demonstrated the applicability of polymers as phase-change materials (PCM) in latent heat storages (LHS). By the use of high-density polyethylene (HDPE), polypropylene (PP) and polyamide 6 (PA 6) a broad application temperature range from 100 °C to 250 °C can be covered. They can therefore be utilized for low- and intermediate temperature applications according to the categories established in the introduction. The conducted research further revealed the challenges that come along with the use of polymers in the melt state. During the long-term exposure of HDPE no thermal degradation outside the oxygen diffusion depth occurred. This implied that the PCM's dimensions significantly impact its long-term stability as the specimen surface determines the area through which atmospheric oxygen diffuses into the PCM. The diffused oxygen initiates degradation and results in a loss of the storage capacity. Thus, a small surface in regard to the volume of the PCM or an inert atmosphere should be considered during the design of a LHS. Nonetheless, the polymers' facile adaptability to the requirements (enhancement of thermal conductivity) renders them a highly interesting PCM class as each PCM can be fitted to the design and the application of the LHS. Additionally, their commercial availability and thus cost-effectiveness as well as the possibility to use recycled polymers instead of virgin material contribute to a combined economic and ecologic motivation for utilizing polymers as PCM.

However, as this thesis focused on HDPE for the long-term stability investigations, further research is necessary to fully exploit the potential of the other two selected polymeric PCM (i.e. PP and PA) in order to reach market maturity for the entire above designated application temperature range. For this purpose, it would be interesting to investigate their long-term stability and the long-term stability of their compounds. Another interesting future field of research for polymeric PCM would be the optimization of the polymer synthesis process. As polymers have not been applied largely as PCM yet, their synthesis might still be optimized to achieve a maximum crystallinity by using different process temperatures, catalysts etc. Furthermore, copolymers could be synthesized that possess two melting

peaks to possess two storing temperatures. This might also be done by blending different polymers or polymers with existing PCM such as paraffins.

For the functionalization of the polymeric PCM, a broad spectrum of fillers with varying filler loadings and particle geometries was investigated. As all compounds including their specimens were fabricated identically and their TC was determined accordingly, material- and technology-induced impacts on the compound's final TC could thereby be eliminated which enabled comparability of each filler's efficiency in enhancing the TC for the first time (as opposed to the individual results from the scientific literature). The obtained results therefore serve as solid base for further work regarding the efficient TC enhancement of polymers.

Along with the increase in TC, the expanded graphite increased the viscosity of the compound over the neat HDPE significantly. At filler loadings of 5 vol% and above, the compound's flowability without external force application was lost which was not desirable for the application in storage tanks where the granule is poured into. However, this characteristic could be used for additive manufacturing where dimensionally stable and thus container-free LHS can be fabricated according to the individual applications.

Even though further research is still necessary, the conducted research in the course of this thesis might have contributed to pave the way for the application of polymeric PCM. It gave rise to new ideas for the use of polymeric PCM and hopefully encourages other scientists to expedite their field of research towards this very interesting topic.